TECHNISCHE UNIVERSITÄT MÜNCHEN

Wissenschaftszentrum Weihenstephan für Ernährung, Landnutzung und Umwelt Lehrstuhl für Entwicklungsgenetik

A circular RNA derived from the *Tulp4* gene regulates synaptic transmission and working memory

Natalia Soledad Pino Delgado

Vollständiger Abdruck der von der Fakultät Wissenschaftszentrum Weihenstephan für Ernährung, Landnutzung und Umwelt der Technischen Universität München zur Erlangung des akademischen Grades eines

Doktors der Naturwissenschaften

genehmigten Dissertation.

Vorsitzende:	Prof. Dr. Aphrodite Kapurniotu
Prüfer der Dissertation:	1. Prof. Dr. Wolfgang Wurst
	2. Prof. Angelika Schnieke, Ph.D.

Die Dissertation wurde am 20.11.2019 bei der Technischen Universität München eingereicht und durch die Fakultät Wissenschaftszentrum Weihenstephan für Ernährung, Landnutzung und Umwelt am 22.04.2020 angenommen.

1 Table of contents

2 Table of figures

3 Summary

Circular RNAs (circRNAs) have recently emerged as a large class of long non-coding RNAs evolutionarily conserved through the eukaryote kingdom, displaying cell-, tissue-, and stage-specific expression patterns. CircRNAs originate by a 'backsplicing' reaction, wherein a downstream splice donor site attacks an upstream splice acceptor site to form a unique sequence –known as the head-to-tail junction– not present in messenger RNAs. Most circRNAs are derived from protein-coding genes, containing one or multiple adjacent exons. Some of them may include intronic sequences as well as untranslated regions and can be originated from the antisense strand. To date, perhaps due to their sequence heterogeneity, no generalized function has been ascribed to circRNAs. However, although the function of most circRNAs remains largely unknown, some have been shown to work in microRNA sequestration, transcriptional regulation, modulating alternative splicing outcome, and serving as scaffolds for the formation of protein complexes. Recently, few circRNAs have been reported to act as templates for translation.

The identification and characterization of circRNAs have been hampered mainly due to the difficulties of working with low abundance molecules and the restriction of specifically targeting the unique, short head-to-tail junction. Therefore, circRNA research grows mainly supported by single circRNA studies. In this project, we have focused on a brain-enriched circRNA derived from the *Tulp4* gene, which is the most abundantly expressed, coding-sequence-derived circRNA in neurons. Using loss-of-function models, we report that circTulp4 plays a role in early neuronal development and, most notably, in excitatory synaptic neurotransmission. Furthermore, we could correlate the deficit in neurotransmission with a decreased number of excitatory synaptic contacts on dendritic spines.

In order to assess the physiological phenotype of depleting circTulp4 *in vivo*, CRISPR/Cas9 was used to target the circRNA-specific splice acceptor site, preventing its biogenesis while preserving the transcription of the linear isoform of *Tulp4*. Acute hippocampal slices derived from mutant mice recapitulated the electrophysiological outcome recorded from circTulp4-deficient neurons in culture and in hippocampal slices transfected via the *in utero* electroporation technique. Moreover, behavioral phenotyping revealed circTulp4^{KO} mouse displayed novelty-induced increased locomotor activity, aberrant sensorimotor recruitment, and substantial cognitive deficits. This behavioral phenotype is well-related with mouse models displaying glutamatergic neurotransmission and/or synaptic plasticity impairments, which suggests convergent molecular mechanisms.

Overall, the present study reveals novel and physiological insights into the most predominantly expressed, coding-sequence-derived circRNA in neurons. CircTulp4 acts in the finely regulated process of excitatory synaptic transmission and its depletion strongly impacts spatial working memory.

4 Zusammenfassung

Zirkuläre RNAs (circRNAs) haben sich vor kurzem als große Klasse von langen, nicht-kodierenden RNAs, die in Eukaryoten evolutionär hoch konserviert sind, herausgestellt. Sie zeigen zell-, gewebe- und entwicklungsspezifische Expressionsmuster. CircRNAs entstehen durch eine „backsplicing“ Reaktion bei der ein downstream Spleißdonor mit einen upstream Spleißakzeptor reagiert und eine neue Sequenz –*head-to-tail junction* genannt– bilden, welche nicht in der Boten-RNA zu finden ist. Die Mehrzahl der circRNAs entstammt proteinkodierenden Genen und beinhaltet ein oder mehrere aufeinander folgende Exons. Manche enthalten Intron-Sequenzen oder untranslatierte Regionen und können auch vom Gegenstrang stammen. Bisher konnte circRNAs keine allgemeine Funktion zugeschrieben werden, was möglicherweise auf ihre Sequenzheterogenität zurückzuführen ist. Obwohl die Funktion der meisten circRNAs weiterhin größtenteils unbekannt ist, wurde für einige eine Funktion in der Bindung von microRNAs, der Transkriptionsregulation, der Modulierung von alternativem Spleißen, sowie als Gerüst für die Formierung von Proteinkomplexen, gezeigt. Kürzlich wurde zudem beschrieben, dass einige wenige als Translationsmatrizen dienen.

Die Identifizierung und Charakterisierung von circRNAs wurde hauptsächlich dadurch erschwert, dass die Moleküle in sehr geringer Konzentration vorliegen, sowie der Tatsache, dass eine spezifische Adressierung der charakteristischen *head-to-tail junctions* aufgrund ihrer Kürze sehr schwierig ist. Deshalb gibt es Fortschritte in der circRNA Forschung vor allem durch Studien von einzelnen circRNAs. In dieser Arbeit lag der Schwerpunkt auf einer circRNA die Ihren Ursprung im *Tulp4* Gen hat und welche die am häufigsten exprimierte, aus kodierenden DNA-Sequenzen stammende, circRNA in Nervenzellen ist. Durch die Verwendung von gentechnischen loss-of-function Werkzeugen können wir hier zeigen, dass circTulp4 eine Rolle in der frühen neuronalen Entwicklung und vor allem in der exzitatorischen synaptischen Reizleitung spielt. Darüber hinaus konnten wir das Defizit der neuronalen Reizleitung mit einer verringerten Anzahl von exzitatorischen Synapsen auf dendritischen Dornfortsätzen in Verbindung bringen.

Um den Phänotyp eines Fehlens von circTulp4 *in vivo* zu untersuchen wurde der circRNA-spezifische Spleißakzeptor mit Hilfe von CRISPR/Cas9 zerstört um die Biogenese von circTulp4 zu unterbinden, gleichzeitig aber die Transkription der linearen Isoform aufrecht zu erhalten. Elektrophysiologische Untersuchungen an hippocampalen Hirnschnitten von Mausmutanten zeigten dieselben Ergebnisse wie zuvor circTulp4-defiziente Neuronen in Kultur, sowie hippocampale Hirnschnitte die via *in utero* Elektroporation transfiziert wurden. In

Verhaltensexperimenten zeigten diese circTulp4^{KO} Mäuse darüber hinaus eine durch eine neue Umgebung induzierte Hyperlokomotion, eine veränderte sensomotorische Rekrutierung und erhebliche kognitive Defizite. Dieser Verhaltensphänotyp ähnelt dem von Mäusen mit verringerter glutamaterger Neurotransmission und/oder synaptischer Plastizität, stark. Dies legt ähnliche zugrunde liegende molekulare Mechanismen nahe.

Zusammenfassend gibt diese Arbeit neue Einblicke in die Physiologie der am häufigsten exprimierten, aus kodierenden DNA-Sequenzen stammende, circRNA in Nervenzellen. CircTulp4 beeinflusst die exakt regulierten Prozesse der exzitatorischen synaptischen Reizleitung und ihr Fehlen hat einen starken Effekt auf das räumliche Arbeitsgedächtnis.

5 Introduction

5.1 THE TRANSCRIPTOME COMPLEXITY

The development of deep sequencing technology in parallel with bioinformatic tools for its analysis have revealed a stunning conservation of the number of genes found in organisms as diverse as *Caenorhabditis elegans*, *Mus musculus* and *Homo sapiens*, suggesting that species complexity cannot only be explained by protein-coding sequences (Lander et al., 2001; Mattick, 2003; Waterston et al., 2002).

Diverse mechanisms acting at multiple levels can lead to complexity. Alternative splice variants may create functional diversity in protein isoforms, presenting different domain combinations. The use of alternative gene starts can also increase transcriptional diversity; or the use of varied 5'- and 3'-ends generating the structural basis for the regulation of messenger RNA (mRNA) turnover, translation and subcellular localization.

Previous studies focused on transcriptional output, and the extensive annotation efforts of the ENCODE project have underscored the pervasiveness with which genomes are transcribed (Carninci et al., 2005; Dunham et al., 2012; Koch et al., 2008). Nearly 80 % of the eukaryotic genome is represented in processed transcripts that seem to lack protein-coding capacity (Birney et al., 2007; Carninci et al., 2005; Dunham et al., 2012). These findings in association with observations that non-coding DNA increases with species complexity posited attention in exploring the non-coding RNA world.

In the following sections, different mechanisms contributing to transcriptome complexity –in particular in the mammalian central nervous system (CNS)– will be given.

5.1.1 Alternative splicing is prevalent in nervous system tissues

Alternative splicing (AS) of primary transcripts is an essential mechanism during gene expression that results in increased transcriptomic and proteomic diversity and also post-transcriptionally regulates mRNA levels. Its frequency is highly variable among species and increases with species complexity (Barbosa-Morais et al., 2012; Merkin et al., 2012), with around 95 % of human multi-exonic genes subjected to AS (Pan et al., 2008; Wang et al., 2008).

Alternative splicing is especially prevalent and highly conserved in nervous system tissues of vertebrates (Barbosa-Morais et al., 2012; Jelen et al., 2007; Merkin et al., 2012; Raj & Blencowe, 2015). Current evidence suggests that such high frequencies may contribute to the nervous system functional complexity, playing a role in various biological processes such as cell differentiation, morphogenesis, the formation of complex neuronal networks, and the establishment/plasticity of synapses (Norris & Calarco, 2012; Zheng & Black, 2013).

A conserved set of *cis*-acting elements in exons and flanking introns known as the core splicing signals (5'- and 3'-splice sites, branch site, and polypyrimidine tract) guides the interactions between spliceosomal components and precursor mRNA (pre-mRNA). Most of the *cis*-regulatory elements that are predictive of the tissue-specific splicing pattern are located within 300 nucleotides around the splice sites. These regions are highly enriched in binding sites of RNA-binding proteins (RBPs) and, in general, are more conserved than distal intronic sequences (Barash et al., 2010; Xiong et al., 2015). The core splicing signals, however, are not sufficient to ensure correct splice site selection and to regulate AS. These decisions are further regulated by the combinatorial control of short, degenerate RNA motifs known as exonic/intronic splicing enhancers or silencers, which are bound by *trans*-acting splicing factors. The combination of variable *cis*-acting elements and *trans*-acting factors is responsible for cell type-, condition-, and species-specific changes in alternative splicing.

Noticeably, despite the presence of multiple variants of a gene, most of the human genes express a single major transcript variant (Gonzàlez-Porta et al., 2013).

5.1.2 Non-coding RNAs dominate the transcriptional output of mammalian CNS genome

The protein-centric view of molecular biology has been defied by the discovery of nuclear introns and RNA interference (RNAi), and most recently by the advances in genome sequencing technology, which lead to the identification of a large number of non-coding transcripts.

Based upon the fact that 95 % of pre-mRNAs is represented by intronic RNA and observations suggesting that a large number of non-coding RNA (ncRNA) transcripts do not contain substantial open reading frames and may represent at least half of all the transcripts, it is estimated that 97-98 % of the transcriptional output of the human genome is non-protein-coding RNA (Dunham et al., 2012). The relevance of the main participants in gene expression –transfer RNA (tRNA) and ribosomal RNA (rRNA)– was already established in the 1950s. However, the importance of short- and long-non-coding RNAs is only now starting to be unveiled.

NcRNAs are broadly and arbitrarily sub-classified according to their size into small non-coding RNAs (sncRNAs) –ranging from 20 to 200 nt– and long non-coding RNAs (lncRNAs), with sizes from 200 nt to more than 1 Kb. SncRNAs can comprise 10 % of the transcription detected in human cells. Three major families have been described in eukaryotic cells: micro-RNAs (miRNAs), piwi-interacting RNAs (piRNAs) and small-interfering RNAs (siRNAs). Though these families are different in their origin, they share specific biogenesis steps and regulatory mechanisms. Generally, sncRNAs regulate genomic output at transcriptional or post-transcriptional levels with the help of two main groups of proteins: processors and effectors. Processors are the nucleases responsible for excising small RNAs from specific RNA transcripts; while effectors are a diverse group of RBPs acting in the stabilization, transport and regulatory activity of the sncRNA over its cognate target (Faehnle & Joshua-Tor, 2007; Murchison & Hannon, 2004).

Like protein-coding mRNAs, lncRNAs are transcribed by RNA Polymerase II (Pol II), and many are also 5'-capped, spliced, and polyadenylated (Quinn & Chang, 2016). LncRNA genes are oriented in the sense or antisense direction of the host gene, can be located intergenically, or be divergently transcribed from a neighboring gene through a shared promoter. At the molecular level, lncRNAs can regulate the expression of neighboring genes in *cis* (Engreitz et al., 2016; Guil & Esteller, 2012) or distant genes in *trans* (Chu et al., 2011; Johnsson et al., 2013) through the interaction with DNA, RNA or protein partners. Besides, recent studies have shown that transcripts annotated as lncRNAs have the potential to encode functional micropeptides (Andrews & Rothnagel, 2014; Nelson et al., 2016). Noteworthy, any particular lncRNA gene might play multiple roles depending on the accessibility of low free-energy conformation motifs

at a time (Bassett et al., 2014; Dethoff et al., 2012). The final effectors driving RNA free-energy landscapes can be RBPs, helicases, metabolites, or various ions.

A striking 40 % (equivalent to 4.000-20.000) of the lncRNA genes annotated in the human genome have a brain-specific expression (Derrien et al., 2012). The expression of many of them is dynamically regulated during mammalian CNS development and neural stem cell (NSC) differentiation (Aprea et al., 2013; Belgard et al., 2011; Mercer et al., 2010; Ramos et al., 2013), and in some cases can be regulated by neuronal activity (Barry et al., 2014; Lipovich et al., 2012). Furthermore, it is often restricted to specific brain regions, showing a high degree of cell-type specificity, even surpassing that of protein-coding genes (Liu et al., 2016; Molyneaux et al., 2015; Ramos et al., 2013).

Circular RNA transcripts –described as belonging to the lncRNA family– are introduced in the following section.

5.2 CIRCULAR RNAS

Circular RNA molecules were first described in mammalian cells in 1979 as an RNA viral genome (Hsu & Coca-Prados, 1979). Although some studies have subsequently reported the existence of circular RNAs (Capel et al., 1993; Cocquerelle et al., 1992; Nigro et al., 1991; Zaphiropoulos, 1996), their underrepresentation and low expression levels have long supported the notion of these molecules as non-functional by-products of the spliceosomal machinery. The advent of RNA-sequencing technology and novel computational algorithms found these molecules to be ubiquitously expressed and conserved in the whole eukaryote kingdom (Ashwal-Fluss et al., 2014; Memczak et al., 2013; Salzman et al., 2012).

There are different types of circular RNA molecules, generated by distinct mechanisms (See **Table 1** and **Figure 1**). Some viroids and viruses have a circular RNA genome, multiplying it from a single initiation event through rolling circle replication. Other circular RNAs are by-products of RNA processing, as circular RNA intron and circular RNA processing intermediate. However, the majority of circular molecules derives from protein-coding genes (circRNAs) and span complete exons (Ashwal-Fluss et al., 2014; Guo et al., 2014; Rybak-Wolf et al., 2015; You et al., 2015).

Using RNA-sequencing technology, other groups and us have shown circRNA´s expression pattern to be tissue and developmental-stage-specific (Rybak-Wolf et al., 2015; Venø et al., 2015; Westholm et al., 2014; You et al., 2015). Interestingly, in the mammalian brain, up to 20 % of the protein-coding genes produce circRNAs. Previously, we have found circRNAs to be highly abundant in different neuronal tissues and cell types, upregulated during neuronal development and, most importantly, highly enriched in synapses (Rybak-Wolf et al., 2015). This specific localization suggests that circRNAs might have an important role in the regulation of neurotransmission and synaptic plasticity.

In the following subsection, different mechanisms giving rise to circRNAs will be described.

Table 1. Characteristics of different types of circular RNA molecules. Adapted from (Lasda & Parker, 2014).

	Circular RNA	Phosphodiester bond	Organism	Function	Reference
Genome	viral	3’ → 5’; 2’ → 5’	Human and plants	Replication	(Côté & Perreault, 1997; Flores et al., 2011)
Intronic	Group I	3’ → 5’; 2’ → 5’	Virus, bacteria, eukaryotes	Mobile genetic element	(Cech, 1990; Grabowski et al., 1981)
	Group II		Bacteria, archaea, eukaryote organelles	Mobile genetic element	(Li-Pook-Than & Bonen, 2006; Molina-Sánchez et al., 2006)
	tRNA processing	3’ → 5’	Archaea and Metazoa	Can contain snoRNAs	(Abelson et al., 1998; Lu et al., 2015)
	Lariat introns	2’ → 5’	Eukaryotes	Transcriptional regulation	(Gardner et al., 2012; Talhouarne & Gall, 2018; Zhang et al., 2013)
Processing intermediate	rRNA precursor	3’ → 5’	Archaea and algae	Rearrange genomic order of sequence	(Danan et al., 2012; Tang, 2002)
	Permuted tRNA	3’ → 5’			(Soma et al., 2007)
Non-coding	snoRNA and RNase P	3’ → 5’	Archaea	Stability	(Danan et al., 2012)
Exonic	circRNAs	Backsplicing	Eukaryotes	Transcriptional and post-transcriptional regulation	(Hansen et al., 2013; Li et al., 2015; Memczak et al., 2013)

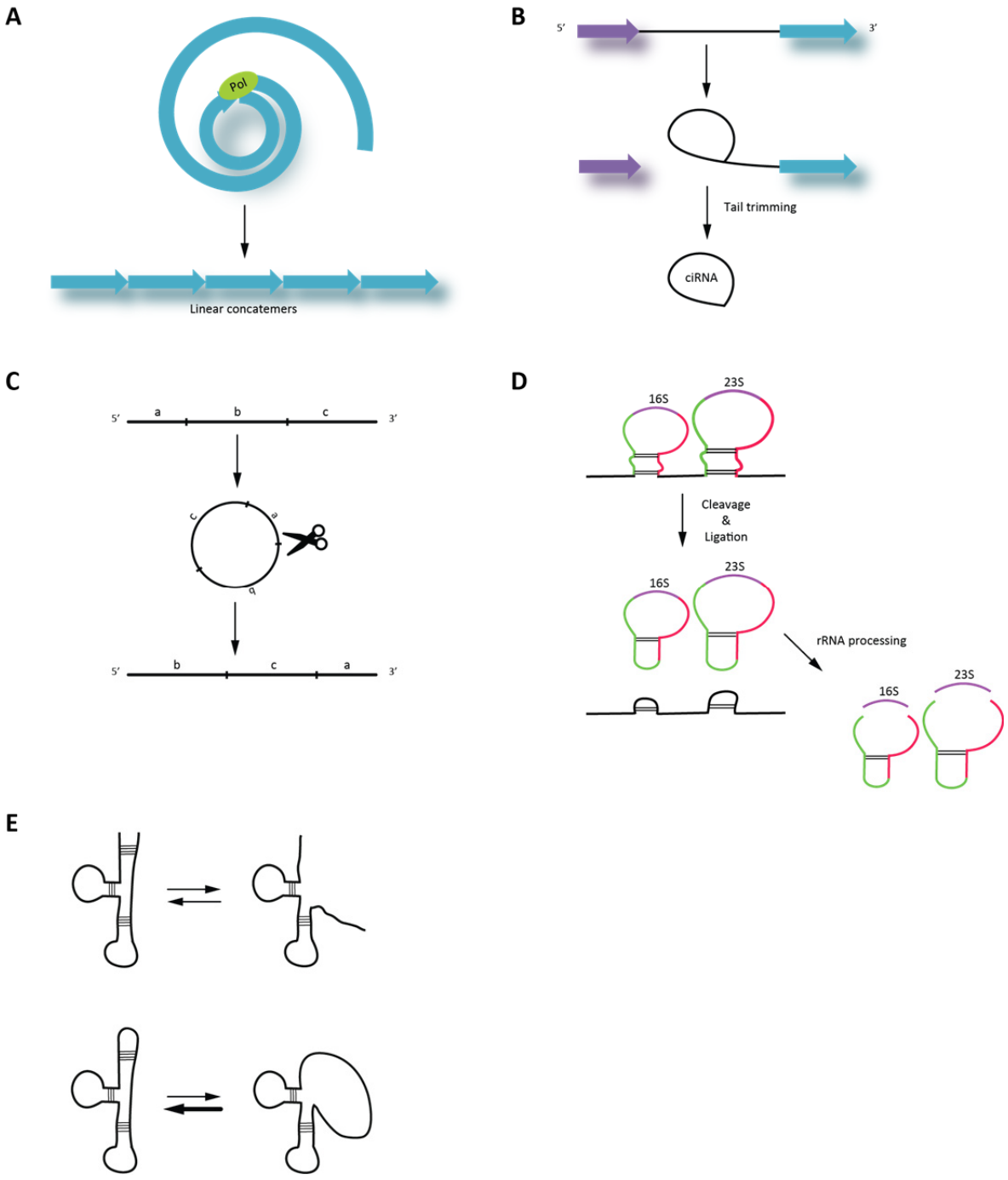

Figure 1. The biogenesis of different types of circular RNA molecules.
(A) Viroids and the hepatitis delta virus have circular single-stranded RNA genomes and are replicated via rolling circle replication. A host DNA-dependent RNA polymerase (green) originates multiple genomic copies in linear concatemers that are then separated into linear monomers and finally ligated into circular RNAs. **(B)** Circular intronic RNAs (ciRNAs) are originated by the eukaryotic spliceosomal machinery. The lariat intron somehow evades normal debranching and degradation, and instead undergoes a 'tail trimming' downstream from the branchpoint, resulting in a stable molecule. **(C-D)** Circular molecules can also be produced as intermediates in RNA processing reactions. **(C)** In some algae and archaea circularization is critical in the biogenesis of permuted tRNA genes, allowing for sequence rearrangements. **(D)** In some archaea, the 16S and 23S ribosomal subunits are excised from linear precursor molecules that are circularized and then further processed to produce the mature rRNAs. rRNA regions are indicated in purple; upstream and downstream regions contained within the circular intermediate are green and red, respectively. **(E)** Circular non-coding RNAs, such as RNaseP and some small nucleolar RNAs (snoRNAs), are produced in some archaeal species from excised circularized tRNA introns. Circularization of functional non-coding RNAs could protect them from

degradation by exonucleases and could also facilitate proper folding by imposing structural constraints. Adapted from (Lasda & Parker, 2014).

5.2.1 CircRNA biogenesis

Circular and linear (mRNAs) transcripts of a host gene derive from Pol II primary transcripts by reactions catalyzed by the canonical spliceosomal machinery (Ashwal-Fluss et al., 2014; Starke et al., 2015; Wang & Wang, 2015). Unlike canonical splicing, the so-called "backsplicing" reaction that originates circRNAs involves the attack of a 5'-splice donor site to an upstream 3'-splice acceptor site (see **Figure 2A**). The resulting RNA molecules are single-stranded, covalently closed, and are characterized by a unique sequence not present in mRNAs, the head-to-tail junction. CircRNAs can contain one or multiple adjacent exons, include intronic sequences as well as untranslated regions (UTRs), and can also be originated from the antisense strand (Memczak et al., 2013). Of note, many circRNAs can be produced from one gene *locus* by alternative backsplicing events and/or alternative splicing within circRNAs containing multiple exons (Zhang et al., 2016). Due to the lack of 5'-cap and poly-A tail ends, circular transcripts are endowed with natural resistance to endonucleases. In comparison with their linear counterparts that have a half-life of 8-9 h in human cells (Garneau et al., 2007; Neff et al., 2012), circRNA´s half-life exceeds 24-48 h (Enuka et al., 2016).

As shown in **Figure 2**, spliceosomal backsplicing can be facilitated by two features of pre-mRNA, and a third recently demonstrated mechanism:

- An intron lariat generated by skipping alternative exons (**Figure 2B**). This mechanism implies that either splicing event may influence the other and that backsplicing is subjected to the same regulatory inputs as alternative splicing (Barrett et al., 2015; Kelly et al., 2015).
- Reverse complementary sequences (**Figure 2C**) in the flanking introns of the circularized exons (Ivanov et al., 2015; Kramer et al., 2015; Liang & Wilusz, 2014; Zhang et al., 2014).
- *Trans*-acting factors (**Figure 2D**). Muscleblind, Adar1, Quaking and the immune factors NF90 and NF110 enhance circRNA formation by bridging splice sites in close proximity (Ashwal-Fluss et al., 2014; Conn et al., 2015; Ivanov et al., 2015; Li et al., 2017).

In 2016, a study led by Li Yang and Ling-Ling Chen showed −using 4-thiouridine (4sU) tagging of nascent RNAs− that circRNA processing from pre-mRNA is extremely low efficient endogenously compared to canonical splicing and mostly occurs post-transcriptionally (Zhang et al., 2016). Besides, polyadenylation signal mutagenesis of circRNA-producing host genes can eliminate circRNA production (Liang & Wilusz, 2014). Furthermore, suppression of co-transcriptional 3'-

end processing results in enhanced circRNA levels due to increased read-through transcription past the poly-A signals by Pol II (Liang et al., 2017).

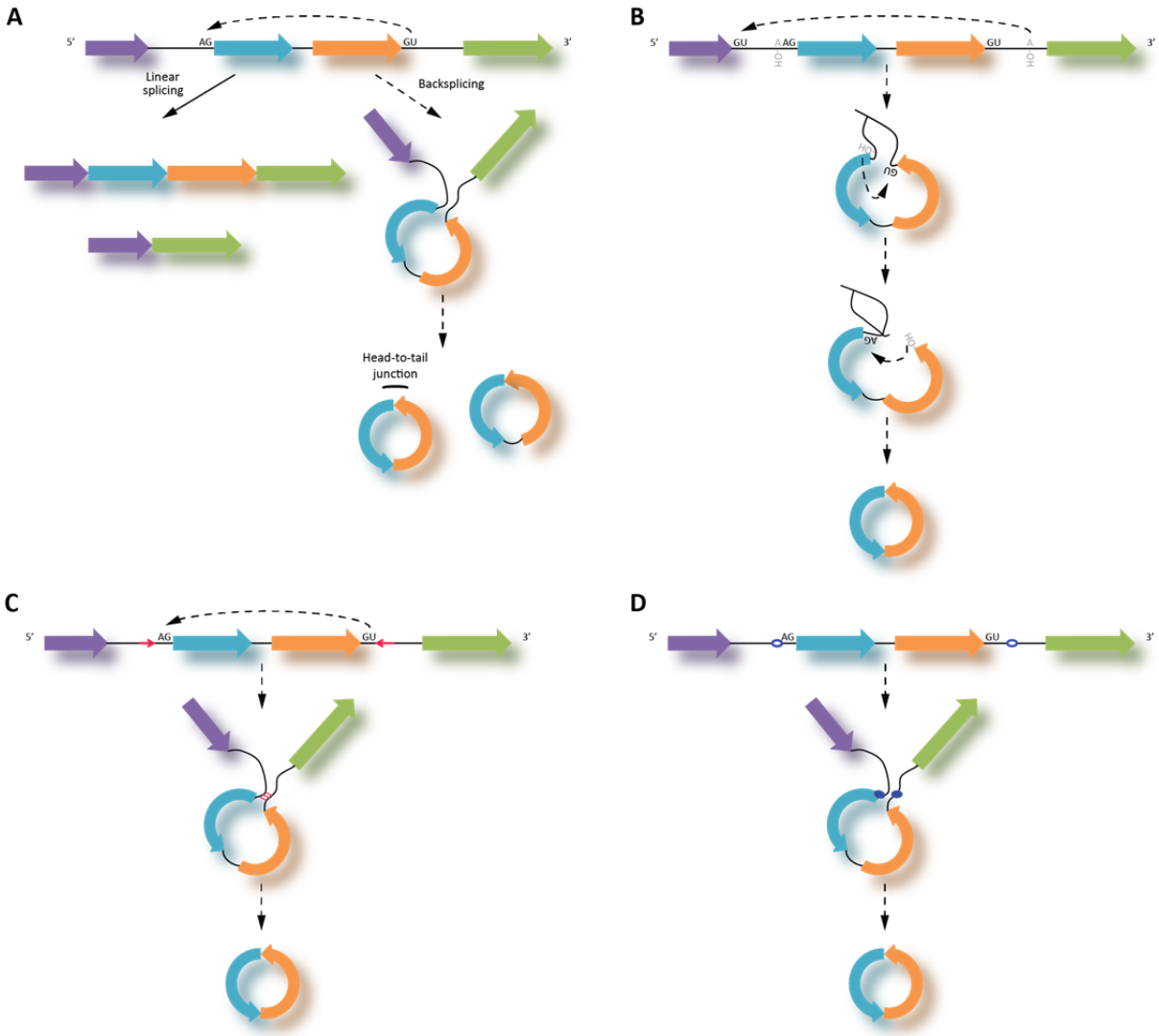

Figure 2. Mechanisms of circRNA biogenesis.
(A) The spliceosomal machinery catalyzes circularization through backsplicing. Differently from linear splicing, in a backsplicing event a downstream 5'-splice donor site is joined to an upstream 3'-splice acceptor site to produce a covalently closed circular molecule. **(B)** In the intron lariat model, circRNA formation starts with a linear splicing produced by skipping exons and then the intron lariat containing the skipped exons is further backspliced to produce a circular molecule. **(C)** Reverse complementary sequences (red) in the introns flanking circularized exons can promote circRNA biogenesis by forming RNA duplexes that bring the splicing sites nearby. **(D)** *Trans*-acting factors (blue) may also bind to introns flanking circularized exons, juxtaposing them and by that facilitating backsplicing.

On the other hand, a previous study found circRNAs to be bound to chromatin extracted from flies' heads, suggesting co-transcriptional generation, and that flies having a slow polymerase have lower levels of circRNAs (Ashwal-Fluss et al., 2014). In agreement with those results, in 2017 Wilusz's Lab showed that depleting core spliceosomal components increases global

circRNA levels, though the effect sizes vary depending on the factor depleted and the circRNA examined (Liang et al., 2017). To explain the different sensitivity of the splicing events upon spliceosome inhibition, they propose a model in which first exonic sequences are identified in the pre-mRNA (see **Figure 3**). Initially, the small nuclear ribonucleoproteins (snRNPs) U1 and U2 bind at opposing sites of each exon and form cross-exon interactions that are stabilized by additional factors, such as SR proteins. Under normal conditions, cross-exon interactions are converted into cross-intron interactions to generate a canonically spliced mRNA. When spliceosome components are limiting, cross-exon interactions are inefficiently converted into active cross-intron interactions, favoring circRNA yield. In this context, further stabilization of cross-exon interactions may be achieved by base pairing of complementary sequences in the flanking introns (Zhang et al., 2016).

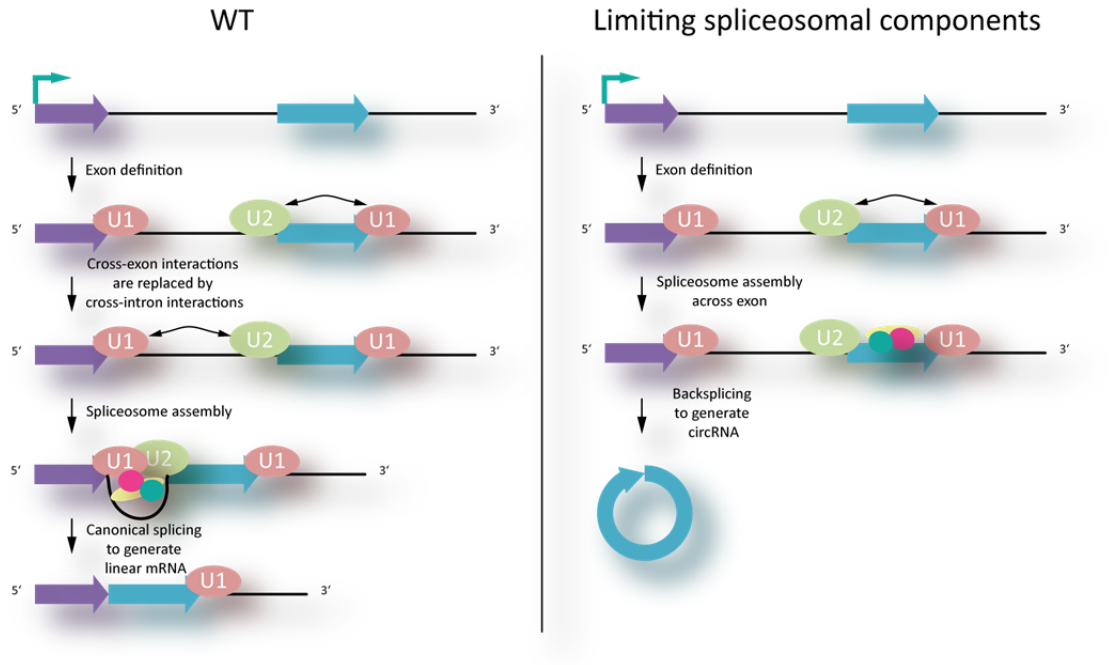

Figure 3. CircRNA levels increase when spliceosomal components are limiting.
During exon definition, splicing complexes form across exons; snRNP U1 binds the downstream 5'-splice site, snRNP U2 the upstream polypyrimidine tract and branch point sequence, while additional splicing factors stabilize the protein-protein interactions. In a wild-type (WT) context (left), these cross-exon interactions are then replaced by cross-intron interactions, enabling full assembly of the spliceosome and generation of mRNA. When spliceosomal components are limiting (right), the full spliceosome assembles across an exon, facilitating backsplicing and formation of circRNA. Adapted from Liang et al., 2017.

5.2.2 Detection challenges

The generalized prevalence of circular transcripts has long been underestimated due to several reasons. Unlike small RNAs, circRNAs do not segregate easily by size or electrophoretic motility from other RNA species. Second, the molecular technics generally used in RNA studies destroy circularity because they involve either sample amplification, molecule fragmentation, or both. Microarray, the most globally used technic for transcriptome analysis before the upcome of high-throughput sequencing, does not allow distinguishing between circular and linear transcripts of a host gene.

Furthermore, due to the lack of free ends circRNAs cannot be identified by RACE (rapid amplification of cDNA ends) or by poly-A enrichment previous to RNA sequencing (Jeck & Sharpless, 2014). Even nowadays the identification of circRNAs is not automatic but relies on bioinformatic post-processing of RNA-sequencing data that detects the characteristic head-to-tail junction by its non-collinearity with the genome (Memczak et al., 2013; Rybak-Wolf et al., 2015) (See **Figure 4**). Until a few years ago, this was a restriction set by most bioinformatic algorithms that resulted in circular molecules being filtered out from RNA-sequencing data.

The first systemic identifications of circRNAs were taken with skepticism by some researchers in the RNA field, arguing that these molecules could represent by-products of the spliceosomal machinery without any functional relevance (Guo et al., 2014). However, an increasing number of reports contradict this notion. To begin with, circRNAs are not only highly abundant, with around 15 % of the active genes in a cell producing circular transcripts (Barrett et al., 2015), but also in many cases their expression levels are weakly correlated with their linear counterparts, suggesting specific regulation (Jeck et al., 2013; Salzman et al., 2012). In addition, the majority of circRNAs are cytoplasmic, while most spliceosomal by-products accumulate at the site of transcription (Moore & Proudfoot, 2009). Furthermore, circRNAs are evolutionarily conserved at both, their sequence and level of expression, in particular in the brain (Rybak-Wolf et al., 2015).

Finally, different groups have recently shown functionality for some circRNAs both under physiological conditions and disease (Du et al., 2016; Hansen et al., 2013; Memczak et al., 2013; Zheng et al., 2016).

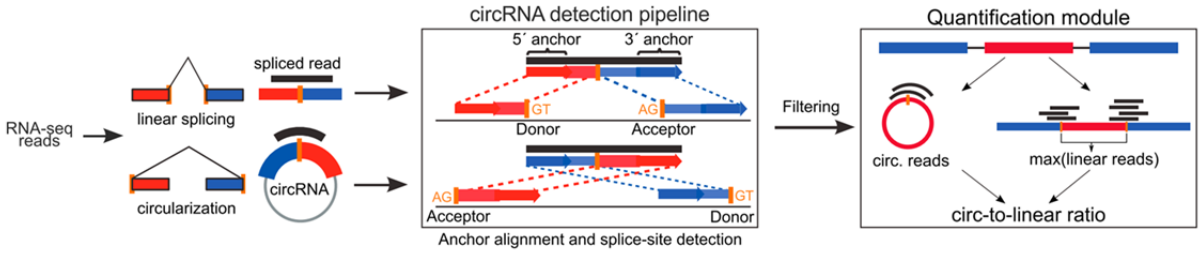

Figure 4. CircRNA detection and quantification module.
Junction-spanning reads are aligned to the genome; if the alignment is sequential it represents a linear transcript, while if the reads blast in reverse orientation to the genome it corresponds to circular transcripts (head-to-tail spliced reads). For quantitative analysis of circRNA, circ-to-linear ratio was calculated as head-to-tail spliced reads divided the maximum number of linear reads flanking the circularized exons. From Rybak-Wolf et al., 2015.

5.2.3 Potential and proven functions of circRNAs

Despite the large number of circRNAs identified in the past few years, the function of only a small fraction of them could be experimentally proven. CDR1as is the most highly expressed circRNA in mammals, particularly in the brain, and the best characterized one. Through its over 70 binding sites to miR-7, CDR1as acts as a miRNA sponge (Hansen et al., 2013; Memczak et al., 2013). Conditional knockdown of CDR1as reduces the expression of miR-7 targets, showing an effect in migration pattern in a cellular system. Exogenous expression in zebra fish brain, which does not express CDR1as, causes developmental anomalies (Memczak et al., 2013). In mice, constitutive knockout of *Cdr1 locus* shows dysfunction of excitatory synaptic transmission associated with neuropsychiatric disorders (Piwecka et al., 2017). Interestingly, *Cdr1* knockout mouse also shows an increased level of miR-7 targets, suggesting different regulatory mechanisms of miR-7 levels according to the scenario (Kleaveland et al., 2018; Piwecka, et al., 2017).

In addition to CDR1as, other circRNAs have been suggested to act as miRNA sponges. Mouse testis-specific circSRY contains 16 binding sites to miR-138 (Hansen et al., 2013). CircHIPK3 binds and inhibits miR-134, arresting human cellular growth (Zheng et al., 2016). Interestingly, circHIPK3 possesses 18 total binding sites for 9 different miRNAs, opening the possibility that under specific conditions inefficient miRNA-sponging circRNAs can become functional. CircBIRC6 regulates human pluripotency and differentiation by sequestering miR-34a and miR-145 (Yu et al., 2017). CircHIPK2 regulates astrocyte activation via the cooperation of autophagy and endoplasmic reticulum stress by sponging miR124-2HG (Huang et al., 2017). However, miRNA sponging is not a generalized function of circRNAs. Backspliced exons are not predominantly enriched in cross-linking datasets exploring AGO2-bound RNAs, neither are miRNA binding sites

in non-poly-A enriched RNA-sequencing libraries (Guo et al., 2014; Salzman et al., 2013; You et al., 2015).

Although the majority of circular molecules are located in the cytoplasm, those retaining intronic sequences −exon-intron circular RNAs (EIcircRNAs)− are restricted to the nucleus (Li et al., 2015). It has been shown that the knockdown of a couple of EIcircRNAs reduces the transcription of their host genes by affecting EIcircRNA-U1 snRNP-Pol II complex formation at their promoters (Li et al., 2015). EIcircPAIP2, for example, regulates the transcription level of its parental gene *PAIP2*, which is a translational inhibitor of memory-related genes through PABP (poly-A binding protein) (Khoutorsky et al., 2013; Li et al., 2015). Thus, EIcircPAIP2 may indirectly play a role in memory.

As described in **Section 5.2.1**, the biogenesis of circRNAs through a lariat precursor implies that they could function in the regulation of alternative splicing, determining with their generation the fate of the remaining pre-mRNA. As a matter of fact, different research groups have shown a correlation between exon skipping and occurrence of backsplicing events (Ashwal-Fluss et al., 2014; Barrett et al., 2015; Kelly et al., 2015). However, it remains largely unknown which factors influence on the balance between canonical linear splicing and backsplicing.

CircRNAs can also bind and form complexes with RBPs subsequently regulating the mode of action of associated proteins. Fly circMbl regulates alternative splicing of the host gene by binding to MBL splicing factor (Ashwal-Fluss et al., 2014). Highly expressed in mammalian heart circFOXO3 can promote cardiac senescence by interaction with the anti-senescent protein ID-1, the transcription factor E2F1 and the anti-stress proteins FAK and HIF1a (Du et al., 2017b; Du et al., 2016). CircANRIL modulates rRNA maturation by interacting with PES-1, an essential 60S-pre-ribosomal factor. Suppression of ribosome biogenesis in vascular smooth muscle cells and macrophages results in nucleolar stress and cell death, key cellular events in atherosclerosis (Holdt et al., 2016). Recently, a study has shown that circRNAs may also serve as a reservoir of the immune factors NF90/NF110, which in response to viral infection are released from circRNP complexes and exported to the cytoplasm (Li et al., 2017).

Furthermore, as the majority of circRNAs derive from coding sequences, several studies have explored whether they are translatable. Their lack of 5'-cap and poly-A tail ends suggests their translation should occur in a cap-independent manner. CircRNA-derived proteins have been expressed when adding IRES (internal ribosome entry sites) to constructs bearing circRNA sequences (Conn et al., 2015; Li et al., 2016; Wang & Wang, 2015), but studies investigating circRNA association with ribosomes reported that only a small proportion is associated with

polysomes, suggesting that being a template for translation of peptides is not a property shared by the majority of circular transcripts (Guo et al., 2014; Jeck et al., 2013; Yang et al., 2017). Nevertheless, three recent studies have shown the endogenous translation of circRNAs (Legnini et al., 2017; Pamudurti et al., 2017; Yang et al., 2017). For example, human circZNF609 plays a role in myoblast proliferation and is associated with heavy polysomes. Although its translation has been shown from engineered tagged vectors and the endogenous *locus*, circZNF609-derived protein contribution to the biological process is still unclear (Legnini et al., 2017). Another study showed by ribosome footprinting that a group of circRNAs expressed on fly heads is associated with translating ribosomes and that circMbl generates a protein (Pamudurti et al., 2017). Noteworthy, these two circRNAs contain IRES to allow the low initiation efficiency cap-independent translation, and share the start codons with their hosting mRNAs (Legnini et al., 2017; Pamudurti et al., 2017), suggesting that circRNA-derived polypeptides play similar roles or act as dominant negative competitors to their mRNA-encoded proteins. Recently, circRNA translation −from both a reporter and endogenous *loci*− was also shown to be driven by m6A modification (Yang et al., 2017).

Moreover, although not a demonstration of biological function but of utility, circRNAs' secretion in extracellular vesicles (Kim et al., 2017; Li et al., 2015) and their detection in body fluids, such as saliva (Bahn et al., 2015) and blood (Memczak et al., 2015), makes them suitable candidates as biomarkers of disease. A major advantage of using circRNAs as clinical biomarkers compared with traditional ones is that they may compensate for low organ specificity due to their tissue-specific expression.

Considering both, the vast sequence heterogeneity of circRNAs and available (although limited) experimental evidence, the prevailing view is that circular transcripts exert their function through diverse molecular mechanisms (see **Figure 5** for an overlook). For this reason, current experimental approaches to characterize the function of circRNAs are oriented to individual candidates.

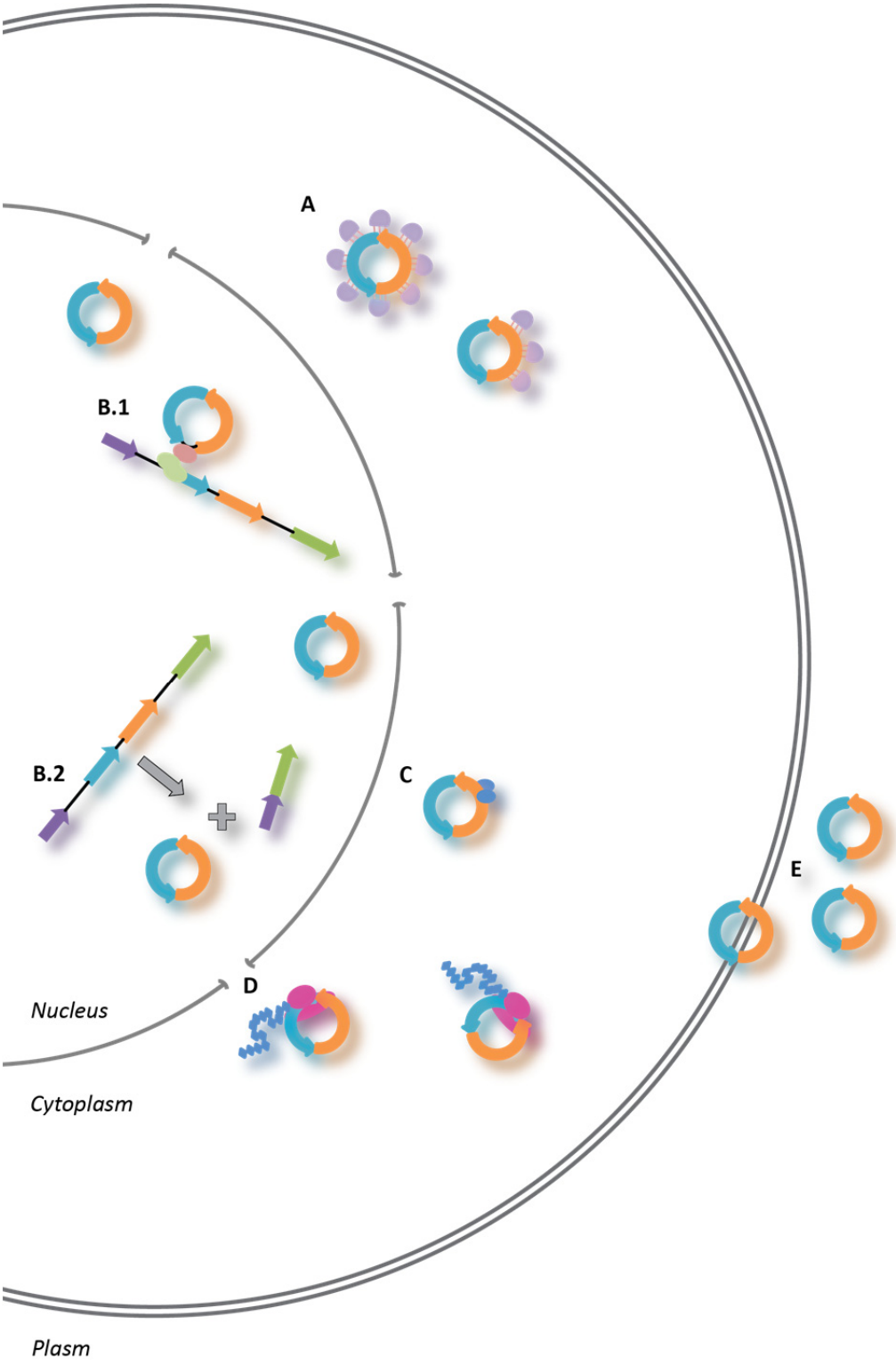

Figure 5. Mechanisms of circRNA functions.
(A) circRNAs can act binding and sequestering miRNAs (purple), protecting target mRNAs from degradation; **(B)** may regulate gene expression of its host gene by interacting with Pol II (subunits in green and pink) **(B.1)**, or by affecting the splicing of its linear counterpart **(B.2)**; **(C)** can serve as scaffolds for the assembly of protein complexes, regulating the mode of action of associated proteins (blue); **(D)** may serve as templates for translation under specific circumstances (ribosome in fuchsia, polypeptide in blue); **(E)** may be transported through exosomes, potentially serving as biomarkers.

5.2.3.1 Are circRNA functions related with that of their host genes?

Aside from EIcircRNAs and circMbl, the function of a circRNA does not necessarily need to be correlated with the function of its host gene. Examples are circRNAs known to act as miRNA sponges (Hansen et al., 2013; Huang et al., 2017; Kleaveland et al., 2018; Yu et al., 2017; Zheng et al., 2016); circRNAs that serve as platforms for the assembly of protein complexes (Du et al., 2017b; Du et al., 2016; Holdt et al., 2016; Li et al., 2016); and some circRNAs that serve as templates for translation (Yang et al., 2018; Zhang et al., 2018b).

As it will be described below, in the present work first 6 circRNA candidates were selected and their expression levels along neuronal development and in neuronal- compared with astrocytic-primary cultures were characterized, to end up focusing on the functional characterization of one of them, circTulp4 (see **Section 8.1.2**).

What is the function of the linear transcript of *Tulp4*? *Tulp4* codes for a protein belonging to the tubby-like proteins family (TULPs), which in vertebrates encompasses the founding member TUB and related TULPs 1 to 4 (Li et al., 2001; North et al., 1997). The tubby-like family is characterized by a conserved C-terminal 'tubby domain' consisting of a β barrel enclosing a central α helix that interacts with specific membrane phosphoinositides (PIPs) (Ikeda et al., 2002a; Santagata et al., 2001). TULP4 is the most distantly related TULP family member, sharing only a 40-48 % sequence identity with other tubby family proteins at the conserved tubby domain (Li et al., 2001). Studies on tissue distribution showed that they are all predominantly express in the nervous system (Ikeda et al., 2002b; Ikeda et al., 2001; Kleyn et al., 1996; Li et al., 2001; Nishina et al., 1998; North et al., 1997). In mouse, *Tulp4* mRNA localized in brain and testis, while in human the full-length transcript was detected in brain, skeletal muscle, kidney and placenta (Li et al., 2001). Fly homolog TUSP (tubby domain superfamily protein) is detected after embryonic stage 12 in bilateral groups of cells in the brain and in the antennal-maxillary sensory neurons (Ronshaugen et al., 2002).

Aside of binding to specific PIPs, which accounts for their reversible plasma membrane localization, the tubby domain has also been suggested to bind double-stranded DNA, an interaction depending in part on the positively charged surface of this domain (Boggon et al., 1999; Hu et al., 2009). Although the amino-termini of these proteins are diverse, they share several characteristics with the acid-globule activation domains of some transcription factors. Of note, all TULP family members have nuclear localization signals (NLS), but only the Tub NLS has been mapped experimentally (Santagata et al., 2001). Transcription activation capacity was shown for Tub using one-hybrid assays (Boggon et al., 1999). However, the role of these proteins

as transcriptional regulators remains unclear, downstream TULPs-regulated genes have not been identified, and acidic-domain-GAL4 fusions (used in the one-hybrid assays) can non-specifically activate transcription (Sadowski et al., 1988).

TULP4 amino-terminus is large and contains WD40 repeats and a suppressor of cytokine signaling (SOCS) domain. WD40 repeats are 40 amino acids motifs enriched in tryptophan and aspartic acid residues which have been reported in diverse eukaryotic proteins displaying various functions, including pre-mRNA processing, signal transduction, cytoskeleton assembly, and cell cycle control (Smith et al., 1999). The SOCS domain interacts with generic components of the E3 ubiquitin ligase complexes facilitating ubiquitination (Kile et al., 2002; Li et al., 2001). So far, the specific substrates for these E3 ubiquitin ligases are unknown.

5.2.4 CircRNAs and human disease

In agreement with their role in gene regulation, increasing evidence associates circRNAs with human disease.

Since miRNAs are major players in the pathogenesis of human cancers (Kohlhapp et al., 2015; Rupaimoole et al., 2016), circRNAs acting as miRNA sponges are likely to be involved in cancer. CircITCH is significantly downregulated in different cancer types, such as esophageal squamous cell carcinoma, lung cancer, colorectal cancer and hepatocellular carcinoma (Guo et al., 2017; Huang et al., 2015; Li et al., 2015; Wan et al., 2016). CircITCH contains several miRNA binding sites including seed matches to oncogenic miR-7 and miR-214, suggesting it may regulate their activity inhibiting cancer progression, a mechanism that would also involve ITCH overexpression and suppression of Wnt/β-catenin signaling pathway (Li et al., 2015; Wan et al., 2016). Another example is circPVT1, which is upregulated in gastric cancer patients and acts promoting cell proliferation through sequestering members of the miR-125 family (Chen et al., 2017).

circFoxo3, derived from the tumor-suppressor gene *Foxo3*, is involved in cancer development through protein-scaffolding mechanisms. Through the interaction with p53 and MDM2 it may indirectly upregulate the expression of its host gene (Du et al., 2017a); and by forming a circFoxo3–p21–CDK2 ternary complex it prevents CDK2 from promoting cell cycle progression (Du et al., 2016).

Furthermore, well-established cancer-associated chromosomal translocations and genomic DNA amplifications may also promote cancer development through circRNA biogenesis. PML/RARα, the most recurrent translocation in promyelocytic leukemia, originates fusion-circRNAs, derived from the rearranged genome, that contribute to transformation and promote cell survival

(Guarnerio et al., 2016). CircPRKCI, which derives from the gene *protein kinase C iota*, is frequently amplified in lung cancer. *In vitro* experiments downregulating circPRKCI impair cellular proliferation and migration (Qiu et al., 2018).

The high stability of circRNAs and accumulation during aging (Gruner et al., 2016; Westholm et al., 2014) could link them with neurodegenerative diseases. For example, CA1 hippocampal samples from sporadic Alzheimer´s disease (AD) patients have decreased CDR1as expression compared to age-match controls (Lukiw, 2013). A recent study has shown *in vitro* that CDR1as decrease is accompanied by an increase on miR-7 levels and concomitant decrease on miR-7 targets, among them UBE2A (ubiquitin protein ligase A) which is responsible for the clearance of amyloid peptides in AD and other degenerative disorders (Zhao et al., 2016). Additionally, FUS (fused in sarcoma) was recently found to regulate a group of circRNAs in motor neurons derived from murine embryonic stem cells (Errichelli et al., 2017).

CircRNAs are emerging as important regulators of cellular physiology and as potential biomarkers of disease diagnostic and prognostic (see **Section 5.2.3**). Although a detailed description of the mechanism of action (or even the biological relevance) of many disease-regulated circRNAs is still at early developmental stages, it seems possible that in the near future they could be used as therapeutic targets. For example, overexpression of specific circRNAs sponging oncogenic miRNAs or of circANRIL, that confers atheroprotection (Holdt et al., 2016), could modulate cancer and atherosclerosis progression, respectively. Alternatively, it may be possible to interfere with circRNA biogenesis by introducing antisense oligonucleotides complementary to the head-to-tail junction, backsplice signals, inverted repeat sequences in the pre-mRNA, and binding sites for *trans*-acting factors involved in backsplicing. Antisense approaches aiming to influence splicing patterns in pathological conditions are already in development (Lee et al., 2017).

5.3 GENERAL PRINCIPLES OF NEURONAL DEVELOPMENT AND FUNCTION IN THE MAMMALIAN CNS

The central goal of modern neuroscience is to decipher the cellular and molecular events that ultimately explain perception, action, learning and memory. Expressed in other words, how the activity of defined neural circuitries relates to complex mental processes.

To appreciate how a precise function is carried out by a neural circuitry, first, the structural components and mechanisms of signalization between individual neurons −the basic units of the brain− must be examined. The most distinctive feature of neurons is their polarized morphology. Early in development, the cell undergoes a multipolar phase in which apparently identical short neurites extend and retract until one undergoes a prolonged period of growth becoming the definitive axon (Dotti et al., 1988). Polarization underlies the ability of neurons to integrate and propagate information within the brain and throughout the body.

Neurons communicate among each other via synapses, the majority of which are established, in the mammalian forebrain, between pre-synaptic axon terminals and post-synaptic dendritic sites (or dendritic protrusions, called spines). For reference, the human brain contains an estimated amount of 100 billion neurons (10^{11}), supported by an equal number of glial cells, and interconnected through a 1.000 to 10.000 fold higher number of synapses (10^{14}-10^{15}) (Azevedo et al., 2009; Kandel et al., 2000).

The formation, maintenance and elimination of proper connections in the brain are essential to all complex mental processes and because of that, they are subjected to tight regulation. Disruption of any of the progressive events that assemble neural circuitries, including neuronal migration, axon and dendrite development, synaptogenesis and synapse function leads to severe neurodevelopmental, neuropsychiatric and neurodegenerative diseases (Herms & Dorostkar, 2016; Liu, 2011; Riccomagno & Kolodkin, 2015; Ting et al., 2012).

The development and functions of neurons can be studied using different experimental systems, which will be described in the following sections.

5.3.1 Modeling neuronal development in culture: dissociated primary neurons

Over a century ago, Ross Harrison published findings on the developing neuron after cultivating for the first time living tissues of vertebrates outside their bodies (Harrison, 1910). Since then, techniques for culturing neurons *in vitro* have evolved to answer aspects of neuronal development, function, interconnectivity, as well as bases and mechanisms of neuronal disease. Much of the progress done in neuronal culture until today involves dissociated embryonic or neonatal neuronal tissue (Banker & Cowan, 1977).

Although it is possible to culture neurons virtually from every region of the vertebrate nervous system, hippocampal and cortical cultures have proven to be the most popular due to the cell-type composition and accessibility. The hippocampus has a relatively homogeneous nerve cell population composed of around 90 % excitatory glutamatergic pyramidal cells and a remaining 10 % of GABA-ergic interneurons (Benson et al., 1994; Soriano et al., 1994). The cerebral (neo-) cortex has two morphologically distinguishable principal neuronal cell types, excitatory glutamatergic pyramidal cells and stellate (granule) cells, representing the GABA-ergic interneurons (Bayer et al., 1991; Marín-Padilla, 1992; McConnell, 1995; Supèr & Uylings, 2001). Isolation of hippocampal and cortical neurons from late-stage rodent embryos −mouse embryonic day (E) 17.5-18.5− contains relatively few glial cells and decreases shearing damage to axons and dendrites due to fewer adhesion contacts (Brewer, 1997).

Although confined to a two-dimensional organization, neurons in culture resemble their *in vivo* counterparts in their time course of development as well as in morphological and functional properties (Barnes & Polleux, 2009). Five characteristic developmental stages can be distinguished in dissociated hippocampal and cortical neurons growing under controlled growth conditions (Barnes & Polleux, 2009; Dotti et al., 1988) (**Figure 6**). At stage 1 (days *in vitro* (DIV) 0), freshly attached, immature post-mitotic neurons display lamellipodia surrounding most of the circumference of the cell. The appearance of discrete motile patches at intervals results in the emergence of stage 2 (DIV 1-2) neurons bearing multiple immature neurites. At stage 3 (DIV 2-4), one of the neurites begins to grow at a much faster rate becoming many times longer than the rest of neurites, and acquiring axonal identity. This selective elongation is the hallmark of neural polarization (Craig & Banker, 1994; Dotti et al., 1988), the initial break in symmetry during neuronal development. Stage 4 (DIV 4-15) is characterized by rapid axon growth, and extensive dendritic outgrowth and branching. Finally, by stage 5 (> DIV 15) neurons are terminally differentiated and reach functional polarization. Mature neurons form functional synaptic

contacts among each other and generate electric currents (Akemann et al., 2010; Bartlett & Banker, 1984; Fletcher et al., 1994; Segal, 1983).

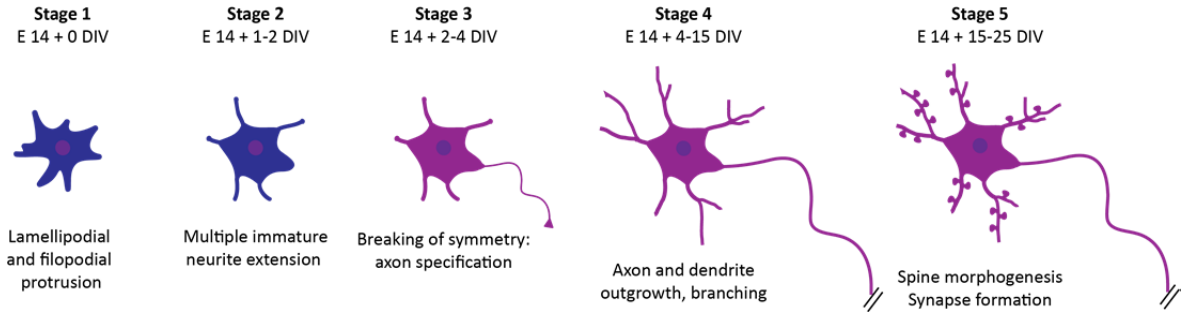

Figure 6. Development and polarization of primary neurons in culture.
In dissociated cultures, post-mitotic neurons isolated from embryonic mouse hippocampus and cortex travel through a sequence of well-defined stages. Stage 1 (DIV 0): unpolarized, freshly plated neurons are surrounded by lamellipodia and filopodia that display high protrusive dynamics. Stage 2 (DIV 1-2): neurons develop several minor immature neurites. Stage 3 (DIV 2-4): neuronal symmetry breaks, the axon (purple) is specified by its faster growth in comparison with the remaining neurites, which will adopt dendritic identity. Stage 4 (DIV 4-15): rapid and extensive axon and dendrite outgrowth. Stage 5 (> DIV 15): neurons are terminally differentiated into mature pyramidal neurons carrying functional synapses formed between dendritic spines and axonal boutons (purple spots on dendrites). Adapted from Barnes & Polleux, 2009; Dotti et al., 1988.

Forty years after the first description of primary neuronal cell cultures by Banker and Cowan (Banker & Cowan, 1977), the methods for culturing primary neurons have changed only minimally (Kaech & Banker, 2006), but considerable progress has been made in the technologies available for its study.

Gene expression can be altered in individual neurons at different developmental stages using calcium-, lipid- or electroporation-based transfection methods, as well as viral-mediated gene transfer (Janas et al., 2006; Jiang & Chen, 2006; Kaech & Banker, 2006; Zeitelhofer et al., 2007). By these means, it is possible to study the effects of downregulating or overexpressing specific genes in the context of neuronal development (Lewis et al., 2013; Siddiqui & Craig, 2011; Zeringue & Constantine-Paton, 2004). For addressing questions related to the early stages of neuronal maturation, such as neurite outgrowth, electroporation of embryonic heads (*ex vivo* electroporation) combined with primary neuronal culture provides a low cost and rapid approximation to the *in vivo* environment (Lizarraga et al., 2012). In addition, with the advent of genome engineering technology for the generation of *in vivo* models, neuronal cultures offered a valuable way to analyze the effect of the mutated gene. In particular, post-natal aspects of neural development in engineered animals that carry a late embryonic or post-natal lethal gene mutation.

Fluorescently tagged proteins are commonly employed to study subcellular localization and cellular trafficking of proteins as well as for live-cell imaging studies to analyze dynamic processes in living neurons or as reporters for intracellular processes (Feng & Arnold, 2016; Kaech et al., 2012).

Furthermore, as neurons establish functional connections in culture, it is possible to record electrophysiological parameters in cells subjected to gene manipulation, pharmacological treatment or derived from genetically modified animals (Bolton et al., 2000; Copi et al., 2005; Song et al., 2002; Yang et al., 1993).

Although primary neuronal cultures have successfully addressed cellular and molecular mechanisms underlying complex processes building up the mammalian nervous system, they cannot recapitulate the intricate interplay that different brain regions have *in vivo*. Many neurodevelopmental processes like neuronal migration, cellular differentiation into neuronal and glial lineages, even neurite outgrowth are controlled by external cues from the brain's microenvironment. Moreover, higher brain functions, such as learning and memory, emotional and motor behavior, as well as the underlying synaptic circuits can only be analyzed in living organisms.

The following section describes techniques used in this project with the aim of studying circRNAs relevance in a physiological context.

5.3.2 Approaches to study neuronal development and function under physiological conditions

5.3.2.1 *In utero* electroporation technique

Electroporation combined with surgery is a quick and highly efficient method to address gene expression regulation in a spatio-temporally restricted manner. Compared with the generation of transgenic and gene knockin mice and the construction of recombinant viruses, *in utero* electroporation is quickly performed with relatively simple equipment. Furthermore, several different nucleic acids can be simultaneously transfected into the same cells by electroporation (Mikuni et al., 2016; Saito, 2006; Saito & Nakatsuji, 2001).

The developing CNS is particularly targetable by electroporation due to the number of dividing neuronal progenitors adjacent to the ventricles (Goldstein et al., 1989). Neurons derived from electroporated progenitors express the transfected nucleic acid for a long time, probably due to the lack of neuronal cell division. The persistent gene expression in neurons implicates that this method can be used to analyze gene expression regulation not only in the embryo but also in the adult.

Because many different types of neurons are generated at a specific embryonic stage, the expression of transfected nucleic acids can be restricted to some types of neurons by choosing the stage at which *in vivo* electroporation is performed (Kawauchi & Saito, 2008; Mizutani, 2005; Saito & Nakatsuji, 2001).

During *in utero* electroporation, nucleic acids are microinjected into the brain ventricle of E 12.5-15.5 mouse embryos *in utero* and square-wave electric pulses are delivered with forceps-type electrodes (Saito, 2006) (**Figure 7**).

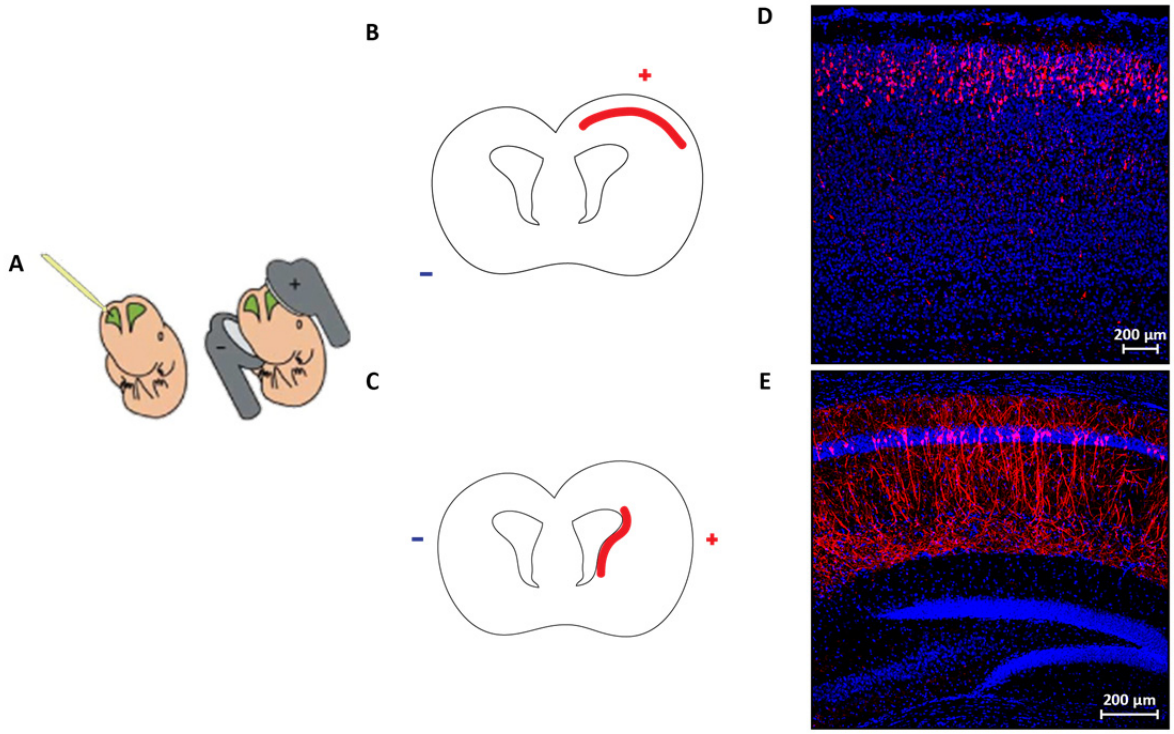

Figure 7. Transfection of embryonic mouse CNS cells by *in utero* electroporation.
(A) DNA is microinjected into the lateral ventricles of E 14.5-15.5 mouse embryos using glass capillaries. The embryo is gently held with forceps-type electrodes and electric pulses are delivered. **(B-C)** Schematic overview showing electrodes position in relation to the targeted brain region. Electric current is delivered towards the cathode. **(D-E)** Mouse coronal brain sections showing that red fluorescent protein (RFP), used as transfection control, is expressed after electroporation. DAPI staining (blue) was performed to visualize cell nuclei. Scale bars represent 200 µm. **(D)** E 14.5 mouse embryos were *in utero* electroporated targeting the neocortex and brains were analyzed at P 60. RFP-expressing pyramidal neurons are found in the cortical plate, below the marginal zone. **(E)** E 15.5 mouse embryos were transfected targeting the hippocampus and brains were analyzed at P 60. RFP-expressing pyramidal neurons are found in the CA1 layer of the hippocampus.

5.3.2.2 Generation of genetically modified mice

The development of recombinant DNA technology during the 1970s represented for molecular biologists not only the possibility to study gene´s structure and function but also to harness them for the advance of medicine and biotechnology. Together with DNA double-stranded breaks (DSBs), homologous recombination (HR)-mediated targeting was one of the breakthroughs in genome manipulation. Allowing the precise integration of exogenous DNA through repair templates that contain sequence homology to the donor site, HR facilitated the generation of knockin and knockout animal models via manipulation of germline-competent stem cells (Capecchi, 1989, 2005). The difficulty to generate DSBs at a specified *locus* and the time and costs involved in generating mice through conventional gene-targeting methods paved the way for the development of a series of programmable nuclease-based genome editing technologies

during recent years. Meganucleases, zinc-finger nucleases (ZFNs), and transcription activator-like effector nucleases (TALENs) all recognize specific DNA sequences through protein-DNA interactions (Bogdanove & Voytas, 2011; Ménoret et al., 2013; Urnov et al., 2010; Wefers et al., 2013; Wefers et al., 2014). Meganucleases were not widely adopted due to a lack of clear correspondence between the protein residues and their target DNA sequence specificity. ZFNs and TALENs exhibit context-dependent specificity and the construction of arrays with the desired DNA binding specificity is labor intensive. Most recently, a fourth type of nuclease-based genome editing technology was introduced. CRISPR (clustered regularly interspaced short palindromic repeats) Cas9 (CRISPR-associated) toolbox allows for genetic manipulation on the basis of simpler RNA-guided DNA recognition. The class 2 type II DNA-targeting endonuclease from *Streptococcus pyogenes* Cas9 was the first Cas effector to be harnessed for genome engineering. (For a review of CRISPR systems and applications see Hsu et al., 2014; Knott & Doudna, 2018).

Regardless of the endonuclease of choice, DNA DSBs generated at a specific genomic *locus* are repaired by error-prone non-homologous end joining (NHEJ), resulting in mutant alleles (Carbery et al., 2010; Geurts et al., 2009; Sung et al., 2013; Tesson et al., 2011; Wang et al., 2013; Wefers et al., 2013). Alternatively, if a single-stranded DNA (ssDNA) or a donor plasmid with homology arms flanking the DSB is provided, a defined modification can be inserted into the genome by high-fidelity HR (Brown et al., 2013; Cui et al., 2011; Meyer et al., 2010; Yang et al., 2013).

CRISPR/Cas systems evolved as an adaptive immunity mechanism of microbes against viral infections. Microbes capture snippets of foreign genetic elements and incorporate them into their genomic CRISPR array. Posterior transcription of CRISPR arrays originates CRISPR RNAs (crRNAs) that bind to and direct Cas nucleases to specifically degrade target nucleic acids (Barrangou et al., 2007; Marraffini & Sontheimer, 2008; Brouns et al., 2008). A third component is necessary in the biogenesis and processing of crRNA in type II CRISPR systems, a non-coding transactivating crRNA (tracrRNA) (Deltcheva et al., 2011). The dual crRNA-tracrRNA can be fused into a chimeric single-guide RNA (sgRNA) (Jinek et al., 2012). Finally, a protospacer adjacent motif (PAM) flanking the 3´-end of the DNA target site dictates the DNA target search mechanism of Cas9 (Marraffini & Sontheimer, 2010; Mojica et al., 2009) (**Figure 8**).

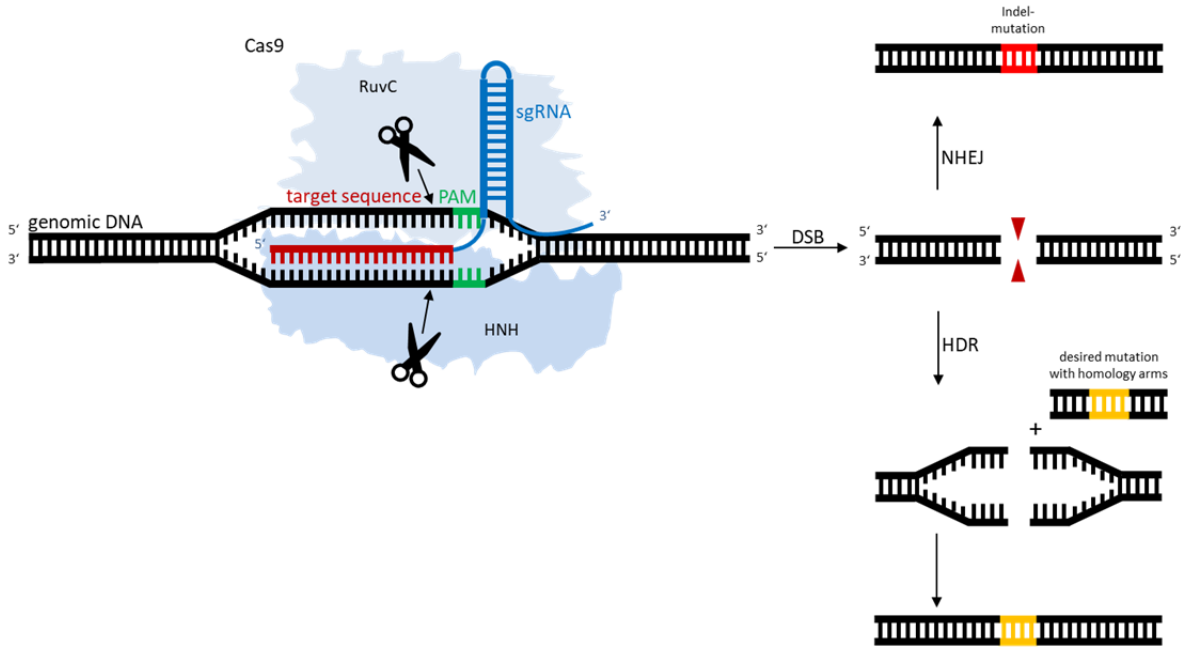

Figure 8. Class 2 type II CRISPR/Cas system and usage in genome editing.
Scheme showing Cas9 enzyme directed by a sgRNA (blue) encoding a 20 nt spacer (red) to a complementary target dsDNA (black) proximal to a PAM (green). Upon correct base-pairing, HNH and RuvC nuclease domains activate (scissors) cleaving both strands of the target gene. The double-strand break can be repaired either by NHEJ (upper right corner) leading to small indels that generally introduce a premature STOP codon or by HDR (lower right corner) where precise modifications are introduced by the usage of repair templates carrying homology arms to the target gene.

Genetically modified mice are extensively used in research for understanding conserved mammalian gene function in a physiological context, and for modeling human disease. The conventional generation of mutant mice by HR in embryonic stem (ES) cells is laborious and costly. Gene-targeted ES cell clones need to be selected and injected into WT mouse blastocysts to generate chimeric mice, which then have to be bred to generate single-gene mutant offspring, a procedure that usually takes 9-12 months (Capecchi, 2005; Friedel et al., 2007). Direct co-injection of Cas9 and *locus*-specific sgRNAs into WT zygotes circumvents time disadvantages associated with ES cells working, thus allowing for the efficient generation of mice carrying mutations in single and multiple genes, as well as of mice carrying endogenous reporters and conditional alleles (Brandl et al., 2015; Yang et al., 2013). **Figure 9** shows schematically the procedure for the generation of gene-modified mice by CRISPR/Cas.

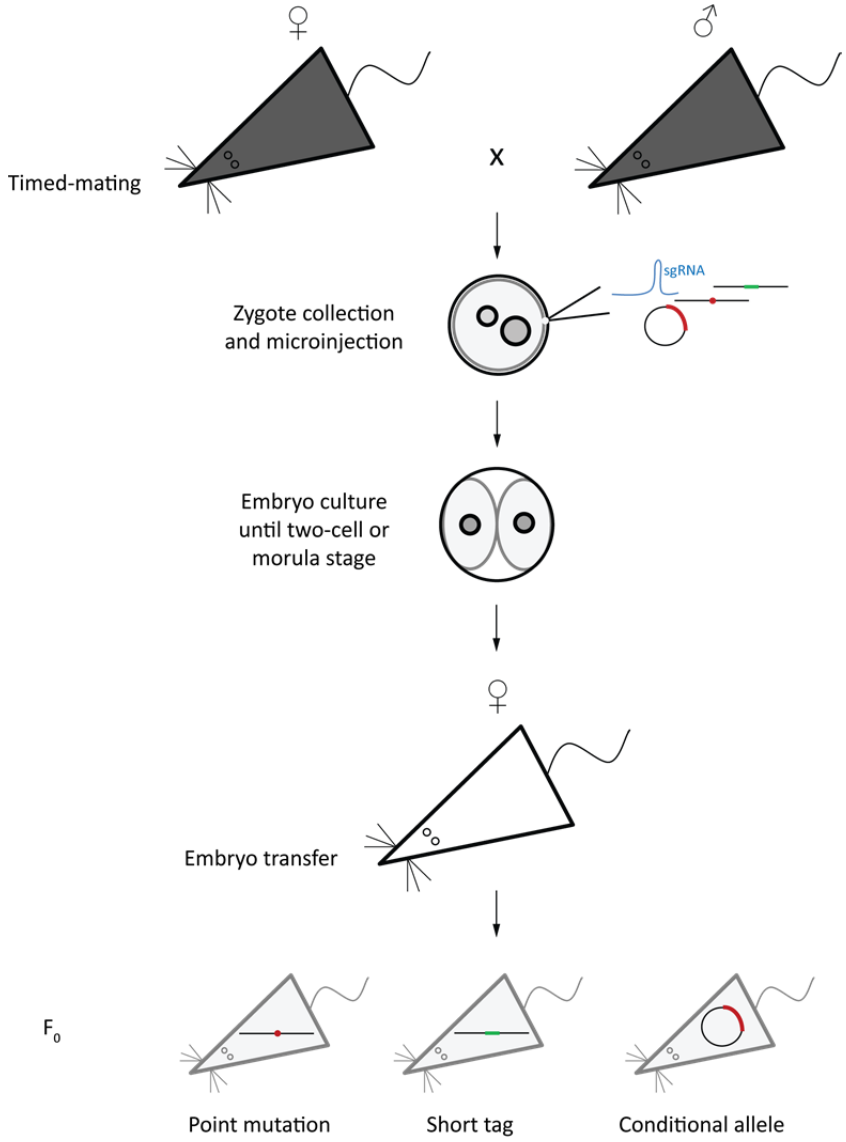

Figure 9. Procedure for the generation of genetically modified mice by CRISPR/Cas.
C57Bl6/N donor females are treated with hormones three days before microinjection and mated on day 0. Zygotes are collected at day 1, microinjected with CRISPR/Cas9 reagents, and transferred to pseudopregnant CD1 foster mothers (mated to vasectomized males) either at two-cell or morula stage. Three weeks after birth, F_0 pups derived from the microinjected zygotes can be evaluated by genotyping. For this project, mouse zygotes were microinjected with Cas9 protein plus mRNA, sgRNA and a repair template ssDNA or donor plasmid to generate point mutations, tag insertion or a conditional knockin mouse, respectively.

Compared with ZFNs and TALENs, the main advantages of CRISPR/Cas-mediated genome engineering are the efficiency of targeting genomic *loci* and the ease of designing, constructing and delivering multiple sgRNAs. As with other techniques, there are also limitations: i) Off-target mutation rate appears to be a problem when working with cell lines, but rare in targeted mice derived from CRISPR/Cas zygote injection (Li et al., 2013; Wang et al., 2013; Yang et al., 2013). ii) Mice generated by CRISPR/Cas injection into the zygote are frequently mosaics and might require breeding and genetic transmission for the production of mutant mice.

5.3.3 Synaptogenesis and spinogenesis in the mammalian CNS: basis of excitatory neurotransmission

Neuronal circuits are assembled during development by the formation of synaptic contacts. The majority of excitatory synaptic contacts in the mammalian CNS are composed of a pre-synaptic axon terminal containing synaptic vesicles (SVs) and a protein-rich post-synaptic density (PSD) (Harris, 1999; Hering & Sheng, 2001; Sheng & Hoogenraad, 2007). The formation of dendritic spines coincides with the main period of synaptogenesis during the first few weeks after birth in many regions of the developing rodent brain. During the first stages of synaptogenesis, the majority of synapses on pyramidal neurons are located on the dendritic shafts; however, as spines begin to form, excitatory synapses on spines gradually replace the dendritic shaft population (Yuste & Bonhoeffer, 2004). In the adult, very few excitatory synapses onto excitatory neurons are located on the dendritic shaft, and the vast majority of spines contain a single excitatory synapse (Harris et al., 1992; LeVay, 1973).

In excitatory neurons −such as the hippocampal and cortical pyramidal neurons− the incoming action potentials moving along the axon cause the fusion of docked SVs filled with the neurotransmitter glutamate (Burns & Augustine, 1995; Phillips et al., 2001). Once released, glutamate diffuses across the synaptic cleft and binds to the two major classes of ionotropic glutamate receptors enriched in the PSD, the N-methyl-D-aspartic acid receptor (NMDAR) and the α-amino-3-hydroxy-5-methyl-4-isoxazolepropionic acid receptor (AMPAR) (Hollmann, 1994). Opening of the NMDARs and AMPARs then leads to an influx of ions, local depolarization, and activation of voltage-gated ion channels as well as a number of signaling cascades. Multiple depolarization events sum up and propagate to the cell body where, if an electrical threshold is reached, a new action potential is generated in proximity to the cell body at the axon hillock (**Figure 10A**).

The properties of synaptic transmission can be assessed electrophysiologically by measuring the electrical effects of released neurotransmitter on the post-synaptic membrane. The whole-cell configuration of the patch-clamp technique (see **Section 7.9**) allows low noise, high sensitive electrical currents measurements across the plasma membrane. When reading miniature responses (total blockade of action potentials formation and propagation), one can distinguish pre- from post-synaptic events, as these responses are the result of spontaneous transmitter release from a single SV. The frequency of miniature excitatory/inhibitory post-synaptic currents (m(E/I)PSCs) is dependent upon vesicular release, while the amplitude reflects the activation of the post-synaptic receptors. Furthermore, holding the potential of the recording micropipette at

specific voltages allows to record specific receptor-mediated synaptic currents. In addition, measuring the relative contributions of excitatory and inhibitory synaptic inputs in a defined neural microcircuit, so-called E/I ratio, allows the assessment of the status of the brain microcircuit. An E/I ratio is balanced if across a range of conditions it remains constant. Misbalances in the E/I ratio are associated with human neurodevelopmental pathologies, such as schizophrenia, autism spectrum disorders, Down syndrome, Rett syndrome and Fragile X syndrome, among others.

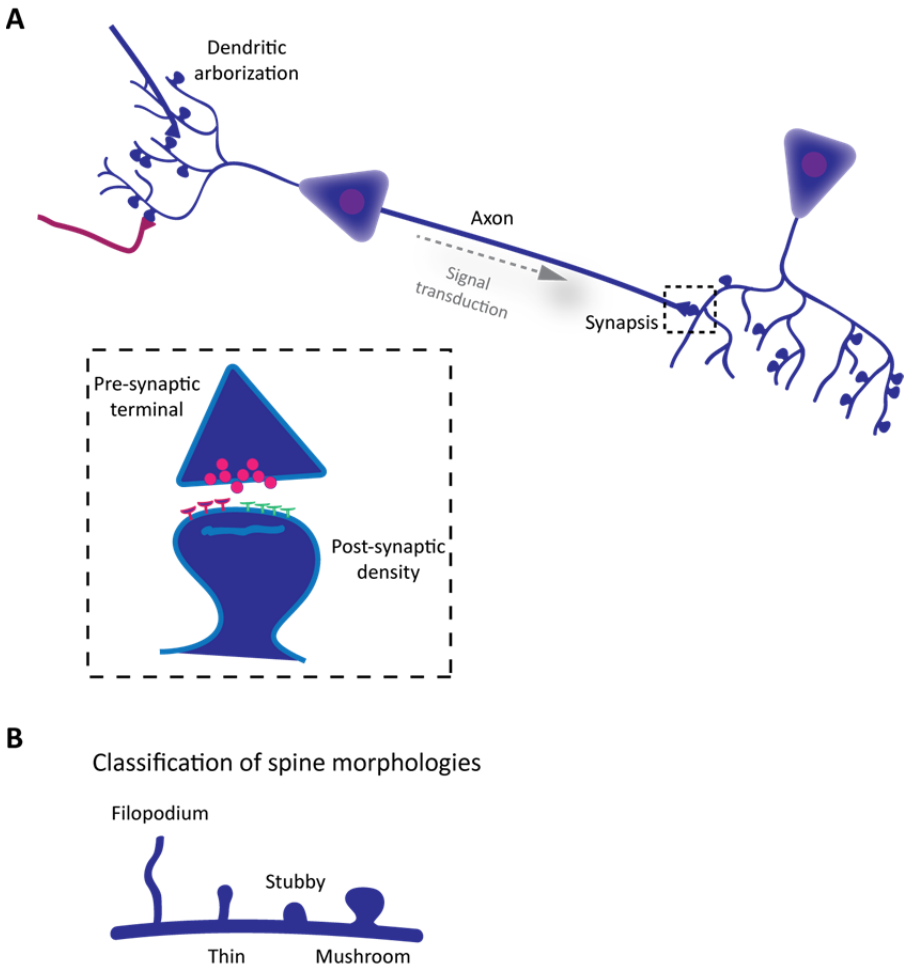

Figure 10. Excitatory synapses in the mammalian CNS.
(A) During early post-natal mammalian brain development, spine formation coincides with synaptogenesis. Excitatory synapses are formed between pre-synaptic axon terminals of one neuron and post-synaptic dendritic protrusions, called spines, on the following neuron. Lower panel (dashed-line square inset) shows in higher magnification a diagram of a synapse; the pre-synaptic terminal contains synaptic vesicles full with the neurotransmitter glutamate and scaffolding proteins, the post-synaptic density contains glutamate-receptors and a large number of scaffolding and signaling proteins. **(B)** Dendritic protrusions are traditionally classified according to their morphology as filopodia (hair-like structure), thin, stubby (lacking head and neck configuration), and mushroom-like spines according to Peters and Kaiserman-Abramof's classification of 1970.

5.3.3.1 Spine stabilization and synaptic plasticity

The introduction of two-photon microscopy combined with the development of methods to label single cells with genetically encoded fluorescent proteins has allowed for the *in vivo* visualization of dendritic structure within intact brain circuits. Similar to the morphological progression observed during development (see **Figure 10B**), there is considerable capacity for spine sculpting, even across the stable excitatory dendritic scaffold of adult neurons *in vivo* (Lee et al., 2006; Mizrahi & Katz, 2003; Trachtenberg et al., 2002). The presence and strength of excitatory synapses is closely related with spine morphology (Asrican et al., 2007; Beique et al., 2006; Harris et al., 1992; Matsuzaki et al., 2001; Noguchi et al., 2005; Zito et al., 2009). In the adult cortex and hippocampus, ~ 25 % of spines are mushroom-shaped while > 65 % are thin shaped (Harris et al., 1992; Peters & Kaiserman-Abramof, 1970).

Spine formation and stabilization are processes regulated by neuronal activity; stimuli that in culture affect synaptic strength also influence spine volume and stabilization. For this reason, methods that allow for the visualization of spine density and size have been used to infer the locations of excitatory synapses in cultures, slices and *in vivo*, and as metrics to assess normal excitatory circuit health and development (reviewed in Rochefort & Konnerth, 2012).

A variety of stimuli influence neuronal circuitry sculpting and rewiring, including certain patterns of synaptic activity (Engert & Bonhoeffer, 1999; Hosokawa et al., 1995; Kirov & Harris, 1999; Maletic-Savatic et al., 1999; Nägerl et al., 2004; Yuste & Bonhoeffer, 2001), learning and memory formation (Bourne & Harris, 2007; Gruart et al., 2006; Neves et al., 2008; Whitlock et al., 2006), stress (Fuchs et al., 2006; Goldwater et al., 2009; Radley et al., 2008), hormones (McEwen et al., 1991), changes in temperature (Roelandse & Matus, 2004), normal aging (Dumitriu et al., 2010; Woolley et al., 1990) as well as chronic substance abuse (Kauer, 2004). The process of experience-dependent changes in synaptic connectivity is called synaptic plasticity. Underlying dendritic spine remodeling, as well as changes in strength and function of synaptic connectivity, are dynamic rearrangements on the spine actin cytoskeleton (Hotulainen & Hoogenraad, 2010).

Two different mechanisms operate within different ranges of neuronal activity to homeostatically regulate synaptic strength without compromising information stored as distributed synaptic weights (Bridi et al., 2018). Synaptic scaling of excitatory synapses has been demonstrated both *in vitro* and *in vivo*, and in spinal neurons and cortical and hippocampal pyramidal neurons (Lissin et al., 1998; O'Brien et al., 1998; Thiagarajan et al., 2005; Turrigiano et al., 1998). This mechanism strengthens up or down a population of synapses over a time scale of several hours by increasing or decreasing the accumulation of glutamate receptors in the post-

synaptic membrane, and/or by modulating the number of pre-synaptic glutamate release sites or the release probability. Compensatory changes in the unit strength of excitatory synapses can be measured by mEPSCs. In addition, synapses are regulated by a variety of short- and long-lived processes –collectively categorized as Hebbian plasticity– some of which lead to decreased synaptic strength and others that lead to enhancement. Synaptic facilitation is a form of short-term plasticity that enhances synaptic transmission in the timescale of hundreds of milliseconds. It can be seen with pairs of stimuli, in which the second post-synaptic potential can be up to five times the size of the first (Zucker & Regehr, 2002). Facilitation has been proposed to play a critical role in working memory, which involves the short-term storage of information for subsequent retrieval and decision making (Jackman & Regehr, 2017). Two forms of long-term plasticity represent major accepted cellular models for learning and memory in the brain (see **Section 5.3.3.2**): long-term potentiation (LTP) and long-term depression (LTD). Prolonged enhancement of synaptic transmission at a synapse results in LTP and synapse strengthening (Hill & Zito, 2013; Kopec et al., 2006; Lang et al., 2004; Matsuzaki et al., 2004; Nägerl et al., 2004), whereas during LTD a persistent weakening of synaptic transmission occurs (Nägerl et al., 2004; Zhou et al., 2004).

The assembly and remodeling of functional neural circuits requires precise spatial and temporal control. Disruptions of the distinct molecular mechanisms that tightly regulate synapse formation, stabilization and elimination are linked to brain malfunction and neurological disease. Altered synaptic receptor trafficking, abnormal spine morphology, increased or decreased synaptic density, and defective synaptic function have been reported in neuropsychiatric disorders such as schizophrenia, major depression and addiction (Glantz & Lewis, 2000; Kauer & Malenka, 2007; Lau & Zukin, 2007; Stockmeier et al., 2004), and in cognitive diseases, including mental retardation, fragile X syndrome and autism (Dölen & Bear, 2008; Südhof, 2008). Furthermore, neurodegenerative diseases as Alzheimer's disease (AD), Parkinson's disease (PD) and Huntington's disease –all characterized by gradual neuronal death, leading to decline in motor, cognitive and intellectual functions– are also associated to early abnormal dendritic growth and spine loss (Anderton et al., 1998; Plotkin & Surmeier, 2015; Selkoe, 2002).

5.3.3.2 Learning and memory: principles and behavioral models

One of the most challenging goals of neuroscience is to understand how the nervous system acquires- (learning) and stores and later on retrieves- (memory) information derived from the sensory world. The idea that changes in the strength of synapses within diverse neural circuits could mediate the storage of information acquired during learning has both theoretical and experimental support (Bliss & Lømo, 1973; Hebb, 1949; Jones, 1994; Kandel, 2001; Scoville & Milner, 1957). The synaptic plasticity and memory hypothesis states: *activity-dependent synaptic plasticity is induced at appropriate synapses during memory formation, and is both necessary and sufficient for the encoding and trace storage of the type of memory mediated by the brain area in which that plasticity is observed* (For a review see Martin et al., 2000).

Memory has different forms and is distributed across many different brain regions. Observations derived from activity-dependent synaptic plasticity experiments, as well as from lesions, suggest an important role for the hippocampus in episodic memory in animals and humans (Gruart et al., 2006; Scoville & Milner, 1957; Whitlock et al., 2006). The hippocampus is a tractable model system for studies of synaptic plasticity due to its simple laminar pattern of neurons and synaptic pathways (perforant, mossy fiber, and Schaffer collateral pathways) (see **Figure 11**). These anatomical characteristics make the hippocampus suitable for electrophysiological, genetic, and molecular cell biological manipulations. The transverse hippocampal slice preparation (Skrede & Westgaard, 1971) enables pharmacological agents to be rapidly washed on and off, allowing intracellular and patch-clamp recordings. In addition, hippocampal neuronal cultures (see **Section 5.3.1**) facilitate molecular manipulations to analyze the effect of downregulating or overexpressing specific proteins. As an example, autophosphorylation of a protein at a specific residue has been tracked and studied at multiple organizational levels in the hippocampus; going from isolated synaptic membranes to the behavioral analysis of animals with specific molecular defects (Giese et al., 1998).

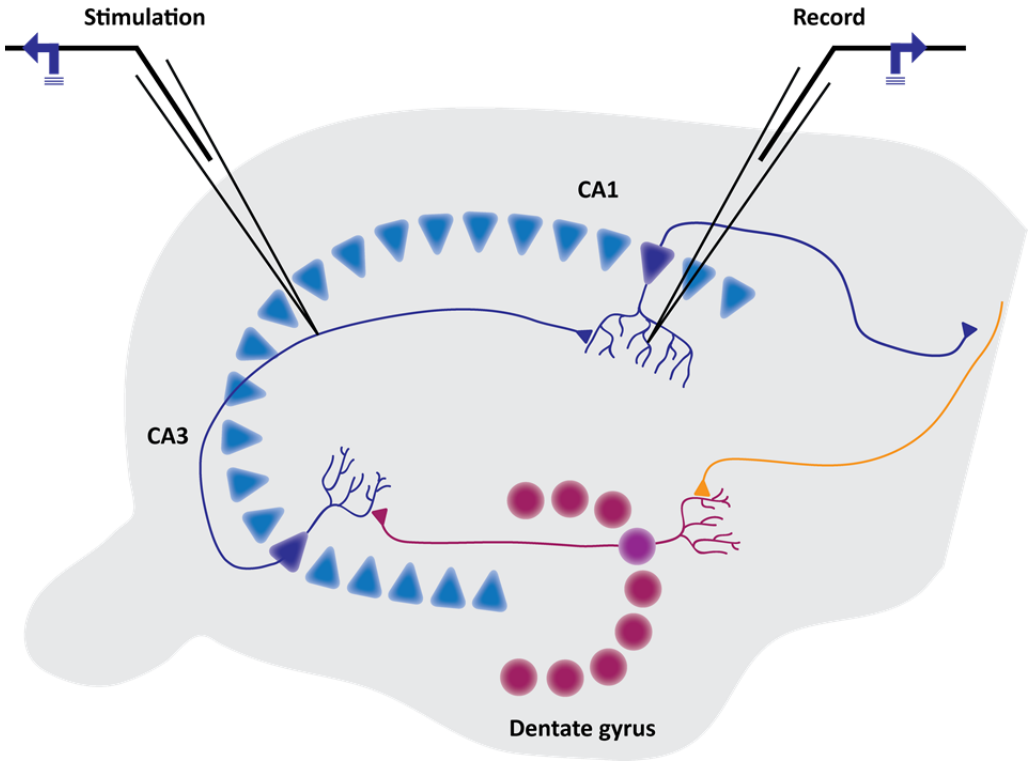

Figure 11. The tri-synaptic hippocampal circuit.
Diagram representing a transverse slice of the rodent hippocampus with the preserved excitatory synaptic pathways. In the perforant pathway, axons from the entorhinal cortex project onto the dendrites of dentate granule cells; in the mossy fiber pathway, dentate granule axons contact with CA3 pyramidal neuron dendrites; and in the Schaffer collateral pathway, CA3 axons synapse on CA1 pyramidal neuron dendrites. Electrodes can be used to record CA1 neurons reaction to CA3 pre-synaptic axonal stimulation. Adapted from Ho et al., 2011.

In humans, episodic memory refers to the ´what, when and where´ elements of an event-related memory. In animals, only the ´what´ and ´where´ can be assessed by behavioral tests where contextual cues are implemented. Following, the most common behavioral tests to assess memory impairment and/or hippocampus integrity in animals are summarized.

Cognition-based tests

Testing of cognitive functions in new genetically modified mouse lines, in particular in disease models, constitutes a substantial area of behavioral neuroscience. Yet, only a small fraction of cognitive testing aims a detailed understanding of underlying cognitive processes, and it should be considered that no single test is specific for a single cognitive domain.

The Y-maze spontaneous alternation test assesses spatial working memory, the ability to keep a memory item active in mind until a response is made, after which another item will replace it from the active memory. The test is based on rodents' natural curiosity to explore new environments, therefore typically preferring to investigate a new arm of the maze rather than returning to one that was previously visited (Dellu et al., 2000; Wall et al., 2003). Different areas

of the brain, including hippocampus, septum, basal forebrain, and prefrontal cortex are involved in this task.

The novel object recognition test evaluates recognition memory. The test is based on rodents´ natural preference to spend more time exploring a novel object than a familial one (Van Gaalen & Steckler, 2000). The task is believed to relay on hippocampal and perirhinal cortex function.

Social interaction tests

Social behavior can be defined as any behavior that influences, or is influenced by, other members of the same species. Social recognition tasks are applied to analyze social memory, namely the ability to discriminate between familiar and unfamiliar stimuli (Richter et al., 2005). Social interaction is analyzed as the time spent investigating a novel animal, as well as the amount and duration of grooming behavior, sexual interaction, and otherwise undefined interactions. This test is useful in identifying social amnesia in transgenic mouse lines exhibiting social interaction deficits, such as autism models, as well as part of the phenotyping of new transgenic mouse lines.

Intellicages

The Intellicage is an automated testing chamber used to test cognitive ability of socially housed mice. This testing device allows for the evaluation of up to 15 animals in their home environment, free of the confounding presence of the human experimenter, thanks to the individual identification with implanted transponders (Vannoni et al., 2014). Place learning is a cognitive protocol that measures the animal´s ability to learn that water is only available in a specific location in the cage. Reversals of the place are effective at testing flexibility of learning a new place, while probe trials are effective at testing the animal´s long term memory.

The Intellicage also allows for sensitive behavioral testing of sensorimotor and locomotor abilities.

Pre-pulse inhibition (PPI) of the acoustic startle reflex (ASR)

The ASR is a fast flinching response to an unexpected intense auditory stimulus present across different species. Its magnitude can be modulated by a variety of experimental manipulations and pathological conditions, making it a useful behavioral tool to analyze the neuronal basis of information processing as well as behavioral plasticity (Koch, 1999). The PPI is a measure of the ability of a weaker stimulus (pre-pulse) to attenuate the flinching response to an intense stimulus, this is the ability to successfully integrate and inhibit redundant sensory information (Swerdlow et al., 2001). Deficits in PPI have been reported in a variety of human disorders such

as: schizophrenia, bipolar disorder, Huntington's disease, fragile X syndrome, and autism. Importantly, in the absence of confounding factors like hearing loss or motor deficits, ASR and PPI give complementary information, namely: sensorimotor recruitment and sensorimotor gating, respectively.

6 Aims of the thesis

In this project, the characterization of six abundantly expressed circRNA candidates selected from RNA-sequencing libraries derived from frontal cortex, primary neuronal cultures along development, and synaptosomes was assessed. As circTulp4 revealed a high, neuron-specific expression level, all the research efforts were centered on its investigation, answering the next experimental questions: i) is circTulp4 playing a role in neuronal development?; ii) does it act in synaptic activity?; iii) could circTulp4 act through a translated peptide?; and iv) what is circTulp4 role *in vivo*?. To this end, a battery of genetic and molecular tools was developed to regulate circTulp4 expression levels in different experimental models, going from cell lines to living mice. In this context, a circTulp4^{KO} mouse line was developed, the first mouse model of specific circRNA depletion. The characterization of physiological, behavioral and electrophysiological alterations in this mouse line provides a comprehensive assessment of circTulp4 endogenous function.

7 Materials and methods

7.1 REAGENTS, BUFFERS AND SOLUTIONS

Unless stated otherwise, all chemicals and reagents were obtained from Roche applied science, Sigma-Aldrich and Roth or Merck.

Agarose gel electrophoresis

6x DNA loading buffer (orange)

1 g orange G (Sigma-Aldrich)

10 mL 2 M TRIS/HCl, pH 7.5

150 mL glycerol

Adjust volume to 1 L with H_2O.

1x TRIS acetate EDTA (TAE) buffer

4.84 g tris(hydroxylmethyl)-aminomethane (TRIS, Sigma-Aldrich)

1.142 mL acetic acid (Karl Roth)

20 mL 0.5 M ethylendiaminetetraacetate (EDTA, Sigma-Aldrich), pH 8.0

800 mL H_2O

Adjust to pH 8.3 with acetic acid.

Protein isolation and Western Blot

RIPA buffer

20 mM TRIS/HCl

150 mM NaCl

1 mM Na_2EDTA

1 mM EGTA

1 % NP-40

1 % Sodium deoxycholate

2.5 mM Sodium pyrophosphate

Add protease inhibitor mix.

4x Protein Loading buffer

50 % (V/V) Glycerol

125 mM Tris-HCl, pH 6.8

4 % SDS

0.08 % (W/V) Bromophenol blue

5 % β-Mercaptoethanol

10x SDS-PAGE running buffer

1 % (W/V) SDS

250 mM Tris

1920 mM Glycine

Adjust to pH 8.3.

1x Transfer buffer

0.025 M Tris

0.192 M Glycine

20 % Methanol

Adjust to pH 8.3.

1x TBS

50 mM Tris

150 mM NaCl

Adjust to pH 7.6.

Fluorescent *in situ* hybridization

10x Phosphate buffered saline (PBS)

1.37 M NaCl

27 mM KCl

200 mM Na_2HPO_4 x 12 H_2O (Merck)

20 mM KH_2PO_4 (Merck)

Adjust volume to 1 L with H_2O.

Adjust to pH 7.4.

DEPC- H_2O

1 L H_2O

1 mL diethylpyrocarbonate (DEPC)

Incubate overnight and autoclave 2x.

20 % paraformaldehyde (PFA)

20 % W/V paraformaldehyde (Sigma-Aldrich)

in 1x PBS

Adjust to pH 7.4.

20x Saline-sodium citrate (SSC)

3 M NaCl (Karl Roth)

300 mM sodium citrate (Sigma-Aldrich)

Adjust to pH 7.4.

Bacterial growth

LB medium

1 % (W/V) bacto-tryptone

0.5 % (W/V) bacto-yeast-extract

1.5 % (W/V) NaCl

1.5 % (W/V) bacto-agar (for agar plates)

Adjust to pH 7.4 with NaOH.

7.2 CONSUMABLES, ANTIBODIES, PRIMERS, OLIGOS AND PLASMIDS

Table 2. Kits used throughout this study.

Kit	Company
Wizard Genomic DNA purification Kit	Promega
QIAquick Spin Miniprep Kit	QIAGEN
QIAGEN Plasmid Maxi Kit	QIAGEN
QIAquick PCR Purification Kit	QIAGEN
QIAquick Gel Extraction Kit	QIAGEN
RNeasy Mini Kit	QIAGEN
RNA 6000 Nano Kit	Agilent Technologies
SuperScript VILO cDNA Synthesis Kit	Invitrogen
View miRNA ISH Cell Assay Kit	Affimetrix
TOPO TA Cloning Kit pCRII TOPO	Invitrogen
Rapid DNA Dephos & Ligation Kit	Roche
QuickChange Lightning Site-Directed Mutagenesis Kit	Agilent Technologies

Table 3. Enzymes.

Enzyme	Company
Taq DNA Polymerase (REDTaq ReadyMix)	Sigma-Aldrich
Q5 High-Fidelity DNA Polymerase (2x Master Mix)	New England BioLabs
Taq DNA Polymerase (LongAmp Taq 2x Master Mix)	New England BioLabs
Proteinase K	Sigma-Aldrich
RNAse A	Promega
T4 DNA Polymerase	Roche
T4 DNA Ligase	Roche
Restriction enzymes with buffer	New England BioLabs

Table 4. Antibodies.

Antibody	Supplier
anti-neurofilament	Abcam, #ab204893
anti-VGlut1	NeuroMab, #73-006, clone N28/9
anti-TULP4	Aviva Systems Biology, #ARP39410_P050
anti-HA	BioLegend (previously Covance, # MMS-101P)
anti-HA	Sigma-Aldrich, #H3663, clone HA-7
Alexa Fluor 488 goat α-mouse IgG	Invitrogen, #A11029
Alexa Fluor 594 goat α-mouse IgG	Invitrogen, #A11032

Alexa Fluor 647 goat α-mouse IgG	Invitrogen, #A21236
α-mouse-IgG HRP	CST, #7076

Table 5. Genotyping primers.

Name	Sequence 5´ → 3´	Amplicon (bp)	Detection of
Fw SA KO_2	CCGGCAGGAACAAGGGATAG	646	Wild-type circTulp4^{KO} (following
Rv SA KO	GGTGCTCCAGCTGATGCTTA		digestion with DdeI: 446 + 200 bp)
Fw Rosa 5' HA	AAAGTCGCTCTGAGTTGTTAT	252	Wild-type
Fw eGFP	GGTGAACTTCAAGATCCGCC	2044 + 396	Mutant
Rv Rosa 3' HA	CACACCAGGTTAGCCTTTAAGCC		
Fw eGFP_Refojo	CCTACGGCGTGCAGTGCTTCAGC	345	Mutant
Rv eGFP_Refojo	CGGCGAGCTGCACGCTGCCGTCCT		

Table 6. Primers for qRT-PCR.

Name	Sequence 5´ → 3´	Amplicon (bp)	Detection of
Fw Sv2b_circ	TTTTGGTGAGCACGTGCATGG	142	CircRNA
Rv Sv2b	ATGACAAACACTCTCCAGCTGTGG	123	Linear
Fw Sv2b_linear	CATCTTCTGGATGACTGGAGGC		
Fw Slc24a2_circ	CTTCCAGCTCATGATACACACCC	80	CircRNA
Rv Slc24a2	CGGTAAAGTTGGCCCATCC	184	Linear
Fw Slc24a2_linear	GTGGTGGGAAAGCTTACTCC		
Fw Adcy1	CCAGGAGCTGGTGAAACTGC	120	CircRNA
Rv Adcy1_circ	AAGATCCGCACGAAGACGCC	90	Linear
Rv Adcy1_linear	CCAAGGATCTTGATTCGGCG		
Fw Mfsd6	TGTTCAGTCCTGAGTCATGTGTCC	147	CircRNA
Rv Mfsd6_circ	TATCATCAGCAGCCATGGCTTACC	101	Linear
Rv Mfsd6_linear	GCCAGGCCAATGTATAAAACCC		
Fw Aagab	CCTGAATCTACAGGTGTAAAGCGG	158	CircRNA
Rv Aagab_circ	TTGTTATCGATGGTCCAGGGG	108	Linear
Rv Aagab_linear	TGAGTTGAGAAGGCTGAAGCC		
Fw Dgki_circ	CTTCAGCCTTGGATTTGATGC		
Rv Dgki_circ	AAACTTGTCCTCTTCTTCTTCCGG	97	CircRNA
Fw Dgki_linear	ATGACATCCATCAGGTGCAA	84	Linear
Rv Dgki_linear	CTGGGACAGACTGGGGAAT		

Fw Ksr2_circ	ATGGAGCCAACCAGGAAGAGTGC		
Rv Ksr2_circ	TTCTTCTTGCAGGACAGCTGTCG	119	CircRNA
Fw Ksr2_linear	CATGCTAGAGAAACTGCCAAAG	102	Linear
Rv Ksr2_ linear	GGTGAGGCAGCTGATGCT		
Fw Tom1l2_circ	TCTCTCCCAAGAATAACCCTCCC		
Rv Tom1l2_circ	CTAAGCCGCTTCTTTAGAGCCC	98	CircRNA
Fw Tom1l2_linear	CGTCAACGATGACCTCAACA	61	Linear
Rv Tom1l2_linear	GGACCTGTACCTCTCGAACCT		
Fw Tasp1_circ	CTGGTGCTCTTGCTACAGATGC		
Rv Tasp1_circ	GGAAAAGAGCATCCTTCCATCC	93	CircRNA
Fw Tasp1_linear	AGAGCATGTGCGTGGGATA	67	Linear
Rv Tasp1_linear	GGGAGTCGTGAAATGTGAGTC		
Fw Cds1_circ	TACCACAGGTTCATATCCTTCGCC		
Rv Cds1_circ	CGCCTCTGGCATCGAGATCT	83	CircRNA
Fw Cds1_linear	TGTCAGTATTTGATGGCAACG	76	Linear
Rv Cds1_linear	GCACTTTGCTGGGATTCG		
Fw Zpf445_circ	GCTCAGCGCAATCTTTATCGGG		
Rv Zpf445_circ	ATAGTCAGGCACCGAGACAGCAGG	90	CircRNA
Fw Zpf445_linear	TCCTGGAGAATTATGGGAATGT	77	Linear
Rv Zpf445_linear	GGCTTCTAGCCAGGAGATCA		
Fw Pi4ka_circ	TTAGCCCAGAACGTGGCATACC		
Rv Pi4ka_circ	AATGCAATCACTGCATCTCTCCG	152	CircRNA
Fw Pi4ka_linear	TCAACACAGTACTTTCACTGGC	94	Linear
Rv Pi4ka_linear	TCTACTGGGCACATGCAAAGC		
Fw Pi4k2a_circ	TGCCTTGTTCTCAACCAGG		
Rv Pi4k2a_circ	AGCCACTTGGTCCACTTAGG	164	CircRNA
Fw Pi4k2a_linear	GGCTAGCTTTCCCACTGAAG	92	Linear
Rv Pi4k2a_linear	CTGAGAGAACGGGACTTTCG		
Fw Snhg11_circ	TCACACTCTCGTGGGACAACCC		
Rv Snhg11_circ	GAAAGCCCTGAACAATCCTGGC	139	CircRNA
Fw Snhg11_linear	GAGGGGACATGAGAGGTGTC	78	Linear
Rv Snhg11_linear	TGTTGGGGAGTACGTTCCTT		
Fw Rims2_circ	CATTGGGGCCAAAATGGTAGC		
Rv Rims2_circ	CATCACTTACATCACTGTCCGAGG	150	CircRNA
Fw Rims2_linear	CAGCAAAAACAACCCAATGA	60	Linear
Rv Rims2_linear	CATTTCAAATTGTTGGTGCAG		
Fw Sntg1_circ	CAGAAATTTCCCTGTAAACCAGC	84	CircRNA
Rv Sntg1_circ	CGTTTTAAGAATGACACTGTCAGG	93	Linear

Fw Sntg1_linear	GCATGTGATCTGGCAGTGAG		
Rv Sntg1_linear	AGTCCTGGATACCCCGACA		
Fw Myrip_circ	TCTTCTGAGGAGAACAACCAGG		
Rv Myrip_circ	CACTCTTCGGTTTGGTCAGC	144	CircRNA
Fw Myrip_linear	GAGAGACTTCAATCTTCGCAAAA	63	Linear
Rv Myrip_linear	GCCAGCCTCTGCTTCATC		
Fw 4933406I18Rik_circ	AGGACGTGTGCAGATGGAAACC		
Rv 4933406I18Rik_circ	TAGAGCAGTCTTAGTGCCTGGC	130	CircRNA
Fw 4933406I18Rik_linear	AAGTAAGGAAGAGTTTGTTTTCTCC	73	Linear
Rv 4933406I18Rik_linear	A AACATCCAGTTGGTTGTCCAC		
Fw Cdr1as_circ	GCAGTGTCTCCAGTGTATCGG	93	CircRNA
Rv Cdr1as_circ	GGAAGACCTTGGTACTGGCACC		
Fw Tulp4_circ	TCACTGTCGCAGAGATAGGAGT	153	CircRNA
Rv Tulp4_circ	GGCACTTGATATGTTTGTTTTCC		
Fw Dtnb_circ	CAGAACTGCTTTTGGCGTGG		CircRNA
Rv Dtnb_circ	ACTGAAAACACGGTCAACTTGC		
Fw Magi1_circ	CATAGTCCACCCGGAGAATGAGG	116	CircRNA
Rv Magi1_circ	GAAAGCTGTAATCCACACCAGGC		
Fw Fat3_circ	TATCAGAGATGGCAGTGGTCTTGG	118	CircRNA
Rv Fat3_circ	GATGCAAGAAGGAGGCTTTGTGC		
Fw HomerI_circ	GACAGACGATGAGAGAACACCC		CircRNA
Rv HomerI_circ	ACAGTAACTGCATGCTTGCTGG		
RPL19 for	GCATCCTCATGGAGCACAT		Mouse housekeeper gen
RPL19 rev	CTGGTCAGCCAGGAGCTT		
TBP for	GTGATGTGAAGTTCCCCATAAGG		Mouse housekeeper gen
TBP rev	CTACTGAACTGCTGGTGGGTCA		(Shibata et al., 2008)

Table 7. Oligos

Name	Sequence 5´ → 3´	Purpose
N19_scrambled	GCGCGCTTTGTAGGATTCG	For cloning into shRNA-expressing plasmids
N19_circTulp4#1	CAACAGTGAGAGTTGTAAG	For cloning into shRNA-expressing plasmids
N19_circTulp4#2	CAGTGAGAGTTGTAAGAGT	For cloning into shRNA-expressing plasmids
N19_circTulp4#3	CACAACAGTGAGAGTTGTA	For cloning into shRNA-expressing plasmids
N20_gRNA_SA_circTulp4#1	AGAGTTGTAAGAGTCCATCC	For cloning into Pbs_U6_chimaeric RNA
N20_gRNA_SA_circTulp4#2	GTAAAACAACGACAAAAAAG	For cloning into Pbs_U6_chimaeric RNA
ssODN_SA_circTulp4	ACACACACATGCATATATACATATATATATACAC ACACACACATATCCTCTTTTTTGTCGTTGTTTTACT CAGTTGTAAGAGTCCATCCAGTACCTTCCAGTCA TGAATAATCTGATGGCTCCTGAATTAACCGGGAA AA	Donor template for deleting the splicing acceptor site from circTulp4
N20_gRNA_Met_Tulp4#1	TTGGAATCGCTGCAAAGCAC	For cloning into Pbs_U6_chimaeric RNA
N20_gRNA_Met_Tulp4#2	TGTATGCAGCAGTGGAACAT	For cloning into Pbs_U6_chimaeric RNA
N20_gRNA_Met_Tulp4#3	ATGTATGCAGCAGTGGAACA	For cloning into Pbs_U6_chimaeric RNA
N20_gRNA_Met_Tulp4#4	AAAAAGTATGTATGCAGCAG	For cloning into Pbs_U6_chimaeric RNA
ssODN_HA_N-Tulp4	AAAATAAGCCAATAAAAGAACTTGGTTTGAAATT CCTCAGTACTTTTAAAGTGAAATACTTCATTGAA AAAAGTATGTACCCTTACGACGTTCCAGACTACG CTATGTATGCTGCAGTGGAACATGGTCCTGTGCT TTGCAGCGATTCCAACATCCTCTGCCTGTCCTGG AAGGGGCGTGTTCCCAAGAGTGAGAAGGAG	Donor template for expressing HA-tag fusion TULP4 from endogenous promoter
N20_gRNA_Stop_circTulp4#1	GCCATCAGATTATTCATGAC	For cloning into Pbs_U6_chimaeric RNA
N20_gRNA_Stop_circTulp4#2	TATTCATGACTGGAAGGTCC	For cloning into Pbs_U6_chimaeric RNA

N20_gRNA_Stop_circTulp4#3	TCCAGTCATGAATAATCTGA	For cloning into Pbs_U6_chimaeric RNA
N20_gRNA_Stop_circTulp4#4	TCAGATTATTCATGACTGGA	For cloning into Pbs_U6_chimaeric RNA
ssODN_HA_C-circTulp4	TACATATATATATACACACACACACATATCCTCTT TTTTGTCGTTGTTTTACAGAGTTGTAAGAGTCCAT CCAGGACCTTTCAGTCATACCCTTACGAGGTTCC AGACTACGCTTGAATAATCTGATGGCTCCTGAAT TAACCGGGAAAACAAACATATCAAGTGCCATTTG AAGACTCTGTCTATCTATG	Donor template for expressing HA-tag fusion TULP4 from endogenous promoter

Table 8. Plasmids

Plasmid name	Purpose	Source
pcRII-TOPO	TOPO cloning vector	Invitrogen
pSUPER.neo+gfp	Expression of shRNAs (H1 promoter)	OligoEngine, #VEC-PBS-0005/6
pSico	Cre-inducible expression of shRNAs (U6 promoter)	Tyler Jacks. Addgene, #11578
pcDNA3.1(+) Laccase2 MCS exon vector	circRNA expression in mammalian cells	Jeremy Wilusz. Addgene, #69893
pcDNA3_CAG-RFP	Transfection control vector	Damián Refojo
pcDNA3_CAG-GFP	Transfection control vector	Damián Refojo
Pbs_U6_chimaeric RNA	gRNA cloning as dsDNA sequence	Cloned, Oskar Ortiz
pCAG-Cas9v2-wt-162A	Cas9 WT expression under CAG promoter	Cloned, Benedikt Wefers
PX459	All-in-one vector, for Cas9 WT expression (Cbh promoter) and cloning backbone for gRNA	Lucas Pontel
pROSA26 0.8	Gene targeting vector bearing 800 bp homology arms to *Rosa26*	Cloned, Oskar Ortiz
pROSA26 0.8_pSico_sh-circTulp4	Donor vector for conditional expression of sh-circTulp4	Cloned
pROSA26 long HA	Gene targeting vector bearing 1 Kb left and 4.5 Kb right homology arms to *Rosa26*	Cloned, Davina Fisher
pROSA26 long HA_pSico_sh-circTulp4	Donor vector for conditional expression of sh-circTulp4	Cloned

1A_mVenus_Neo	For PCR amplification-based tagging of endogenous genes. Expression of C-terminal fusion proteins	Lucas Pontel
1C_Neo_eGFP	For PCR amplification-based tagging of endogenous genes. Expression of N-terminal fusion proteins	Lucas Pontel
pEASY Flox	Tri-loxP vector for conditional gene targeting. Selectable marker: G418	Klaus Rajewsky. Addgene, #11725
pEASY Flox (-DTA)+HA_N-Tulp4	Donor vector for expression of HA-tagged TULP4 (endogenous promoter).	Cloned

7.3 NUCLEIC ACID METHODS

7.3.1 Genomic DNA preparation

DNA preparation from cell cultures

For genomic DNA extraction from cell lines, Wizard Genomic DNA Purification Kit (Promega) was used according to manufacturer´s instructions.

For mESCs, a protocol kindly shared by Dr. Claudia Seisenberg (IDG, High-Throughput Molecular Genetics) was used. 96 well plate frozen cells were thawed for 5 min on ice, after which 30-60 µL Lysis Buffer [TE 1x, KCl 50 mM, $MgCl_2$ 2 mM, RNaseA 200 µg/mL] followed by 2-4 µL Proteinase K (20 mg/mL) was added. The plate was shacked and centrifuged 1 min at 400 rpm before incubating it for an o.n. in a humid box at 60 ºC. Next day, the plate was centrifuged 1 min at 400 rpm, and 15 µL reactions were transferred to a new 96 well plate where Proteinase K was heat-inactivated 2 min at 90 ºC. 2 µL of the lysate were seed on an agarose gel to estimate quality and DNA amount. 1:3-1:4 dilution was used for genotyping PCR reaction.

DNA preparation from animal tissue

Genomic DNA for genotyping PCRs was isolated from tail tissue and ear punches. Wizard Genomic DNA Purification Kit (Promega) was used according to manufacturer´s instructions to establish genotyping PCRs. Afterwards, HotSHOT genomic DNA preparation (Truett et al., 2000) from ear punches was regularly used. Briefly, the tissue sample was digested in 75 µL Alkaline Lysis Reagent [NaOH 25 mM, EDTA 0.2 mM, pH 12.0] for 30 min at 95 ºC. After heating, samples were cooled down to 4 ºC, and 75 µL Neutralization Buffer [Tris-HCl 40 mM, pH 7.0] was added. 1 µL of the lysate was used for genotyping PCR reaction.

7.3.2 Plasmidic DNA preparation

Plasmidic DNA was prepared using DNA isolation Kits from QIAGEN (Mini- and Plasmid Maxi- Kit) according to the manufacturer's instructions. For MiniPreps, a single colony was inoculated in 2-3 mL LB medium with a selective antibiotic o.n. on a shaker at 37 ºC. For MaxiPreps, 500 µL of an o.n. MiniPrep, or a bacterial glycerolstock was added to 200 mL LB medium with the appropriate antibiotic and incubated o.n. on a shaker at 37 ºC.

7.3.3 Polymerase chain reaction (PCR)

For amplification of DNA fragments up to 1 Kb, REDTaq® ReadyMix™ PCR Reaction Mix (Sigma-Aldrich) was used according to manufacturer´s instructions.

For larger DNA fragments amplifications, LongAmp® Taq DNA Polymerase was used following a modified protocol:

Template DNA (50 ng)	1 µL
5x Buffer	5 µL
5 mM dNTPs	1.25 µL
Fw primer (10 pmol)	2.5 µL
Rv primer (10 pmol)	2.5 µL
100 % DMSO	0.5 µL
Taq DNA Polymerase	1 µL
H_20	11.25 µL
Total reaction	25 µL

PCRs were carried out in Eppendorf thermocyclers with modifications of the following program:

Step		Cycles	Temperature (ºC)	Time
Preincubation		1	95 ºC	5 min
Amplification	Denaturation		95 ºC	30 sec
	Annealing	30	X	30 sec
	Elongation		72 ºC	Y
Elongation		1	72 ºC	5 min
Cooling		1	10 ºC	∞

The annealing temperature (X) and the elongation time (Y) were adjusted according to the melting temperature of the primers and the amplicon size, respectively. LongAmp® Taq DNA Polymerase elongation temperature is 65 ºC instead of 72 ºC.

7.3.4 Cloning procedures

DNA restriction digests

Unless otherwise stated, restriction enzymes and working buffers from New England Biolabs (NEB) were employed. Plasmidic DNA was digested according to manufacturer´s instructions, in general 1-2 h at 37 ºC with 5 units/µg of the restriction enzyme in corresponding buffers. Fragment sizes were analyzed by agarose gel electrophoresis.

DNA gel extraction

For DNA fragment´s purification out of an agarose gel, QIAquick Gel Extraction Kit (QIAGEN) was used following manufacturer´s instructions. The DNA concentration and quality were determined by spectrophotometry.

Ligation of DNA fragments

For ligating and insert into a linearized vector, Rapid DNA Ligation Kit (Roche) was used. 50 ng of vector DNA was ligated to 3x molar excess of insert DNA. The appropriate amount of insert was calculated as following: m insert (ng) = 3 x 50 ng x (bp of insert / bp of vector). T4 DNA ligase and corresponding buffer were added in a total volume of 20 µL, and incubated for 5 min at RT. Heat shock transformation using 1-2 µL of the ligation product was performed in chemocompetent bacteria.

In cases were recircularization of the linearized vector was favored, Rapid DNA Dephos & Ligation Kit (Roche) was employed according to manufacturer´s instructions.

TOPO TA Cloning

For ligation of Taq polymerase-amplified PCR products into a plasmid vector, inserts were cloned into the pCRII-TOPO vector (TOPO TA cloning Dual promoter Kit, Invitrogen), containing Sp6 and T7 promoters for efficient *in vitro* transcription. The TOPO cloning reaction was set up as follows: 1-4 µL PCR product, 1 µL salt solution and 1 µL pCR®II-TOPO® vector in 6 µL final volume. After 5-30 min incubation at RT, depending on the length of the amplicon to be inserted, 1-4 µL of the mixture was transformed into chemically competent bacteria as described above. For blue-white selection of the colonies, 40 µL of 40 mg/mL X-Gal were added to the LB-agar plates.

pSUPER cloning

For stable expression of short interfering RNAs (siRNAs) in mammalian cells, pSUPER RNAi System (pSUPER.neo+GFP) was employed following OligoEngine protocol (Brummelkamp et al., 2002). The vector contains a Polymerase III H1 promoter for the production of small RNA transcripts from well-defined transcription start, lacking polyadenosine tails, and with a termination signal consisting of five thymidines in a row. A pair of custom oligonucleotides containing, among other features, a 19 nt sequence (N19) derived from the RNA transcript of the gene targeted for suppression were ordered, annealed and cloned between BglII and XhoI restriction sites. After transformation, the presence of positive clones was checked by analytic

digestion with EcoRI and XhoI, followed by fragment size analysis in agarose gel. The presence of correct insertion was also confirmed by sequencing.

pSICO cloning

For the conditional expression of shRNAs, pSICO plasmid was used (Addgene #11578). pSICO vector contains a Polymerase III U6 modified promoter that allows for Cre-dependent shRNA expression. After Cre-mediated recombination, a cytomegalovirus (CMV)-enhanced GFP stop/reporter cassette is excised, generating a functional U6 promoter. Similar to the pSUPER system, N19 oligos 5' phosphorylated and PAGE purified were ordered, annealed and cloned between HpaI and XhoI restriction sites. After transformation, positive clones can be checked by analytic digestion with SacII and NotI, followed by fragment size analysis in agarose gel. The presence of correct insertion was also confirmed by sequencing.

Sequencing

Sequencing reactions were carried out by GATC (www.eurofinsgenomics.eu) or by Sequiserve (www.sequiserve.de) according to the complexity of the DNA sample.

7.3.5 RNA isolation and quantitative real-time PCR (qRT-PCR)

RNA preparation

RNA extraction from cells and tissue was performed following a protocol that combines the instructions from TRIzol (Invitrogen) and RNeasy Mini Kit (QIAGEN). Cells were harvested in 1 mL TRIzol per 10 cm dish; for tissue 1 mL TRIzol was used per 30 mg sample. Homogenization was carried out by pipetting (cells) or using TURRAX (IKA Labortechnik) (tissue samples). 300 µL chloroform was subsequently added and vortexed for 15 s before incubating for 5 min at RT. Phenol and aqueous phases were separated by centrifugation at 15.000 rpm for 15 min and at 4 ºC. The aqueous supernatant containing the RNA was then transferred to a fresh 2 mL Eppi, precipitated with 1 volume absolute ethanol, and vortexed. Up to 700 µL of the mixture was then transferred to an RNeasy Mini spin column and centrifuged at 13.000 rpm for 15 s. Posterior steps were followed according to manufacturer´s instructions.

RNA concentration and purity were calculated by spectrophotometry, measuring absorbance at 260, 230 and 280 nm (A260, A230 and A280). In water, A260 = 1 corresponds to 40 µg of RNA per mL. The total yield of RNA sample was calculated as follows: concentration (µg/mL) x volume of sample (mL), where concentration = 40 x A260 x dilution factor. Pure RNA has an A260/280

ratio of around 2; lower values indicate the presence of contaminants that absorb in the UV, such as protein and phenol. A260/230 ratios lower than 2 also indicate the presence of contaminants such as carbohydrates, phenol, EDTA.

RNA integrity was measured on the Agilent 2100 Bioanalyzer (Agilent Technologies) using the Agilent RNA 6000 Nano Kit (Agilent Technologies). This analysis based on electrophoresis through microchannel was conducted following the manufacturer's protocol.

cDNA synthesis

First strand cDNA synthesis from high-quality RNA was performed using SuperScript™ VILO™ cDNA Synthesis Kit (Invitrogen) following manufacturer's instructions. A control reaction lacking the reverse transcriptase was included to test for genomic DNA contamination. cDNA was stored at -20 ºC.

Quantitative RT-PCR (qRT-PCR)

qRT-PCR was carried out in a LightCycler480 System using SYBR Green I Master (Roche). A mastermix reaction was set up as follow (volume per sample): 1 µL forward primer (10 µM), 1 µL reverse primer (10 µM), 5 µL SYBR Green I Master, and 1 µL H_20. 8 µL mastermix were pipetted into each well of a 96 well- or 384 well-plate (Sarstedt). Subsequently, 2 µL diluted template cDNA (1:10 or 1:20) were added, the well-plate was sealed with a clear film (Sarstedt) and quickly spun down before placing it into the machine. A regular 3-step PCR protocol followed by a melting curve analysis was applied for all runs conducted. Each sample (diluted template cDNA) was always run per triplicates.

Relative expression levels were determined using the $2^{-\Delta\Delta CT}$ method (Livak & Schmittgen, 2001), normalized to the housekeeping genes *Rpl19* and *Tbp*, and related to the data of the control sample. All calculations were based on an assumed PCR efficiency of 2.

Absolute expression levels were determined using the Second Derivative Maximum method (LightCycler® 480 Software version 1.5). For the standard curves, serial dilutions of qRT-PCR products were used as standard samples and their dilution factors were plotted against corresponding CP values. The number of circRNA molecules per neuron was calculated considering the amount of RNA isolated from 50.000 cells/mL seeded, and the molecular mass of the circRNA.

7.3.6 Site-directed mutagenesis

The QuickChange Lightning Site-Directed Mutagenesis Kit (Agilent Technologies) was used for generating point mutations, amino acid replacement, or small deletions/insertions according to manufacturer´s instructions.

7.4 PROTEIN BIOCHEMISTRY

7.4.1 Immunoblotting

Protein lysates from tissues or cells were obtained by adding ice-cold RIPA lysis buffer containing protease inhibitors and disrupting using a Turrax (VWR international) for tissue samples, or by pipetting up and down for cells. For better solubilization of membrane proteins, cells were subsequently rotated for 30 min to 1 h, followed by centrifugation at 13.000 rpm for 10 min and recovery of the supernatant containing the proteins. All steps were conducted on ice or at 4 ºC to avoid protein degradation. Until further processing, samples were stored at -80 ºC. Protein concentrations were estimated using Bradford assay. Prior to immunoblotting, protein samples were separated by 8-14 % SDS-PAGE (Laemmli, 1970) and transferred to 0.45 µm Immobilon-P PVDF membrane (Millipore). To minimize unspecific antibody binding, membranes were blocked in 5 % fat-free milk (Roth) in TBS-T 20 0.01 % (Sigma-Aldrich) for 1 h at RT. Primary antibodies were incubated o.n. at 4 ºC. Secondary horseradish peroxidase-IgG-conjugated antibodies were incubated for 2 h at RT. Following antibody incubation, membranes were always washed 3x 10 min with TBS-T 0.01 %. Signals were revealed by enhanced chemiluminescence reagent (Millipore) and the ChemiDoc imaging system (BioRad).

7.4.2 Mass spectrometry

LC-PRM analyses were carried out with a Q-Exactive Plus hybrid mass spectrometer (Thermo Scientific, San Jose, CA, USA) coupled to an Ultimate 3000 UHPLC system (Dionex) with 0.1 % formic acid as mobile phase A and 95 % ACN/0.1 % formic acid as mobile phase B. The theoretical synthetic peptides (NLRGHNSESCK, GHNSESCK, SPSRTFQS, 1 pmol each) were analyzed to collect MS/MS reference spectra. A mouse brain protein digest (1 µg) was injected onto a nano column (15 cm length, 75 µm diameter, PicoTip Emitter, New Objective, USA) self-packed with C18 (1.9 µm particles, Dr. Maisch GmbH, Germany) and then subjected to a 65 min gradient elution at a flow rate of 300 nL/min, 2 % mobile phase B (0-5 min), elution with 2-40 % mobile phase B (5-40 min), 40-80 % mobile phase B (40-50 min), 2 % mobile phase B (50-65 min). The mass spectrometer was set to collect in PRM mode with an inclusion list for the theoretical peptides (415.53153, 431.17961, 455.22487) following a full MS scan (350-1500 m/z). Full scans were conducted at a resolution of 70,000 at 200 m/z with an AGC setting of 3x106 and a max IT of 200 ms. PRM scans were collected at a resolution of 17,500 at 200 m/z with AGC setting of 2x105 and a max IT of 100 ms. The isolation window was set to 4.0 m/z and NCE was 27. Raw

files were searched with SEQUEST in Proteome Discoverer 2.2 against the Swissprot mouse protein sequence database that included the 3 peptide sequences. Search parameters were: 10 ppm mass tolerance for peptide precursors and 20 mDa (HCD) mass tolerance for fragment ions, carbamidomethylation of cysteine residues as fixed modification and oxidation on methionine as variable modification. The decoy search results indicated < 1 % false discovery rate (FDR).

7.5 CELL CULTURE

All cell culture reagents were purchased from Thermo Fisher Scientific except as otherwise stated, all cell culture dishes were purchased from Nunc® as otherwise stated.

7.5.1 Cell line cultures

Maintenance

Neuro-2a (mouse neuroblastoma) cells were grown in 'growth medium' [DMEM high glucose 1x; 10 % (V/V) heat-inactivated FCS] at 37 ºC in an atmosphere with 5 % CO_2. HT22 (mouse neuroblastoma) cells were grown in 'growth medium' [DMEM; 10 % (V/V) heat-inactivated FCS, Penicillin-Streptomycin (5.000 U/mL); 2 mM L-Glutamine] at 37 ºC and 5 % CO_2.

When reaching confluence, cells were passaged by removing old medium, washing with PBS, and adding 1 mL 0.25 % Trypsin-EDTA 1x to a 10 cm culture. After incubating 5 min at 37 ºC, trypsinization was stopped by adding 10 mL of growth medium and cells were re-suspended by pipetting. Cells were plated at the desired density (cell number was determined with a Neubauer chamber (Roth)) in a new culture dish and fresh growth medium was added.

For long-term storage of cells in liquid nitrogen, confluent cells were trypsinized and subsequently harvested by centrifugation at 1200 rpm for 5 min. Cells of one 10 cm culture dish were re-suspended in 1 mL of freezing medium [DMEM; 10 % (V/V) DMSO] and transferred into cryotubes (Nalgene). Vials were slowly cooled-down to -80 ºC in Mr. Frosty freezing containers (Nalgene) and the next day transferred to liquid nitrogen. To thaw cells, a frozen vial was quickly warmed up to 37 ºC, thawed cells were transferred to a falcon containing growth medium and subsequently centrifuged at 1200 rpm for 5 min. The cell pellet was re-suspended in 10 mL of growth medium and plated on a culture dish.

Transfection

For transient transfection experiments, cells were seeded at a desired density, if necessary on Poly-D-Lysine (Sigma-Aldrich)-coated cell culture plates and 24 h later transfected with the respective expression vectors using lipofectamine 2000 according to the manufacturer protocol. For CRISPR transfections X-tremeGENE HP DNA Transfection Reagent (Sigma-Aldrich) was used instead.

7.5.2 Primary neuronal cultures

Preparation of hippocampal and cortical cultures

Hippocampi and cortices were extracted from embryonic day (E) 17.5-18.5 mice, collected in 'dissection solution' [HBSS, 1 M HEPES, 10 % Penicillin-Streptomycin (5.000 U/mL)] and digested with 0.25 % Trypsin-EDTA 1x at 37 ºC with gentle shaking. After 20 min, trypsinization was stopped by washing 2x with DMEM supplemented with 10 % FCS and further tissue disaggregation was achieved with a fire-polished Pasteur pipette to yield dissociated cells. Cells were centrifuged at 900 rpm for 5 min, the pellet was carefully re-suspended in Neurobasal-A medium supplemented with B27, and the number of living cells was calculated from a Trypan Blue stained cell dilution. Cells were plated at the desired density ($5x10^4$ cells/well in a 24-well plate, $5\text{-}10x10^6$ cells/10 cm plate) on Poly-D-Lysine (0.05 mg/mL, 30.000-70.000 MW, Sigma-Aldrich)-, Laminin (1 µg/mL, Sigma-Aldrich)-coated cell culture plates or on 12 mm glass coverslips (Menzel) and maintained in Neurobasal-A medium supplemented with 2 % B27 and 0.5 mM GlutaMAXI at 37 ºC and 5 % CO_2.

Transfection

Plated neurons were transfected following a modified calcium-phosphate protocol (Jiang & Chen, 2006). For 4 wells of a 24 well-plate 1 mL of transfection mixture was prepared in a sterile 1.5 mL eppendorf tube as is detailed next: sufficient quantity to complete 1 mL of Ampuwa H_2O, followed by 12.5 µL 1 M $CaCl_2$ (fast vortexing) and 7-9 µg plasmid DNA was added by pipetting up and down 10x. During slow vortexing, 50 µL 2x BBS [50 mM BES, 280 mM NaCl, 1.5 mM Na_2HPO_4, pH 7.26] were added drop-wise to the formal mixture and finally 900 µL 37 ºC pre-warmed Neurobasal-A medium supplemented with 2 % B27 and 0.5 mM GlutaMAXI (fast vortexing). After incubating 15 min at RT, the conditioned medium was collected from the plated neurons and stored, and the transfection mixture was applied for a duration depending on the age and density of the neuronal culture. Next, transfected neurons were washed 8x with warm HBSS buffer containing 0.01 M HEPES, and finally conditioned medium, filled up with new Neurobasal-A medium, was pipetted back onto the neurons.

To study early developmental steps, such as polarization, neurite formation and axonal outgrowth, mouse embryo brains were *ex vivo* transfected before plating.

7.5.3 Mouse embryonary stem cells (mESCs) cultures

Maintenance

JM8 mESCs were grown in gelatin-coated [0.1 % (V/V) gelatin (Sigma-Aldrich) in H_2O] 10 cm plates with 'growth medium' [500 mL KnockOut™ DMEM; 12 % (V/V) FCS (PAN-Biotech); 6 mL L-Glutamine 200 mM 100x; 6 mL β-Mercaptoethanol (Sigma-Aldrich); 72 µL ESGRO® Recombinant Mouse LIF Protein (Sigma-Aldrich)] at 37 ºC in an atmosphere with 5 % CO_2.

When reaching confluence, cell were passaged by removing old medium, washing with PBS, and adding 1.5 mL Trypsin 2x+G [500 mL PBS; 0.1 g EDTA (Sigma-Aldrich); 0.5 g D-(+)-Glucose (Sigma-Aldrich); 5 mL chicken serum; 20 mL 2.5 % Trypsin 10x]. After incubating for ~5 min at 37 ºC, trypsinization was stopped by adding 10 mL of growth medium and cells were re-suspended by pipetting. Upon centrifugation for 5 min at 1200 rpm, cells were re-suspended in 1 mL growth medium and seeded at the desired density ($2x10^6$ cells per 10 cm plate) in a gelatin-coated plate containing 9 mL of fresh growth medium.

For the long-term storage of cells in liquid nitrogen, a similar protocol to cell line storage was used (**Section 7.5.1**).

Transfection

Human Stem Cell Nucleofector® Kit 2 and Nucleofector® 2b electroporator (Lonza) were used according to the following protocol. Two 10 cm gelatin-coated plates were prepared in advance per electroporation. When reaching confluence, cells were washed with PBS and trypsinized by adding 1 mL Trypsin 2x+G to a 10 cm plate. After incubating for ~5 min at 37 ºC, trypsinization was stopped by adding 5 mL growth medium and cells were re-suspended by pipetting. Upon mixing in a Falcon containing 15 mL growth medium, cells were counted to a density of $5x10^6$ cells per electroporation and separated in a new Falcon. Before transfecting, cells were spun-down, most of the medium was removed, and 100 µL of Nucleofector® solution 2 was added. Upon mixing, cells were transferred to u-bottomed wells containing the DNA mix, mixed 3-4 times and transferred to an electroporation cuvette (program A-23). Immediately after electroporation, transfected cells were transferred into a Falcon containing 4 mL growth medium, 1.5 mL and 3.5 mL were plated in each of the two 10 cm plates. The two following days growth medium was replaced, and from the third day on the medium was changed to 'selection medium' [growth medium; 150 µg/mL G418] and daily changed until

colonies were visible. ~30 colonies per electroporation were picked and expanded up to 6 copies; 4 copies for long-term storage and 2 copies for genotyping.

7.6 FLUORESCENT *IN SITU* HYBRIDIZATION (FISH)

FISH was performed using the QuantiGene ViewRNA miRNA ISH Cell Assay (Affimetrix) following manufacturer's protocol. In brief, wild-type and transfected primary neurons, grown on glass coverslips, were fixed in 4 % PFA in 1x PBS for 1 h at RT. Upon washing 3x with 1x PBS, cells were equilibrated with Cross-Linking Buffer QM 2x for 10 min at RT and the target was cross-linked with 0.16 M EDC for 1 h at RT and rocking. After washing 3x with 1x PBS, cells were permeabilized with Detergent Solution QC for 10 min at RT and digested with Working Protease Solution for 10 min at RT. A 2x and 3x washing steps with 1x PBS were performed after permeabilization and after digestion, respectively. Cells were then hybridized with Working Probe Solutions for 3 h at 40 ºC in a dry incubator, washed 3x in Wash Buffer (soaking 3 min in between), and stored in Storage Buffer until next day at 4 ºC. After no more than 24 h, cells were washed 2x with Wash Buffer and consecutively hybridized with Working PreAmplifier Mix Solution, Working Amplifier Mix Solution, and Label Probe Working Solution, each time for 1 h at 40 ºC. After each hybridization step, 3x washing steps with Wash Buffer (soaking 3 min in between) were followed. For Fast Red development, cells were incubated with AP-Enhancer for 5 min at RT, AP-Enhancer was removed and Fast Red Substrate was incubated at 40 ºC for 45 min. Afterwards, cells were washed 2x with 1X PBS, fixed in 4 % PFA in 1x PBS for 10 min at RT, and washed again 3 times with 1X PBS. Finally, coverslips were stained with DAPI and mounted with anti-fading VectaShield medium (Vector).

Images were taken using a confocal microscope (Zeiss LSM 710).

7.7 IMMUNOCHEMISTRY

Transfected cells, grown on glass coverslips, were fixed in 4 % (V/V) PFA, 4 % (W/V) sucrose in 1x PBS for 20 min at RT. Both, primary neuronal cultures as brain coronal sections were first permeabilized by washing 3x with PBS-TritonX-100 0.1 % (V/V) for cultures, or 3x PBS-TritonX-100 0.3% (V/V) for sections, for 10 min at RT with slow rocking. Upon washing with 1x PBS for 5 min, blocking was performed with 5 % BSA (W/V) in PBS-TritonX-100 0.1 % (V/V) for 1 h for cells, or 5% goat serum in PBS-TritonX-100 0.01% (V/V) for 2 h for sections, at RT with slow rocking. After 2x washing with 1x PBS for 5 min, samples were incubated with primary antibodies diluted at an appropriate concentration in 5 % BSA (W/V) in PBS-TritonX-100 0.01 % at 4 ºC o.n. Alexa dye-conjugated secondary antibodies (Invitrogen) diluted in blocking solution were incubated for 2 h for cells, or 5 h for sections, at RT with slow rocking. Antibody incubation was always followed by washing 3x with PBS-TritonX-100 0.1 % (V/V) for cells, or PBS-TritonX-100 0.01% (V/V) for sections, for 5 min with slow rocking. Samples were stained with DAPI and mounted with anti-fading VectaShield medium (Life Technologies).

Neuronal morphology analysis

For the analysis of axons/dendrites in culture, primary hippocampal neurons were fixed at DIV 5 and images were taken from at least three independent preparations. Axons were traced with open access NeuronJ (ImageJ, https://imagej.nih.gov/ij/) and further evaluated with the same software to calculate total length and branching.

Dendritic spine and VGlut1 signal quantification

Images were taken using a confocal microscope (Zeiss LSM 710). Neuronal cultures were first explored in search of healthy-shaped neurons, with high fluorescence values and sufficiently spaced dendrites to the end of individually photograph them. The exploration was performed using a Plan-Apochromat 40x/1.4 Oil DIC M27 oil immersion objective and individual dendrites were photographed with the same objective, adding digital zoom. For IUE coronal sections, exploration was performed with a Plan-Apochromat 10x/0.45 M27 instead, checking that transfected neurons belong to the CA1 region of the hippocampus. A Plan-Apochromat 40x/1.4 Oil DIC M27 oil immersion objective was then used to photograph the transfected dendrites, using additionally digital zoom. All images were acquired using 1 µm z-steps, ensuring that the

whole dendrite width is contained in the z-axis of the image. Images were post-processed using Fiji software (https://imagej.net/Fiji).

For dendritic spine density quantification, images derived from different focal planes were converted into their maximum projections. The dendritic length was measured using the 'Simple Neurite Tracer' PlugIn in every picture, and with the 'Cell Counter' PlugIn the number of dendritic spines was calculated. Dendritic spine density was expressed as the number of dendritic spines per 10 µm dendritic length. Dendritic spines were defined as protuberances larger than 0.5 µm, but shorter than 1 µm.

For VGlut1 puncta quantification, the signal was first deconvoluted using the 'Iterative deconvolution' PlugIn. For this, first an image of the theoretical point spread function (PSF) was taken using the Born & Wolf optical model of the 'PSF generator' PlugIn, which considers the conditions in which the pictures were shot (refractive index of the immersion medium, the numerical aperture of the objective, pixel size, z-step, wave-length, and image size). Then, deconvolution was done using a number of 5 iterations and a low-pass filter of 4 pixels. Once the image was deconvoluted, a detection threshold was applied to the signal following the 'Isodata' method. Briefly, the image is divided into object and noise taking an initial threshold, and then pixel means are calculated separating them between those under the threshold and those above. Next, the threshold is increased and the process is repeated until the threshold is higher than the combined means. After the intensity threshold was set, signals smaller than 0.15 μm^2 were further filtered out. The final image was merged to the image of the corresponding dendrite and the number of puncta on dendritic spines and on the dendritic shaft was calculated. The resulting values were normalized to the number of spines in the first case, and to the dendritic length in the second case. A punctae was counted positive when the signal was adjacent to the dendrite signal.

7.8 ANIMAL PROCEDURES

Mice were handled according to institutional guidelines and approved by the animal welfare committee of the government of Upper Bavaria. Animal protocol numbers: *mouse generation:* ROB 55.2-2532.Vet 02-14-205; *behavioral characterization:* ROB 55.2-1-54-2532-46-2016. The mice were housed in standard cages in a specific pathogen-free facility on a 12 h light/dark cycle with *ad libitum* access to food and water.

7.8.1 Brain slices preparation

In utero electroporated animals were anesthetized with isoflurane (Piramal Critical Care) and transcardially perfused with a peristaltic pump for 1 min with 1x PBS, 5 min with 4 % PFA (W/V) in 1x PBS, pH7.4, and 1 min with 1x PBS at a flow of 10 mL/min. All solutions were ice cold. Brains were immediately removed, post-fixated for 1 h in 4 % PFA (W/V) in 1x PBS, and cryopreserved in 15 % (W/V) sucrose in 1x PBS, pH 7.6 o.n. at 4 ºC. Brains were then washed with 1x PBS and integrated in a warm solution consisting of 4 % agarose (Invitrogen) in 1x PBS with the aim of cutting 50 µm transversal sections with the vibratome (VT1000 S, Leica). Sections were stored at -20 ºC in cryopreservation solution [20 % (V/V) glycerol, 30 % (V/V) ethylenglycol in 1x PBS, pH7.4] until immunohistochemistry, DAPI staining and mounting.

7.8.2 Generation of mouse models

CRISPR/Cas9 target sites

CRISPR target sites were identified using http://crispr.mit.edu/ as previously described (Ran et al., 2013). Alternative target sequences (see **Section 7.2**, **Table 7**) were selected according to their quality score and cloned as complementary oligonucleotides into the BbsI sites of a pbs-U6-chimaericRNA plasmid designed based on Chen et al. (2013) (Chen et al., 2013). Plasmids pbs-U6-chimaericRNA-gRNA were further validated in Neuro-2a cells using a Cas9-expressing vector designed based on Jinek et al. (2013) (Jinek et al., 2013) to test Cas9 cutting efficiency in mouse genome at the gene of interest *locus*.

Pronuclear microinjection

crRNA and tracrRNA were ordered from Integrated DNA Technologies Inc. The repair template was ordered as a HPLC-purified single-stranded oligodeoxynucleotide (ssODN) from Metabion.

RNAs and ssODNs were diluted in $T_{10}E_{0.1}$ injection buffer [10 mM Tris-HCl, 0.1 mM EDTA], filtrated through a centrifugal filter (Ultrafree, PFTE, Millipore) and stored in single-use aliquots at -80 ºC. On the day of injection, a thawed aliquot containing 0.6 pmol/µL crRNA/tracrRNA heteroduplex, 50ng/µL ssODN, and 25 ng/ µL Cas9 mRNA was added Cas9 protein to a final concentration of 50 ng/µL. For microinjections, zygotes were obtained by mating of C57BL/6N males with super-ovulated C57BL/6N females (Charles River). Zygotes were injected into one pronucleous and transferred into pseudo-pregnant CD1 female mice to obtain live pups.

7.8.3 Behavioral tests

With the exception of the IntelliCage, all behavioral experiments were carried out in adult female and male mice (age 11-18 weeks), which were habituated to test room conditions one week before testing. All behavioral tests were performed during the light phase. For the IntelliCage, only adult female mice (age 32 weeks) were tested. In order to minimize possible carryover effects of the different behavioral tests, the sequence of tests was arranged from least to most stressful.

Open field (OF) test

The OF test was originally designed to characterize general locomotor activity and anxiety-related behavior in a novel environment. The analysis was carried out as described before (Hölter & Glasl, 2012). In brief, mice were placed in a square OF arena (WLH 45.5 x 45.5 x 39.5 cm), illuminated with 200 lux in the center, and surrounded by infrared beams (ActiMot, TSE, Bad Homburg, Germany). Behavior was recorded for 20 min, during which several parameters were analyzed, including distance traveled, number of rearings, time in center [%] and distance in center [%] in 5 min bins.

Acoustic startle response (ASR) and pre-pulse inhibition (PPI)

The ASR/PPI aims to characterize two dissociable functions: sensorimotor recruitment (ASR) and sensorimotor gating (PPI) (Koch, 1999; Swerdlow et al., 2001). The latter reflecting the ability of an animal to successfully integrate and inhibit irrelevant sensory information. The experimental apparatus consisted of an outer sound-attenuated chamber and an inner load cell platform that recorded the startle response (SR-LAB, San Diego Instruments SDI, San Diego, CA, USA). After an acclimation period of 5 min, the response to a 110 dB pulse was measured. For PPI assessment, the capacity of a weaker acoustic pre-pulse of varying intensities (67, 69, 73 or 81 dB) to

attenuate a 110 dB pulse was calculated as a percentage score. For each acoustic pre-pulse trial, % PPI= 100 x (S – PPi_S)/S. Where S is the basal startle amplitude at 110 dB and PPi is the startle amplitude after pre-pulse presentation. The protocol consisted of 10 blocks, each including every trial condition in a pseudo-randomized order. ASR was also elicited 10 times at 110 dB without a pre-pulse in order to determine the baseline response and assess habituation effects.

Modified SHIRPA

The primary behavioral observation screen is a modification of the Irwin procedure (Irwin, 1968), in which the general health status and evaluation of basic neurological and motor functions are assessed. First, the mouse is placed in a clear cylinder to observe body posture and tremors. Then, is transferred into an arena (WLH 26 × 42 × 18 cm) in which a Perspex sheet on the floor is marked with 15 squares. Here, several other parameters are taken, including locomotor activity which is recorded during the first 30 sec by counting the number of squares being crossed.

Y-maze test

Spatial memory was investigated in the Y-Maze, which consisted of three identical arms (WLH 5 × 30 × 15 cm) placed at 120° from each other and illuminated in the center with 100 lux (Wall et al., 2003). When tested in the Y-maze, normal mice show a preference to explore the least recently visited arm, thus tending to alternate visits between the three arms. To do so, the mouse must maintain a record of the most recently visited arm and continuously update it. Therefore, alternation behavior is a measure of spatial working memory. During testing, each mouse was placed at the end of one arm and allowed to move freely through the maze during a 5 min session. Total numbers of arm entries were collected cumulatively over the 5 min, accounting for locomotor activity. The percentage of spontaneous alternations (SPAs)–defined as consecutive entries into all three arms without repetitions in overlapping triplet sets– was calculated as the ratio of total alternations to total number of triplets x 100. The percentage of alternate arm returns (AARs)–defined as triplet sets that include a return into the first arm, e.g. ABA– was calculated as the ratio of alternate arm returns to total arm entries × 100.

Social discrimination test

Social discrimination was analyzed as previously described (Feil et al., 2009). The procedure consisted of two trials, each of 4 min exposures to an unfamiliar animal (ovariectomized 129Sv females). Before the first exposure, the test animal was allowed to move freely in a fresh cage

for a 2 h period, after which an unfamiliar animal was presented. After a retention interval of 2 h, the test animal was re-exposed to the now familiar animal, together with an additional new unfamiliar animal. The duration of investigatory behavior of the test animal towards the unfamiliar animal was recorded by a trained observer with a handheld computer. A social recognition index was calculated as the ratio between the time spent investigating the unfamiliar mouse to the time spent investigating both the familiar and unfamiliar mice.

IntelliCage

Female mice were implanted with microtransponders (implantable RF tags; DATAMARS SA, Bedano/Lugano, Switzerland). Implantation was performed under a brief isofluorane anesthesia, subcutaneously injecting the transponders into the skin fold in the back of the neck of the animal. Five days after, animals were placed into the IntelliCages and allowed to habituate for 5 days: all doors in the corners open, mice learned to drink from the corners. Followed by a 14 days nosepoke habituation: all doors closed, mice learned that they have to nosepoke for a door to open and give access to the drinking spout. In this study, three different test modules were evaluated: i) 7 days place learning: each mouse is assigned to only one corner where nosepoking will lead to door opening and access to the drinking spout. Corner assignments are distributed evenly over all 4 corners of the cage. ii) 7 days reversal learning: each mouse corner assignments were switched to the corner diagonally opposite of the previously correct one. iii) 10 days patrolling: each mouse corner assignments switch after each correct drinking event to the next corner of the cage in a clock-wise direction. The animals learn that they have to ‘patrol’ the corners in a clock-wise direction for water access.

During each module, mice were monitored for their licking (drinking) behavior; any mouse which did not master the module completely was removed from the analysis. Thus, the following mice were excluded: Place learning: n = 1 WT; Reversal learning: n = 2, with one WT and one KO; Patrolling: n = 2 KO.

7.9 ELECTROPHYSIOLOGY

Slice preparation

Mice were anesthetized and decapitated 4-6 weeks after IUE. Brains were removed into a chilled solution containing (mM): 110 choline-Cl−, 2.5 KCl, 2 NaH_2PO_4, 25 $NaHCO_3$, 0.5 $CaCl_2$, 7 $MgCl_2$, 20 dextrose, 1.3 Na+ -ascorbate, 3.1 Na+ -pyruvate, and 4 kynurenic acid. The right hippocampus was dissected and 400 µm thick slices were cut transversally to the longitudinal axis in a vibratome and transferred to a chamber containing artificial cerebrospinal fluid (ACSF; mM): 125 NaCl, 2.5 KCl, 2.3 NaH_2PO_4, 25 $NaHCO_3$, 2 $CaCl_2$, 1.3 $MgCl_2$, 1.3 Na+ -ascorbate, 3.1 Na+-pyruvate, and 10 dextrose (315 mOsm). Slices were bubbled with 95 % O_2/5 % CO_2 and maintained at 30 ºC for >1 h before experiments started. Salts were acquired from Sigma-Aldrich.

Electrophysiological single-cell recordings

Recorded neurons were visually identified by fluorescence and infrared DIC video Microscopy. Whole-cell recordings were performed using microelectrodes (4–5 MΩ) filled with (mM): 130 CsOH, 130 D-gluconic acid, 2 $MgCl_2$, 0.2 EGTA, 5 NaCl, 10 HEPES, 4 ATP-tris, 0.3 GTP-tris, 10 phosphocreatine.

For evoked monosynaptic excitatory post-synaptic currents (EPSC) and inhibitory post-synaptic currents (IPSC) recordings, a stimulating electrode was placed at the *stratum radiatum* to activate Schaffer collateral axons. EPSCs were isolated by voltage clamping pyramidal neurons at the reversal potential of the IPSC measured for each individual neuron (∼-60 mV). In turn, IPSCs were recorded at the reversal potential of the EPSC (∼0 mV). When present, direct monosynaptic IPSC elicited in the presence of kynurenic acid (KYN, Sigma-Aldrich) was subtracted from the total IPSC.

For recordings of the miniature excitatory and inhibitory postsynaptic currents (mEPSCs and mIPSCs, respectively), tetrodotoxin containing ACSF (0.5 µM; Alomone labs) was bath perfused. mEPSCs and mIPSCs were recorded at the reversal potential of inhibition (-60 mV) and excitation (0 mV) respectively, in gap free mode.

In experiments where the intrinsic responses to current pulses were evaluated, a potassium gluconate internal solution was used (mM): 120 potassium gluconate, 4 $MgCl_2$, 10 HEPES buffer, 0.1 EGTA, 5 NaCl, 20 KCl, 4 ATP-tris, 0.3 GTP-tris, and 10 phosphocreatine (pH = 7.3; 290 mOsm).

Recordings were obtained using Multiclamp 700B amplifiers, (Molecular Devices), digitized, and acquired at 20 KHz onto a personal computer using the pClamp10 software. Membrane

capacitance and input resistance were obtained from current traces evoked by a hyperpolarizing step of 10 mV. Series resistance was typically 10–20 MΩ, and experiments were discarded if higher than 40 MΩ.

7.10 STATISTICAL ANALYSIS

All results are presented as mean ± standard error of the mean (SEM), unless otherwise stated, and were analyzed using GraphPad Prism version 5.01. For data with homogeneous variances, a two-tailed t-test was used for single comparisons and two-way ANOVA was used for multiple comparisons. In case of inhomogeneous variances, Mann-Whitney U test was used instead. Time-dependent measures including segmented distance traveled and number of rearings, startle response and for progression analysis in the three modules of the Intellicage were assessed by two-way ANOVA with repeated measures (RM-ANOVA). Whenever significant interaction effects or main effect were found by the ANOVAs, Bonferroni post-hoc tests were carried out to locate simple effects. Statistical significance was defined as $p < 0.05$.

8 Results

8.1 CIRCRNA EXPRESSION ANALYSIS DURING NEURONAL DEVELOPMENT

8.1.1 Circular and linear isoforms of a gene are differentially regulated along neuronal development

As the first aim of this project, the expression profile of the 20 most highly expressed circRNAs derived from a whole mouse brain RNA-sequencing library (see **Table 9**. Memczak et al. (2013)) was characterized along primary neuronal culture development.

The absolute expression level of circular and linear isoforms of selected genes was assessed by qRT-PCR. For that, primary cortical neurons obtained from embryonic mice were cultured for 1, 7, 14, 21 and 28 days *in vitro* (DIV). Standard curves were generated from serial qRT-PCR product dilutions, and absolute expression was calculated considering primers efficiency (see **Section 7.3.5** for quantitative analysis description). As observed in **Figure 12**, most of the candidates showed a similar expression pattern for both RNA isoforms, with no changes throughout development. However, while for some candidates the levels of the circular isoform were significantly higher than their linear counterpart (*Tasp1, Cdr1as, Snhg11, Mfsd6, Slc24a2, 4933406I18Rik*), others showed the opposite configuration with higher linear isoform levels compared with the respective circular isoform (*Aagab, Rims2, Tom1l2, Cds1, Adcy1, Sv2b*). Interestingly, a more dynamic expression pattern of the two RNA isoforms was also observed; *Dgki* circular isoform expression increased along development while its corresponding linear isoform decreased. Taken together, these results indicate that the expression levels of circular and linear isoforms of a gene can be uncoupled, pointing towards a specific regulation of circRNA expression and therefore suggesting potential divergent functions of both RNA isoforms.

A notable outcome of measuring circRNA candidates' absolute expression is that with few exceptions, the majority of the candidates are expressed at low levels, with an estimation in the order of ten molecules per neuron.

Table 9. Top twenty most highly expressed circRNAs. RNA-sequencing data from Memczak et al., 2013 was filtered to preserve only candidates present in whole mouse brain.

Header descriptions	
chrom	Chromosome name
start	Start position (zero based)
end	End position (exclusive)
name	circRNA identifier
score	Total number of reads supporting the head-to-tail splice junction
strand	Strand orientation of the candidates
samples	Samples where the circRNAs are detected
unique_reads	How many unique reads support the head-to-tail splice junction
genomic_length	Genomic distance between the circRNA's splice sites
best_transcript	Transcript ID which has the best overlap with the circRNA (see Suppl. Methods.).
spliced_seq_length	Length of the inferred spliced sequence
gene	Gene corresponding to the transcript that best overlaps with the circRNA
annotation	circRNas annotation; ALT_ACCEPTOR: acceptor site not in our catalog , ALT_DONOR: donor site not in our catalog, ANNOTATED: both splice sites in our catalog, ANTISENSE: ANTISENSE to

#chrom	start	end	name	score	strand	samples	unique_reads	genomic_length	best_transcript	spliced_seq_length	gene	annotation
chr7	82281183	82293974	mm9_circ_005710	26	-	mm_brain1,mm_brain2	16	12791	NM_153579	589	Sv2b	ANNOTATED,CDS,INTERNAL,coding
chrX	58436422	58439349	CDR1as	25	+	mm_brain1,mm_brain2	13	2927	NM_001166658	2927	Cdr1	ANTISENSE,CDS,UTR3,UTR5,coding,upstream_start
chr4	86719091	86722061	mm9_circ_000696	18	-	mm_brain1,mm_brain2	14	2970	NM_001110240	148	Slc24a2	ANNOTATED,CDS,INTERNAL,coding
chr1	22336373	22384029	mm9_circ_003161	17	-	mm_brain1,mm_brain2	13	47656	NM_001012623	14924	Rims1	ALT_ACCEPTOR,CDS,INTERNAL,coding,intronic
chr11	6978890	7009115	mm9_circ_004272	17	+	mm_brain1,mm_brain2	13	30225	NM_009622	381	Adcy1	ANNOTATED,CDS,INTERNAL,coding
chr1	52765007	52766599	mm9_circ_009434	16	-	mm_brain1,mm_brain2	13	1592	NM_178081	1592	Mfsd6	ANNOTATED,CDS,INTERNAL,UTR5,coding
chr9	63464492	63467038	mm9_circ_005795	16	+	mm_brain1,mm_brain2	12	2546	NM_025857	462	Aagab	ANNOTATED,CDS,INTERNAL,coding
chr6	36979762	37008028	mm9_circ_013516	16	-	mm_brain1,mm_brain2	8	28266	NM_001081206	649	Dgki	ANNOTATED,CDS,INTERNAL,coding
chr9	120341470	120350699	mm9_circ_017648	16	+	mm_brain1,mm_brain2	8	9229	NM_144557	866	Myrip	ANNOTATED,CDS,INTERNAL,coding
chr5	117950721	117955648	mm9_circ_004874	15	+	mm_brain1,mm_brain2	12	4927	NM_001114545	292	Ksr2	ANNOTATED,CDS,INTERNAL,coding
chr11	60083819	60088504	mm9_circ_003952	15	-	mm_brain1,mm_brain2	9	4685	NM_001039092	229	Tom1l2	ANNOTATED,CDS,INTERNAL,coding
chr17	34873839	34954233	mm9_circ_010282	14	-	mm_brain1	11	80394	NM_009780	75527	C4b	ALT_ACCEPTOR,CDS,UTR5,coding,upstream_start
chr4	131908420	131908873	mm9_circ_013552	14	-	mm_brain1,mm_brain2,mm_brain3	10	453	NR_003270	453	Snhg3	ALT_ACCEPTOR,ALT_DONOR,INTERNAL,intronic,ncRNA
chr2	139772892	139777315	mm9_circ_011578	14	-	mm_brain1,mm_brain2	9	4423	NM_001159641	199	Tasp1	ANNOTATED,CDS,INTERNAL,coding
chr5	102210393	102227535	mm9_circ_004198	13	+	mm_brain1,mm_brain2	10	17142	NM_173370	463	Cds1	ANNOTATED,CDS,INTERNAL,coding
chr5	37573319	37585543	mm9_circ_004341	13	+	mm_brain1	8	12224	None	12224	None	INTERGENIC
chr7	121462966	121464765	mm9_circ_006185	12	-	mm_brain1,mm_brain2	10	1799	NR_029437	301	4933406I18Ri	ANNOTATED,INTERNAL,ncRNA
chr9	122765816	122766279	mm9_circ_013827	12	-	mm_brain1,mm_brain2	10	463	NM_173364	186	Zfp445	ANNOTATED,CDS,INTERNAL,coding
chr15	74878871	74941057	mm9_circ_004432	12	-	mm_brain1,mm_brain2	9	62186	NM_001252058	62186	Ly6c1	ALT_ACCEPTOR,CDS,UTR5,coding,upstream_start
chr16	17373442	17389550	mm9_circ_007694	12	-	mm_brain1,mm_brain2	7	16108	NM_001001983	700	Pi4ka	ANNOTATED,CDS,INTERNAL,UTR5,coding
chr19	42175126	42175327	mm9_circ_007095	11	+	mm_brain1,mm_brain2	7	201	NM_145501	201	Pi4k2a	ANNOTATED,CDS,INTERNAL,coding
chr2	158208239	158208899	mm9_circ_017587	10	+	mm_brain1,mm_brain2	8	660	NM_175692	660	Snhg11	ALT_ACCEPTOR,ALT_DONOR,INTERNAL,UTR3,coding
chr15	39417135	39448056	mm9_circ_015883	9	+	mm_brain1,mm_brain2	9	30921	NM_053271	415	Rims2	ANNOTATED,CDS,INTERNAL,coding
chr1	8544805	8614962	mm9_circ_009692	9	-	mm_brain1	8	70157	NM_027671	486	Sntg1	ANNOTATED,CDS,INTERNAL,coding

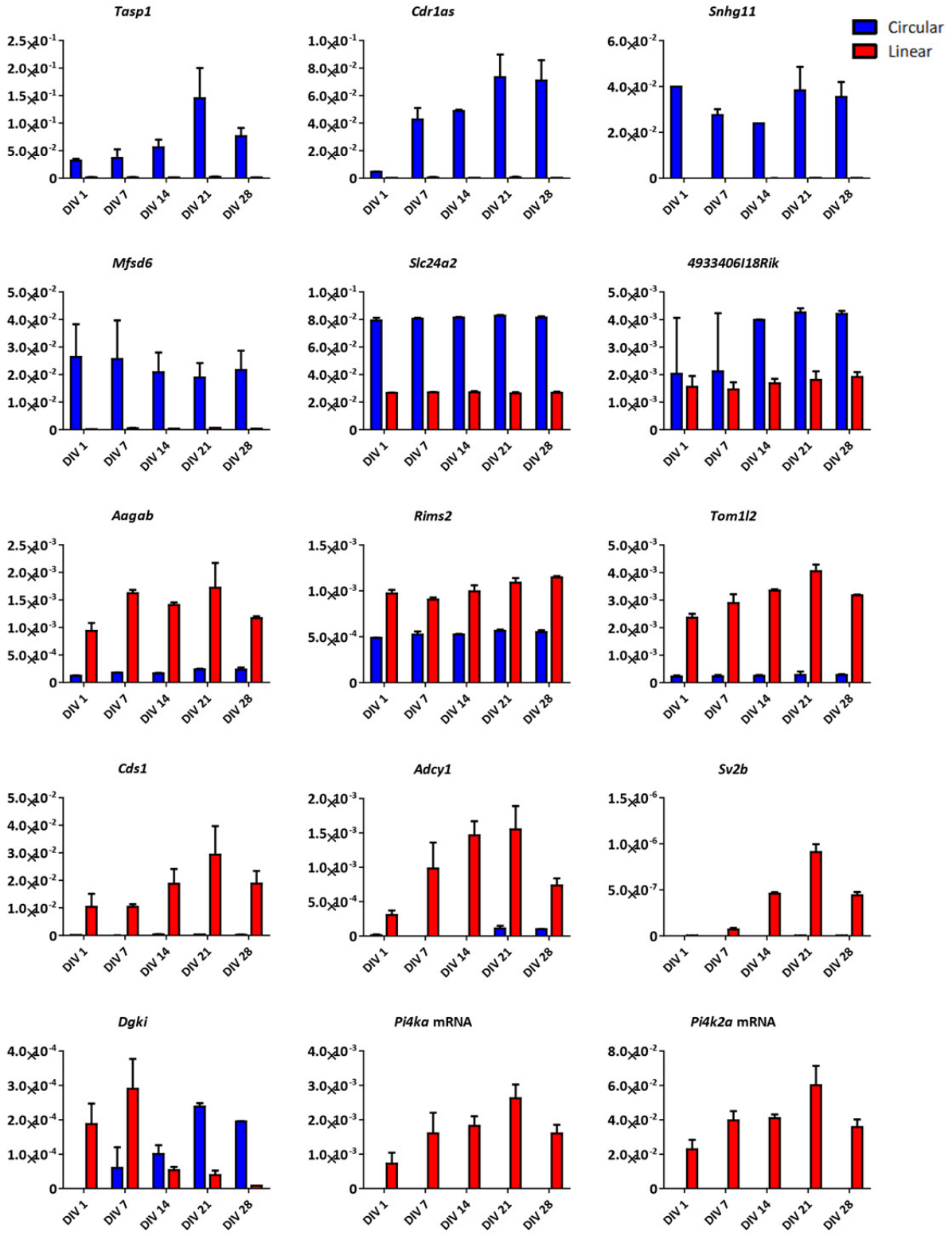

Figure 12. Expression levels of circular and linear isoforms of candidate genes along neuronal development. RNA was isolated from primary cortical neurons at the indicated DIV and absolute quantification was assessed by qRT-PCR; n = 2 independent neuronal cultures. Y-axes represent number of attomoles (10^{-18} moles). Candidates which graphs are not shown had unreliable cross-point values (CP > 35) or double temperature of melting.

8.1.2 CircRNA candidates´selection

In collaboration with Dr. Sebastián Kadener at the Hebrew University of Jerusalem, RNA-sequencing libraries derived from primary frontal cortex neurons along development and from synaptosomal fractions were generated. Based on their abundancy in these RNA-sequencing libraries, and considering the host gene involvement in synaptic function (Rybak-Wolf et al., 2015; You et al., 2015), six circRNA candidates were selected for further analysis: Cdr1as, circTulp4, circDtnb, circMagi1, circFat3 and circHomer1. First, relative expression was assessed by qRT-PCR in primary cortical neurons cultured for 1, 7, 14, 21 and 28 DIV (**Figure 13A**). Except for circTulp4, which is constantly expressed throughout neuronal development, the other five circRNA candidates showed an increased expression level upon development. The expression profiles observed recapitulated the data obtained from RNA-sequencing, where the number of readings over the head-to-tail junction was normalized to the total amount of readings (**Figure 13B**).

With the aim of testing whether the expression levels of the six circRNA candidates measured in primary neuronal cultures are representative only of neurons or also of astrocytes, primary astrocytic cultures were prepared and their relative expressions were calculated normalizing to the house-keeping gene *Rpl19* (data was shown as part of Florencia Merino´s master thesis). CircTulp4 is not only the most highly expressed circRNA in neuronal cultures after CDR1as (**Figure 13C**), but also the first candidate belonging to the most representative circular type, protein-coding-derived circRNA. For this reason, I focused on analyzing its function and mechanism of action using a variety of technics that will be presented throughout the Results section.

As revealed by qRT-PCR (**Figure 13D**), circular and linear RNA isoforms of *Tulp4* have similar expression patterns and express at the same levels along neuronal development.

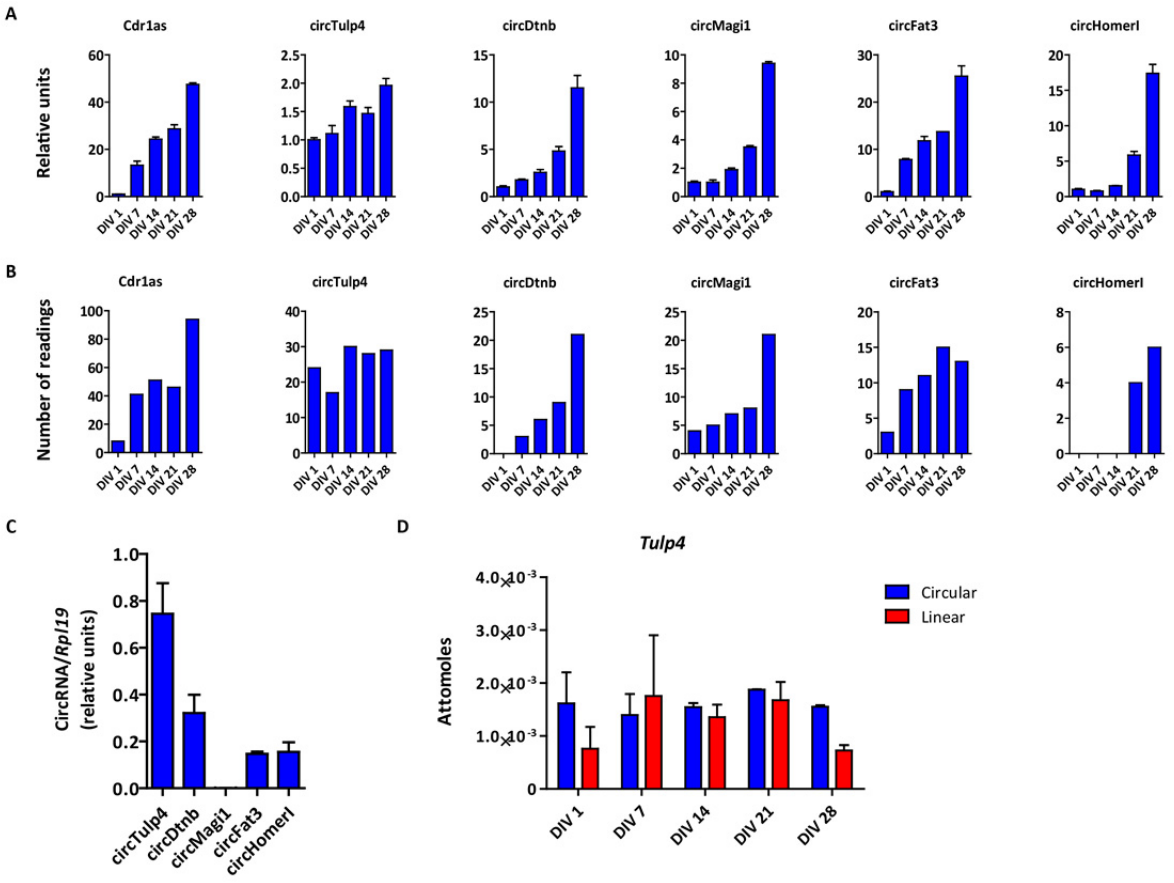

Figure 13. CircTup4 is constantly expressed along neuronal development and is specifically abundant in neurons.
(A) RNA was isolated from primary neuronal cultures at the indicated DIV and relative expression was assessed by qRT-PCR; n = 1 neuronal culture, with samples run per triplicates. While the majority of candidates increased its expression level along neuronal development, circTulp4 displayed a constant, steady expression level. **(B)** Number of readings of circRNA-specific head-to-tail junctions normalized to the total amount of readings confirming the qRT-PCR results. **(C)** Comparison of the expression level of the circRNA candidates in neurons. RNA was isolated from primary neuronal cultures and relative expression was assessed by qRT-PCR; n = 3 independent cultures. CDR1as was taken out of the graph as it is the candidate of another research group. **(A,C)** RNA expression was always normalized to the house-keeping gene *Rpl19*. **(D)** Circular and linear *Tulp4* absolute expression level. RNA was isolated from primary cortical neurons at the indicated DIV; n = 2 independent cultures.

8.1.3 Genetic strategies for studying circRNA function

As for protein-coding genes, the function of circular transcripts can be studied by the use of the two classic genetic approaches: loss-of-function and gain-of-function. In the next subsections, genetic tools designed for selectively regulating circRNA´s expression level are described.

8.1.3.1 CircRNA downregulation

RNA interference is a well-established tool to knockdown the expression of specific genes *in vitro* and *in vivo*. Short hairpin RNA (sh-RNA) constructs targeting mouse circTulp4 head-to-tail junctions (sh-circTulp4) were cloned into the pSUPER.neo+gfp vector (OligoEngine), from which they are expressed under the control of the human polymerase III H1 promoter. Three sh-circRNAs differing only in a couple of nucleotides to the left or right of the head-to-tail junction were designed. A scrambled sh-RNA sequence (sh-scrambled) containing 5 base pair mismatches to any known mouse or human gene served as a control. Silencing efficiency was tested in Neuro-2a cell line by qRT-PCR. As shown in **Figure 14**, the three different sh-RNAs against circTulp4 were equally good at silencing the circular RNA isoform of *Tulp4*, but sh-circTulp4#1 showed a tendency to reduce the linear counterpart. For the following experiments, sh-circTulp4#2 (referred from now on as sh-circTulp4) was selected as downregulating tool.

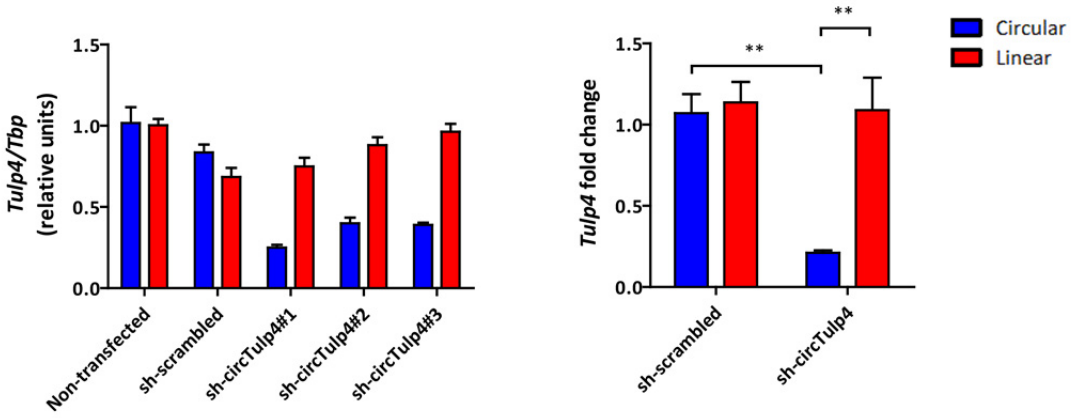

Figure 14. Validation of circTulp4 silencing efficiency by pSUPER constructs in Neuro-2a cell line.
RNA expression was normalized to the house-keeping gene *Tbp*. Left, data are given as mean ± SEM from n = 5 independent cultures. Right, data are given as mean ± SEM from n = 3 independent cultures. RNA expression was also normalized to the transfection efficiency measured by *EGFP* expression. *CircTulp4 expression:* sh-circTulp4, 0.211 ± 0.014 vs sh-scrambled, 1.070 ± 0.117; two-way ANOVA, Bonferroni post-test, t = 4.599, **p < 0.01. *Sh-circTulp4 treatment:* circular, 0.211 ± 0.014 vs linear, 1.090 ± 0.199; two-way ANOVA, Bonferroni post-test, t = 4.703, **p < 0.01.

8.1.3.2 CircRNA overexpression

A construct overexpressing circTulp4 was generated based on the pcDNA3.1(+) Laccase2 MCS exon vector, described and kindly shared by Jeremy Wilusz (Kramer et al., 2015). Briefly, *Drosophila laccase2* gene is known to produce an abundant circRNA both *in vitro* and *in vivo*. Laccase2 MCS exon vector contains a pair of minimal inverted repeats from the

DNAREP1_DM family transposons that are part of the > 9 kb intronic sequences flanking the circularizable *laccase2* exon 2, and an artificial 63 nt exon composed of restriction enzyme sites (see **Figure 15A**). In comparison with "CircRNA Mini Vector" (Liang & Wilusz, 2014), Laccase2 MCS exon vector generates significantly less amount of linear RNA.

For the generation of circTulp4 overexpressing construct (OE-circTulp4), its cDNA sequence was cloned into the multiple restriction site of Laccase2 MCS exon vector. Overexpression of the circular isoform was confirmed in Neuro-2a cell line (see **Figure 15B**).

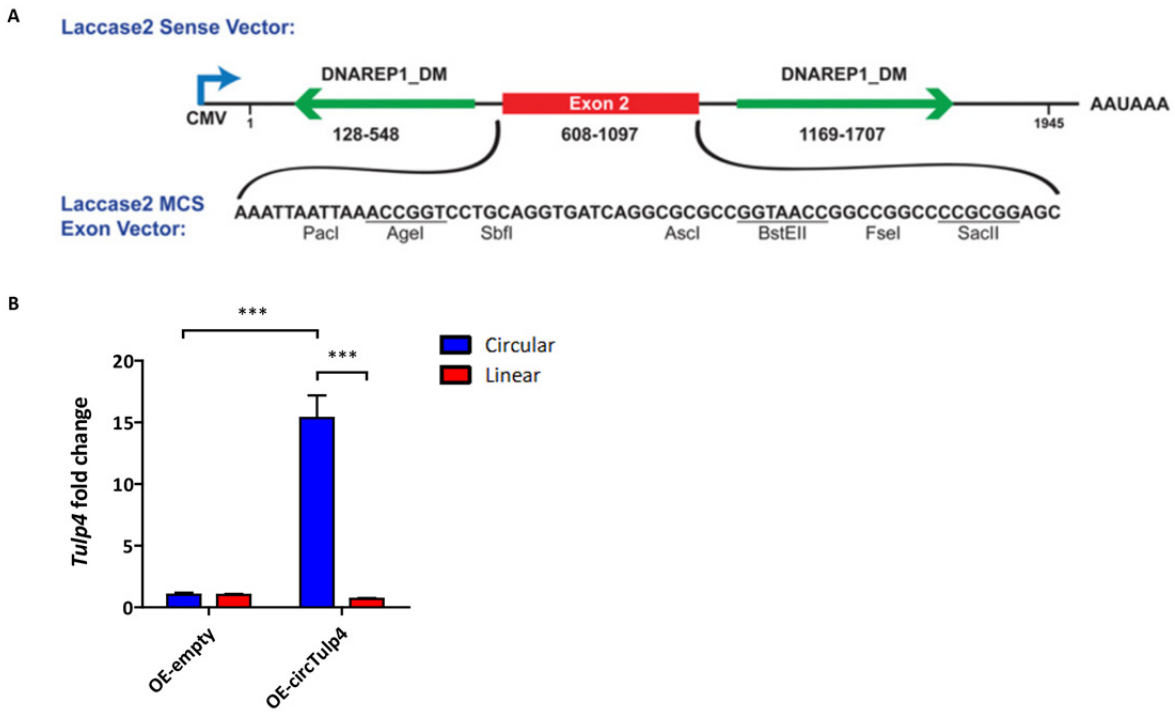

Figure 15. CircRNA expression plasmid for efficient expression in mammalian cells.
(A) The Laccase2 MCS exon vector. From Kramer et al., 2015. **(B)** Efficiency validation of OE-circTulp4 in Neuro-2a cell line. Data are given as mean ± SEM from n = 3 independent cultures. RNA expression was normalized to the house-keeping gene *Tbp* and to the transfection efficiency measured by *EGFP* expression. *CircTulp4 expression:* OE-circTulp4 = 15.35 ± 1.840 vs OE-empty = 1.024 ± 0.160; two-way ANOVA, Bonferroni post-test, t = 10.95, ***p < 0.001. *OE-circTulp4 treatment:* circular = 15.35 ± 1.840 vs linear = 0.698 ± 0.057; two-way ANOVA, Bonferroni post-test, t = 11.20, ***p < 0.001.

8.2 CIRCTULP4 LOCALIZATION IN MATURE NEURONS

Identifying the subcellular localization of an uncharacterized molecule is one of the first steps towards unveiling its function. To this end, a fluorescent *in situ* hybridization (FISH) approach (QuantiGene ViewRNA ISH Cell Assay, Affymetrix) based on the design of an oligo pair probe that specifically recognizes the head-to-tail junction of circTulp4 was chosen. Detection at single-molecule resolution was achieved after several steps of branched DNA signal amplification, hybridization of a labeled probe oligonucleotide conjugated to alkaline phosphatase, and the addition of Fast Red Substrate. To distinguish *bonafide* signal from background noise, a negative control that underwent the entire assay procedure except for adding the labeled probe was included (**Figure 16A**). Additionally, the specificity of the circRNA probe was controlled by regulating the circRNA levels through primary hippocampal neurons transfection with sh-circTulp4 or OE-circTulp4 (**Figure 16B-C**). **Figure 16A** shows that under control conditions circTulp4 is expressed mostly in the soma of mature neurons. In **Figure 16B,** sh-circTulp4 transfected neurons show a decrease in the number of circular molecules when compared with sh-scrambled treated neurons. Accordingly, OE-circTulp4 transfected neurons showed an increment of circTulp4 molecules per soma, while the OE-empty transfected neurons expressed a similar number as the sh-scrambled transfected ones (**Figure 16C**). Unfortunately, due to the high-density of the primary neuronal cultures, it was not possible to distinguish whether circTulp4 is expressed in dendritic processes and, most importantly, specifically in spines.

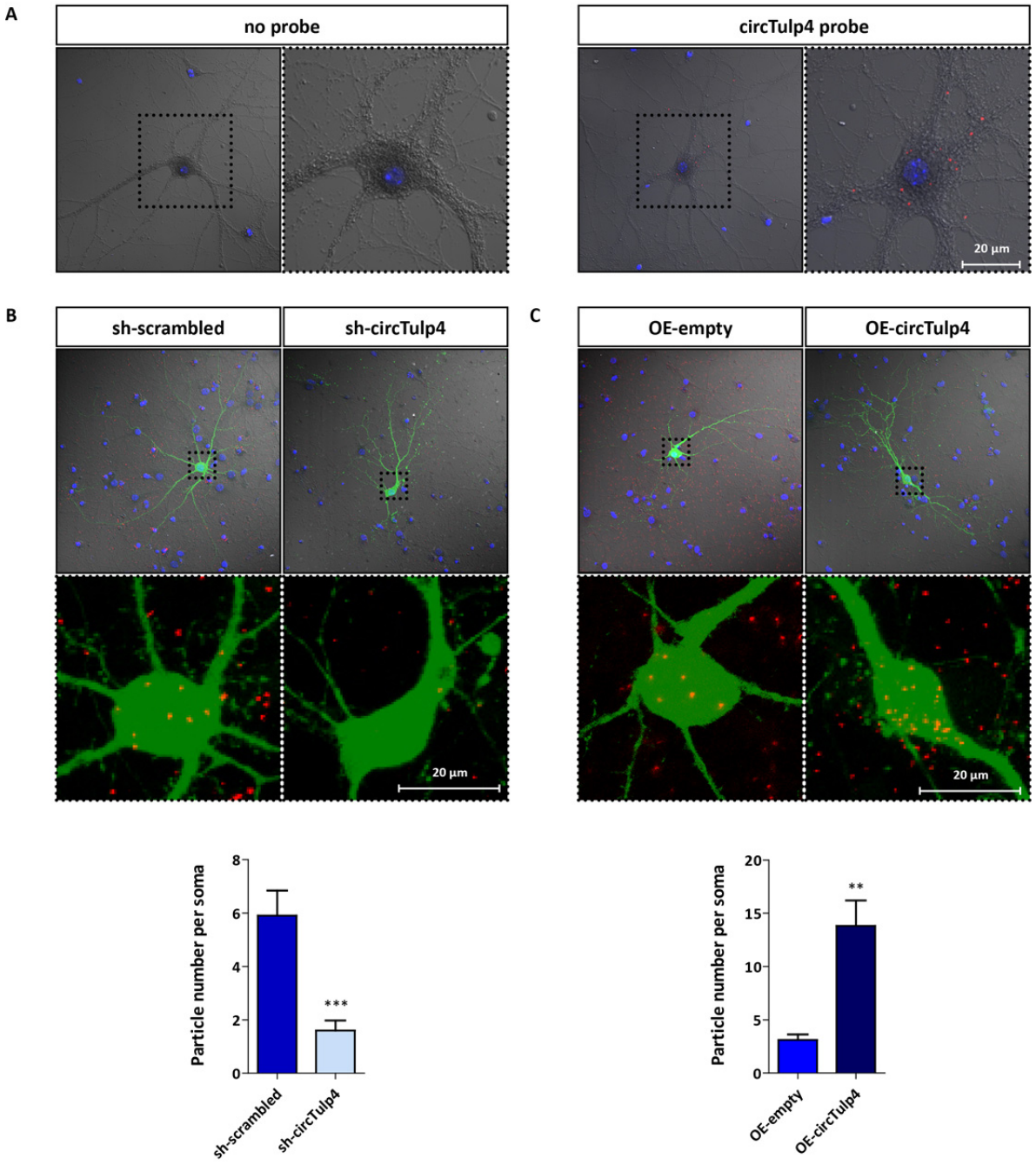

Figure 16. Detection of circTulp4 by FISH in primary hippocampal neurons cultured at high-density.
(A) Differential interference contrast (DIC) photomicrographs of primary WT hippocampal neurons stained with DAPI (blue channel) to visualize cell nuclei. Left, no probe control assay. Right, high-resolution FISH against circTulp4 shows the circular molecule expresses predominantly in the soma of hippocampal neurons. Right panels show detail (dashed-line square insets) in higher magnification. Scale bar represents 20 µm. **(B-C)** Primary hippocampal neurons were transfected at DIV 12 with sh-circTulp4 or OE-circTulp4 constructs to control probe specificity. Upper panels show DIC photomicrographs of GFP (green channel) co-transfected neurons, cell nuclei were stained with DAPI (blue channel) and circTulp4 was detected after addition of fast red substrate (red channel). Lower panels show details in higher magnification. Scale bars represent 20 µm. Data are given as mean ± SEM; Mann-Whitney U test, **p < 0.01, ***p < 0.001; n = 10 neurons from one culture. **(B)** sh-circTulp4 = 1.6 ± 0.371 vs sh-scrambled = 5.9 ± 0.948; U = 4.5, p = 0.0006. **(C)** OE-circTulp4 = 13.8 ± 2.394 vs OE-empty = 3.100 ± 0.526; U = 7, p = 0.0012.

8.3 CIRCTULP4 IS INVOLVED IN AXO-DENDRITIC DEVELOPMENT

As circTulp4 is constantly expressed throughout neuronal development, we set out to study its function starting from a morphological analysis of axonal and neurite outgrowth all through to dendritic development, including spine morphology. Mouse embryo brains were *ex vivo* electroporated with sh-circTulp4 or the sh-scrambled control, hippocampal primary neuronal cultures were prepared and fixed at different developmental time points to evaluate the morphology of transfected neurons. **Figure 17A-B** show the deleterious consequences of downregulating circTulp4 on axonal and neurites development at DIV 3. CircTulp4-deficient neurons displayed a delayed polarization and axonal outgrowth compared to the control neurons. However, these neurons remained viable, showing at DIV 10 a recovery in axonal length, whereas dendritic impairment became more notorious (**Figure 17B**). As an additional developmental point, primary hippocampal neurons were Ca^{2+} transfected at DIV 12 with the pSUPER constructs and spine morphology was evaluated at DIV 21. As shown in **Figure 17C**, no phenotype was detected. (See **Section 8.4.2** for a quantitative analysis).

In order to quantitatively analyze the observed axonal phenotype, *ex vivo* electroporations were repeated; hippocampal neuronal cultures were prepared, fixed at DIV 5, and immunostained with an antibody anti-neurofilament. **Figure 18A** shows circTulp4-deficient neurons displayed a significant increment in the number of axonal branches when comparing to the control, sh-scrambled transfected ones (sh-circTulp4 = 11.41 ± 0.971 vs sh-scrambled = 4.727 ± 0.476; Mann-Whitney U test, U = 550, $p < 0.0001$). Interestingly, no alterations were found in the total axonal length, although a slight reduction in the length of the main axonal shaft was observed (**Figure 18B**).

Figure 17. CircTulp4 regulates early neuronal development.
(A-B) Mouse embryo brains were *ex vivo* electroporated with sh-circTulp4 or the sh-scrambled control; primary hippocampal cultures were prepared and fixed at the indicated DIV. Scale bars represent 50 µm. **(A)** Sh-circTulp4 transfected neurons displayed delayed axonal and neurite outgrowth, as it is observed at DIV 3. **(B)** At a later stage (DIV 10), downregulation of circTulp4 rendered severe impairment in dendritic development. **(C)** DIV 21 sh-circTulp4 transfected neurons did not show any effect on dendritic spine morphology when comparing to sh-scrambled transfected neurons. Scale bar represents 5 µm.

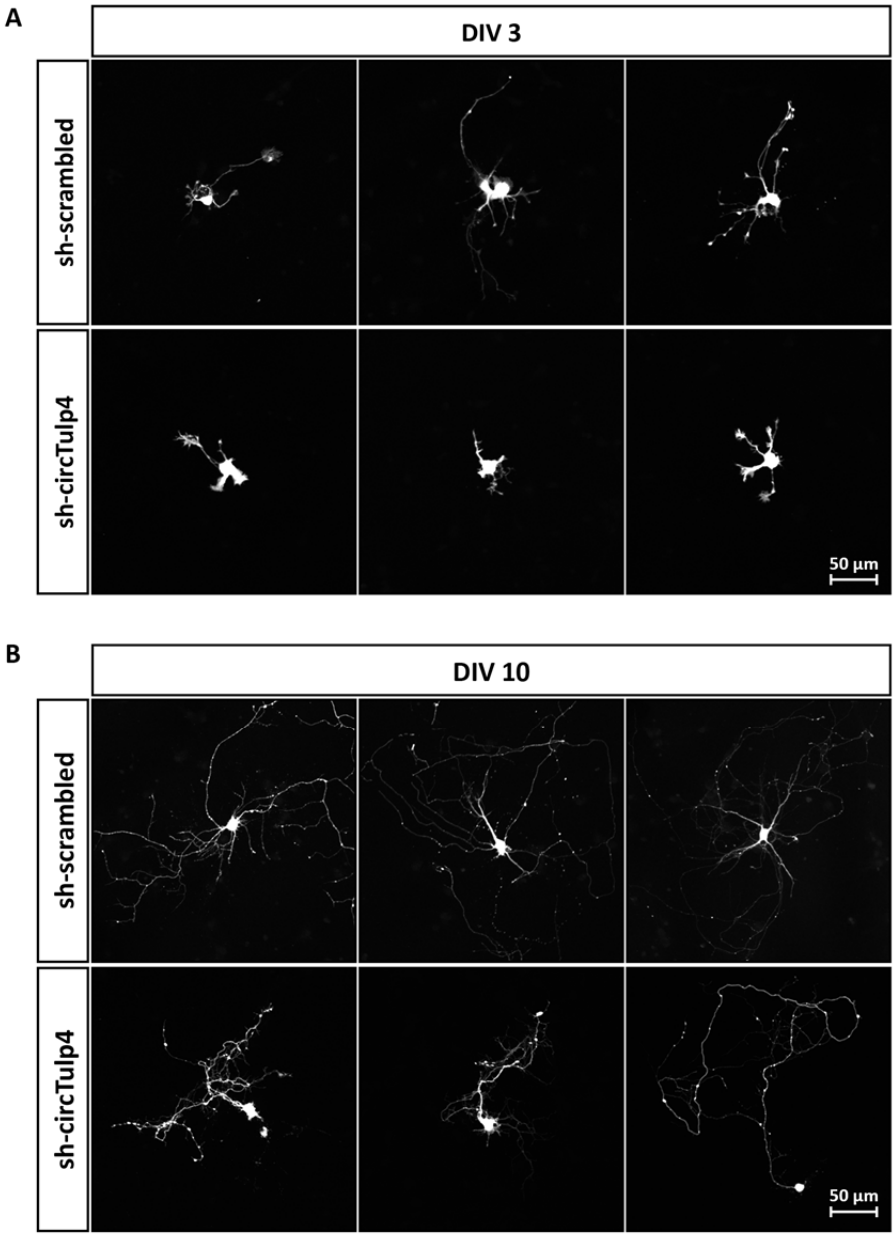
A
DIV 3
sh-scrambled
sh-circTulp4
50 µm
B
DIV 10
sh-scrambled
sh-circTulp4
50 µm
C
sh-scrambled
sh-circTulp4
5 µm

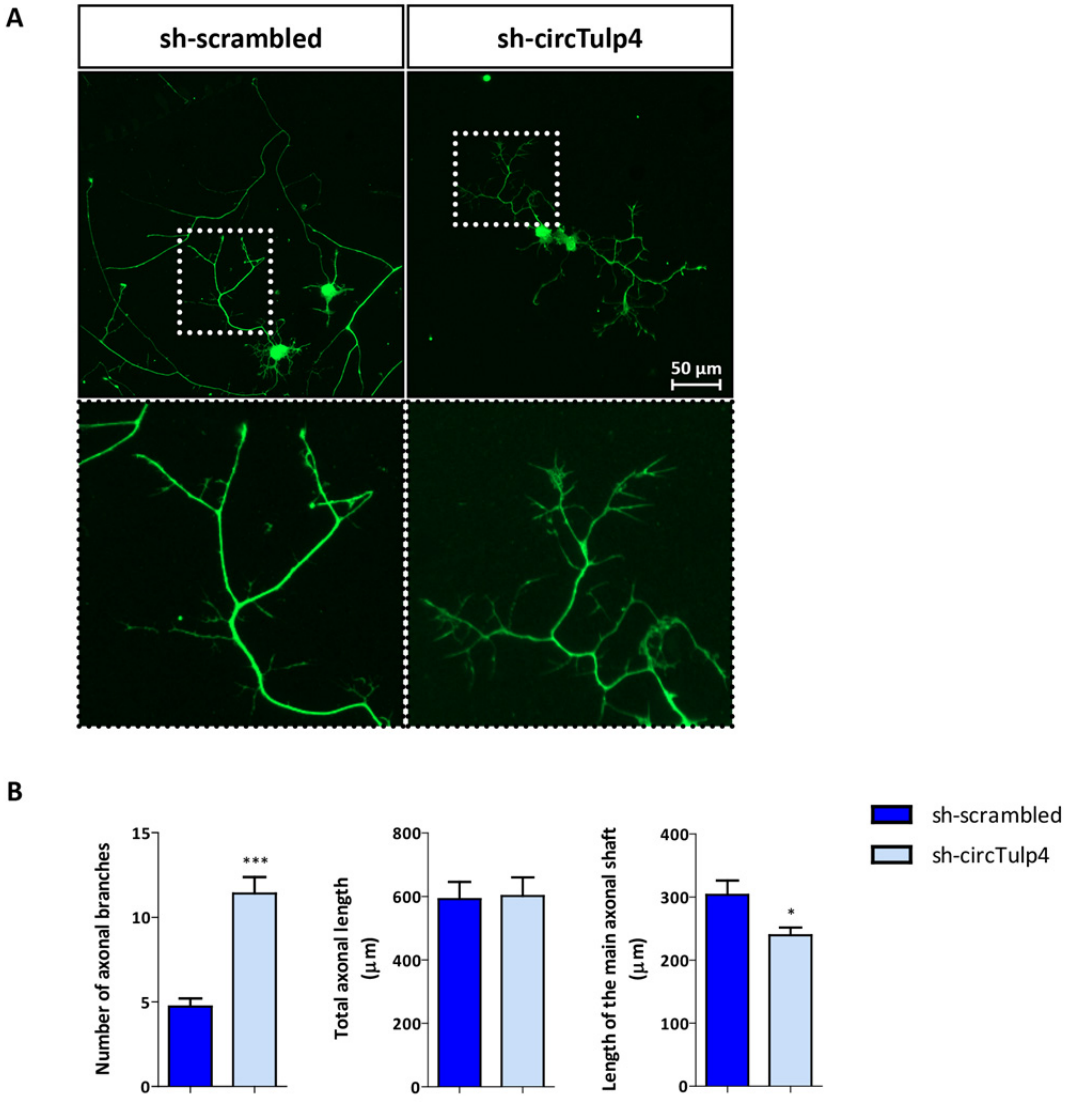

Figure 18. Downregulation of circTulp4 increases axonal branching without affecting total axonal length.
(A-B) Mouse hippocampal neurons were *ex vivo* electroporated before plating with sh-circTulp4 or the sh-scrambled control. Neurons were fixed at DIV 5 and immunostained with an antibody α-neurofilament. **(A)** Morphological characterization of circTulp4-deficient neurons in comparison with control neurons. Lower panel shows details (dashed-line square insets) in higher magnification. Scale bars represent 50 µm. **(B)** Quantification of axonal branching and length revealed that sh-circTulp4 transfected neurons have a significant increment of axonal branching number without alterations in the total axonal length (sh-circTulp4 = 601.7 ± 58.83 µm vs sh-scrambled = 591.4 ± 54.91 µm; U = 734.5, ns). The main axonal shaft length, however, remained slightly reduced (sh-circTulp4 = 239.5 ± 12.09 µm vs sh-scrambled = 303.7 ± 22.39 µm; U = 973.5, p = 0.0228) in comparison to sh-scrambled transfected neurons. Data are given as mean ± SEM; Mann-Whitney U test, *p < 0.05, ***p < 0.0001; n = 45 neurons from three independent experiments.

8.4 CIRCTULP4 REGULATES SYNAPTIC ACTIVITY IN PRIMARY NEURONAL CULTURES

To assess the function of circTulp4 in synaptic transmission, a collaboration with Dr. Antonia Marín-Burgin at the Biomedicine Research Institute of Buenos Aires (IBioBA-MPSP) was established.

8.4.1 CircTulp4 downregulation alters excitatory neurotransmission

In order to electrophysiologically characterize the effects of downregulating circTulp4 in culture, DIV 12 primary hippocampal neurons were Ca^{2+} transfected with sh-circTulp4 or the sh-scrambled control, and patch-clamp recordings were performed between DIV 21-25. The experimental design allowed us to distinguish the pre-synaptic WT neuron from the post-synaptic sh-circTulp4 transfected neuron (co-transfected with a fluorescent protein-expressing vector), in which AMPAR-mediated miniature post-synaptic currents were recorded. Sh-circTulp4 transfected neurons showed a strong reduction in the frequency of miniature excitatory post-synaptic currents (mEPSC) when compared to control cells (sh-circTulp4 = 1.492 ± 0.392 Hz vs sh-scrambled = 5.125 ± 0.877 Hz; Mann-Whitney U test, U = 8, p = 0.0016). However, no significant alteration in amplitude values was observed, suggesting that the drop in the frequency is a consequence of a decreased number of functional synapses. Importantly, no differences in miniature inhibitory post-synaptic currents (mIPSC) were registered, indicating a specific effect of circTulp4 on excitatory neurotransmission (**Figure 19**).

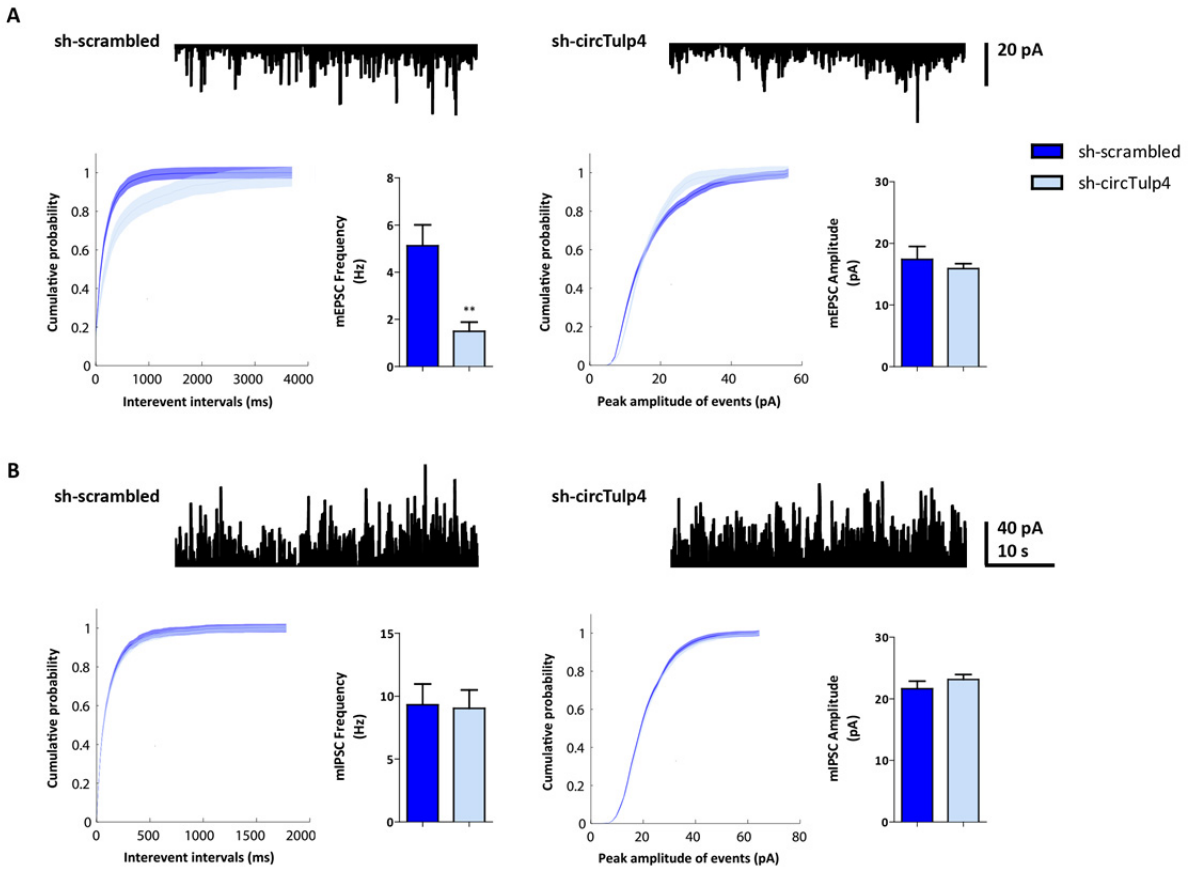

Figure 19. Downregulation of circTulp4 in primary neuronal cultures reduces the frequency of AMPAR-mediated mEPSC.
Mouse primary hippocampal neurons were transfected at DIV 12 with sh-circTulp4 or the sh-scrambled control and electrophysiological patch-clamp recordings were done between DIV 21-25 in collaboration with Dr. Marín-Burgin at the IBioBA-MPSP. **(A-B)** Data are given as mean ± SEM; Mann-Whitney U test, **p < 0.01; for mEPSCs n = 13 neurons for sh-circTulp4, n = 8 neurons for sh-scrambled; for mIPSCs n = 11 neurons for sh-circTulp4, n = 8 neurons for sh-scrambled. **(A)** Top, representative recordings of AMPAR-mediated mEPSCs illustrating the effect of downregulating circTulp4 (right). A strong reduce in mEPSC frequencies was observed in sh-circTulp4 transfected neurons compared to control neurons. No significant changes were recorded in the amplitude of mEPSCs (sh-circTulp4 = 15.91 ± 0.809 pA vs sh-scrambled = 17.39 ± 2.089 pA; U = 51, ns). **(B)** Top, representative recordings of mIPSCs showing the lack of effect of downregulating circTulp4 on mIPSCs in the same cells (*Frequency:* sh-circTulp4 = 9.020 ± 1.473 Hz vs sh-scrambled = 9.314 ± 1.659 Hz; U = 40, ns/ *Amplitude:* sh-circTulp4 = 23.12 ± 0.815 pA vs sh-scrambled = 21.62 ± 1.221 pA; U = 31, ns). These results suggest that circTulp4 exerts a specific role in excitatory neurotransmission.

8.4.2 CircTup4 downregulation reduces the number of pre-synaptic excitatory punctae on spines

A strong reduction in mEPSCs frequency is generally interpreted as a decreased probability of pre-synaptic release, or as a reduction in the number of synapses. As in our electrophysiological experiment the pre-synaptic neuron is wild-type, the phenotype observed in sh-circTulp4 transfected neurons can be explained by: (i) a reduction in the number of spines; (ii) a reduction

in the number of excitatory pre-synaptic contacts or; (iii) an increment in the number of silent synapses. In order to answer whether circTulp4 regulates excitation by regulating numbers of glutamatergic inputs, first the number of dendritic spines was quantified. For that, primary hippocampal neurons were Ca^{2+} transfected at DIV 13 with sh-circTulp4 or the sh-scrambled control, plus a GFP expressing vector to visualize dendritic protrusions, and were evaluated at DIV 21. As observed in **Figure 20A-B**, circTulp4 downregulation did not alter spine numbers when compared to control neurons. Next, the number of excitatory inputs was examined (see **Section 7.7** for quantitative analysis description). Immunostaining with an α-VGlut1 antibody revealed that the number of excitatory pre-synaptic punctae was decreased in sh-circTulp4 transfected neurons, and this decrease was explained by a specific reduction of pre-synaptic contacts on spines (sh-circTulp4 = 0.678 ± 0.022 vs sh-scrambled = 0.890 ± 0.028; unpaired t-test, $t_{(78)}$ = 5.875, $p < 0.0001$) and not on dendritic shafts (**Figure 20B**).

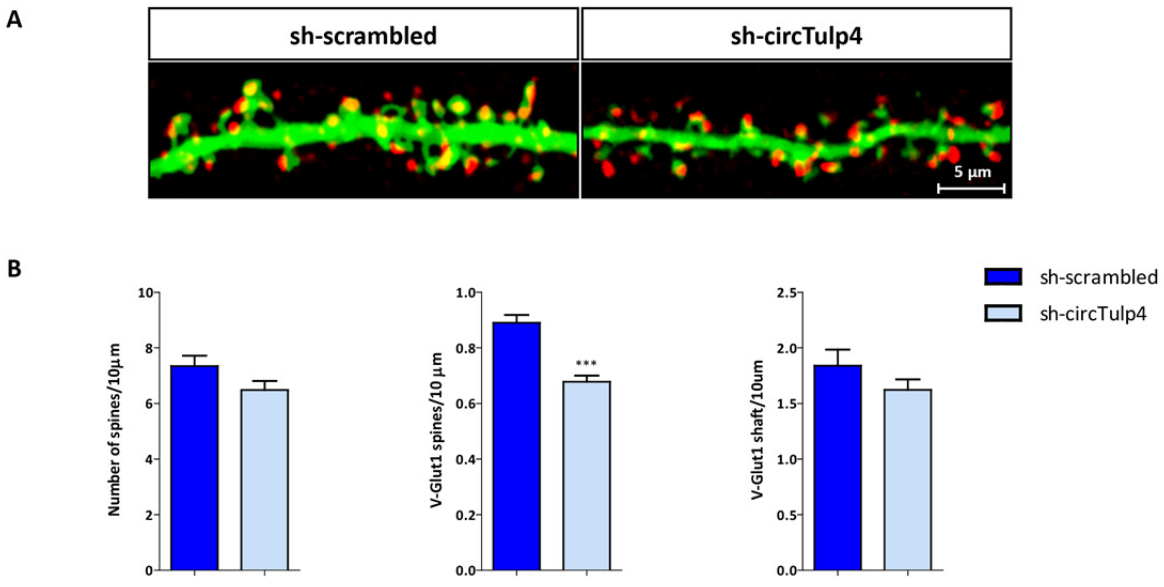

Figure 20. Downregulation of circTulp4 in culture reduces the number of pre-synaptic excitatory punctae on spines.
Mouse hippocampal neurons were transfected at DIV 13 with sh-circTulp4 or the sh-scrambled control, and quantitative analysis of dendritic spine density and of pre-synaptic excitatory punctae (VGlut1) was carried out at DIV 21. **(A)** Immunostaining against VGlut1. Cultures were co-transfected with a GFP expressing vector (green channel) and labeled with an α-VGlut1 antibody (red channel) to visualize only excitatory pre-synaptic contacts (merge, yellow). Scale represents 5 µm. **(B)** Downregulation of circTulp4 did not alter synaptic density (left, sh-circTulp4 = 6.483 ± 0.326 vs sh-scrambled = 7.343 ± 0.378; unpaired t-test, $t_{(78)}$ = 1.720, ns), but specifically diminished the number of excitatory pre-synaptic contacts on spines (middle) and not on dendritic shafts (right). Data are given as mean ± SEM; unpaired t-test, ***$p < 0.0001$; n = 40 neurons derived from three independent neuronal cultures.

8.5 WHAT IS THE MECHANISM OF ACTION OF CIRCTULP4?

Given the general low expression of circRNAs, we reasoned that a biological effect could be exerted through a process that involves an amplification mechanism. The amplification could be achieved, for instance, by acting as a scaffold for the activation of some enzymes. Another possible mechanism is that some circRNAs act as templates for the translation of peptides. Regarding the latter, circRNAs have been demonstrated to be translatable both *in vitro* and *in vivo* (Abe et al., 2015; Wang & Wang, 2015), and in the past few years direct evidence of endogenous translation has been reported (Legnini et al., 2017; Pamudurti et al., 2017; Yang et al., 2018; Yang et al., 2017; Zhang et al., 2018a; Zhang et al., 2018b).

8.5.1 CircTulp4 could serve as a translational template

A circRNA-specific open reading frame (ORF) is found in the sequence of circTulp4 (named as TULP4-95aa). Of note, this hypothetic peptide shares the start codon with its hosting gene, but a distinct C-terminus for TULP4-95aa appears upon reading over the head-to-tail junction (see **Figure 21A**). To assess the existence of TULP4-95aa *in vivo*, first an anti-TULP4 antibody (Aviva System Biology) designed against the shared N-terminus of TULP4 and TULP4-95aa was tested. Protein extracts derived from primary neuronal cultures along development and from different mouse brain tissues at diverse developmental points failed to show a specific signal (data not shown).

As an alternative approach, and in order to clearly distinguish between the hypothetic TULP4-95aa and the TULP4-1547aa full-length protein, the specific circTulp4 C-terminus was targeted for endogenous HA-tag labeling using CRISPR technology (**Figure 21A**). For that, single-cell labeling of endogenous proteins by CRISPR/Cas9-mediated HDR (SLENDR) (Mikuni et al., 2016) was used. Briefly, a sgRNA expressing plasmid, Cas9 expressing plasmid, and a single-stranded donor oligonucleotide (ssODN) were *in utero* electroporated into mouse embryo brains (E 14-15). **Figure 21B** shows α-HA-tag immunostained brains of six-week-old pups. In the upper panel, GFP co-transfected neurons are observed. The lower panels are a blow-up showing the first evidence that circTulp4 could be endogenously translated.

A drawback of the SLENDR technique is the impossibility to get enough protein material to assess TULP4-95aa by Western Blot (WB). Stewart-Ornstein & Lahav were designing a family of plasmids that upon PCR amplification serve as double-stranded donor templates to express fusion proteins after HDR (Stewart-Ornstein & Lahav, 2016). As neurons, non-replicating post-

mitotic cells, do not count with the homologous recombination machinery, Neuro-2a cell line was used. Unfortunately, and perhaps due to the short 40 bp homology arms, this approach showed to be unsuccessful in our hands.

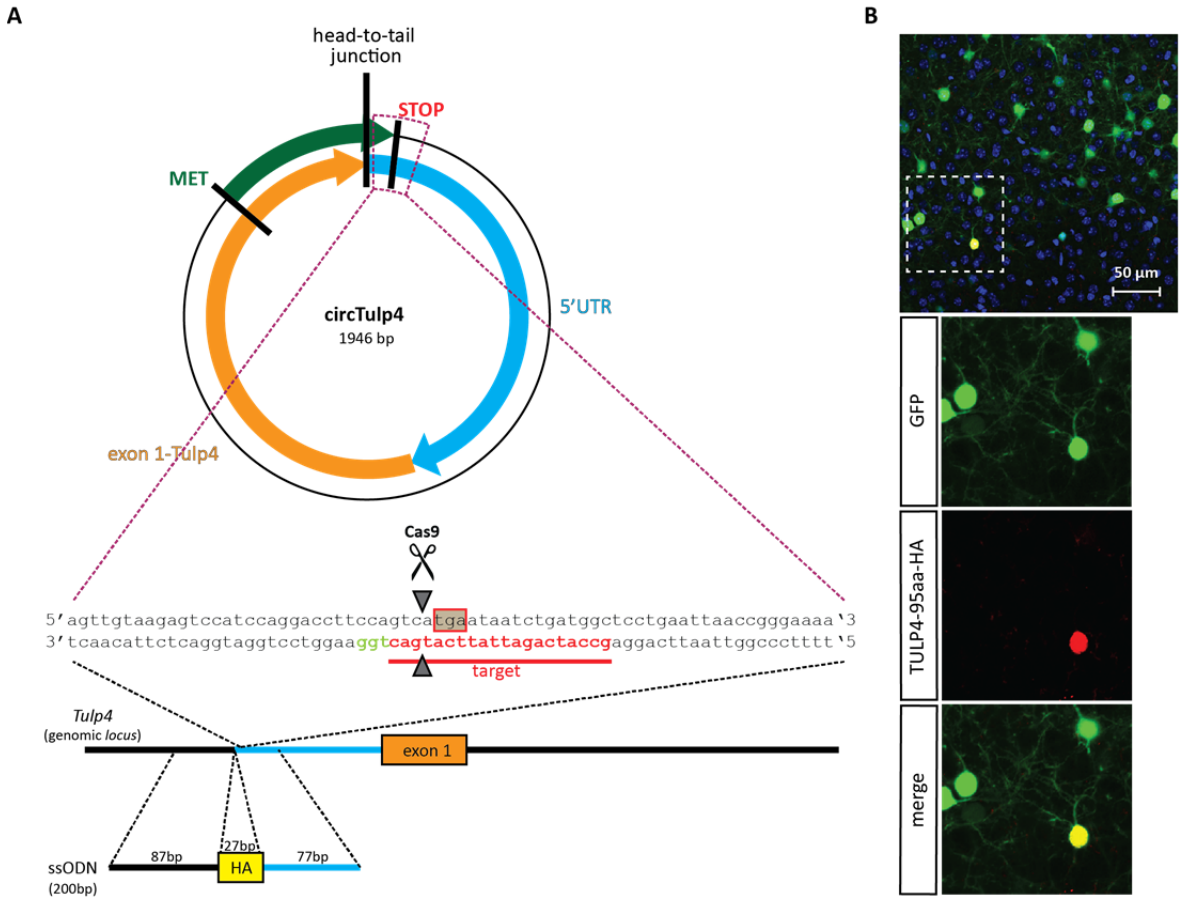

Figure 21. SLENDR strategy for testing whether circTulp4 acts as a template for translation.
(A) Diagram of circTulp4 and circTulp4-derived peptide (TULP4-95aa) depicting the shared start codon (MET) with *Tulp4*-derived protein and the specific stop codon (STOP) generated upon reading over the head-to-tail junction. Lower part: graphical representation of mouse *Tulp4* genomic *locus* showing the target site for Cas9, sgRNA and ssODN. **(B)** Mouse embryo brains (E 14-15) were *in utero* electroporated with CRISPR tools and a GFP expressing plasmid as a transfection control. Six-week-old pups brains were dissected and immunostained with an antibody α-HA-tag (red channel). The upper panel shows transfected cortical neurons (green channel). Scale bar represents 50 µm. Lower panels show a blow-up of the dashed-line square inset, depicting that circTulp4 could be endogenously translated (merge, yellow).

As a second tactic, a donor vector bearing ~1 Kb homology arms and a floxed geneticin-resistant cassette for clonal selection was designed to introduce an HA-tag in the N-terminus of TULP4. Upon correct HDR, TULP4-1547aa full-length protein should be distinguishable from the shorter TULP4-95aa by Western Blot. As shown in **Figure 22**, a band corresponding to the HA-tagged TULP4 full-length protein, but no band corresponding to the tagged TULP4-95aa was observed in Neuro-2a protein extracts 24 h post-transfection, without selection.

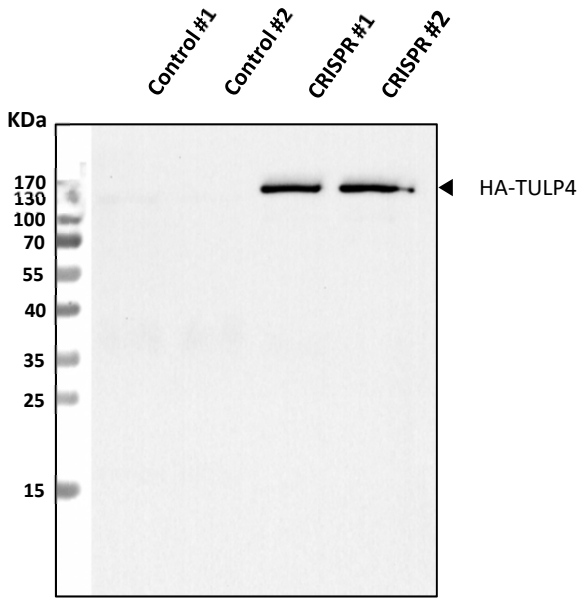

Figure 22. HA-tagged TULP4 full length-protein is expressed in CRISPR transfected Neuro-2a cells. Western Blot analysis of protein extracts from WT (control) and CRISPR transfected (CRISPR) Neuro-2a cells subjected to immunoblotting with an α-HA-tag antibody. Neuro-2a cells were transfected with a Cas9 expressing plasmid, a sgRNA expressing plasmid and a donor vector that upon HDR introduces a HA-tag to the N-terminus of TULP4. 24h post-transfection, cells were harvested, protein was extracted, and the WB was performed.

Reasoning that the above outcome could be due to the low efficiency associated to cap-independent translation, two parallel strategies were initiated. First, a clonal selection process in CRISPR transfected Neuro-2a cells to enriched the protein sample in cells that have incorporated the tag through HDR and by that increase WB sensitivity. Second, a collaboration with Prof. Dr. Christoph Turck at the Max-Planck-Institute for Psychiatry was established to analyze WT mouse samples by mass spectrometry in search of the hypothetical TULP4-95aa. In addition, arguing that neuron-specific protein factors could be required for circTulp4 translation, mouse embryonic stem cells (mESCs) were CRISPR-edited using the *Tulp4* N-terminus tagging donor vector.

Repeated clonal selection by limiting dilution in Neuro-2a cells was unsuccessful in our hands; no clone bearing only the desired mutations was obtained. On the other hand, mESCs were successfully transfected with the same CRISPR elements used for Neuro-2a cells. Upon clonal selection and genotyping, three clones with the correct HDR event were identified (data not shown). However, the high antibody background noise did not allow us to detect the ~11 KDa HA-tagged TULP4-95aa peptide. For mass spectrometry, WT mouse hippocampal lysates were analyzed using three synthetic predicted circTulp4-derived peptides as standards. None of the three target sequences was identified (data not shown).

8.6 GENERATION OF AN ENGINEERED MOUSE MODEL TO STUDY CIRCTULP4 ROLE *IN VIVO*

The results described in **Section 8.3** and **Section 8.4** confirm the relevance of circTulp4 in cell culture systems and *ex vivo* experiments. In order to unveil the actual physiological role of circTulp4, we set out to generate the first murine model of a circRNA depletion. For that, a CRISPR-based strategy was designed, the generation of a full knockout mouse model based on the specific depletion of the circular isoform of *Tulp4* gene through direct mutation of the canonical splice acceptor site.

Before evaluating the effects of depleting circTulp4 in an *in vivo* model, the expression of circular and linear isoforms of *Tulp4* was measured by qRT-PCR in various wild-type C57Bl6/N mouse tissues. **Figure 23** shows the expression of both RNA isoforms normalized to the house-keeping gene *Rpl19*. Interestingly, circTulp4 levels were found to be higher not only in brain-derived regions, as it was observed before by RNA-sequencing (Rybak-Wolf et al., 2015), but also in eyes. These results make us speculate that circTulp4 expression might be circumscribed to nervous tissue, probably being specifically expressed in the retina. Further experiments need to be performed to test this hypothesis.

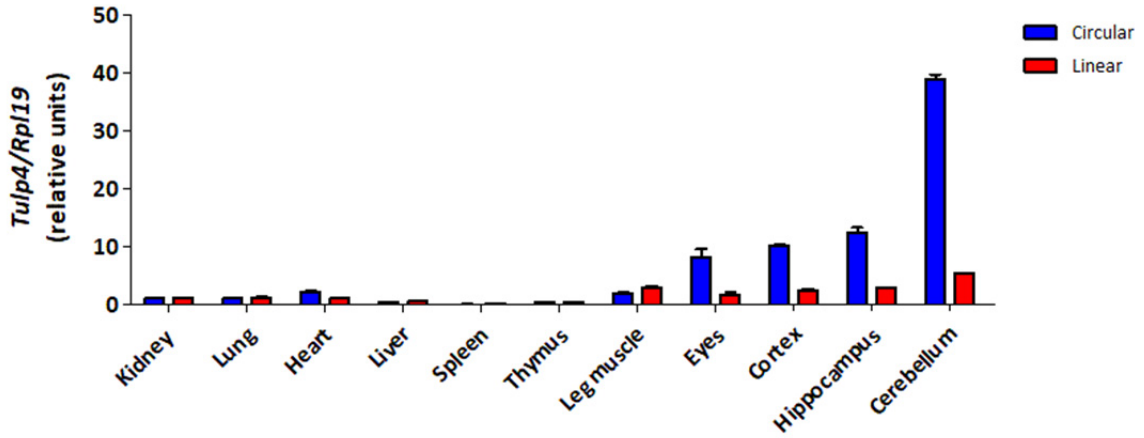

Figure 23. CircTulp4 expression is enriched in mouse brain tissues and eyes.
Circular and linear isoforms expression level of *Tulp4* gene were measured in various WT C57Bl6/N tissues by qRT-PCR, normalized to the house-keeping gene *Rpl19* and arbitrarily normalized to the value of circTulp4 in kidney. Data are given as mean ± SEM; n = 2 mice.

With the aim of generating a specific knockout mouse model for the circular transcript of *Tulp4*, the splice acceptor (SA) site involved in circTulp4 biogenesis was targeted for mutagenesis. As shown in **Figure 24A**, circTulp4 sequence consists of exon 1 of the major linear transcript variant of *Tulp4* gene (ENSMUST00000039655.2) and its 5'UTR. As a first step towards the development of a KO mouse, *Tulp4* 5'UTR was analyzed with MATInspector software in search of transcription factor binding sites (TFBSs) which mutagenesis could interfere in the biogenesis of the different RNA isoforms of *Tulp4*. **Table 10** shows the outcome of the *in silico* analysis, where two different TFBSs were overlapping with the SA site of circTulp4, namely: Alternative splicing variant of FOXP1, activated in ESCs; and Binding site for a Pbx1/Meis1 heterodimer. Since the exchange of the two target-bases does not modify the core sequences of the two TFBSs, it is unlikely to affect their binding probability to this genomic position. Therefore, the generation of an animal model of depletion of circTulp4 via this approach was continued.

After verifying by DNA-sequencing *Tulp4* genomic DNA sequence, sgRNAs were designed (http://crisr.mit.edu/), and four were selected according to their score number for further cleavage efficiency testing in Neuro-2a cell line (data not shown). From this testing, two sgRNAs were selected for the *in vivo* strategy and ssODNs were designed accordingly. C57Bl6/N mouse pronuclei were injected with a synthetic sgRNA, Cas9 enzyme plus Cas9 mRNA, and a ssODN that upon HDR replaces the canonical splicing acceptor site AG by TC. One additional mutation was added to the PAM site to avoid ssODN recognition and cleavage by Cas9 (see **Figure 24B**). Given the high efficiency of Cas9 double-strand breaks, seven out of fourteen pups born presented indels, and one pup (#5) happened to be a mosaic founder (**Figure 24C,** upper panel). TOPO subcloning of genotyping PCR products derived from pup #5 showed the existence of at least one allele with the correct three point mutations (**Figure 24C,** lower panel).

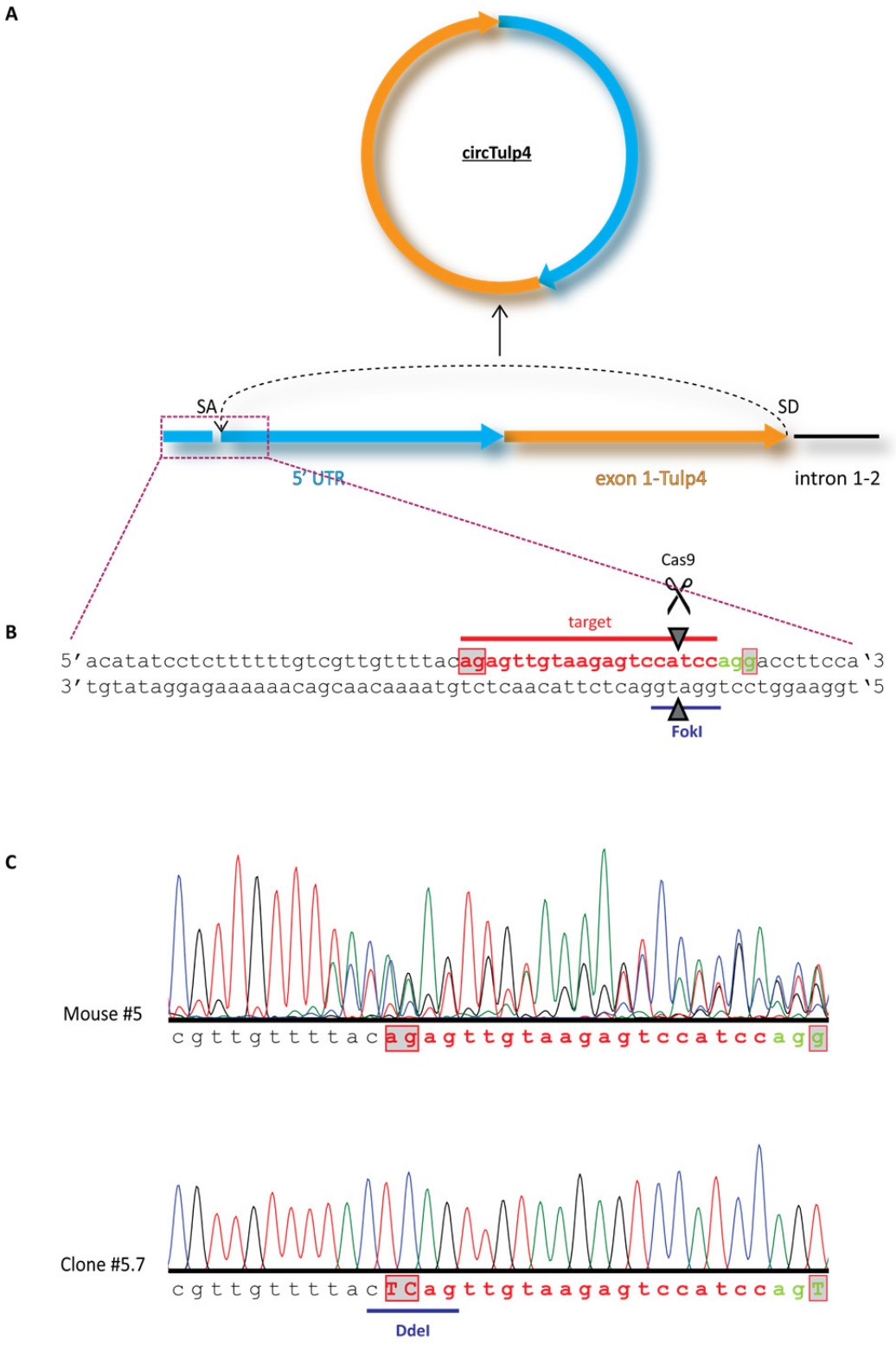

Figure 24. Generation of circTulp4^{KO} mouse model.
(A) Diagram depicting circTulp4 genomic DNA sequence and the splicing sites involved in its biogenesis. SA: splice acceptor site; SD: splice donor site. **(B)** Fragment of the ssODN used as repair template highlighting the sgRNA (sgRNA#1) and desired mutations introduced by the approach (red boxes). FokI: restriction site that disappears upon efficient Cas9 cutting. **(C)** DNA-sequencing results for the mosaic founder mouse #5 and of the DH5α clone #5.7 generated by TOPO subcloning the PCR products derived from founder mouse. Lower panel shows that at least one allele contains the desired three point mutations. DdeI: restriction site that appears upon AG to TC base exchange (used for mouse line genotyping). (Pronuclei microinjections were done in

collaboration with Dr. Florian Giesert at the Institute of Developmental Genetics (IDG), Helmholtz-Zentrum München).

Table 10. *Tulp4* 5'UTR sequence analysis. The 5' untranslated region of mouse *Tulp4* gene was analyzed for potential transcription factor binding sites using MatInspector Release 8.2 (MatBase Version 9.4). Opt: optimized matrix similarity; "from-to": indicates the nucleotide position where the potential TFBS was found; sim: similarity. Highlighted in red the canonical splice acceptor sequence of circTulp4 included in two TFBSs. (MatInspector analysis was done in collaboration with Dr. Dietrich Trümbach at the Institute of Developmental Genetics (IDG), Helmholtz-Zentrum München).

Family/matrix	Detailed Matrix Information	Opt.	From-to	Strand	Core sim.	Matrix sim.	Sequence (capitals: core sequence)
V$POU3F3.01	POU class 3 homeobox 3 (POU3F3), OTF8	0,81	34-48	-	1	0,847	tatatGCATgtgtgt
V$OCT3_4.02	POU domain, class 5, transcription factor 1	0,88	32-50	-	1	0,929	tatatatGCATgtgtgtgt
V$POU3F3.01	POU class 3 homeobox 3 (POU3F3), OTF8	0,81	37-51	+	1	0,892	cacatGCATatatac
V$CABL.01	Multifunctional c-Abl src type tyrosine kinase	0,97	88-98	-	1	0,976	aaAACAacgac
V$FOXP1_ES.01	Alternative splicing variant of FOXP1, activated in ESCs	1	87-103	-	1	1	tctgtaaAACAacgaca
V$DMP1.01	Cyclin D-interacting myb-like protein, DMTF1 - cyclin D binding myb-like transcription factor 1	0,82	111-125	-	1	0,824	gtcctGGATggactc
V$CP2.02	LBP-1c (leader-binding protein-1c), LSF (late SV40 factor), CP2, SEF (SAA3 enhancer factor)	0,84	116-134	-	1	0,861	gACTGgaaggtcctggatg
V$NFKAPPAB65.01	NF-kappaB (p65)	0,87	119-133	+	1	0,898	ccaggaccTTCCagt
V$NRF2.01	Nuclear respiratory factor 2	0,86	118-138	-	1	0,87	tcatgactGGAAggtcctgga
V$SOX9.06	SRY (sex-determining region Y) box 9, dimeric binding sites	0,68	120-142	+	1	0,754	caggaccttccaGTCAtgaataa
V$PIT1.01	Pit1, GHF-1 pituitary specific pou domain transcription factor	0,92	133-147	-	1	0,94	tcagaTTATtcatga
V$GC_SBE.01	GC-rich Smad1/5 binding element	0,94	146-156	+	1	0,953	gatggCTCCtg
V$LTSM.01	LTSM elements with 7 bp spacer	0,82	145-159	-	1	0,824	attcaggagcCATCa
V$PROP1.01	Prophet of Pit 1, PROP paired-like homeobox 1	0,84	146-166	-	1	0,857	ccggttAATTcaggagccatc
V$HOXB4.01	Homeobox B4 / Hox-2phi	0,84	148-166	-	1	0,855	ccggttAATTcaggagcca
V$NKX25.02	Homeo domain factor Nkx-2.5/Csx, tinman homolog low affinity sites	0,88	148-166	-	1	0,899	ccggtTAATtcaggagcca
V$PCE1.01	Photoreceptor conserved element 1	0,89	150-166	-	1	0,904	ccggtTAATtcaggagc
V$LBX2.01	Ladybird homeobox 2	0,89	149-167	+	1	0,902	ggctcctgAATTaaccggg
V$LHX1.01	LIM homeobox 1	0,82	147-169	+	1	0,829	atggctcctgAATTaaccgggaa
V$NKX61.01	NK6 homeobox 1	0,91	152-166	-	1	0,914	ccggTTAAttcagga

V$HMGA.01	HMGA family of architectural transcription factors (HMGA1, HMGA2)	0,88	148-170	-	1	0,892	tttcccggttAATTcaggagcca
V$HOXC4.01	Homeobox C4 / Hox-3epsilon	0,84	151-169	+	1	0,864	ctcctgAATTaaccgggaa
V$CART1.02	Cartilage homeo protein 1	0,84	151-171	+	1	0,862	ctcctgAATTaaccgggaaaa
V$TST1.01	POU-factor Tst-1/Oct-6	0,9	153-171	+	1	0,962	cctgaATTAaccgggaaaa
V$OVOL1.01	Zinc finger transcription factor OVO homolog-like 1	0,8	155-169	-	1	0,814	ttcccgGTTAattca
V$GRHL1.01	Grainyhead-like 1 (LBP32, MGR, TFCP2L2)	0,86	158-170	-	1	0,892	tttcccGGTTaat
V$E2F.01	E2F, involved in cell cycle regulation, interacts with Rb p107 protein	0,75	158-174	+	1	0,856	attaaccggGAAAacaa
V$FOXP1_ES.01	Alternative splicing variant of FOXP1, activated in ESCs	1	163-179	+	1	1	ccgggaaAACAaacata
V$CABL.01	Multifunctional c-Abl src type tyrosine kinase	0,97	168-178	+	1	0,973	aaAACAaacat
V$HFH3.01	HNF-3/Fkh Homolog 3 (FOXI1, Freac-6)	0,97	166-182	+	1	0,98	ggaaaacAAACatatca
V$LACTOFERRIN.01	Lactotransferrin and delta-lactoferrin, growth-inhibiting protein 12	0,89	180-188	-	1	0,984	gGCACttga
V$NKX25.01	Homeo domain factor Nkx-2.5/Csx, tinman homolog, high affinity sites	1	176-194	+	1	1	catatcAAGTgccatttga
V$SMARCA3.01	SWI/SNF related, matrix associated, actin dependent regulator of chromatin, subfamily a, member 3	0,96	185-195	+	1	0,985	tgCCATttgaa
V$CHR.01	Cell cycle gene homology region (CDE/CHR tandem elements regulate cell cycle dependent repression)	0,92	187-199	+	1	0,931	ccatTTGAagact
V$HSF1.04	Heat shock factor 1	0,76	109-133	+	0,973	0,809	aagagtccatccaggaccTTCCagt
V$HSF1.01	Heat shock factor 1	0,84	118-142	-	0,952	0,844	ttattcatgactGGAAggtcctgga
V$TCFCP2L1.01	Transcription factor CP2-like 1 (LBP-9)	0,87	150-168	-	0,927	0,872	tcCCGGttaattcaggagc
V$HSF1.03	Heat shock factor 1	0,76	143-167	+	0,868	0,787	tctgatggctccTGAAttaaccggg
V$PIT1.01	Pit1, GHF-1 pituitary specific pou domain transcription factor	0,92	38-52	-	0,855	0,953	tgtatATATgcatgt
V$PIT1.01	Pit1, GHF-1 pituitary specific pou domain transcription factor	0,92	41-55	+	0,855	0,952	tgcatATATacatat
V$USF.04	Upstream stimulating factor 1/2	0,9	175-191	-	0,851	0,911	aatggCACTtgatatgt
V$PAX8.01	PAX 2/5/8 binding site	0,88	119-147	-	0,85	0,901	tcagattattcATGActggaaggtcctgg
V$YB1.01	Y box binding protein 1, has a preference for binding ssDNA	0,88	4-16	+	0,818	0,888	ttgatTTGCtact

V$MYBL2.01	v-myb myeloblastosis viral oncogene homolog (avian)-like 2 (BMYB), dimeric binding site	0,75	160-180	+	0,814	0,774	taaccgggaAAACaaacatat
V$CUX1.01	Cut-like homeobox 1, dimeric binding site	0,69	135-157	-	0,813	0,754	tcaggagCCATcagattattcat
V$HOXC9.01	Homeobox C9 / Hox-3beta	0,83	128-144	+	0,805	0,88	tccagtcaTGAAtaatc
V$POU3F3.01	POU class 3 homeobox 3 (POU3F3), OTF8	0,81	132-146	+	0,784	0,83	gtcatGAATaatctg
V$PDX1.01	Pdx1 (IDX1/IPF1) pancreatic and intestinal homeodomain TF	0,74	136-154	+	0,783	0,744	tgaataatcTGATggctcc
V$HOXC10.01	Homeobox C10/ Hox-3iota	0,83	186-202	-	0,777	0,83	cagagtctTCAAatggc
V$DMRT4.01	Doublesex and mab-3 related transcription factor 4	0,79	4-24	+	0,775	0,863	ttgatttgcTACTttaaaata
V$POU3F3.01	POU class 3 homeobox 3 (POU3F3), OTF8	0,81	42-56	-	0,762	0,836	tatatGTATatatgc
V$IRX6.01	Iroquois homeobox 6	0,85	46-58	-	0,756	0,857	tataTATGtatat
V$IRX6.01	Iroquois homeobox 6	0,85	47-59	+	0,756	0,857	tataCATAtatat
V$POU3F3.01	POU class 3 homeobox 3 (POU3F3), OTF8	0,81	45-59	+	0,754	0,823	tatatACATatatat
V$BRN3.03	POU class 4 homeobox 3 (POU4F3), BRN3C	0,83	127-145	-	0,754	0,855	agattatTCATgactggaa
V$NFY.03	Nuclear factor Y (Y-box binding factor)	0,81	1-15	-	0,75	0,845	gtagCAAAtcaaagt
V$GZF1.01	GDNF-inducible zinc finger protein 1 (ZNF336)	0,73	22-34	-	0,75	0,78	TGTGtatatatat
V$GZF1.01	GDNF-inducible zinc finger protein 1 (ZNF336)	0,73	24-36	-	0,75	0,789	TGTGtgtatatat
V$GZF1.01	GDNF-inducible zinc finger protein 1 (ZNF336)	0,73	26-38	-	0,75	0,768	TGTGtgtgtatat
V$GZF1.01	GDNF-inducible zinc finger protein 1 (ZNF336)	0,73	54-66	-	0,75	0,78	TGTGtatatatat
V$GZF1.01	GDNF-inducible zinc finger protein 1 (ZNF336)	0,73	56-68	-	0,75	0,789	TGTGtgtatatat
V$GZF1.01	GDNF-inducible zinc finger protein 1 (ZNF336)	0,73	58-70	-	0,75	0,768	TGTGtgtgtatat
V$PBX1_MEIS1.02	Binding site for a Pbx1/Meis1 heterodimer	0,77	89-105	+	0,75	0,778	tcgtTGTTttac**ag**agt
V$BRN3.01	Brn-3, POU-IV protein class	0,78	130-148	+	0,75	0,852	cagtcatgaATAAtctgat

For germline transmission, the founder male #5 was bred to wild-type C57Bl6/N female mice. Mutant allele transmission was confirmed by genotyping PCR followed by digestion with DdeI restriction enzyme, and by DNA-sequencing (**Figure 25A**) shows a representative genotyping PCR). Heterozygous litter was further mated, and the expression of circTulp4 was assessed by qRT-PCR in homozygous, heterozygous and WT offspring, using *Rpl19* as the house-keeping gene. **Figure 25B** shows circular and linear RNA expression levels of *Tulp4* in homozygous mutant mice (circTulp4^{KO}) compared to control littermates (circTulp4^{Ctrl}). Surprisingly, circTulp4 expression was not fully depleted, in particular in those tissues where it is normally enriched under WT conditions. Sequencing results revealed that the qRT-PCR product detected is not circTulp4, but a circular variant (circTulp4_v) produced by the usage of the next downstream AG splice acceptor site (**Figure 25C**). This cryptic SA site would be tissue-specifically selected upon depletion of circTulp4, an observation supported by sequencing results from WT mice.

Figure 25B also shows a slight increment in the expression of linear Tulp4 in the homozygous brain-derived tissues and eyes. Further experiments are needed to demonstrate whether this slight increase in linear Tulp4 contributes or not to the circTulp4^{KO} mice phenotype.

CircTulp4^{KO} mice were viable, fertile and did not show any obvious abnormality in adult brain anatomy (data not shown).

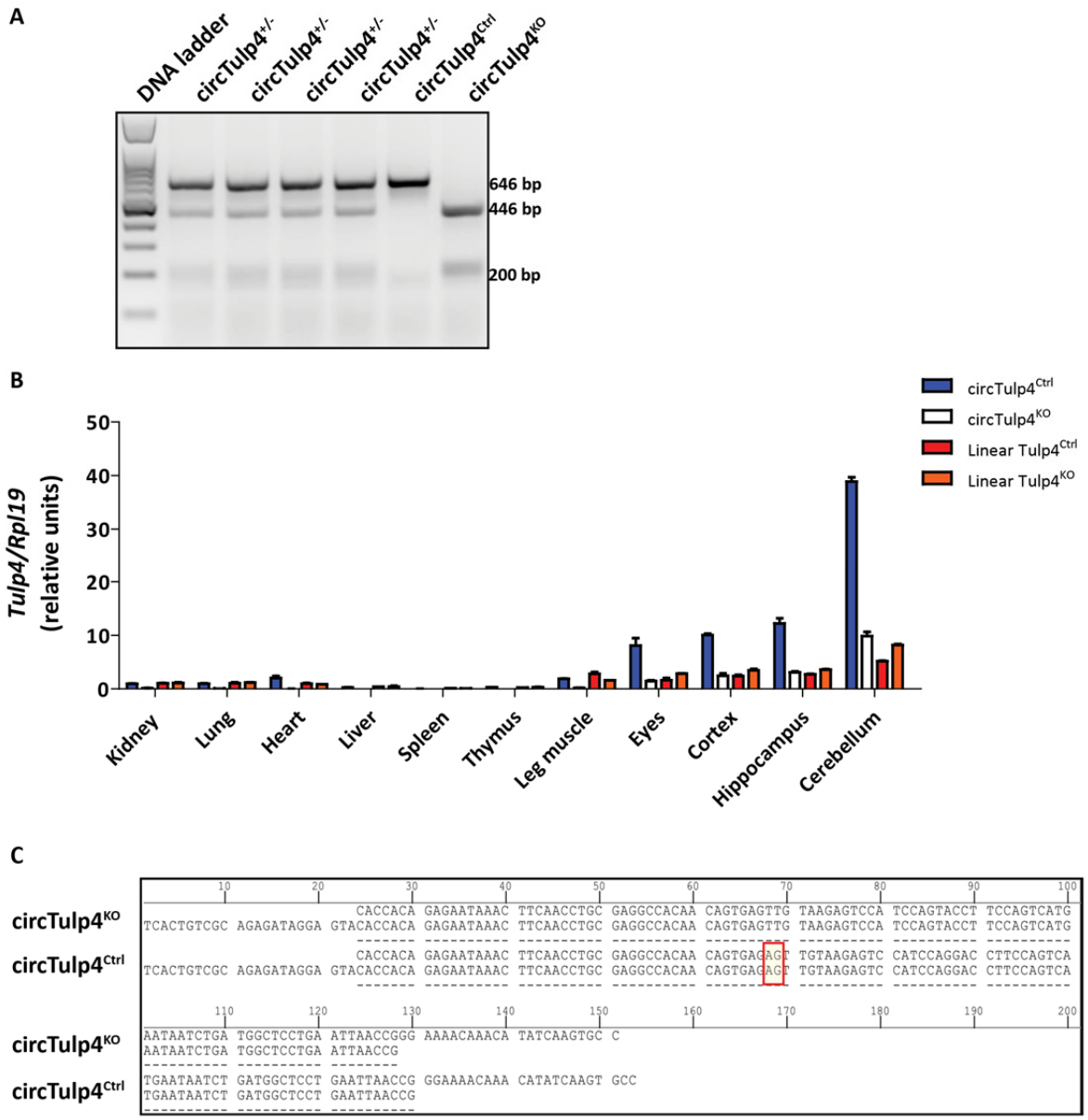

Figure 25. Expression-based characterization of circTulp4^{KO} mouse.
(A) Representative genotyping PCR. Primers Fw SA KO_2 and Rv SA KO amplify a 646 bp fragment of *Tulp4*, consecutive digestion with the DdeI restriction enzyme allows distinguishing between the different genotypes by restriction fragment sizes. circTulp4^{Ctrl}: 646 bp; circTulp4^{KO}: 446 bp + 200 bp; circTulp4$^{+/-}$: 646 bp + 446 bp + 200 bp. **(B)** Quantitative PCR validation of the KO model. Circular and linear RNA isoforms of *Tulp4* gene were measured in various WT and KO C57Bl6/N tissues, normalizing to the house-keeping gene *Rpl19* and arbitrarily to circTulp4 expression in kidney. Data are given as mean ± SEM; n = 2 mice. **(C)** Sequencing alignment of KO against WT mouse data showing that upon mutagenesis of the splice acceptor site of circTulp4 a new circular variant is generated using the next AG cryptic site in the sequence. The red box shows the canonical splice acceptor site in the WT mouse that is depleted in circTulp4^{KO}.

8.6.1 CircTulp4^{KO} mice show an impairment in excitatory neurotransmission

Given the electrophysiological results obtained in primary hippocampal neurons in which circTulp4 expression was downregulated (see **Section 8.4.1**), we set out to characterize the neurotransmission properties of hippocampal neurons in the circTulp4^{KO} mouse. For that, we again collaborated with Dr. Marín-Burgin at the IBioBA-MPSP to measure the miniature synaptic currents in the Schaffer collateral-CA1 synapses in acute hippocampal slices. As shown in **Figure 26**, hippocampal CA1 neurons displayed a strong reduction in the frequency of mEPSCs (circTulp4^{KO} = 0.117 ± 0.010 Hz vs circTulp4^{Ctrl} = 0.258 ± 0.043 Hz; Mann-Whitney U test, U = 16, p = 0.017), with a modest increase in the amplitude, probably due to compensatory mechanisms. Additionally, no alterations were recorded in the frequency and amplitude of mIPSCs.

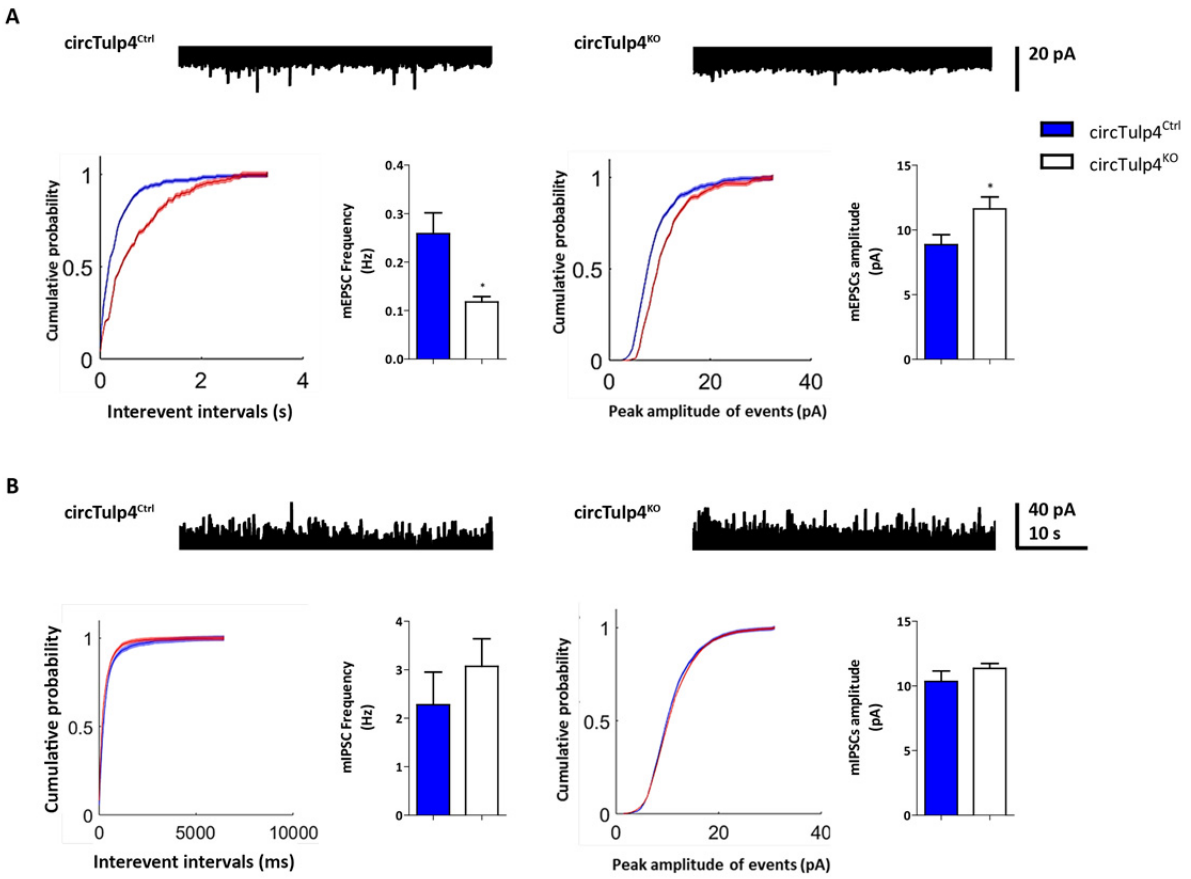

Figure 26. CircTulp4^{KO} mice display a strong reduction in the frequency of AMPAR-mediated mEPSCs. Electrophysiology in acute hippocampal slices of six-week-old mice, done in collaboration with Dr. Marín-Burgin at the IBioBA-MPSP. **(A-B)** Cumulative probability graphs have color definition changed for easier identification; blue represents circTulp4^{Ctrl}, while red circTulp4^{KO}. Data are given as mean ± SEM; Mann-Whitney U test, *p < 0.05; unpaired t-test, *p < 0.05; for mEPSCs n = 9 neurons for circTulp4^{KO}, n = 10 neurons for circTulp4^{Ctrl}; for mIPSCs n = 7 neurons for circTulp4^{KO}, n = 6 neurons for circTulp4^{Ctrl}. **(A)** Top, representative recordings of AMPAR-mediated mEPSCs illustrating the effect of depleting circTulp4 (right). In comparison with WT

littermate controls, the mean frequency of mEPSCs was strongly reduced in CA1 neurons of circTulp4^{KO} mouse. A moderate but statistically significant increase in the amplitude of circTulp4^{KO} neurons was also recorded (circTulp4^{KO} = 11.62 ± 0.937 pA vs circTulp4^{WT} = 8.85 ± 0.786 pA; unpaired t-test, $t_{(17)}$= 2.273, p = 0.036), probably reflecting compensatory mechanisms. **(B)** Top, representative recordings of mIPSCs showing the lack of effect of depleting circTulp4 on mIPSCs.

In the KO mice, circTulp4 expression is depleted not only in the pre- and post-synaptic compartments but also in glial cells. To assess the specific effect of downregulating circTulp4 only in the post-synaptic compartment, electrophysiological measurements were performed on acute hippocampal brain slices which were *in utero* electroporated (E 15.5) with sh-circTulp4 or the sh-scrambled control. For a clear distinction, post-synaptic currents were measured in sh-circTulp4 transfected neurons co-transfected with an RFP expressing plasmid. As shown in **Figure 27A**, circTulp4-deficient neurons showed a strong reduction in mEPSCs frequency when compared to sh-scrambled control neurons (sh-circTulp4 = 0.050 ± 0.007 Hz vs sh-scrambled = 0.470 ± 0.094 Hz; Mann-Whitney U test, U = 0, p = 0.0014). Of note, the frequency of mIPSCs was also slightly decreased in neurons transfected with sh-circTulp4 (**Figure 27B**). These results suggest that under physiological conditions the inhibitory circuits try to compensate for the decreased frequency of excitatory transmission, maintaining synaptic homeostasis. As observed in cultured neurons, we did not observe any changes in the amplitude of both mEPSCs and mIPSCs.

Figure 27. Sh-circTulp4 *in utero* electroporated acute hippocampal slices display a reduction in the frequency of mEPSCs and a compensatory drop in the frequency of mIPSCs.
Electrophysiological measurements were performed in CA1 neurons of six-week-old mice, done in collaboration with Dr. Marín-Burgin at the IBioBA-MPSP. **(A-B)** Data are given as mean ± SEM; Mann-Whitney U test, **p < 0.01, *p < 0.05; for mEPSCs n = 7 neurons for sh-circTulp4, n = 8 neurons for sh-scrambled; for mIPSCs n = 10 neurons for sh-circTulp4, n = 7 neurons for sh-scrambled. **(A)** Top, representative recordings of AMPAR-mediated mEPSCs illustrating the effect of downregulating circTulp4. In comparison with sh-scrambled control cells, the mean frequency of mEPSCs was strongly reduced. No changes in the amplitude were recorded. **(B)** Top, representative recordings of mIPSCs showing a significant reduction in the frequency of mIPSCs upon downregulating circTulp4 (sh-circTulp4 = 2.523 ± 0.673 Hz vs sh-scrambled = 3.667 ± 0.264 Hz; Mann-Whitney U test, U = 14, *p = 0.045).

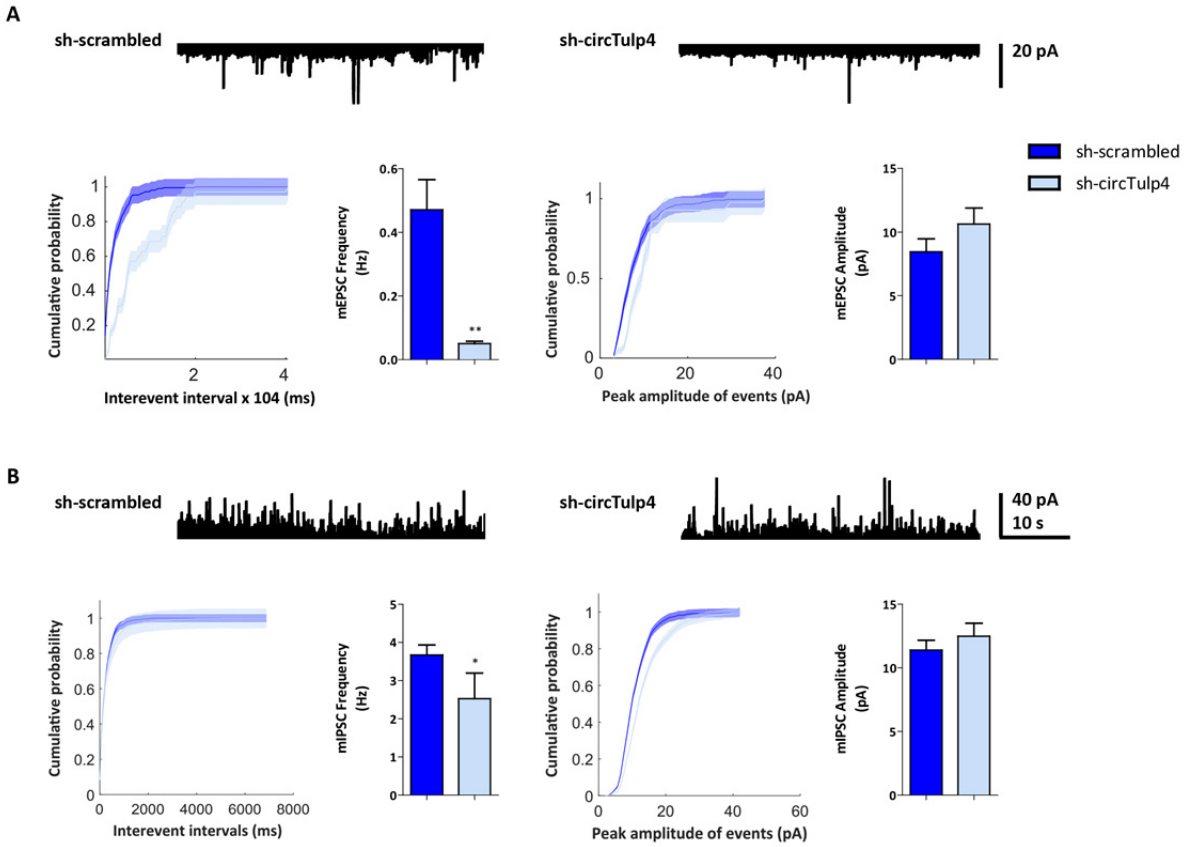

With the aim of validating the previously observed effects of downregulating circTulp4 over the number of excitatory inputs in a physiological context, mouse embryo brains were *in utero* electroporated with sh-circTulp4 or the sh-scrambled control. Dendritic spine density and the number of VGlut1 punctae were analyzed in acute hippocampal slices from P 45 mice. As observed in **Figure 28A-B**, circTulp4 downregulation did not alter spine numbers when compared to control neurons. Immunostaining with α-VGlut1 confirmed the reduction in the number of excitatory pre-synaptic contacts in sh-circTulp4 transfected neurons. Once again, this reduction was explained by a lower number of pre-synaptic contacts on spines (sh-circTulp4 = 0.631 ± 0.026 vs sh-scrambled = 0.897 ± 0.028; unpaired t-test, $t_{(69)}$ = 6.679, $p < 0.0001$) and not on dendritic shafts (**Figure 28B**).

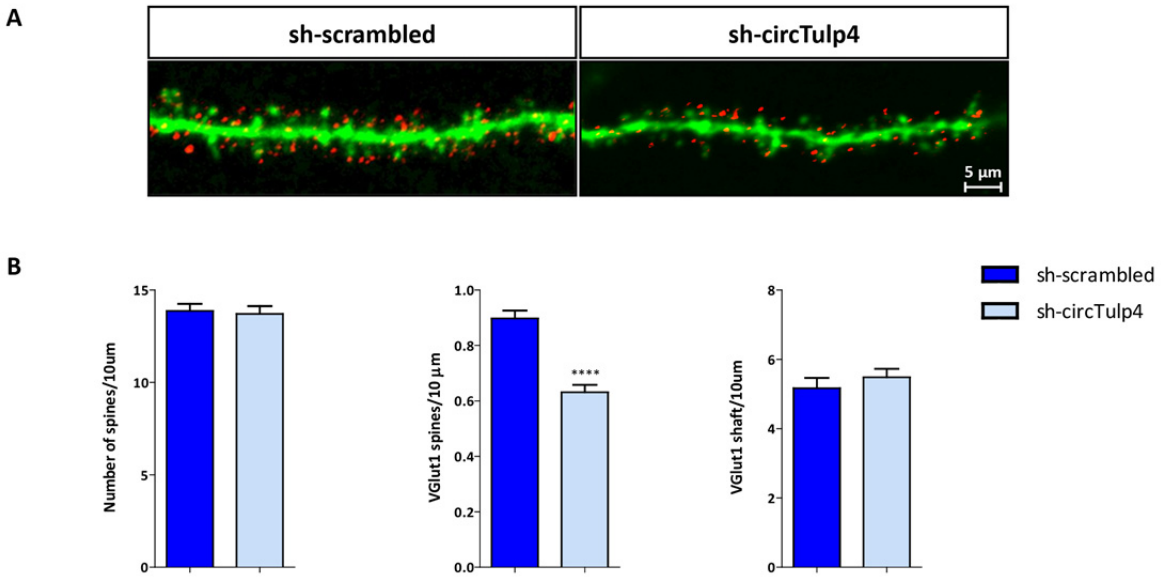

Figure 28. Downregulation of circTulp4 under physiological conditions reduces the number of excitatory pre-synaptic contacts on spines.
Mouse embryo brains were *in utero* electroporated at E 15.5 with sh-circTulp4 or the sh-scrambled control, and quantitative analysis of dendritic spine density and of pre-synaptic excitatory punctae (VGlut1) was carried out at P 45. **(A)** Immunostaining against VGlut1. Mouse embryo brains were co-transfected with a GFP expressing vector (green channel) and acute hippocampal slices were labeled with an α-VGlut1 antibody (red channel) to visualize only excitatory pre-synaptic contacts (merge, yellow). Scale represents 5 µm. **(B)** Downregulation of circTulp4 did not alter synaptic density (left, sh-circTulp4 = 13.71 ± 0.424 vs sh-scrambled = 13.87 ± 0.380; unpaired t-test, $t_{(79)}$ = 0.271, ns), but specifically reduced the number of excitatory pre-synaptic contacts on spines (middle). Data are given as mean ± SEM; unpaired t-test, ****p < 0.0001; n = 40 neurons derived from three mice.

In agreement with the excitatory transmission dysfunction registered by mPSCs recordings in primary neuronal cultures and acute hippocampal slices derived both from circTulp4^{KO} mouse and IUE mouse brains, we also observed a strong imbalance in the ratio of excitatory to inhibitory synaptic membrane currents (E/I balance) *in vivo*. **Figure 29A** shows a decrease in the EPSC versus IPSC slope for the circTulp4^{KO} mice in comparison with WT controls. Furthermore, **Figure 29B** illustrates that the mean E/I ratio is strongly decreased in circTulp4^{KO} mice at all stimulation frequencies applied.

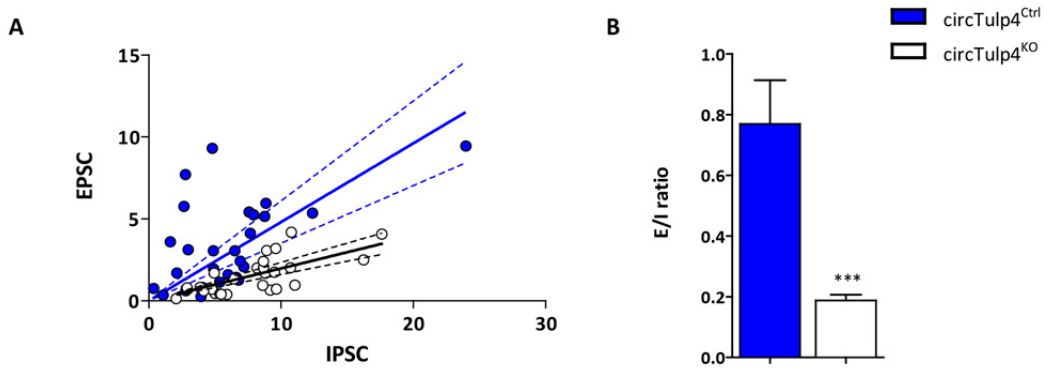

Figure 29. E/I ratio is strongly reduced in circTulp4^{KO} mice.
Electrophysiology in acute hippocampal slices of six-week-old mutant mice. Post-synaptic currents were recorded at different holding potentials to yield EPSC and IPSC. **(A)** Slope circTulp4^{KO} mice: 0.160 to 0.234; slope WT mice: 0.351 to 0.609 (95 % CI). **(B)** Data represent mean E/I ratios ± SEM measured at different frequencies of stimulation (circTulp4^{KO} = 0.187 ± 0.018 vs circTulp4^{Ctrl} = 0.769 ± 0.144; Mann-Whitney U test, U = 97, ***p < 0.0001; n = 27 neurons *per* condition.

Different factors contribute to synaptic E/I balance, including synaptic transmission. Although we have consistently shown in different systems that the downregulation of circTulp4 affects the post-synapse, it remains unclear whether the pre-synapse is also altered by downregulating circTulp4 levels. In order to analyze specific alterations in pre-synaptic properties, we further studied paired-pulse facilitation (PPF) in acute hippocampal slices of six-week-old circTulp4^{KO} mice. For that, pre-synaptic Schaffer collateral axons were stimulated with two consecutive pulses and the evoked responses of post-synaptic CA1 neurons were registered. As reflected in **Figure 30**, circTulp4^{KO} mice had a higher paired-pulse ratio in comparison with WT controls (circTulp4^{KO} = 2.587 ± 0.269 vs circTulp4^{WT} = 1.828 ± 0.221; unpaired t-test with Welch's correction, $t_{(13.96)}$ = 2.176, p < 0.047). In other words, the probability of release of the pre-synaptic neuron when it receives an action potential was increased in circTulp4-deficient neurons, and this was mainly due to a decrease in the first pulse stimulation response (**Figure 30A**). Steady-state changes in the basal probability of neurotransmitter release could potentially account for the observed PPF in the KO mice. In other words, the increased facilitation may not be due to an alteration in the short-term plasticity mechanism *per se*, but it may result from a reduced initial synaptic potential (due to reduced neurotransmitter release) leading to a greater relative increase in the second synaptic potential.

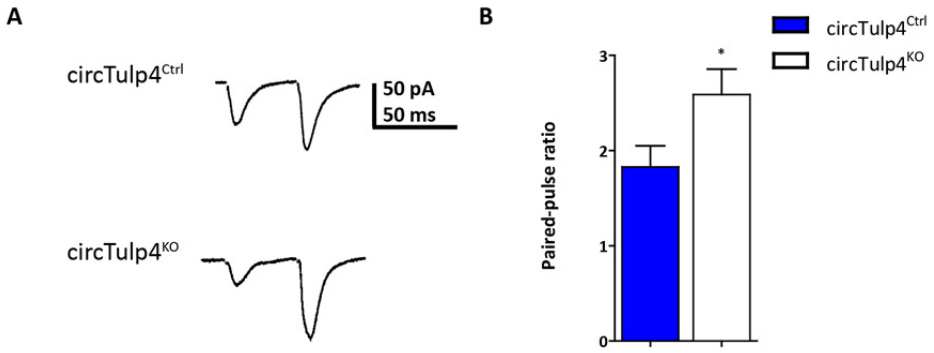

Figure 30. Paired-pulse facilitation is enhanced in circTulp4^{KO} mice.
(A) Example traces of evoked responses upon stimulation of the Schaffer collateral pathway with a paired stimuli (50 ms interstimulus interval). **(B)** Data represent mean paired-pulse ratios ± SEM; unpaired t-test with Welch's correction, *p < 0.05; n = 9 neurons from three mutant mice, n = 7 neurons from three WT mice.

8.6.2 Behavioral effects of circTulp4 depletion

In order to investigate possible behavioral effects related to the strong excitatory synaptic dysfunction observed in circTulp4^{KO} hippocampus, we set out to phenotypically analyze the mouse line following the pipeline N 'General neuro-behavioral assessment' at the German Mouse Clinic (GMC). For this collaboration, 25 heterozygous matings were set up to analyze a total of 60 animals divided into four groups: 15 homozygous circTulp4^{KO} males and respective 15 male littermate controls (circTulp4^{Ctrl}), and 15 homozygous circTulp4^{KO} females with its 15 female littermate controls. To reduce heterogeneity, only animals differing in no more than 10 days were tested.

CircTulp4^{KO} animals did not show differences in autonomous and muscle functions compared to the control group, as revealed by a modified SHIRPA protocol, grip strength, accelerating rotarod and ladder beam (data not shown). However, circTulp4^{KO} female mice showed a substantial increase in body weight, and this difference was observed through the entire eight-week pipeline (**Figure 31**).

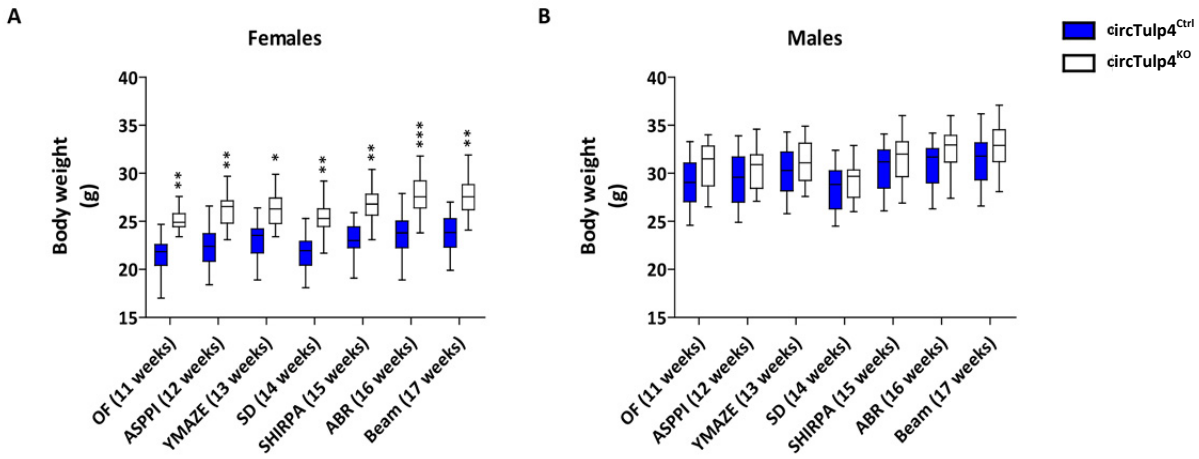

Figure 31. CircTulp4^{KO} female mice show increased body weight.
Data are presented as box-and-whisker plots showing the body weight for tested **(A)** Females. **(B)** Males. Box limits represent first and third quartiles, center line represents median, and whiskers represent the minimum and maximum values. OF: open field; ASPPI: acoustic startle/pre-pulse inhibition; SD: social discrimination; ABR: auditory brainstem response; Beam: balance beam. *Statistically significant from control mice; RM-ANOVA, Bonferroni post-test, ***p < 0.001, **p < 0.01, *p < 0.05; n = 10 animals per group.

Table 11 shows two-way ANOVA analyses for some of the tests shown in this section, including open field, SHIRPA, hot plate, Y-maze and social discrimination.

Table 11. Two-way ANOVA table with genotype and sex as main factors.

	Genotype			Sex			Genotype x Sex		
	F	dF	p	F	dF	p	F	dF	p
Open Field									
Distance travelled (m)	8.306	1, 51	0.0058	3.678	1, 51	0.0607	0.639	1, 51	0.4278
Rearings (#)	4.399	1, 51	0.0409	1.665	1, 51	0.2028	3.042	1, 51	0.0872
Center time (%)	2.899	1, 51	0.0947	0,000	1, 51	0.9878	0.139	1, 51	0.7108
Whole arena average speed (cm/s)	7.068	1, 51	0.0105	4.804	1, 51	0.0330	0.284	1, 51	0.5963
Periphery average speed (cm/s)	7.266	1, 51	0.0095	5.884	1, 51	0.0189	0.072	1, 51	0.7898
Center average speed (cm/s)	1.527	1, 51	0.2222	3.837	1, 51	0.0556	1.734	1, 51	0.1938
SHIRPA									
Locomotor activity	6.395	1, 52	0.0145	4.820	1, 52	0.0326	0.081	1, 52	0.7766
Hot plate									
First response	5.368	1, 52	0.0245	0.646	1, 52	0.4251	0.186	1, 52	0.6679
Second response	3.778	1, 52	0.0574	0.475	1, 52	0.4937	1.591	1, 52	0.2128
Y-maze									
Entries (#)	8.934	1, 50	0.0043	4.688	1, 50	0.0352	0.567	1, 50	0.4550
Spontaneous alternations (%)	4.574	1, 50	0.0374	2.453	1, 50	0.1236	0.476	1, 50	0.4933
Alternate arm returns (%)	4.640	1, 50	0.0361	1.834	1, 50	0.1818	0.222	1, 50	0.6395
Social discrimination									
Investigation time (s)	0.142	1, 52	0.7081	36.37	1, 52	< 0.0001	2.842	1, 52	0.0978
Recognition index	1.261	1, 52	0.2667	8.176	1, 52	0.0061	0,745	1, 52	0.3920

The open field (OF) test was employed to assess novelty-induced locomotion, exploration and anxiety-related behavior. As shown in **Figure 32A**, circTulp4^{KO} mice exhibited increased horizontal and vertical locomotor activity compared to littermate controls, represented by total distance travelled (circTulp4^{KO} = 259.2 ± 5.996 m vs circTulp4^{WT} = 229.2 ± 8.779 m; two-way ANOVA genotype, $F_{(1,51)}$ = 8.306, p = 0.0058) and by total number of rears (circTulp4^{KO} = 153.5 ± 5.498 vs circTulp4^{WT} = 136.2 ± 6.843; two-way ANOVA genotype, $F_{(1,51)}$ = 4.399, p = 0.0409). This phenotype was further accompanied by an increment in the average speed in the whole arena and in the periphery, but not in the anxiogenic center (**Table 11**, **Figure 32B**). Hyperactive behavior was also evidenced in the SHIRPA, where the number of squares crossed in 30 s was quantified (circTulp4^{KO} = 22.25 ± 1.398 vs circTulp4^{WT} = 17.86 ± 1.182; two-way ANOVA genotype, $F_{(1,52)}$ = 6.395, p = 0.0145) (**Figure 32B**). In agreement with the center average speed, there were no significant genotype differences in the time spent in the center (**Figure 32D**).

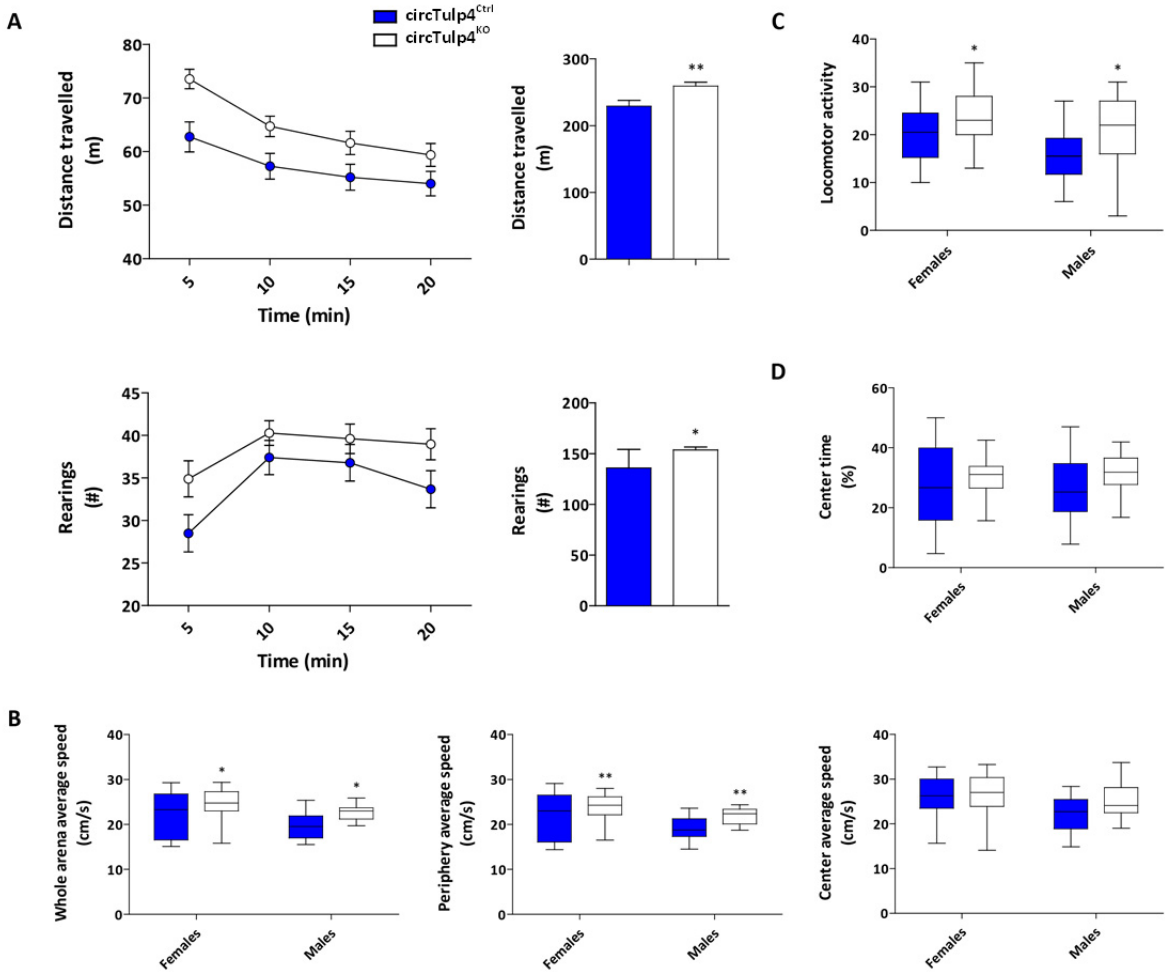

Figure 32. CircTulp4^{KO} mice exhibit locomotor hyperactivity.
(A) Revealed by an increased total distance traveled and total number of rears, and **(B)** by an increased in whole average speed and periphery average speed in the OF test. **(C)** Further supported by the number of squares crossed in 30 s in the SHIRPA protocol. **(D)** No differences in the time spent in the anxiogenic center were observed in the OF test. **(A-D)** Data are given as mean ± SEM. *Statistically significant from littermate controls; two-way ANOVA **p < 0.01, *p < 0.05; n = 26-30.

CircTulp4^{KO} mice showed increased sensorimotor recruitment in the acoustic startle response (ASR) at 110 dB (RM-ANOVA, sound pressure level x genotype $F_{(5,270)}$ = 9.178, p < 0.0001; genotype $F_{(1,270)}$ = 11.90, p = 0.0011, Bonferroni post-test, p < 0.001) and at 81 dB when corrected by body weight (RM-ANOVA, sound pressure level x genotype $F_{(4,216)}$ = 5.795, p = 0.0002; genotype $F_{(1,216)}$ = 4.579, p = 0.0369, Bonferroni post-test, p < 0.001) (**Figure 33A**). In addition, thermal sensitivity –measured in the hot plate test– was also found increased in circTulp4^{KO} mice; with faster reaction times in the first response (two-way ANOVA, genotype $F_{(1,52)}$ = 5.368, p = 0.0245) (**Figure 33C**). Of note, no significant genotype differences on sensorimotor gating in the pre-pulse inhibition test were detected (**Figure 33B**).

To control for the possible effects that hyperactive behavior can have over the interpretation of anxiety-related behavior, elevated plus maze (EPM) was performed at the IBioBA-MPSP in Buenos Aires. CircTulp4^{KO} mice revealed an increase in anxiety-related behavior, by spending less time in the open arms compared to control littermates (data was shown as part of Florencia Merino's master thesis). Together, these results suggest that circTulp4^{KO} mice display novelty-induced hyperactivity, aberrant sensorimotor recruitment and overall increased anxiety-related behavior.

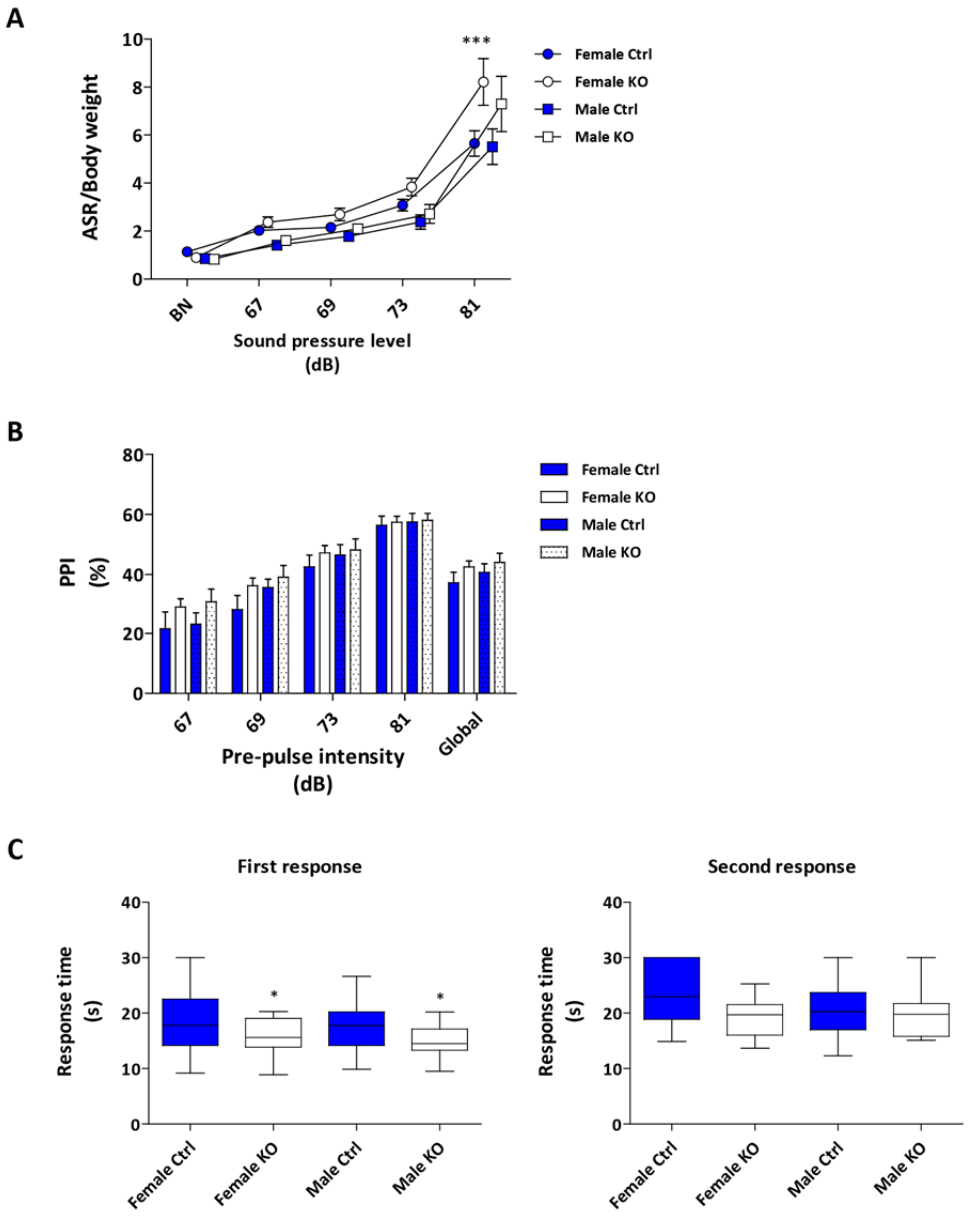

Figure 33. CircTulp4^{KO} mice display increased sensorimotor recruitment.
(A) Revealed by the acoustic startle response test. CircTulp4^{KO} mice display an increased ASR compared to littermate controls at 110 dB and at 81 dB when corrected by body weight. Data are given as mean ± SEM. *Statistically significant from littermate controls; RM-ANOVA for sound pressure level-dependent analysis, Bonferroni post-test, ***p < 0.001; n = 13-15. **(B)** No significant differences were observed in the PPI test. **(C)**

The aberrant sensorimotor recruitment was further supported by decreased latencies in the first response to the hot plate test. Box limits represent first and third quartiles, center line represents median, and whiskers represent the minimum and maximum values.*Statistically significant from littermate controls; two-way ANOVA, *p < 0.05; n = 13-15.

Cognitive performance tested by the Y-maze was severely affected in circTulp4^{KO} mice, which showed decreased percentage of spontaneous alternations (circTulp4^{KO} = 66.83 ± 2.080 % vs circTulp4^{WT} = 72.40 ± 1.616 %; two-way ANOVA, genotype $F_{(1,50)}$ = 4.574, p = 0.0374) and increased alternate arm returns (circTulp4^{KO} = 32.18 ± 2.062 % vs circTulp4^{WT} = 26.66 ± 1.530 %; two-way ANOVA, genotype $F_{(1,50)}$ = 4.640, p = 0.0361) (**Figure 34A**, middle and right), parameters that cannot be obscured by the reported novelty-induced hyperactivity. Notably, KO mice also displayed an increased number of arm entries compared to control littermates (**Table 11**, **Figure 34A**, left), further supporting the described hyperactivity. Although hippocampal-dependent spatial memory in the Y-maze was impaired, circTulp4^{KO} mice did not show alterations in the novel object recognition test, performed at the IBioBA-MPSP in Buenos Aires (data not shown), neither in the social discrimination protocol (**Figure 34B**).

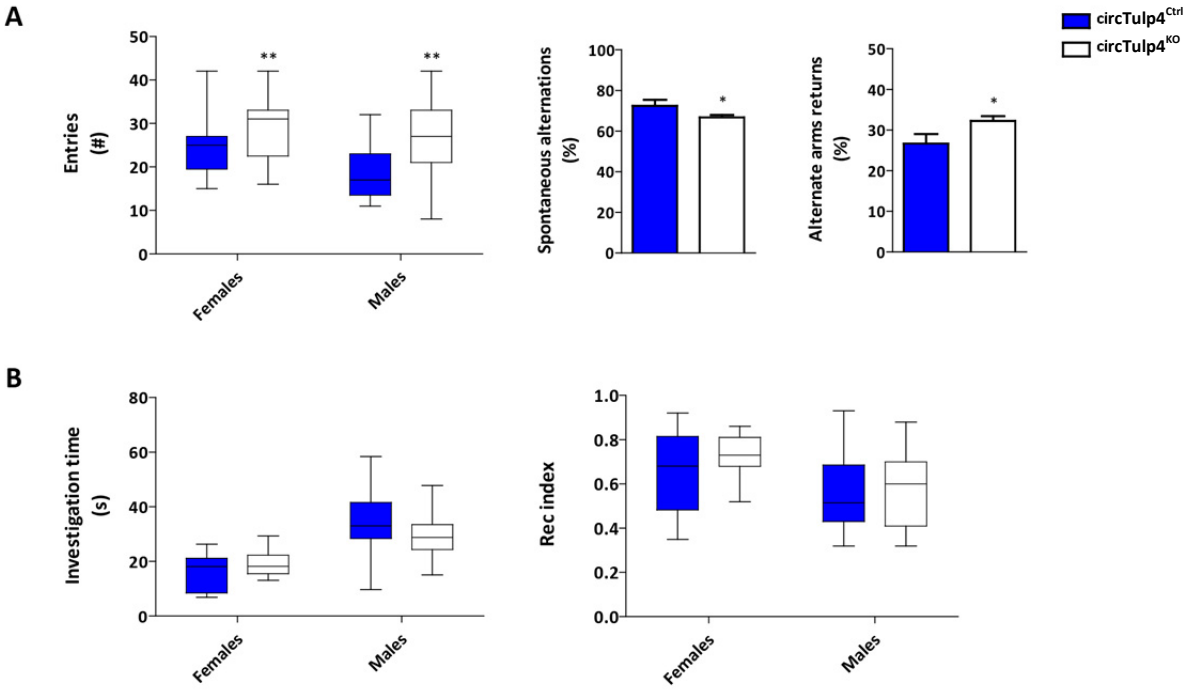

Figure 34. CircTulp4^{KO} mice show strong spatial working memory alterations.
(A) As shown by decreased spontaneous alternations (middle) and increased alternate arms return (right), parameters that are independent of circTulp4^{KO} hyperactivity. Data are given as mean ± SEM. *Statistically significant from littermate controls; unpaired t-test, *p < 0.05; n = 26-28. **(B)** Box-and-whisker plots showing no genotype significant differences in either investigation time (left) or recognition memory (right) in the social discrimination test. **(A,B)** Box limits represent first and third quartiles, center line represents median, and whiskers represent the minimum and maximum values. n = 13-15 per group.

Upon the strong working memory alterations observed in the Y-maze and given that no differences in motor function or motor coordination were recorded between circTulp4^{KO} and control littermates (data not shown), we decided to replace the gait analysis in pipeline N with IntelliCage to further characterize cognitive alterations. Three modules were analyzed in the home cage environment of the IntelliCage: place learning, reversal learning and patrolling (see **Section 7.8.3**). CircTulp4^{KO} mice revealed decreased error rate in the place learning test compared to control mice (RM-ANOVA, time x genotype $F_{(6,138)} = 5.432$, $p < 0.0001$; genotype $F_{(1,138)} = 8.365$, $p = 0.0082$, Bonferroni post-test, $p < 0.001$, $p < 0.01$) (**Figure 35A**, left). Interestingly, the faster reduction of error rate in circTulp4^{KO} mice was accompanied by decreased locomotor activity, as revealed by the number of visits (RM-ANOVA, genotype $F_{(1,138)} = 4.910$, $p = 0.0369$) and nosepoke activity (RM-ANOVA, time x genotype $F_{(6,138)} = 3.294$, $p = 0.0046$; genotype $F_{(1,138)} = 16.66$, $p = 0.0005$, Bonferroni post-test, $p < 0.001$, $p < 0.01$) (**Figure 35C,** left). Although not significant (**Figure 35A**, middle), mutants showed lower error rates than control mice in reversal learning. In the patrolling module, both genotypes required a week to learn the task, after which mutants demonstrated again a lower error rate than control mice (RM-ANOVA, time x genotype $F_{(9,135)} = 2.589$, $p = 0.0087$; genotype $F_{(1,135)} = 12.10$, $p = 0.0034$, Bonferroni post-test, $p < 0.001$, $p < 0.01$) (**Figure 35A**, right). In this case, both genotypes increased activity levels until they learned the task (**Figure 35B-C**, right), after which activity dropped dramatically.

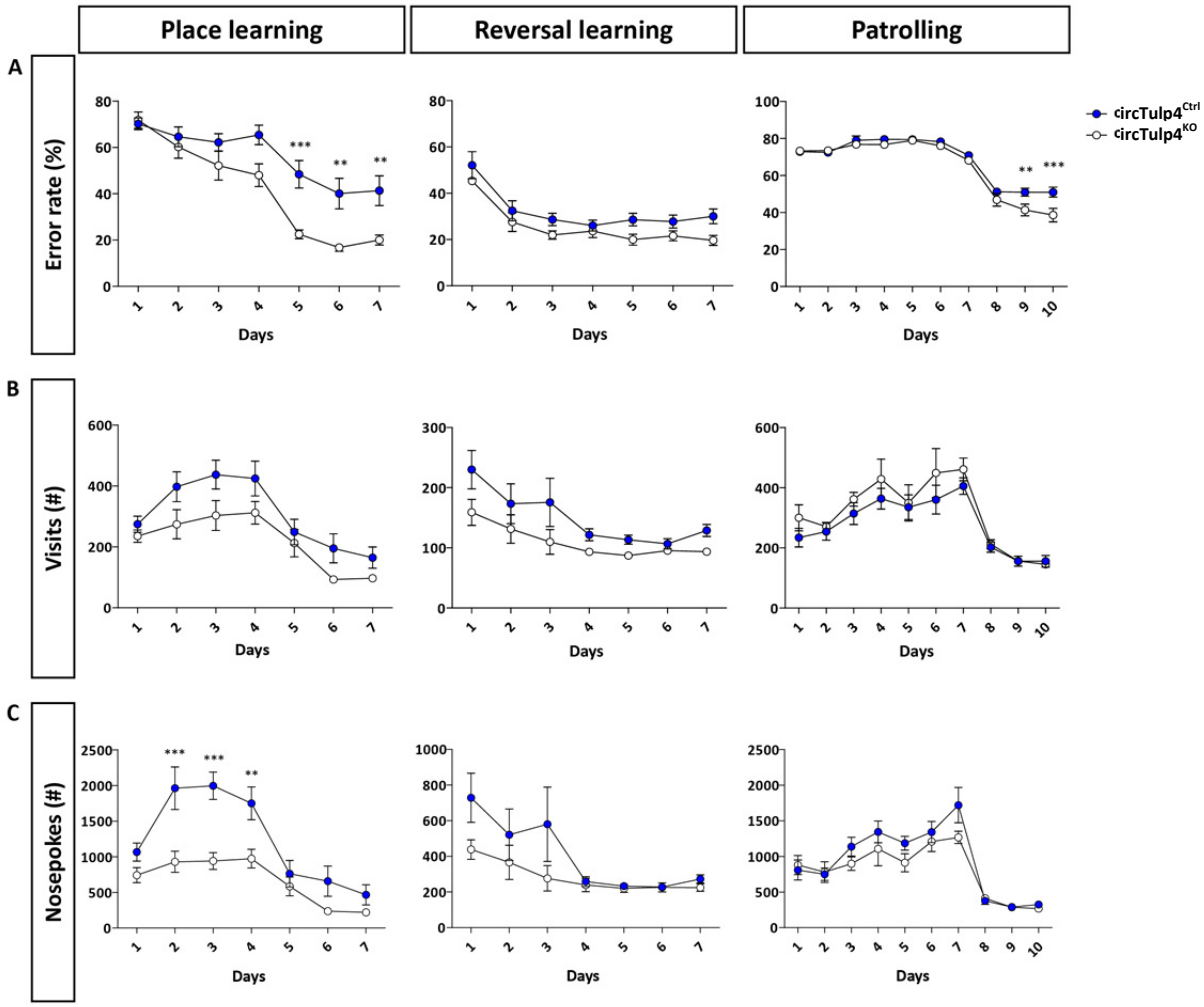

Figure 35. CircTulp4^{KO} mice display improved learning compared to controls in the IntelliCage.
(A) As suggested by a faster error rate reduction. **(B-C)** Locomotor activity measures. Left column, the better performance of KO animals in the place learning module was accompanied by a lower number of visits and reduced nosepoke activity. Right column, in the patrolling task both groups needed a week to learn, after which KO displayed a lower error rate. Data are given as mean ± SEM. *Statistically significant from littermate controls; RM-ANOVA for time-dependent analysis, Bonferroni post-test, ***p < 0.001, **p < 0.01; n = 12-14 females only.

Overall, our data indicate that circTulp4^{KO} mice show novelty-induced hyperactivity, aberrant sensorimotor recruitment, and specific alterations in cognitive function.

9 Discussion

Covalently closed single-stranded transcripts exist across all branches of life (Ebbesen et al., 2017; Lasda & Parker, 2014; Salzman, 2016; Vicens & Westhof, 2014; Wilusz, 2018). Although different types of circular molecules have been described (see **Section 5.2**), the most abundant one is represented by backspliced circRNAs, in particular, those derived from protein-coding sequences. Generated by the spliceosome machinery, this group of circRNAs has recently been found to be abundantly expressed in a wide range of eukaryotic species.

At the beginning of this project, a systematic analysis of circRNA abundance in the (mammalian) central nervous system was missing. To date, we know that circRNAs are highly enriched in neuronal tissues derived from mouse, pig, human, and also in fly (Ashwal-Fluss et al., 2014; Rybak-Wolf et al., 2015; Venø et al., 2015; Westholm et al., 2014; You et al., 2015). Indeed, many of the circRNA-producing genes are exclusively expressed in the brain or, if expressed in other tissues as well, the percentage of transcripts producing circRNAs is significantly higher in the brain (You et al., 2015), suggesting a neural-specific regulation of circRNA biogenesis. We and others have previously shown that circRNA levels are dynamically regulated during neuronal differentiation and development (Rybak-Wolf et al., 2015; You et al., 2015), following bursts of electrical activity (You et al., 2015), and accumulate with age (Gruner et al., 2016; Westholm et al., 2014), and many of them are enriched in synapses (Rybak-Wolf et al., 2015; You et al., 2015). Furthermore, circRNAs are evolutionary conserved across species, and the degree of conservation increases with their expression level (Chen et al., 2015; Danan et al., 2012; Dong et al., 2017; Guo et al., 2014; Jeck et al., 2013; Memczak et al., 2013; Rybak-Wolf et al., 2015; Salzman et al., 2012; Wang et al., 2014).

CircTulp4 is the most abundant, coding-sequence-derived circRNA in neurons. This study aimed to unveil –mainly through loss-of-function approaches in cellular systems and, most notably, under physiological contexts– the function and mechanism of action of this molecule. The first aim was to assess the expression level of selected circRNA-producing genes, including *Tulp4,* in primary neurons along development in culture and in primary astrocytic cultures in comparison with neuronal ones, to uncover specific RNA expression profiles. Second, to investigate circTulp4 intracellular localization and to study morphological effects of downregulating its expression in primary neuronal cultures. Third, as circTulp4 is predominantly expressed in synapses, to electrophysiologically characterize the effects of depleting its expression in hippocampus-derived neurons. Finally, a constitutive circTulp4 knockout mouse was generated by specifically

introducing a two-base-pair exchange in its splicing acceptor site, enabling the morphological and electrophysiological loss-of-function characterization *in vivo*. In addition, possible behavioral alterations were explored by subjecting the animals to a general battery of neurological tests. Cognitive alterations, known to be associated with hippocampus malfunction, were further analyzed.

9.1 EXPRESSION ANALYSIS OF CIRCRNA CANDIDATES

Characterizing the expression level of molecules of unknown function is one of the first mandatory steps towards unveiling their potential biological roles. Compared to protein-coding mRNAs, most circRNAs exhibit low abundance (Guo et al., 2014; Memczak et al., 2013; Salzman et al., 2013). However, although some circRNAs express more or less ubiquitously, the majority of them display cell-, tissue- and/or developmental stage-specific expression profiles (Conn et al., 2015; Rybak-Wolf et al., 2015; Salzman et al., 2013; Westholm et al., 2014).

How do circRNAs derived from the same *loci* (and presenting the same *cis*-regulatory elements) can display cell-type-specific expression profiles? Recently, a genome-wide siRNA library targeting all human genes with a circRNA expression reporter was applied to screen for potential *trans*-acting factors regulating circRNA biogenesis (Li et al., 2017). Immune response factors containing dsRNA binding domains (dsRBDs) were found to promote circRNA production by stabilizing intronic RNA pairs (Li et al., 2017). However, in spite of all the knowledge gained over the past few years in circRNA biogenesis (Aktaş et al., 2017; Ashwal-Fluss et al., 2014; Conn et al., 2015; Errichelli et al., 2017; Fei et al., 2017; Ivanov et al., 2015; Khan et al., 2016; Rybak-Wolf et al., 2015), several RBPs associated with circRNA processing and function remain to be explored (Li et al., 2018). In particular, it would be interesting to investigate what drives the specific expression of circRNAs in the brain.

Since circular and linear isoforms of a gene are transcribed by Pol II and spliced by the canonical splicing machinery from a unique pre-mRNA (see **Section 5.2.1**), different expression levels of these RNA isoforms would imply the existence of distinct molecular mechanisms regulating their biogenesis and, therefore, suggest circRNA biological relevance. Here, 20 genes with high circRNA-production capacity were selected from a mouse whole brain RNA-sequencing library (Memczak et al., 2013) and the absolute expression level of their circular and linear RNA isoforms was characterized along neuronal development in primary cultures. As it has also been reported by others (Venø et al., 2015; You et al., 2015), our circRNA candidates showed different relations with their linear counterparts; sometimes displaying higher abundance, sometimes

lower and, in one case, opposite regulation (see **Section 8.1.1**, **Figure 12**). Their dynamic expression patterns, at times independent from the linear transcript levels, support the notion that at least some circRNAs might play biological roles. It is important to note that this first expression analysis exploration was not in agreement with the RNA-sequencing results shown by Memczak et al. (2013), although we did not evaluate expression levels in mouse whole brain. Those differences may derive from the intrinsic quantitative accuracy of both methodologies, being qRT-PCR superior to RNA-sequencing (Kristensen et al., 2019). In addition, RNA-sequencing data processing requires not only bioinformatics expertise but also the development of standard normalization methods for accurate identification and quantification of circRNAs, which has been evolving and refined together with the circRNA field (Hansen, 2018).

The specific abundance of circRNAs in nervous tissues, their overall increased expression during neuronal development, and their preferential biogenesis from host genes with synaptic-related function (Rybak-Wolf et al., 2015; You et al., 2015), shifted our interest towards investigating six candidates from the overlapping RNA-sequencing outcome derived from synaptosomal fractions- and primary frontal cortex neurons along development- libraries (Rybak-Wolf et al., 2015). In this project, we have focused on circTulp4, the second most abundantly expressed circRNA in neurons, but the first candidate when considering the more prevalent group of circRNAs, those derived from protein-coding sequences (see **Section 8.1.2**, **Figure 13C**). As it has been shown in **Figure 13D**, circTulp4 displayed constant expression level across neuronal development, while linear Tulp4 paralleled its expression pattern both in kinetics and in abundance. However, circTulp4 was found to be enriched in synaptosomal fractions (Rybak-Wolf et al., 2015), which, in the context of these new results, suggests specific transportation of the circular isoform of *Tulp4* upon spinogenesis/synaptogenesis. Furthermore, circTulp4 was found to be differentially regulated from its linear counterpart when *Tulp4* expression levels were assessed in mouse WT-derived tissues (see **Section 8.6**, **Figure 23**). CircTulp4 specific brain abundance could be explained by the natural resistance to degradation of circRNAs (see **Section 5.2.1**); non-replicative cells, as post-mitotic neurons are, would accumulate circRNAs over time. However, circTulp4 is not particularly enriched in muscle (**Figure 23**), another tissue composed of post-mitotic cells. Moreover, *Tulp4* mRNA expression is not restricted to nervous tissue. In agreement with the RNA profiling data sets generated by the Mouse ENCODE project (Gene ID: 68842), *Tulp4* was found to be expressed rather ubiquitously; with high abundance in leg muscle and eyes, and at lower levels in kidney, lung, heart, liver, thymus and spleen. Two tissues were *Tulp4* has been reported to be expressed abundantly, ovaries and testis, were not included in

the expression screening. Moreover, *Tulp4* expression has also been assessed by Northern Blot. Using a probe expanding over exons 7 to 9 (ENSMUST00000039655.2, Ensembl release 96 - April 2019) –and by that not recognizing circTulp4– Li et al. (2001) reported a 7 Kb transcript containing the full-coding sequence in mouse brain and testis, while a second major 2 Kb transcript was also detected in brain (Li et al., 2001). Until date, this second transcript has not been reported in the updated databases. The difference in expression patterns between Li et al. (2001) and us most likely derives from the intrinsic sensitivity of the technics employed.

Given that *Tulp4* is highly expressed in nervous tissues, and that circTulp4 expression parallels its expression in neuronal cultures along development, it is tempting to speculate that the high abundance of circTulp4 observed in eyes probably derives from the retina. Of note, the expression profile of circRNAs during postnatal rat retina development has been analyzed to detect possible changes associated with physiological neuronal apoptosis (Han et al., 2017). A circRNA derived from *Tulp4* was found at postnatal day (P) 3, but not at P 7 or P 14. As the expression profile of circRNAs was not analyzed in the mature retina, neither the host gene expression, further experiments need to be performed to prove whether circTulp4 is indeed specifically expressed in the retina.

In the present work, phenotypes associated with specific circTulp4 depletion are being described. Since circTulp4 function is unknown, as well as if it is related to its host gene, following, reported *Tulp4* depletion phenotypes are provided to enrich our discussion. Fly *Tulp4* homologue (*Tusp*) mutants (Yoon et al., 2017) have been recently reported to display a reduction in the assembly of the ternary 7S synaptobrevin-syntaxin-SNAP-25 (SNARE) ternary complex. Though the transcription of each gene of the individual SNARE complex component was not changed, these data suggest that TUSP is a novel regulator of neurotransmitter release. In vertebrates, mutations in *Tulp4* are associated with short stature, cleft lip, and cleft palate (Conte et al., 2016; Lango et al., 2010). Recently, a *Tulp4* knockout mouse line generated by CRISPR/Cas9-mediated exon 4 deletion was found to be subviable (http://www.mousephenotype.org/data/genes/MGI:1916092). Heterozygous phenotype is currently under investigation, but the molecular mechanisms underlying the pre-weaning homozygous lethality remain to be explored. The different strategies that we have undertaken, assure the phenotypes described cannot be attributed to *Tulp4* loss-of-function.

9.2 CIRCTULP4 LOCALIZES IN THE NEURONAL SOMA AND PROCESSES, AND REGULATES BRANCHING ARCHITECTURE IN CULTURE

Another mandatory step towards investigating the unknown function of a molecule is to assess its intracellular localization. To determine circTulp4 localization in primary neuronal cultures, a high-resolution fluorescent *in situ* hybridization (FISH) assay was chosen. Although other groups have also made use of probes targeting the circRNA-specific head-to-tail junction, some of them skipped probe specificity testing, while others tackled it indirectly by choosing RNase R treatment to deplete linear RNAs, or the use of probes designed to detect non-contiguous regions of two exons that could not form head-to-tail junctions (Piwecka et al., 2017; Venø et al., 2015; You et al., 2015). Recently, Zaghlool et al. (2018) developed an *in situ* sequencing approach, suitable for circRNA screening, using circularizable padlock probes in combination with rolling circle amplification and sequencing (Zaghlool et al., 2018). While cellular localization was controlled by adding a padlock probe targeting the lncRNA *Malat1* (which is predominantly expressed in nucleus), they did not assay probe specificity. In this project, we have tested the specificity of the probe by down- and up-regulation of circTulp4 levels using the constructs mentioned above (see **Sections 8.1.3** and **8.2**). These controls exclude the possibility that the circTulp4 probe is binding to the linear isoform of *Tulp4* even though they share partial homology. Furthermore, background noise was controlled by following all manufactory steps except for adding the labeled probe.

CircTulp4 was detected in neuronal cell bodies and processes, as visualized by co-transfection with a GFP-expressing plasmid (**Figure 16**). These results further support the functionality of circTulp4, as aberrant by-products of splicing would normally accumulate at the site of transcription (Moore & Proudfoot, 2009).

The establishment of a functional neuronal circuit relies on proper synaptic connectivity between axon and dendrites, and between neurons and effector cells. Neuronal branching and pruning are in the core of such an intricate connection complexity; a single axon can form multiple synaptic contacts via bifurcation of its extending tip or via lateral branching from the axonal shaft, while dendrite arborization not only increases synaptic capacity but, in addition, is essential for sensory perception. Here we showed that circTulp4-deficient neurons displayed considerably shorter neurites than controls at DIV 3, recovering axonal length (with increased axonal arborization) by DIV 5, while dendritic elongation remained impaired (see **Section 8.3**). The morphological delay observed in circTulp4-deficient neurons with a greater effect over

processes destined to become post-synaptic is suggestive of connectivity alterations. (See **Sections 8.4** and **8.6.1**, and its respective discussion in **Section 9.4.1**). Dendrites are the primary sites of synaptic connections and therefore also the site where synaptic inputs are integrated and processed to ultimately propagate as action potentials (Häusser et al., 2000; London & Häusser, 2005; Vetter et al., 2001). During differentiation and development, neuronal cells undergo dynamic changes in shape, size and functional specialization. These morphological changes are based on cytoskeletal reorganization regulated by actin-binding proteins, Rho pathway signaling proteins, synaptic scaffolding proteins, adhesion molecules and locally secreted neuropeptide hormones. Alterations of the cytoskeletal organization result in impaired neuritogenesis, a phenomenon that takes place in most of neurodevelopmental and neurodegenerative diseases (Kulkarni & Firestein, 2012). Moreover, pathological conditions that lead to altered higher-order brain functions also cause abnormal dendritic architectures; examples being stress paradigms (Liston et al., 2006) and drug abuse (Lu et al., 2012).
Interestingly, sh-circTulp4 *in utero* electroporated animals showed no gross morphological anomaly in the brain. This observation indicates that circTulp4 is not essential for vitality and that under physiological conditions compensatory mechanisms act to restore neuronal circuit functionality.

Currently, the effects of depleting circTulp4 on neuronal morphology are being evaluated *in vivo*. For that, Thy1-eGFP mice –expressing eGFP in a subset of neurons, including pyramidal neurons in the hippocampus and cortex, and granule neurons in the dentate gyrus (Feng et al., 2000)– are being crossed with circTulp4^{KO} mice. Axonal processes –which can typically be seen extending towards the midline and crossing to the contralateral side– will be traced to quantify axonal length and branching.

9.3 NO EVIDENCE INDICATES THAT CIRCTULP4 ACTS THROUGH A TRANSLATED PEPTIDE

Recent evidence has revealed that non-coding RNAs (ncRNAs) can initiate protein translation *in vivo* (Lauressergues et al., 2015; Magny et al., 2013; Nelson et al., 2016). These observations, together with experiments showing the translatable capacity of synthetic circRNAs (Chen & Sarnow, 1995; Wang & Wang, 2015), raised curiosity over the possibility that endogenous circRNAs can encode for peptides.

To date, three different strategies have been employed to identify ORFs in ncRNAs, including conservation analysis across species; examination of codon content and coding features that would differentiate potential coding ORFs from non-coding ones; and translational approaches (Andrews & Rothnagel, 2014). Nevertheless, identifying circRNA-derived peptides faces various difficulties. First, circRNAs are thought (and shown) to be inefficiently translated; their lack of 5'- and 3'- ends suggests ribosomes should be recruited by a mechanism that depends on an internal ribosome entry site (IRES), and cap-independent translation is known to be highly inefficient. Second, conservation analysis of circRNA ORFs relies on the stop codons generated upon reading over the head-to-tail junction, and this is limited by the proximity to the conserved splice site and by the possibility that the stop codon is not circRNA specific. Third, similarly, mass spectrometry identification is based on the detection of circRNA unique peptide sequences (usually short) encoded downstream of the head-to-tail junction.

In this work, the capacity of cirTulp4 to originate a peptide was explored being that, similar to other circRNAs-derived peptides, TULP4-95aa shares the same start codon as its protein-coding host gene (Legnini et al., 2017; Pamudurti et al., 2017) and encounters an in-frame stop codon upon reading over the head-to-tail junction. To prove or dismiss the hypothesis that circTulp4 codes for a peptide, different but complementary approaches were taken (see **Section 8.5**). First, CRISPR/Cas9 tagging of the endogenous *Tulp4* gene, following Mikuni et al. (2016) strategy, indicated possible translation of TULP4-95aa when targeting the specific in-frame stop codon (see **Figure 21**). Second, transfection of an N-terminus tagged *Tulp4* donor vector showed the full-length protein but not TULP-95aa in non-clonal selected Neuro-2a cells (see **Figure 22**), arguing once more that cap-independent translation is lowly efficient. Third, transfection of mESCs with the same N-terminus tagged *Tulp4* donor vector, followed by clonal selection and genotyping, also failed to show the ~11 KDa HA-tagged TULP4-95aa band in a WB.

A similar strategy was followed by Legnini et al. (2017) and circZNF609-derived peptide in mESCs (Legnini et al., 2017). After transfection, clonal selection and genotyped, only one clone carrying one allele with the expected flag and other with a small deletion that prevented circularization was obtained. They also reported low translation efficiency and high background in Western Blot analysis. Therefore, a strategy chosen by different research groups has been immunoprecipitation followed by mass spectrometry analysis (Legnini et al., 2017; Pamudurti et al., 2017; Yang et al., 2018; Yang et al., 2017b; Zhang et al., 2018b).

Here, we have chosen parallel reaction monitoring (PRM)-mass spectrometry to assess the existence of TULP4-95aa. As selected reaction monitoring (SRM)-mass spectrometry, this technique achieves the reproducibility and sensitivity that the shotgun approach lacks and allows to determine absolute abundance (Lange et al., 2008; Peterson et al., 2012). The main advantage of PRM over the traditional SRM approach is that it can provide quantitative data over a wider dynamic range in complex samples; the presence of interfering ions in a full mass spectrum is less disruptive to overall spectral quality than interference in a narrow mass range (Peterson et al., 2012). The utilization of this high-resolution mass spectrometry technic revealed that circTulp4 does not act through a translated peptide, which will further indicate that the endogenous tagged peptide detected by the SLENDR approach is either an off-target or a protein derived from an upstream ORF sharing the same stop codon with TULP4-95aa.

Recently, it has been reported that circRNAs containing the translational start codon from the host gene are more abundantly expressed and conserved than other circRNA groups (including CDS, CDS-3'UTR, 5'UTR, and non-coding). However, cross-species sequence analysis, extensive ribosome profiling, mass spectrometry analysis, and experimental data on a selected panel of this group of circRNAs did not indicate translation of this or any other circRNA (Stagsted et al., 2018). Our results in combination with these new insights suggest that it is very unlikely that circTulp4 is actually translated. However, it remains possible that circTulp4 translation occurs only under specific conditions that have not yet been investigated.

Interestingly, a very recent study lead by L-L Chen's Lab reported that many examined circRNAs tend to form 16-26 bp imperfect RNA duplexes and act as inhibitors of dsRNA-activated protein kinase (PKR). PKR acts in early cellular innate immune responses and was shown to be activated upon poly-(I:C) stimulation or viral infection by RNase L circRNA global degradation (Liu et al., 2019).

In order to explore other circTulp4 possible mechanisms of action, we aim to investigate its interactome by performing pull-down assays with a probe against the specific head-to-tail junction. We expect RNA-sequencing and mass spectrometry data obtained from the immunoprecipitates will allow us to generate new hypotheses about other potential mechanisms of actions to be tested.

9.4 GENERATION OF A CIRCTULP4 DEFICIENT MOUSE MODEL

In 2017, the group led by N. Rajewsky published the first *in vivo* depletion model of a circRNA (Piwecka et al., 2017). The CDR1as knockout (KO) mouse presented specific miRNA deregulation in all brain regions analyzed, as well as upregulation of immediately early genes (IEG), direct mRNA targets of miR-7. They also described impaired sensorimotor gating, a phenotype associated with upregulation of IEG. Furthermore, electrophysiological measurements in single hippocampal neurons derived from CDR1as KO revealed dysfunctional synaptic transmission.

For years it has been assumed that CDR1as is an exceptional circRNA as it is transcribed from a *locus* lacking any mature linear RNA from the same strand. Therefore, Piwecka et al. (2017) designed a mouse model based on the whole deletion of *Cdr1 locus*. However, Salzman's group described −using bioinformatic tools in combination with experimental genetic approaches− linear transcripts containing CDR1as sequence (Barrett et al., 2017). The combined analysis of chromatin modifications and RNA expression revealed CDR1as expression is driven by the nearest annotated transcript upstream, the lncRNA LINC00632 (Barrett et al., 2017). These findings compromise the interpretation of Piwecka et al. (2017) mouse model.

In our *in vivo* model, to specifically knockout the circular RNA isoform of *Tulp4*, a two-base-pair exchange in the canonical SA site that generates circTulp4 upon backsplicing reaction was introduced using CRISPR/Cas9 technology. Further *in silico* investigation of TFBSs in the targeted area (5'UTR) resulted in no core binding domain being affected by the mutation (see **Section 8.6**). Following this strategy, we aimed not to alter linear Tulp4 expression.

Working with CRISPR/Cas 9 technology faces the disadvantage of targeting unexpected gene locations; the so-called off-targets (see **Section 5.3.2.2**). It has been shown that these unspecific alterations are mainly relevant in the context of cellular systems (clonal reproduction) and not for murine models, which are further backcrossed with WT C57Bl6, washing off off-target mutations, if any (Iyer et al., 2015; Wefers et al., 2017). In addition, the homogeneous electrophysiological outcome observed in the different studied systems, regulated by diverse circTulp4 depletion strategies, argued against the potential contribution of unexpected off-target mutations. Nevertheless, the ultimate demonstration of the phenotypical specificity is under current investigation; to do so, electrophysiological parameters will be measured upon rescuing circTulp4 expression in primary circTulp4^{KO}-derived neurons.

CircTulp4^{KO} mouse displayed a strong reduction of the circular RNA isoform expression of *Tulp4*, as assessed by qRT-PCR (see **Figure 25B**). Of note, a slight increase in the linear isoform of *Tulp4* in the different assessed brain regions and eyes was also observed. As shown in **Figure 23**, these

tissues highly express circTulp4 under WT conditions. Differently from *Dgki* (see **Figure 12**) or fly mbl (Ashwal-Fluss et al., 2014), we did not observe opposite regulation of *Tulp4* RNA isoforms in the studied systems. Linear Tulp4 was not increasing its expression with downregulation of circTulp4, neither it was downregulated with circTulp4 overexpression (see **Figure 14** and **Figure 15B**). Further experiments aim to verify if the increment in linear Tulp4 is biologically relevant by determining whether TULP4 overexpression contributes to the phenotypes observed in the circTulp4^{KO} mouse.

Of note, it has not escaped our attention that the approach we have taken for the generation of a murine model of circRNA depletion cannot necessarily be extrapolated to other circRNA candidates. The biogenesis of many circRNAs involves splicing sites which mutations would also alter the generation of their linear counterparts. Other strategies to regulate circRNA isoforms would include:

i) Generation of mice conditionally expressing different sh-RNAs using recombinase-mediated cassette exchange (RMCE) instead of the laborious homologous recombination (Hitz et al., 2007).
ii) RNA-targeting caspases (Kim, 2018) directed to the specific head-to-tail junctions. Cas13b in particular –differently from Cas9– does not require a specific sequence element (protospacer adjacent motif, PAM) in the target site, making it an attractive candidate as an RNA-modulating tool (Cox et al., 2017).

9.4.1 CircTulp4 deficiency impairs excitatory neurotransmission

The assessment of circTulp4 localization together with our synaptosomal RNA-sequencing results, where we found synaptic enrichment of the circular but not the linear isoform of *Tulp4* (Rybak-Wolf et al., 2015), prompted us to investigate possible electrophysiological effects of circTulp4 deficiency.

Here, we demonstrated through recordings of mini excitatory/inhibitory post-synaptic currents and via the assessment of the excitatory/inhibitory ratio that the excitatory neurotransmission is impaired when depleting circTulp4. Similar to what we observed in primary neuronal cultures, patch-clamp recordings on CA1 KO-derived neurons displayed a strong drop in the mEPSCs frequency, accompanied by a slight but significant increase in the amplitude (see **Figure 26**). Decreases in mESPCs frequencies can be interpreted either as a decrease in the probability of pre-synaptic release (Murthy et al., 2001), or in the number of functional synapses; less dendritic spines or fewer synapses onto already established spines (Malenka & Nicoll, 1997). The studies in which hippocampal neurons were transfected with sh-circTulp4 via *in utero* electroporation suggested that alterations in the post-synaptic compartment are sufficient to explain the neurotransmission impairment (see **Figure 27**). This conclusion is supported by the experiment design, where wild-type pre-synaptic neurons could be clearly distinguished from the post-synaptic, sh-circTulp4 transfected neurons. Further quantification of spine density and of the number of excitatory pre-synaptic contacts on sh-circTulp4 transfected neurons revealed no changes in spine number but a decreased number of VGlut1 synaptic contacts on mature dendritic spines (see **Figure 28**). Worth mentioning, the experiments performed in primary neuronal cultures also indicated that the recorded effect on excitatory neurotransmission is not restricted to the Schaffer collateral pathway synapses (see **Figure 19**).

In line with the reduced number of VGlut1 synaptic contacts observed when depleting circTulp4 expression, hippocampal neuronal cultures derived from VGLUT1-deficient mice also showed a drastically reduced excitatory neurotransmission. From 26 % of KO cells, no mEPSCs could be recorded, while the remaining showed a strongly reduced release frequency (Wojcik et al., 2004).

Studies on primary neuronal cultures are limited by the lack of a three-dimensional network where the different components of a brain microcircuit interact to preserve appropriate activity levels within an optimal range. Under physiological conditions, the nervous system responds to environmental changes allowing plastic mechanisms to shape its output and function without compromising the stability and integrity of the information stored or disrupting the processing

mechanisms that rely on differences in synaptic weights (Davis & Bezprozvanny, 2001; Turrigiano & Nelson, 2004). In this context, we interpret the increase in the amplitude of mEPSCs in the KO model as a plastic mechanism to maintain microcircuit homeostasis. Interestingly, neurons transfected via IUE displayed a different compensatory mechanism, a reduction in the frequency of mIPSCs without changes in the amplitudes of excitatory or inhibitory mPSCs. This difference between the KO model and the *in utero* electroporated neurons most likely derives from the fact that in the *in vivo* model all the cells –including pre- and post-synaptic neurons, and glial cells– are depleted from circTulp4 expression, while in the *in utero* electroporated mice only the post-synaptic neurons are.

Although the number of excitatory synaptic contacts on dendritic spines accounts for the reduced excitatory neurotransmission, it does not exclude that other mechanisms –such as the number of silent synapses, or pre-synaptic function alterations– may be contributing. During excitatory synapse maturation, AMPARs are inserted in the post-synaptic membrane after NMDARs (Petralia et al., 1999; Wu et al., 1996), accounting for the developmental decline in the number of 'silent synapses' (exhibiting NMDAR-mediated response but no AMPAR-mediated response) (Durand et al., 1996). Further experiments in circTulp4-deficient neurons aim to investigate whether the proportion of silent synapses is altered in our animal model.

Autapses –connections between a neuron and itself (Ikeda & Bekkers, 2006)– have been described in various brain regions, including the neocortex and the hippocampus (Cobb et al., 1997; Tamás et al., 1997). Although in most cases autapses are sparse *in vivo*, neurons in culture, especially if they are grown in confined spaces, form over a thousand autapses per cell. As a result, we could not fully discard that pre-synaptic alterations contribute to the reduced excitatory neurotransmission observed upon circTulp4 depletion. Facilitation is a pre-synaptic phenomenon observed at many synapses with a low initial probability of neurotransmitter release and is a sensitive indicator of the pre-synaptic function. As shown in **Figure 30**, circTulp4^{KO} mice showed increased paired-pulse facilitation, indicative of increased vesicle fusion, but accompanied by a decreased neurotransmitter release with the first stimulus. This result suggests that the increased facilitation may not derive from changes in the facilitation mechanism *per se*, but from a reduced basal release probability.

Together, our results indicate that circTulp4^{KO} presents excitatory neurotransmission dysfunction, with both pre- and post-synaptic contributions. To further examine pre-synaptic function alterations, possible differences in basal neurotransmitter release between the KO and

WT animals will be assessed. Different experimental designs can attain basal neurotransmitter release differences in indirect and direct ways. First, the level of stimulation required to evoke a criterion extracellular field excitatory post-synaptic potential (EPSP) can be measured. Second, synapses with a decreased release probability are less sensitive than normal synapses to changes that lower neurotransmitter release probability. This means, investigating the effects of lowering the extracellular Ca^{2+}/Mg^{2+} ratio, or of bath applications of the inhibitory agent adenosine, would indirectly indicate whether the basal release probability is altered in the mutant mouse. Lastly, neurotransmitter release can also be directly measured by loading synaptosomes from mutant and WT mice with [^{3}H]-norepinephrine and measuring the Ca^{2+}-dependent release as a function of depolarization. Additionally, synaptic alterations at protein level are currently being investigated in collaboration with Dr. Nils Brose at the Max-Planck-Institute for Experimental Medicine in Göttingen.

The E/I ratio is a measure of the general state of a brain microcircuit; alterations in this balance indicate circuit misregulation and are normally associated with neurodevelopmental disorders (Nelson & Valakh, 2015). As it has been shown in **Figure 29**, in agreement with the excitatory dysfunction revealed by mEPSCs measurements, circTulp4^{KO} mouse also displayed a strong E/I imbalance compared to WT controls. Notably, schizophrenia and autism are examples of disorders hypothesized to have a hypoglutamatergic origin (Nelson & Valakh, 2015). Brain structures implicated in these neurodevelopmental disorders, including the hippocampus, neocortex, and amygdala are predominantly composed of glutamatergic neurons; and glutamate antagonists have been shown to mimic some symptoms.

Electrophysiological recordings have also been performed on CDR1as knockout. EPSCs were studied in single hippocampal neurons at DIV 14-17, revealing a dysfunction of excitatory synaptic transmission (Piwecka et al., 2017). Opposite to circTulp4-deficiency phenotypes here reported, CDR1as KO neurons displayed an increase in mEPSCs frequency compared to control neurons without changes in the amplitude. In addition, the paired-pulse response revealed a strong depression in response to two consecutive stimuli on KO neurons. Their results and ours strongly suggest that at least brain-enriched circRNAs play a role in regulating synaptic transmission.

Overall, in this study we have reported dysfunctional excitatory neurotransmission in circTulp4-deficient neurons, expanding over the Schaffer collateral pathway synapses. Moreover, we

identified alterations in both post- and pre-synaptic compartments. In the next section, the behavioral consequences of depleting circTulp4 *in vivo* will be discussed.

9.4.2 Behavioral alterations of circTulp4^{KO} mouse

Conventional circTulp4 knockout mice have similar behavioral effects as the ones reported in mouse models displaying glutamate transmission- and/or synaptic plasticity-dysfunction, which in turn are associated with schizophrenia and certain neuropsychiatric conditions such as bipolar disorder and attention deficit hyperactivity disorder (Dyck et al., 2011; Garcia-Garcia et al., 2009; Wiedholz et al., 2008). Therefore, three relevant mouse models are being introduced to enrich our discussion:

- Model I: Vesicular glutamate transporter 1 (VGLUT1) knockout mouse (Wojcik et al., 2004), representing a model of reduced glutamatergic neurotransmission. Vesicular glutamate transporters are key players in the major pathway of excitatory neurotransmission in the mammalian brain. From the three known transporters (VGLUT1-3), VGLUT1 and VGLUT2 are predominantly expressed in the adult mouse brain. However, a developmental switch from VGLUT2 to VGLUT1 occurs during the second post-natal week in the hippocampus, cortex and cerebellum (Miyazaki et al., 2003).
- Model II: Synapsin II (Syn II) knockout mouse (Rosahl et al., 1995), representing a model of transmitter release impairment. Synapsins are a family of neuron-specific phosphoproteins –encoded in mammals by three distinct genes *Syn I-III*– that play a prominent role in synaptic homeostasis and plasticity. While Syn III is abundantly expressed during early neuronal development and becomes downregulated in adult animals, Syn I and Syn II start to express during synaptogenesis and continue highly expressed in mature neurons (Ferreira et al., 2000). However, Syn II KO displays the strongest phenotype, with more intense impairments in hippocampal short-term-plasticity than Syn I KO mice (Rosahl et al., 1993), supporting the notion that Syn II plays a more structural role than Syn I in nerve terminal physiology (Cesca et al., 2010).
- Model III: GluR1 knockout mice (Zamanillo et al., 1999), representing a model of severe loss of AMPAR. A major facet of glutamatergic neurotransmission takes action at AMPARs, post-synaptic tetramers composed of one or more glutamate receptor GluR1-4 subunits. Hippocampal CA1 pyramidal cells mainly express GluR1 and GluR2 of the four receptor subunits (Keinänen et al., 1990), and it has been shown that changes in the phosphorylation of GluR1 subunit play a role in the expression of LTP and LTD (Lee et al., 2003).

9.4.2.1 Increased locomotor activity

CircTulp4^{KO} showed increased activity in the novel environment of the open field, SHIRPA and Y-maze tests, but normal activity in a familiar home cage (compare **Figure 32** and Figure 34**A**, left with **Figure 35B-C**). Such phenotypic outcome is suggestive of increased anxiety and /or stress responsivity. Of note, circTulp4^{KO} mice displayed a slight decreased in activity levels compared to controls in the place learning module of the IntelliCages.

VGLUT1 knockout mice showed progressive neurological phenotype after the third post-natal week (Fremeau et al., 2004; Wojcik et al., 2004), therefore only heterozygous mice (VGLUT1+/−) were suitable for behavioral analysis. VGLUT1+/− mice displayed an increase in the total distance traveled after chronic mild stress, suggesting certain vulnerability towards developing abnormalities in locomotor activity after prolonged exposure to stress (Garcia-Garcia et al., 2009). Syn II knockout mice displayed a robust increase in basal locomotor activity when exposed to a novel open field test chamber (Dyck et al., 2009). Interestingly, protein expression analysis from prefrontal cortex tissue revealed decreases in the concentrations of vesicular glutamate (VGLUT1 and VGLUT2) and GABA (VGAT) transporters in Syn II-deficient models (Bogen et al., 2009; Dyck et al., 2011). However, expression of the same proteins was not assessed in the hippocampus. Remarkably, GluR1 knockout mice also exhibited significant hyperactivity when exposed to a new environment such as an open field, but normal locomotor activity in the familiar environment of the home cage (Wiedholz et al., 2008). Furthermore, hyperactivity was still evident after five daily 30 min test exposure, arguing that these mice exhibited behavioral hyperexcitability in response to even modest environmental stimulation. Phenotypic convergence in mice showing glutamatergic dysfunction, as it has been shown for circTulp4^{KO} (see **Sections 8.4** and **8.6.1**), is suggestive of overlapping molecular mechanisms.

9.4.2.2 Aberrant sensorimotor recruitment

CircTulp4^{KO} mice also displayed increased acoustic startle response (ASR), without a change in hearing sensitivity (ABR), and an augmented thermal sensitivity on the hotplate, accounting for aberrant sensorimotor recruitment (see **Figure 33**). Enhanced startle reaction has also been described in VGLUT1-deficient mice (Fremeau et al., 2004; Inta et al., 2012). However, it is worth noticing that enhanced anxiety can also increase the amplitude of the ASR (Koch, 1999). Future experiments aim to further characterize anxiety-related behavior on circTulp4^{KO} mice, as this mood-disorder may act as a confounding factor in other behavioral tests. Most experiments

assessing anxiety-like behavior are based on approach-avoidance conflicts; mice naturally display high levels of exploration of a novel environment but also have an innate aversion to entering exposed, well-lit areas. CircTulp4-deficient mice have shown increased anxiety in the EPM, as revealed by reduced time in the aversive open areas of the plus-maze. At the moment, KO animals and proper controls are being tested in the Dark-Light box (DaLi) test (Hascoët et al., 2001).

Pre-pulse inhibition (PPI) test represents a cross-species measure of sensorimotor gating, and earlier studies have shown that gating deficits are highly correlated with measures of thought disturbance (Braff et al., 1999). CircTulp4^{KO} mice showed no differences in sensorimotor gating compared to littermate controls (see **Figure 33B**).

9.4.2.3 Cognitive deficits

The putative role of glutamate receptor-mediated synaptic plasticity in learning has attracted great attention to rodent hippocampus as a model for studying working memory dysfunctions (Martin et al., 2000). The strong electrophysiological phenotypes observed in circTulp4-deficient hippocampal neurons, indicative of a dysfunctional excitatory connection, would suggest impaired hippocampus-dependent behavioral phenotypes. In this project, we have tested hippocampus-dependent spatial working memory by measuring the percentage of spontaneous alternations (SPAs), while some aspects of attention and locomotor rotational bias were attained by calculating the percentage of alternate arm returns (AARs) in the Y-maze. Since circTulp4^{KO} mice presented increased locomotor activity, they could start making rotations yielding 100 % alternation score without posing any demand on working memory. The decreased percentage of SPAs and the increased percentage of AARs are output parameters confirming altered spatial working memory (see **Figure 34A**).

Similarly, VGLUT1+/− mice exhibited cognitive alterations in the T-Maze test, showing a statistically significant reduced preference to enter the new, unfamiliar arm compared to their littermate controls (Inta et al., 2012). Syn II knockout mice were also shown to exhibit deficits in spatial learning on the Morris water maze (Corradi et al., 2008).

Hippocampal malfunction is known to have two behavioral correlates: i) altered short-term spatial working memory, evidenced by increased visits to an arm that has just been visited in a Y-maze, T-maze or radial maze tasks; and ii) impaired or missing spatial reference memory, typically assessed in a water maze and evidenced by prolonged escape latencies and reduced

searching over the position of removed escape platforms. However, testing hippocampal lesions effects has revealed that spatial reference memory can recover to some extent (Galani et al., 2002; Voikar et al., 2010), and that hippocampal syndrome has a complex behavioral outcome that includes changes in anxiety (Deacon & Rawlins, 2005), increased locomotor activity (Bannerman et al., 2014; Jarrard, 1964), impaired species-typical behavior (Deacon et al., 2002; Deacon & Rawlins, 2005; O'Keefe & Nadel, 1978), diminished sociability (Ely et al., 1976; Maaswinkel et al., 1997; Uekita & Okanoya, 2011), and physiological changes (Ely et al., 1977).

To further optimize the characterization of circTulp4^{KO} cognitive function, mice were subjected to evaluation in the IntelliCage. This system provides the unique possibility to test animals in their social group, decreasing stress levels associated with single housing and thus possibly revealing modest differences that otherwise could be masked (Wolfer et al., 2004).

As it has already been mentioned above, activity levels in the familiar environment of the home cage were not found increased in circTulp4^{KO} mice compared to control littermates, rather the opposite phenotype was observed (**Figure 35B-C,** left) or no statistical difference between genotypes (see **Figure 35B-C,** middle and right). However, to our surprise, circTulp4^{KO} mice showed improved learning in comparison with control mice, as shown by a faster error rate reduction in the three evaluated modules (see **Figure 35A**).

Why did circTulp4^{KO} mice perform better than littermate controls? It has been shown that motivational cues for learning can modify the outcome of behavioral tests, which is nicely exemplified when adding positive or negative reinforcements to classical tasks (Mechan et al., 2009; Reisel et al., 2002). Stress-induced increases in glucocorticoid hormone levels can impact on spatially orientated cognitive performance, resulting in superior reference and working memory (Brinks et al., 2007). Overall, circTulp4^{KO} mice seem to be more stressed by novelty than littermate controls. This interpretation is consistent with the increased locomotion activity in novel environments and absence of general hyperactivity in the IntelliCage, visualized as total number of visits and nosepokes (see **Figure 35B-C**). Following this line of thinking, it is possible that the assignment of a new drinking corner in the IntelliCage (or the weak consequence of having to move to another corner upon incorrect nosepoking) works as an aversive stimulus only on the mutant mice, which then learn faster as a mechanism to decrease the novelty-induced stress. This hypothesis is supported by the tendency towards an increased explorative behavior of WT littermate controls (see **Figure 35B-C**). In the absence of negative reinforcement, mice natural instinct for exploration is too strong to permit effective learning. A second possibility derives from the observed increased body mass in the KO females compared to control

littermates (**Figure 31**). Higher demand on food is normally accompanied by higher water intake, acting the latter as a physiological motivational cue contributing to their better learning performance in the IntelliCage. To further test the first hypothesis, as described in the above section, specific anxiety-related behaviors will be tested. In addition, corticosterone levels will be measured upon a short period of constraint as readout of stress responsivity. Testing the second hypothesis would require detailed food and water intake investigation in an automated metabolic cage. Importantly, the increased body mass was only observed in female circTulp4^{KO}.

Of note, Voikar et al. (2018) recently reported that hippocampal-lesioned female C57BL/6 mice, let to recover for long post-operative times, and evaluated in the IntelliCage, have only marginally impaired the ability to solve simple rewarded spatial preference and reversal tasks (Voikar et al., 2018). The initial experiment design of Voikar et al. (2018), like ours, did not include punishment upon incorrect choices. However, they noticed that when nosepoke errors in the three inappropriate corners were punished by air-puffs, all mice learned the task much faster, and there were no more behavioral outliers (Voikar et al., 2018). The lack of effects on simple spatial learning by hippocampal-lesioned rodents (mostly rats) has been described before (O'Keefe & Nadel, 1978) and it could be explained by other brain structures playing a role in learning such a basic survival task as the position of water supply. Furthermore, Voikar et al. (2018) also showed that tasks requiring precise circadian timing, putative working memory, or when incorrect choices were punished by air-puffs, hippocampal-lesioned mice displayed massive problems (Voikar et al., 2018). Although we cannot predict the outcome of circTulp4^{KO} mice in an IntelliCage design that punishes incorrect choices, we would expect mutant animals to poorly perform in tasks specifically assessing working memory.

Different aspects of spatial memory were not previously revealed by hippocampal lesions studies, but only with studies on subunit or subtype glutamatergic receptors knockout mice (Bannerman, 2009). Interestingly, GluR1 KO mice presented spatial memory dissociations; exhibiting a dramatic impairment in spatial working memory on the T-maze rewarded alternation task, but intact reference memory in the radial maze (Reisel et al., 2002). These results identified a GluR1-dependent, non-associative short-term memory mechanism that is important for performance on spatial working memory tasks, and a GluR1-independent, long-term associative memory mechanism which underlies performance on spatial reference memory tasks. Further molecular characterization of the KO glutamatergic receptors levels/composition needs to be performed to test this hypothesis. Assessing the number of silent synapses would already serve as an indicator of the AMPAR number.

The studies published by Reisel. et al (2002) and Voikar et al. (2008) indicate the need for a comprehensive battery of behavioral tests in circTulp4^{KO} mice assessing separately spatial reference and working memory.

CDR1as KO mice were also subjected to behavioral testing, displaying normal locomotion activity, unaffected anxiety levels, normal social behavior, and no deficits in recognition memory (Piwecka et al., 2017). Although CDR1as is predominantly expressed in excitatory neurons, which are particularly abundant in the hippocampus, it comes as a surprise that hippocampus-dependent working memory was not assessed in CDR1as KO mice. However, they did reveal a behavioral phenotype related to neuropsychiatric disorders, a substantial decrease (between 30-50 %) in the PPI compared to WT controls (Piwecka et al., 2017). Taken together, the altered neuronal activity and behavioral phenotypes linked to circRNA depletion strongly suggest that brain-enriched circRNAs play an essential role in the correct function of the brain.

10 Conclusion and Outlook

The study of circRNAs has progressed at an exponential level in the past few years. The unique covalently-closed circular structure confers circRNAs distinctive characteristics compared to linear RNAs. However, detecting and manipulating circular transcripts faces technical difficulties given their low abundance and the high degree of sequence identity with their linear counterparts. In this study, we addressed this issue by using various molecular and genetic tools designed against the circRNA-specific head-to-tail junction, validating the models by circRNA expression regulation and by the use of different but complementary technics.

Using a loss-of-function approach, we have investigated the function of the circular isoform derived from *Tulp4*. CircTulp4 is the most abundantly expressed coding-sequence-derived circRNA in neurons. Depletion of circTulp4 at early developmental time points in primary neuronal cultures delayed neurite outgrowth. Although axonal length was recovered by DIV 5, the growth of neurites destined to become dendrites remained impaired. Importantly, assessing post- and pre-synaptic function of circTulp4-deficient neurons by electrophysiological recordings revealed a strong impairment in excitatory neurotransmission. This phenotype was further supported by an imbalanced E/I ratio in the mutant mouse model. As a molecular correlate of this electrophysiological outcome, we found a reduction of the number of excitatory synaptic contacts on dendritic spines.

To generate a circTulp4 depletion mouse model, here, we have interfered with the circRNA biogenesis by exchanging a single base-pair in the splice acceptor site using CRISPR/Cas9. CircTulp4^{KO} mouse displayed a specific decrease of circTulp4 expression, accompanied by no-gross morphological anomalies. Notably, KO animals recapitulated the electrophysiological phenotype observed in circTulp4-deficient cultures and in acute hippocampal slices transfected via the *in utero* electroporation technique. In addition, electrophysiological studies in the KO mouse revealed alterations at a pre-synaptic level. Paired-pulse facilitation measurements indicate potential changes in the basal release probability that need to be confirmed by further experiments.

Given the general glutamatergic neurotransmission dysfunction at hippocampal level, it did not come as a surprise that circTulp4^{KO} animals displayed substantial hippocampal-dependent spatial memory alterations. Overall, mutant mice showed novelty-induced increased locomotor activity and impaired working memory. However, when tested in the home cage environment of the IntelliCages, no changes in activity level were detected and mutants showed improved learning

performance in the place learning, reversal learning and patrolling modules, compared with control littermates. We are currently evaluating anxiety-related behaviors to assess for alterations in stress reactivity that could impact on the behavioral phenotypic outcome and interpretation. We also plan to evaluate circTulp4^{KO} at behavioral tasks that allow better distinguishing between spatial reference memory and working memory.

Overall, our results provided novel, comprehensive and, most importantly, physiological insights into the role of the most abundantly expressed, brain-enriched, coding sequence-derived circRNA, circTup4. However, the more we learn, the more evident becomes which questions remain open: How and to what extent do pre- and post-synaptic effects contribute to the deficient excitatory neurotransmission? Is the impairment in excitatory neurotransmission fully explained by the decrease in VGlut1 synaptic contacts, or is the number of silent synapses also altered? How does stress influences on the behavioral outcome of circTulp4^{KO} animals? Are mutants indeed showing spatial memory dissociations? What is the mechanism of action of circTulp4? Which environmental factors modulate circTulp4 expression? Furthermore, it also results intriguing what is TULP4 function in the mammalian brain, and whether it is related to circTulp4. We expect to be able to answer these questions in the near future using the battery of genetic and molecular tools that have been generated at our lab during the past years.

In conclusion, the present study revealed that circTulp4 acts in the finely regulated process of excitatory synaptic transmission and that its depletion strongly impacts spatial working memory.

11 References

Abe, N., Matsumoto, K., Nishihara, M., Nakano, Y., Shibata, A., Maruyama, H., … Abe, H. (2015). Rolling Circle Translation of Circular RNA in Living Human Cells. *Scientific Reports*, *5*, 16435. https://doi.org/10.1038/srep16435

Abelson, J., Trotta, C. R., & Li, H. (1998). tRNA splicing. *Journal of Biological Chemistry*. https://doi.org/10.1074/jbc.273.21.12685

Akemann, W., Mutoh, H., Perron, A., Rossier, J., & Knöpfel, T. (2010). Imaging brain electric signals with genetically targeted voltage-sensitive fluorescent proteins. *Nature Methods*. https://doi.org/10.1038/nmeth.1479

Aktaş, T., Ilik, I. A., Maticzka, D., Bhardwaj, V., Pessoa Rodrigues, C., Mittler, G., … Akhtar, A. (2017). DHX9 suppresses RNA processing defects originating from the Alu invasion of the human genome. *Nature*. https://doi.org/10.1038/nature21715

Anderton, B. H., Callahan, L., Coleman, P., Davies, P., Flood, D., Jicha, G. A., … Weaver, C. (1998). Dendritic changes in Alzheimer's disease and factors that may underlie these changes. *Progress in Neurobiology*. https://doi.org/10.1016/S0301-0082(98)00022-7

Andrews, S. J., & Rothnagel, J. A. (2014). Emerging evidence for functional peptides encoded by short open reading frames. *Nature Reviews Genetics*. https://doi.org/10.1038/nrg3520

Aprea, J., Prenninger, S., Dori, M., Ghosh, T., Monasor, L. S., Wessendorf, E., … Calegari, F. (2013). Transcriptome sequencing during mouse brain development identifies long non-coding RNAs functionally involved in neurogenic commitment. *EMBO Journal*. https://doi.org/10.1038/emboj.2013.245

Ashwal-Fluss, R., Meyer, M., Pamudurti, N. R., Ivanov, A., Bartok, O., Hanan, M., … Kadener, S. (2014). circRNA Biogenesis Competes with Pre-mRNA Splicing. *Molecular Cell*, 1–12. https://doi.org/10.1016/j.molcel.2014.08.019

Asrican, B., Lisman, J., & Otmakhov, N. (2007). Synaptic strength of individual spines correlates with bound Ca 2+-calmodulin-dependent kinase II. *Journal of Neuroscience*, *27*(51). https://doi.org/10.1523/JNEUROSCI.3587-07.2007

Azevedo, F. A. C., Carvalho, L. R. B., Grinberg, L. T., Farfel, J. M., Ferretti, R. E. L., Leite, R. E. P., … Herculano-Houzel, S. (2009). Equal numbers of neuronal and nonneuronal cells make the human brain an isometrically scaled-up primate brain. *Journal of Comparative Neurology*, *513*(5), 532–541. https://doi.org/10.1002/cne.21974

Bahn, J. H., Zhang, Q., Li, F., Chan, T. M., Lin, X., Kim, Y., … Xiao, X. (2015). The landscape of MicroRNA, piwi-interacting RNA, and circular RNA in human saliva. *Clinical Chemistry*. https://doi.org/10.1373/clinchem.2014.230433

Banker, G. A., & Cowan, W. M. (1977). Rat hippocampal neurons in dispersed cell culture. *Brain Research*, *126*(3), 397–425. https://doi.org/10.1016/0006-8993(77)90594-7

Bannerman, D. M. (2009). Fractionating spatial memory with glutamate receptor subunit-knockout mice: Figure 1. *Biochemical Society Transactions*, *37*(6), 1323–1327. https://doi.org/10.1042/bst0371323

Bannerman, D. M., Sprengel, R., Sanderson, D. J., Mchugh, S. B., Rawlins, J. N. P., Monyer, H.,

& Seeburg, P. H. (2014). Hippocampal synaptic plasticity, spatial memory and anxiety. *Nature Reviews Neuroscience*. https://doi.org/10.1038/nrn3677

Barash, Y., Calarco, J. A., Gao, W., Pan, Q., Wang, X., Shai, O., … Frey, B. J. (2010). Deciphering the splicing code. *Nature*. https://doi.org/10.1038/nature09000

Barbosa-Morais, N. L., Irimia, M., Pan, Q., Xiong, H. Y., Gueroussov, S., Lee, L. J., … Blencowe, B. J. (2012). The evolutionary landscape of alternative splicing in vertebrate species. *Science*. https://doi.org/10.1126/science.1230612

Barnes, A. P., & Polleux, F. (2009). Establishment of Axon-Dendrite Polarity in Developing Neurons. *Annual Review of Neuroscience*, *32*(1), 347–381. https://doi.org/10.1146/annurev.neuro.31.060407.125536

Barrangou, R., Fremaux, C., Deveau, H., Richards, M., Boyaval, P., Moineau, S., … Horvath, P. (2007). CRISPR provides acquired resistance against viruses in prokaryotes. *Science*, *315*(5819), 1709–1712. https://doi.org/10.1126/science.1138140

Barrett, S. P., Wang, P. L., & Salzman, J. (2015). Circular RNA biogenesis can proceed through an exon-containing lariat precursor. *ELife*, *4*, 1–18. https://doi.org/10.7554/eLife.07540

Barrett, S., Parker, K. R., Horn, C., Mata, M., & Salzman, J. (2017). ciRS-7 exonic sequence is embedded in a long non-coding RNA locus. *BioRxiv*, 169508. https://doi.org/10.1101/169508

Barry, G., Briggs, J. A., Vanichkina, D. P., Poth, E. M., Beveridge, N. J., Ratnu, V. S., … Mattick, J. S. (2014). The long non-coding RNA Gomafu is acutely regulated in response to neuronal activation and involved in schizophrenia-associated alternative splicing. *Molecular Psychiatry*. https://doi.org/10.1038/mp.2013.45

Bartlett, W. P., & Banker, G. A. (1984). An electron microscopic study of the development of axons and dendrites by hippocampal neurons in culture. II. Synaptic relationships. *The Journal of Neuroscience : The Official Journal of the Society for Neuroscience*. https://doi.org/10.1523/JNEUROSCI.04-08-01954.1984

Bassett, A. R., Akhtar, A., Barlow, D. P., Bird, A. P., Brockdorff, N., Duboule, D., … Ponting, C. P. (2014). Considerations when investigating lncRNA function in vivo. *ELife*, *3*(August2014), 1–14. https://doi.org/10.7554/eLife.03058

Bayer, S. A., Altman, J., Russo, R. J., Dai, X., & Simmons, J. A. (1991). Cell migration in the rat embryonic neocortex. *Journal of Comparative Neurology*, *307*(3), 499–516. https://doi.org/10.1002/cne.903070312

Beique, J.-C., Lin, D.-T., Kang, M.-G., Aizawa, H., Takamiya, K., & Huganir, R. L. (2006). Synapse-specific regulation of AMPA receptor function by PSD-95. *Proceedings of the National Academy of Sciences*, *103*(51), 19535–19540. https://doi.org/10.1073/pnas.0608492103

Belgard, T. G., Marques, A. C., Oliver, P. L., Abaan, H. O., Sirey, T. M., Hoerder-Suabedissen, A., … Ponting, C. P. (2011). A transcriptomic atlas of mouse neocortical layers. *Neuron*. https://doi.org/10.1016/j.neuron.2011.06.039

Benson, D. L., Watkins, F. H., Steward, O., & Banker, G. (1994). Characterization of GABAergic neurons in hippocampal cell cultures. *Journal of Neurocytology*, *23*(5), 279–295. https://doi.org/10.1007/BF01188497

Birney, E., Stamatoyannopoulos, J. A., Dutta, A., Guigó, R., Gingeras, T. R., Margulies, E. H., … De Jong, P. J. (2007). Identification and analysis of functional elements in 1% of the human genome by the ENCODE pilot project. *Nature*, *447*(7146), 799–816. https://doi.org/10.1038/nature05874

Bliss, T. V. P., & Lømo, T. (1973). Long-lasting potentiation of synaptic transmission in the dentate area of the anaesthetized rabbit following stimulation of the perforant path. *The Journal of Physiology*, *232*(2), 331–356. https://doi.org/10.1113/jphysiol.1973.sp010273

Bogdanove, A. J., & Voytas, D. F. (2011). TAL effectors: Customizable proteins for DNA targeting. *Science*. https://doi.org/10.1126/science.1204094

Bogen, I. L., Haug, K. H., Roberg, B., Fonnum, F., & Walaas, S. I. (2009). The importance of synapsin I and II for neurotransmitter levels and vesicular storage in cholinergic, glutamatergic and GABAergic nerve terminals. *Neurochemistry International*. https://doi.org/10.1016/j.neuint.2009.02.006

Boggon, T. J., Shan, W. S., Santagata, S., Myers, S. C., & Shapiro, L. (1999). Implication of tubby proteins as transcription factors by structure- based functional analysis. *Science*. https://doi.org/10.1126/science.286.5447.2119

Bolton, M. M., Pittman, A. J., & Lo, D. C. (2000). Brain-derived neurotrophic factor differentially regulates excitatory and inhibitory synaptic transmission in hippocampal cultures. *The Journal of Neuroscience : The Official Journal of the Society for Neuroscience*. https://doi.org/10.1523/jneurosci.1234-11.2011

Bourne, J., & Harris, K. M. (2007). Do thin spines learn to be mushroom spines that remember? *Current Opinion in Neurobiology*. https://doi.org/10.1016/j.conb.2007.04.009

Braff, D. L., Swerdlow, N. R., & Geyer, M. A. (1999). Symptom correlates of prepulse inhibition deficits in male schizophrenic patients. *American Journal of Psychiatry*. https://doi.org/10.1176/ajp.156.4.596

Brandl, C., Ortiz, O., Röttig, B., Wefers, B., Wurst, W., & Kühn, R. (2015). Creation of targeted genomic deletions using TALEN or CRISPR/Cas nuclease pairs in one-cell mouse embryos. *FEBS Open Bio*, *5*, 26–35. https://doi.org/10.1016/j.fob.2014.11.009

Brewer, G. J. (1997). Isolation and culture of adult rat hippocampal neurons. *Journal of Neuroscience Methods*, *71*(2), 143–155. https://doi.org/10.1016/S0165-0270(96)00136-7

Bridi, M. C. D., De Pasquale, R., Lantz, C. L., Gu, Y., Borrell, A., Choi, S. Y., … Kirkwood, A. (2018). Two distinct mechanisms for experience-dependent homeostasis. *Nature Neuroscience*. https://doi.org/10.1038/s41593-018-0150-0

Brinks, V. (2007). Emotion and cognition in high and low stress sensitive mouse strains: a combined neuroendocrine and behavioral study in BALB/c and C57BL/6J mice. *Frontiers in Behavioral Neuroscience*, *1*(December). https://doi.org/10.3389/neuro.08.008.2007

Brown, A. J., Fisher, D. A., Kouranova, E., McCoy, A., Forbes, K., Wu, Y., … Cui, X. (2013). Whole-rat conditional gene knockout via genome editing. *Nat Methods*, *10*(7), 638–640. https://doi.org/10.1038/nmeth.2516

Brummelkamp, T. R., Bernards, R., & Agami, R. (2002). A system for stable expression of short interfering RNAs in mammalian cells. *Science*. https://doi.org/10.1126/science.1068999

Burns, M. E., & Augustine, G. J. (1995). Synaptic structure and function: Dynamic organization yields architectural precision. *Cell*. https://doi.org/10.1016/0092-8674(95)90160-4

Capecchi, M. R. (1989). Altering the genome by homologous recombination. *Science*, *244*(4910), 1288–1292. https://doi.org/10.1126/science.2660260

Capecchi, M. R. (2005). Gene targeting in mice: Functional analysis of the mammalian genome for the twenty-first century. *Nature Reviews Genetics*. https://doi.org/10.1038/nrg1619

Capel, B., Swain, a, Nicolis, S., Hacker, a, Walter, M., Koopman, P., … Lovell-Badge, R. (1993). Circular transcripts of the testis-determining gene Sry in adult mouse testis. *Cell*, *73*, 1019–1030. https://doi.org/10.1016/0092-8674(93)90279-Y

Carbery, I. D., Ji, D., Harrington, A., Brown, V., Weinstein, E. J., Liaw, L., & Cui, X. (2010). Targeted genome modification in mice using zinc-finger nucleases. *Genetics*, *186*(2), 451–459. https://doi.org/10.1534/genetics.110.117002

Carninci, P., Kasukawa, T., Katayama, S., Gough, J., Frith, M. C., Maeda, N., … Nishiguchi, S. (2005). The transcriptional landscape of the mammalian genome. *Science*, *309*(5740), 1559–1563. https://doi.org/10.1126/science.1112014

Cech, T. R. (1990). Self-splicing of group I introns. *Annual Review of Biochemistry*. https://doi.org/10.1146/annurev.biochem.59.1.543

Cesca, F., Baldelli, P., Valtorta, F., & Benfenati, F. (2010). The synapsins: Key actors of synapse function and plasticity. *Progress in Neurobiology*. https://doi.org/10.1016/j.pneurobio.2010.04.006

Chen, B., Gilbert, L. a., Cimini, B. a., Schnitzbauer, J., Zhang, W., Li, G. W., … Huang, B. (2013). Dynamic imaging of genomic loci in living human cells by an optimized CRISPR/Cas system. *Cell*, *155*(7), 1479–1491. https://doi.org/10.1016/j.cell.2013.12.001

Chen, C. Y., & Sarnow, P. (1995). Initiation of protein synthesis by the eukaryotic translational apparatus on circular RNAs. *Science*. https://doi.org/10.1126/science.7536344

Chen, I., Chen, C. Y., & Chuang, T. J. (2015). Biogenesis, identification, and function of exonic circular RNAs. *Wiley Interdisciplinary Reviews: RNA*. https://doi.org/10.1002/wrna.1294

Chen, J., Li, Y., Zheng, Q., Bao, C., He, J., Chen, B., … Huang, S. (2017). Circular RNA profile identifies circPVT1 as a proliferative factor and prognostic marker in gastric cancer. *Cancer Letters*. https://doi.org/10.1016/j.canlet.2016.12.006

Chu, C., Qu, K., Zhong, F. L., Artandi, S. E., & Chang, H. Y. (2011). Genomic Maps of Long Noncoding RNA Occupancy Reveal Principles of RNA-Chromatin Interactions. *Molecular Cell*. https://doi.org/10.1016/j.molcel.2011.08.027

Cobb, S. R., Halasy, K., Vida, I., Nyíri, G., Tamás, G., Buhl, E. H., & Somogyi, P. (1997). Synaptic effects of identified interneurons innervating both interneurons and pyramidal cells in the rat hippocampus. *Neuroscience*. https://doi.org/10.1016/S0306-4522(97)00055-9

Cocquerelle, C., Daubersies, P., Majérus, M. a, Kerckaert, J. P., & Bailleul, B. (1992). Splicing with inverted order of exons occurs proximal to large introns. *The EMBO Journal*, *11*(3), 1095–1098. https://doi.org/10.1016/0168-9525(92)90213-N

Conn, S. J., Pillman, K. a., Toubia, J., Conn, V. M., Salmanidis, M., Phillips, C. a., … Goodall, G. J. (2015). The RNA binding protein quaking regulates formation of circRNAs. *Cell*, *160*(6), 1125–1134. https://doi.org/10.1016/j.cell.2015.02.014

Conte, F., Oti, M., Dixon, J., Carels, C. E. L., Rubini, M., & Zhou, H. (2016). Systematic analysis of copy number variants of a large cohort of orofacial cleft patients identifies candidate genes for orofacial clefts. *Human Genetics*, *135*(1), 41–59. https://doi.org/10.1007/s00439-015-1606-x

Copi, A., Jüngling, K., & Gottmann, K. (2005). Activity- and BDNF-Induced Plasticity of Miniature Synaptic Currents in ES Cell-Derived Neurons Integrated in a Neocortical Network. *Journal of Neurophysiology*. https://doi.org/10.1152/jn.00155.2005

Corradi, A., Zanardi, A., Giacomini, C., Onofri, F., Valtorta, F., Zoli, M., & Benfenati, F. (2008). Synapsin-I- and synapsin-II-null mice display an increased age-dependent cognitive impairment. *Journal of Cell Science*, *121*(18), 3042–3051. https://doi.org/10.1242/jcs.035063

Côté, F., & Perreault, J. P. (1997). Peach latent mosaic viroid is locked by a 2'5'-phosphodiester bond produced by in vitro self-ligation. *Journal of Molecular Biology*. https://doi.org/10.1006/jmbi.1997.1355

Cox, D. B. T., Gootenberg, J. S., Abudayyeh, O. O., Franklin, B., Kellner, M. J., Joung, J., & Zhang, F. (2017). RNA editing with CRISPR-Cas13. *Science*. https://doi.org/10.1126/science.aaq0180

Craig, A., & Banker, G. (1994). Neuronal polarity. *Annual Review of Neuroscience*, *17*, 267–310. https://doi.org/10.1146/annurev.ne.17.030194.001411

Cui, X., Ji, D., Fisher, D. A., Wu, Y., Briner, D. M., & Weinstein, E. J. (2011). Targeted integration in rat and mouse embryos with zinc-finger nucleases. *Nature Biotechnology*, *29*(1), 64–68. https://doi.org/10.1038/nbt.1731

Danan, M., Schwartz, S., Edelheit, S., & Sorek, R. (2012). Transcriptome-wide discovery of circular RNAs in Archaea. *Nucleic Acids Research*. https://doi.org/10.1093/nar/gkr1009

Davis, G. W., & Bezprozvanny, I. (2001). Maintaining the Stability of Neural Function: A Homeostatic Hypothesis. *Annual Review of Physiology*. https://doi.org/10.1146/annurev.physiol.63.1.847

Deacon, R. M. J., Bannerman, D. M., Kirby, B. P., Croucher, A., & Rawlins, J. N. P. (2002). Effects of cytotoxic hippocampal lesions in mice on a cognitive test battery. *Behavioural Brain Research*. https://doi.org/10.1016/S0166-4328(01)00451-X

Deacon, R. M. J., & Rawlins, J. N. P. (2005). Hippocampal lesions, species-typical behaviours and anxiety in mice. *Behavioural Brain Research*. https://doi.org/10.1016/j.bbr.2004.05.027

Dellu, F., Contarino, A., Simon, H., Koob, G. F., & Gold, L. H. (2000). Genetic differences in response to novelty and spatial memory using a two-trial recognition task in mice. *Neurobiology of Learning and Memory*. https://doi.org/10.1006/nlme.1999.3919

Deltcheva, E., Chylinski, K., Sharma, C. M., Gonzales, K., Chao, Y., Pirzada, Z. A., … Charpentier, E. (2011). CRISPR RNA maturation by trans-encoded small RNA and host factor RNase III. *Nature*, *471*(7340), 602–607. https://doi.org/10.1038/nature09886

Derrien, T., Johnson, R., Bussotti, G., Tanzer, A., Djebali, S., Tilgner, H., … Guigó, R. (2012). The GENCODE v7 catalog of human long noncoding RNAs: Analysis of their gene structure, evolution, and expression. *Genome Research*. https://doi.org/10.1101/gr.132159.111

Dethoff, E. A., Chugh, J., Mustoe, A. M., & Al-Hashimi, H. M. (2012). Functional complexity and regulation through RNA dynamics. *Nature*. https://doi.org/10.1038/nature10885

Dölen, G., & Bear, M. F. (2008). Role for metabotropic glutamate receptor 5 (mGluR5) in the pathogenesis of fragile X syndrome. In *Journal of Physiology*. https://doi.org/10.1113/jphysiol.2008.150722

Dong, R., Ma, X. K., Chen, L. L., & Yang, L. (2017). Increased complexity of circRNA expression during species evolution. *RNA Biology*. https://doi.org/10.1080/15476286.2016.1269999

Dotti, C., Sullivan, C., & Banker, G. (1988). The establishment of polarity by hippocampal neurons in culture. *The Journal of Neuroscience*, *8*(4), 1454–1468. https://doi.org/10.1523/JNEUROSCI.08-04-01454.1988

Du, W. W., Fang, L., Yang, W., Wu, N., Awan, F. M., Yang, Z., & Yang, B. B. (2017a). Induction of tumor apoptosis through a circular RNA enhancing Foxo3 activity. *Cell Death and Differentiation*. https://doi.org/10.1038/cdd.2016.133

Du, W. W., Yang, W., Chen, Y., Wu, Z. K., Foster, F. S., Yang, Z., … Yang, B. B. (2017b). Foxo3 circular RNA promotes cardiac senescence by modulating multiple factors associated with stress and senescence responses. *European Heart Journal*. https://doi.org/10.1093/eurheartj/ehw001

Du, W. W., Yang, W., Liu, E., Yang, Z., Dhaliwal, P., & Yang, B. B. (2016). Foxo3 circular RNA retards cell cycle progression via forming ternary complexes with p21 and CDK2. *Nucleic Acids Research*, *44*(6), 2846–2858. https://doi.org/10.1093/nar/gkw027

Dumitriu, D., Hao, J., Hara, Y., Kaufmann, J., Janssen, W. G. M., Lou, W., … Morrison, J. H. (2010). Selective Changes in Thin Spine Density and Morphology in Monkey Prefrontal Cortex Correlate with Aging-Related Cognitive Impairment. *Journal of Neuroscience*, *30*(22), 7507–7515. https://doi.org/10.1523/JNEUROSCI.6410-09.2010

Dunham, I., Kundaje, A., Aldred, S. F., Collins, P. J., Davis, C. A., Doyle, F., … Lochovsky, L. (2012). An integrated encyclopedia of DNA elements in the human genome. *Nature*, *489*(7414), 57–74. https://doi.org/10.1038/nature11247

Durand, G. M., Kovalchuk, Y., & Konnerth, A. (1996). Long-term potentiation and functional synapse induction in developing hippocampus. *Nature*. https://doi.org/10.1038/381071a0

Dyck, Bailee A., Skoblenick, K. J., Castellano, J. M., Ki, K., Thomas, N., & Mishra, R. K. (2009). Behavioral abnormalities in synapsin II knockout mice implicate a causal factor in schizophrenia. *Synapse*, *63*(8), 662–672. https://doi.org/10.1002/syn.20643

Dyck, Bailey A., Beyaert, M. G. R., Ferro, M. A., & Mishra, R. K. (2011). Medial prefrontal

cortical synapsin II knock-down induces behavioral abnormalities in the rat: Examining synapsin II in the pathophysiology of schizophrenia. *Schizophrenia Research*, *130*(1–3), 250–259. https://doi.org/10.1016/j.schres.2011.05.017

Ebbesen, K. K., Hansen, T. B., & Kjems, J. (2017). Insights into circular RNA biology. *RNA Biology*, *14*(8), 1035–1045. https://doi.org/10.1080/15476286.2016.1271524

Ely, D. L., Greene, E. G., & Henry, J. P. (1976). Minicomputer monitored social behavior of mice with hippocampus lesions. *Behavioral Biology*. https://doi.org/10.1016/S0091-6773(76)91082-8

Ely, D. L., Greene, E. G., & Henry, J. P. (1977). Effects of hippocampal lesion on cardiovascular, adrenocortical and behavioral response patterns in mice. *Physiology and Behavior*. https://doi.org/10.1016/0031-9384(77)90014-2

Engert, F., & Bonhoeffer, T. (1999). Dendritic spine changes associated with hippocampal long-term synaptic plasticity. *Nature*, *399*(May), 66–70. https://doi.org/10.1038/19978

Engreitz, J. M., Haines, J. E., Perez, E. M., Munson, G., Chen, J., Kane, M., … Lander, E. S. (2016). Local regulation of gene expression by lncRNA promoters, transcription and splicing. *Nature*, *539*(7629), 452–455. https://doi.org/10.1038/nature20149

Enuka, Y., Lauriola, M., Feldman, M. E., Sas-Chen, A., Ulitsky, I., & Yarden, Y. (2016). Circular RNAs are long-lived and display only minimal early alterations in response to a growth factor. *Nucleic Acids Research*, *44*(3), 1370–1383. https://doi.org/10.1093/nar/gkv1367

Errichelli, L., Dini Modigliani, S., Laneve, P., Colantoni, A., Legnini, I., Capauto, D., … Bozzoni, I. (2017). FUS affects circular RNA expression in murine embryonic stem cell-derived motor neurons. *Nature Communications*, *8*, 14741. https://doi.org/10.1038/ncomms14741

Faehnle, C. R., & Joshua-Tor, L. (2007). Argonautes confront new small RNAs. *Current Opinion in Chemical Biology*. https://doi.org/10.1016/j.cbpa.2007.08.032

Fei, T., Chen, Y., Xiao, T., Li, W., Cato, L., Zhang, P., … Brown, M. (2017). Genome-wide CRISPR screen identifies HNRNPL as a prostate cancer dependency regulating RNA splicing. *Proceedings of the National Academy of Sciences*. https://doi.org/10.1073/pnas.1617467114

Feil, R., Hölter, S. M., Weindl, K., Wurst, W., Langmesser, S., Gerling, A., … Albrecht, U. (2009). cGMP-dependent protein kinase I, the circadian clock, sleep and learning. *Communicative and Integrative Biology*. https://doi.org/10.4161/cib.2.4.8220

Feng, G., Mellor, R. H., Bernstein, M., Keller-Peck, C., Nguyen, Q. T., Wallace, M., … Sanes, J. R. (2000). Imaging neuronal subsets in transgenic mice expressing multiple spectral variants of GFP. *Neuron*. https://doi.org/10.1016/S0896-6273(00)00084-2

Feng, S., & Arnold, D. B. (2016). Techniques for studying protein trafficking and molecular motors in neurons, *73*(9), 508–515. https://doi.org/10.1002/cm.21274.Techniques

Ferreira, A., Kao, H. T., Feng, J., Rapoport, M., & Greengard, P. (2000). Synapsin III: developmental expression, subcellular localization, and role in axon formation. *The Journal of Neuroscience : The Official Journal of the Society for Neuroscience*. https://doi.org/10.1523/JNEUROSCI.20-10-03736.2000

Fletcher, T., De Camilli, P., & Banker, G. (1994). Synaptogenesis in hippocampal cultures:

evidence indicating that axons and dendrites become competent to form synapses at different stages of neuronal development. *The Journal of Neuroscience*. https://doi.org/10.1523/JNEUROSCI.14-11-06695.1994

Flores, R., Grubb, D., Elleuch, A., Nohales, M. Á., Delgado, S., & Gago, S. (2011). Rolling-circle replication of viroids, viroid-like satellite RNAs and hepatitis delta virus: Variations on a theme. *RNA Biology*. https://doi.org/10.4161/rna.8.2.14238

Fremeau, R. T., Kam, K., Qureshi, Y., Johnson, J., Copenhagen, D. R., Storm-Mathisen, J., … Edwards, R. H. (2004). Vesicular glutamate transporters 1 and 2 target to functionally distinct synaptic release sites. *Science*. https://doi.org/10.1126/science.1097468

Friedel, R. H., Seisenberger, C., Kaloff, C., & Wurst, W. (2007). EUCOMM - The European Conditional Mouse Mutagenesis Program. *Briefings in Functional Genomics and Proteomics*, *6*(3), 180–185. https://doi.org/10.1093/bfgp/elm022

Fuchs, E. (2006). Remodeling of neuronal networks by stress. *Frontiers in Bioscience*, *11*(1), 2746. https://doi.org/10.2741/2004

Galani, R., Obis, S., Coutureau, E., Jarrard, L., & Cassel, J. C. (2002). A comparison of the effects of fimbria-fornix, hippocampal, or entorhinal cortex lesions on spatial reference and working memory in rats: Short versus long postsurgical recovery period. *Neurobiology of Learning and Memory*. https://doi.org/10.1006/nlme.2000.3998

Garcia-Garcia, A. L., Elizalde, N., Matrov, D., Harro, J., Wojcik, S. M., Venzala, E., … Tordera, R. M. (2009). Increased Vulnerability to Depressive-Like Behavior of Mice with Decreased Expression of VGLUT1. *Biological Psychiatry*. https://doi.org/10.1016/j.biopsych.2009.02.027

Gardner, E. J., Nizami, Z. F., Conover Talbot, J., & Gall, J. G. (2012). Stable intronic sequence RNA (sisRNA), a new class of noncoding RNA from the oocyte nucleus of Xenopus tropicalis. *Genes and Development*. https://doi.org/10.1101/gad.202184.112

Garneau, N. L., Wilusz, J., & Wilusz, C. J. (2007). The highways and byways of mRNA decay. *Nature Reviews Molecular Cell Biology*. https://doi.org/10.1038/nrm2104

Geurts, A. M., Cost, G. J., Freyvert, Y., Zeitler, B., Miller, J. C., Choi, V. M., … Buelow, R. (2009). Knockout rats via embryo microinjection of zinc-finger nucleases. *Science*. https://doi.org/10.1126/science.1172447

Giese, K. P., Fedorov, N. B., Filipkowski, R. K., & Silva, A. J. (1998). Autophosphorylation at Thr286of the α calcium-calmodulin kinase II in LTP and learning. *Science*, *279*(5352), 870–873. https://doi.org/10.1126/science.279.5352.870

Glantz, L. A., & Lewis, D. A. (2000). Decreased dendritic spine density on prefrontal cortical pyramidal neurons in schizophrenia. *Archives of General Psychiatry*. https://doi.org/10.1001/archpsyc.57.1.65

Goldstein, S., Fordis, C. M., & Howard, B. H. (1989). Enhanced transfection efficiency and improved cell survival after electroporation of G2/M-synchronized cells and treatment with sodium butyrate. *Nucleic Acids Research*, *17*(10), 3959–3971. https://doi.org/10.1093/nar/17.10.3959

Goldwater, D. S., Pavlides, C., Hunter, R. G., Bloss, E. B., Hof, P. R., McEwen, B. S., & Morrison, J. H. (2009). Structural and functional alterations to rat medial prefrontal

cortex following chronic restraint stress and recovery. *Neuroscience*, *164*(2), 798–808. https://doi.org/10.1016/j.neuroscience.2009.08.053

Gonzàlez-Porta, M., Frankish, A., Rung, J., Harrow, J., & Brazma, A. (2013). Transcriptome analysis of human tissues and cell lines reveals one dominant transcript per gene. *Genome Biology*. https://doi.org/10.1186/gb-2013-14-7-r70

Grabowski, P. J., Zaug, a J., & Cech, T. R. (1981). The intervening sequence of the ribosomal RNA precursor is converted to a circular RNA in isolated nuclei of Tetrahymena. *Cell*, *23*(February), 467–476. https://doi.org/10.1016/0092-8674(81)90142-2

Gruart, A. (2006). Involvement of the CA3-CA1 Synapse in the Acquisition of Associative Learning in Behaving Mice. *Journal of Neuroscience*, *26*(4), 1077–1087. https://doi.org/10.1523/JNEUROSCI.2834-05.2006

Gruner, H., Cortés-López, M., Cooper, D. a., Bauer, M., Miura, P., Danan, M., … Shi, W. (2016). CircRNA accumulation in the aging mouse brain. *Scientific Reports*, *6*(November), 38907. https://doi.org/10.1038/srep38907

Guarnerio, J., Bezzi, M., Jeong, J. C., Paffenholz, S. V., Berry, K., Naldini, M. M., … Pandolfi, P. P. (2016). Erratum: Oncogenic Role of Fusion-circRNAs Derived from Cancer-Associated Chromosomal Translocations (Cell (2016) 165(2) (289???302)). *Cell*, *166*(4), 1055–1056. https://doi.org/10.1016/j.cell.2016.07.035

Guil, S., & Esteller, M. (2012). Cis-acting noncoding RNAs: Friends and foes. *Nature Structural and Molecular Biology*. https://doi.org/10.1038/nsmb.2428

Guo, J. U., Agarwal, V., Guo, H., & Bartel, D. P. (2014). Expanded identification and characterization of mammalian circular RNAs. *Genome Biology*, *15*, 409. https://doi.org/10.1186/PREACCEPT-1176565312639289

Guo, W., Zhang, J., Zhang, D., Cao, S., Li, G., Zhang, S., … Ye, H. (2017). Polymorphisms and expression pattern of circular RNA circ-ITCH contributes to the carcinogenesis of hepatocellular carcinoma. *Oncotarget*. https://doi.org/10.18632/oncotarget.18327

Han, J., Gao, L., Dong, J., Bai, J., Zhang, M., & Zheng, J. (2017). The expression profile of developmental stage-dependent circular RNA in the immature rat retina. *Molecular Vision*, *23*(July), 457–469. Retrieved from http://www.ncbi.nlm.nih.gov/pubmed/28761319

Hansen, T. B. (2018). Improved circRNA identification by combining prediction algorithms. *Frontiers in Cell and Developmental Biology*. https://doi.org/10.3389/fcell.2018.00020

Hansen, T. B., Jensen, T. I., Clausen, B. H., Bramsen, J. B., Finsen, B., Damgaard, C. K., & Kjems, J. (2013). Natural RNA circles function as efficient microRNA sponges. *Nature*, *495*(7441), 384–388. https://doi.org/10.1038/nature11993

Harris, K M. (1999). Structure, development, and plasticity of dendritic spines. *Curr Opin Neurobiol*, *9*(3), 343–348. https://doi.org/nb9308 [pii]

Harris, Kristen M, Jensen, F. E., & Tsao, B. (1992). Three-dimensional structure of dendritic spines and synapses in rat hippocampus (CA1) at postnatal day 15 and adult ages: implications for the maturation of synaptic physiology and long-term potentiation. *The Journal of Neuroscience : The Official Journal of the Society for Neuroscience*, *12*(7), 2685–2705. https://doi.org/10.1016/j.tcb.2009.06.001

Harrison, R. G. (1910). The outgrowth of the nerve fiber as a mode of protoplasmic movement. *Journal of Experimental Zoology*, *9*(4), 787–846. https://doi.org/10.1002/jez.1400090405

Hascoët, M., Bourin, M., & Nic Dhonnchadha, B. A. (2001). The mouse light-dark paradigm: A review. *Progress in Neuro-Psychopharmacology and Biological Psychiatry*. https://doi.org/10.1016/S0278-5846(00)00151-2

Hausser, M., Spruston, N., & Stuart, G. J. (2000). Diversity and dynamics of dendritic signaling. *Science*. https://doi.org/10.1126/science.290.5492.739

Hebb, D. O. (1949). The organization of behavior. *New York: Wiley*. https://doi.org/10.2307/1418888

Hering, H., & Sheng, M. (2001). Dentritic spines: structure, dynamics and regulation. *Nature Reviews Neuroscience*, *2*(12), 880–888. https://doi.org/10.1038/35104061

Herms, J., & Dorostkar, M. M. (2016). Dendritic Spine Pathology in Neurodegenerative Diseases. *Annual Review of Pathology: Mechanisms of Disease*. https://doi.org/10.1146/annurev-pathol-012615-044216

Hill, T. C., & Zito, K. (2013). LTP-Induced Long-Term Stabilization of Individual Nascent Dendritic Spines. *Journal of Neuroscience*, *33*(2), 678–686. https://doi.org/10.1523/JNEUROSCI.1404-12.2013

Hitz, C., Wurst, W., & Kühn, R. (2007). Conditional brain-specific knockdown of MAPK using Cre/loxP regulated RNA interference. *Nucleic Acids Research*, *35*(12). https://doi.org/10.1093/nar/gkm475

Ho, V. M., Lee, J. A., & Martin, K. C. (2011). The cell biology of synaptic plasticity. *Science*. https://doi.org/10.1126/science.1209236

Holdt, L. M., Stahringer, A., Sass, K., Pichler, G., Kulak, N. a., Wilfert, W., … Teupser, D. (2016). Circular non-coding RNA ANRIL modulates ribosomal RNA maturation and atherosclerosis in humans. *Nature Communications*, *7*, 12429. https://doi.org/10.1038/ncomms12429

Hollmann, M. (1994). Cloned Glutamate Receptors. *Annual Review of Neuroscience*, *17*(1), 31–108. https://doi.org/10.1146/annurev.neuro.17.1.31

Hölter, S. M., & Glasl, L. (2012). High-throughput mouse phenotyping. *Neuromethods*. https://doi.org/10.1007/978-1-61779-298-4_7

Hosokawa, T., Rusakov, D. a, Bliss, T. V, & Fine, a. (1995). Repeated confocal imaging of individual dendritic spines in the living hippocampal slice: evidence for changes in length and orientation associated with chemically induced LTP. *The Journal of Neuroscience : The Official Journal of the Society for Neuroscience*, *15*(8), 5560–5573. https://doi.org/0270-6474/95/155560-14

Hotulainen, P., & Hoogenraad, C. C. (2010). Actin in dendritic spines: Connecting dynamics to function. *Journal of Cell Biology*. https://doi.org/10.1083/jcb.201003008

Hsu, M. T., & Coca-Prados, M. (1979). Electron microscopic evidence for the circular form of RNA in the cytoplasm of eukaryotic cells [24]. *Nature*. https://doi.org/10.1038/280339a0

Hsu, P. D., Lander, E. S., & Zhang, F. (2014). Development and applications of CRISPR-Cas9

for genome engineering. *Cell*, *157*(6), 1262–1278. https://doi.org/10.1016/j.cell.2014.05.010

Hu, S., Xie, Z., Onishi, A., Yu, X., Jiang, L., Lin, J., … Zhu, H. (2009). Profiling the Human Protein-DNA Interactome Reveals ERK2 as a Transcriptional Repressor of Interferon Signaling. *Cell*. https://doi.org/10.1016/j.cell.2009.08.037

Huang, G., Zhu, H., Shi, Y., Wu, W., Cai, H., & Chen, X. (2015). Cir-ITCH plays an inhibitory role in colorectal cancer by regulating the Wnt/β-Catenin Pathway. *PLoS ONE*. https://doi.org/10.1371/journal.pone.0131225

Huang, R., Zhang, Y., Han, B., Bai, Y., Zhou, R., Gan, G., … Yao, H. (2017). Circular RNA HIPK2 regulates astrocyte activation via cooperation of autophagy and ER stress by targeting MIR124–2HG. *Autophagy*. https://doi.org/10.1080/15548627.2017.1356975

Ikeda, A, Nishina, P. M., & Naggert, J. K. (2002a). The tubby-like proteins, a family with roles in neuronal development and function. *J Cell Sci*, *115*(Pt 1), 9–14. Retrieved from http://www.ncbi.nlm.nih.gov/pubmed/11801719

Ikeda, Akihiro, Naggert, J. K., & Nishina, P. M. (2002b). Genetic modification of retinal degeneration in tubby mice. *Experimental Eye Research*. https://doi.org/10.1006/exer.2001.1139

Ikeda, A. et al. (2001). Neural tube defects and neuroepithelial cell death in Tulp3 knockout mice. *Human Molecular Genetics*, *10*(12), 1325–1334. https://doi.org/10.1093/hmg/10.12.1325

Ikeda, K., & Bekkers, J. M. (2006). Autapses. *Current Biology*. https://doi.org/10.1016/j.cub.2006.03.085

Inta, D., Vogt, M. A., Perreau-lenz, S., Schneider, M., Pfeiffer, N., Wojcik, S. M., … Gass, P. (2012). Sensorimotor gating , working and social memory deficits in mice with reduced expression of the vesicular glutamate transporter VGLUT1. *Behavioural Brain Research*, *228*(2), 328–332. https://doi.org/10.1016/j.bbr.2011.12.012

Irwin, S. (1968). Comprehensive observational assessment: Ia. A systematic, quantitative procedure for assessing the behavioral and physiologic state of the mouse. *Psychopharmacologia*. https://doi.org/10.1007/BF00401402

Ivanov, A., Memczak, S., Wyler, E., Torti, F., Porath, H. T., Orejuela, M. R., … Rajewsky, N. (2015). Analysis of Intron Sequences Reveals Hallmarks of Circular RNA Biogenesis in Animals. *Cell Reports*, *10*(2), 170–177. https://doi.org/10.1016/j.celrep.2014.12.019

Iyer, V., Shen, B., Zhang, W., Hodgkins, A., Keane, T., Huang, X., & Skarnes, W. C. (2015). Off-target mutations are rare in Cas9-modified mice. *Nature Methods*. https://doi.org/10.1038/nmeth.3408

Jackman, S. L., & Regehr, W. G. (2017). The Mechanisms and Functions of Synaptic Facilitation. *Neuron*, *94*(3), 447–464. https://doi.org/10.1016/j.neuron.2017.02.047

Janas, J., Skowronski, J., & Van Aelst, L. (2006). Lentiviral delivery of RNAi in hippocampal neurons. *Methods in Enzymology*, *406*, 593–605. https://doi.org/10.1016/S0076-6879(06)06046-0

Jarrard, L. E. (1964). Behavior of hippocampal lesioned rats in home cage and novel situations. *Physiology & Behavior*. https://doi.org/10.1016/0031-9384(68)90033-4

Jeck, W. R., & Sharpless, N. E. (2014). Detecting and characterizing circular RNAs. *Nature Biotechnology*. https://doi.org/10.1038/nbt.2890

Jeck, W. R., Sorrentino, J. A., Wang, K., Slevin, M. K., Burd, C. E., Liu, J., … Sharpless, N. E. (2013). Circular RNAs are abundant, conserved, and associated with ALU repeats. *RNA*. https://doi.org/10.1261/rna.035667.112

Jelen, N., Ule, J., Živin, M., & Darnell, R. B. (2007). Evolution of Nova-dependent splicing regulation in the brain. *PLoS Genetics*. https://doi.org/10.1371/journal.pgen.0030173

Jiang, M., & Chen, G. (2006). High Ca2+-phosphate transfection efficiency in low-density neuronal cultures. *Nature Protocols*, *1*(2), 695–700. https://doi.org/10.1038/nprot.2006.86

Jinek, M., Chylinski, K., Fonfara, I., Hauer, M., Doudna, J. A., & Charpentier, E. (2012). A programmable dual-RNA-guided DNA endonuclease in adaptive bacterial immunity. *Science*, *337*(6096), 816–821. https://doi.org/10.1126/science.1225829

Jinek, M., East, A., Cheng, A., Lin, S., Ma, E., & Doudna, J. (2013). RNA-programmed genome editing in human cells. *ELife*, *2013*(2), 1–9. https://doi.org/10.7554/eLife.00471

Johnsson, P., Ackley, A., Vidarsdottir, L., Lui, W. O., Corcoran, M., Grandér, D., & Morris, K. V. (2013). A pseudogene long-noncoding-RNA network regulates PTEN transcription and translation in human cells. *Nature Structural and Molecular Biology*. https://doi.org/10.1038/nsmb.2516

Jones, E. G. (1994). Santiago Ram??n y Cajal and the croonian lecture, March 1894. *Trends in Neurosciences*, *17*(5), 192–193. https://doi.org/10.1016/0166-2236(94)90101-5

Kaech, S., & Banker, G. (2006). Culturing hippocampal neurons. *Nature Protocols*, *1*(5), 2406–2415. https://doi.org/10.1038/nprot.2006.356

Kaech, S., Huang, C.-F., & Banker, G. (2012). General considerations for live imaging of developing hippocampal neurons in culture. *Cold Spring Harbor Protocols*, *2012*(3), 312–318. https://doi.org/10.1101/pdb.ip068221

Kandel, E. R. (2001). The molecular biology of memory storage: A dialogue between genes and synapses. *Science*. https://doi.org/10.1126/science.1067020

Kandel, Eric R, Schwartz, J. H., & Jessell, T. M. (2000). *Principles of Neural Science*. *Neurology* (Vol. 4). https://doi.org/10.1036/0838577016

Kauer, J. A. (2004). Learning Mechanisms in Addiction: Synaptic Plasticity in the Ventral Tegmental Area as a Result of Exposure to Drugs of Abuse. *Annual Review of Physiology*, *66*(1), 447–475. https://doi.org/10.1146/annurev.physiol.66.032102.112534

Kauer, J. A., & Malenka, R. C. (2007). Synaptic plasticity and addiction. *Nature Reviews Neuroscience*. https://doi.org/10.1038/nrn2234

Kawauchi, D., & Saito, T. (2008). Transcriptional cascade from Math1 to Mbh1 and Mbh2 is required for cerebellar granule cell differentiation. *Developmental Biology*, *322*(2), 345–354. https://doi.org/10.1016/j.ydbio.2008.08.005

Keinänen, K., Wisden, W., Sommer, B., Werner, P., Herb, A., Verdoorn, T. A., … Seeburg, P. H. (1990). A family of AMPA-selective glutamate receptors. *Science*. https://doi.org/10.1126/science.2166337

Kelly, S., Greenman, C., Cook, P. R., & Papantonis, A. (2015). Exon Skipping Is Correlated with Exon Circularization. *Journal of Molecular Biology*, *427*(15), 2414–2417. https://doi.org/10.1016/j.jmb.2015.02.018

Khan, M. a, Reckman, Y. J., Aufiero, S., van den Hoogenhof, M. M., van der Made, I., Beqqali, A., … Pinto, Y. M. (2016). RBM20 Regulates Circular RNA Production From the Titin Gene. *Circulation Research*, (July), CIRCRESAHA.116.309568. https://doi.org/10.1161/CIRCRESAHA.116.309568

Khoutorsky, A., Yanagiya, A., Gkogkas, C. G., Fabian, M. R., Prager-Khoutorsky, M., Cao, R., … Sonenberg, N. (2013). Control of synaptic plasticity and memory via suppression of poly(A)-Binding protein. *Neuron*, *78*(2), 298–311. https://doi.org/10.1016/j.neuron.2013.02.025

Kile, B. T., Schulman, B. A., Alexander, W. S., Nicola, N. A., Martin, H. M. E., & Hilton, D. J. (2002). The SOCS box: A tale of destruction and degradation. *Trends in Biochemical Sciences*. https://doi.org/10.1016/S0968-0004(02)02085-6

Kim, K. M., Abdelmohsen, K., Mustapic, M., Kapogiannis, D., & Gorospe, M. (2017). RNA in extracellular vesicles. *Wiley Interdisciplinary Reviews: RNA*. https://doi.org/10.1002/wrna.1413

Kim, V. N. (2018). RNA-targeting CRISPR comes of age. *Nature Biotechnology*, *36*(1), 44–45. https://doi.org/10.1038/nbt.4054

Kirov, S. A., & Harris, K. M. (1999). Dendrites are more spiny on mature hippocampal neurons when synapses are inactivated. *Nature Neuroscience*, *2*(10), 878–883. https://doi.org/10.1038/13178

Kleaveland, B., Shi, C. Y., Stefano, J., & Bartel, D. P. (2018). A Network of Noncoding Regulatory RNAs Acts in the Mammalian Brain. *Cell*, 1–13. https://doi.org/10.1016/j.cell.2018.05.022

Kleyn, P. W., Fan, W., Kovats, S. G., Lee, J. J., Pulido, J. C., Wu, Y., … Moore, K. J. (1996). Identification and Characterization of the Mouse Obesity Gene tubby: A Member of a Novel Gene Family. *Cell*, *85*, 281–290. https://doi.org/10.1016/S0092-8674(00)81104-6

Knott, G. J., & Doudna, J. A. (2018). CRISPR-Cas guides the future of genetic engineering. *Science*, *361*(6405), 866–869. https://doi.org/10.1126/science.aat5011

Koch, F., Jourquin, F., Ferrier, P., & Andrau, J. C. (2008). Genome-wide RNA polymerase II: not genes only! *Trends in Biochemical Sciences*. https://doi.org/10.1016/j.tibs.2008.04.006

Koch, M. (1999). The neurobiology of startle. *Progress in Neurobiology*. https://doi.org/10.1016/S0301-0082(98)00098-7

Kohlhapp, F. J., Mitra, A. K., Lengyel, E., & Peter, M. E. (2015). MicroRNAs as mediators and communicators between cancer cells and the tumor microenvironment. *Oncogene*. https://doi.org/10.1038/onc.2015.89

Kopec, C. D. (2006). Glutamate Receptor Exocytosis and Spine Enlargement during Chemically Induced Long-Term Potentiation. *Journal of Neuroscience*, *26*(7), 2000–2009. https://doi.org/10.1523/JNEUROSCI.3918-05.2006

Kramer, M. C., Liang, D., Tatomer, D. C., Gold, B., March, Z. M., Cherry, S., & Wilusz, J. E.

(2015). Combinatorial control of Drosophila circular RNA expression by intronic repeats, hnRNPs, and SR proteins. *Genes and Development*, *29*(20), 2168–2182. https://doi.org/10.1101/gad.270421.115

Kristensen, L. S., Andersen, M. S., Stagsted, L. V. W., Ebbesen, K. K., Hansen, T. B., & Kjems, J. (2019). The biogenesis, biology and characterization of circular RNAs. *Nature Reviews Genetics*. https://doi.org/10.1038/s41576-019-0158-7

Kulkarni, V. A., & Firestein, B. L. (2012). The dendritic tree and brain disorders. *Molecular and Cellular Neuroscience*. https://doi.org/10.1016/j.mcn.2012.03.005

Laemmli, U. K. (1970). Cleavage of structural proteins during the assembly of the head of bacteriophage T4. *Nature*, *227*(5259), 680–685. https://doi.org/10.1038/227680a0

Lander, E. S., Linton, L. M., Birren, B., Nusbaum, C., Zody, M. C., Baldwin, J., … Morgan, M. J. (2001). Initial sequencing and analysis of the human genome. *Nature*, *409*(6822), 860–921. https://doi.org/10.1038/35057062

Lang, C., Barco, A., Zablow, L., Kandel, E. R., Siegelbaum, S. A., & Zakharenko, S. S. (2004). Transient expansion of synaptically connected dendritic spines upon induction of hippocampal long-term potentiation. *Proceedings of the National Academy of Sciences*, *101*(47), 16665–16670. https://doi.org/10.1073/pnas.0407581101

Lange, V., Picotti, P., Domon, B., & Aebersold, R. (2008). Selected reaction monitoring for quantitative proteomics: A tutorial. *Molecular Systems Biology*. https://doi.org/10.1038/msb.2008.61

Lango Allen H, Estrada K, Lettre G, Berndt SI, Weedon MN, Rivadeneira F, Willer CJ, Jackson AU, Vedantam S, Raychaudhuri S, Ferreira T, Wood AR, Weyant RJ, Segrè AV, Speliotes EK, Wheeler E, Soranzo N, Park JH, Yang J, Gudbjartsson D, Heard-Costa NL, Rand, H. J. (2010). Hundreds of variants clustered in genomic loci and biological pathways affect human height. *Nature*, *467*(7317), 832–838. https://doi.org/10.1038/nature09410.Hundreds

Lasda, E., & Parker, R. (2014). Circular RNAs: Diversity of form and function. *Rna*, *20*(12), 1829–1842. https://doi.org/10.1261/rna.047126.114

Lau, C. G., & Zukin, R. S. (2007). NMDA receptor trafficking in synaptic plasticity and neuropsychiatric disorders. *Nature Reviews Neuroscience*. https://doi.org/10.1038/nrn2153

Lauressergues, D., Couzigou, J. M., San Clemente, H., Martinez, Y., Dunand, C., Bécard, G., & Combier, J. P. (2015). Primary transcripts of microRNAs encode regulatory peptides. *Nature*. https://doi.org/10.1038/nature14346

Lee, H.-K., Takamiya, K., Han, J.-S., Man, H., Kim, C.-H., Rumbaugh, G., … Huganir, R. L. (2003). Phosphorylation of the AMPA Receptor GluR1 Subunit Is Required for Synaptic Plasticity and Retention of Spatial Memory. *Cell*, *112*, 631–643. https://doi.org/10.1016/S0092-8674(03)00122-3

Lee, T., Awano, H., Yagi, M., Matsumoto, M., Watanabe, N., Goda, R., … Matsuo, M. (2017). 2′-O-methyl RNA/ethylene-bridged nucleic acid chimera antisense oligonucleotides to induce dystrophin exon 45 skipping. *Genes*. https://doi.org/10.3390/genes8020067

Lee, W. C. A., Huang, H., Feng, G., Sanes, J. R., Brown, E. N., So, P. T., & Nedivi, E. (2006).

Dynamic remodeling of dendritic arbors in GABAergic interneurons of adult visual cortex. *PLoS Biology*, *4*(2), 271–280. https://doi.org/10.1371/journal.pbio.0040029

Legnini, I., Di Timoteo, G., Rossi, F., Morlando, M., Briganti, F., Sthandier, O., … Bozzoni, I. (2017). Circ-ZNF609 Is a Circular RNA that Can Be Translated and Functions in Myogenesis. *Molecular Cell*, *66*(1), 22-37.e9. https://doi.org/10.1016/j.molcel.2017.02.017

LeVay, S. (1973). Synaptic patterns in the visual cortex of the cat and monkey. Electron microscopy of Golgi preparations. *The Journal of Comparative Neurology*, *150*(1), 53–85. https://doi.org/10.1002/cne.901500104

Lewis, T. L., Courchet, J., & Polleux, F. (2013). Cellular and molecular mechanisms underlying axon formation, growth, and branching. *The Journal of Cell Biology*, *202*(6), 837–848. https://doi.org/10.1083/jcb.201305098

Li-Pook-Than, J., & Bonen, L. (2006). Multiple physical forms of excised group II intron RNAs in wheat mitochondria. *Nucleic Acids Research*. https://doi.org/10.1093/nar/gkl328

Li, F., Zhang, L., Li, W., Deng, J., Zheng, J., An, M., … Zhou, Y. (2015). Circular RNA ITCH has inhibitory effect on ESCC by suppressing the Wnt/β-catenin pathway. *Oncotarget*. https://doi.org/10.18632/oncotarget.3469

Li, Q. Z., Wang, C. Y., Shi, J. Da, Ruan, Q. G., Eckenrode, S., Davoodi-Semiromi, A., … She, J. X. (2001). Molecular cloning and characterization of the mouse and human TUSP gene, a novel member of the tubby superfamily. *Gene*, *273*(2), 275–284. https://doi.org/10.1016/S0378-1119(01)00582-0

Li, W., Teng, F., Li, T., & Zhou, Q. (2013). Simultaneous generation and germline transmission of multiple gene mutations in rat using CRISPR-Cas systems. *Nature Biotechnology*. https://doi.org/10.1038/nbt.2652

Li, X., Liu, C. X., Xue, W., Zhang, Y., Jiang, S., Yin, Q. F., … Chen, L. L. (2016). Coordinated circRNA Biogenesis and Function with NF90/NF110 in Viral Infection. *Molecular Cell*, 1–14. https://doi.org/10.1016/j.molcel.2017.05.023

Li, X., Yang, L., & Chen, L. L. (2018). The Biogenesis, Functions, and Challenges of Circular RNAs. *Molecular Cell*, *71*(3), 428–442. https://doi.org/10.1016/j.molcel.2018.06.034

Li, Y., Zheng, Q., Bao, C., Li, S., Guo, W., Zhao, J., … Huang, S. (2015). Circular RNA is enriched and stable in exosomes: a promising biomarker for cancer diagnosis. *Cell Research*. https://doi.org/10.1038/cr.2015.82

Li, Z., Huang, C., Bao, C., Chen, L., Lin, M., Wang, X., … Shan, G. (2015). Exon-intron circular RNAs regulate transcription in the nucleus. *Nature Structural & Molecular Biology*, *22*(3), 256–264. https://doi.org/10.1038/nsmb.2959

Liang, D., Tatomer, D. C., Luo, Z., Wu, H., Yang, L., Chen, L.-L., … Wilusz, J. E. (2017). The Output of Protein-Coding Genes Shifts to Circular RNAs When the Pre-mRNA Processing Machinery Is Limiting. *Molecular Cell*, 1–15. https://doi.org/10.1016/j.molcel.2017.10.034

Liang, D., & Wilusz, J. E. (2014). Short intronic repeat sequences facilitate circular RNA production, 2233–2247. https://doi.org/10.1101/gad.251926.114.scribed

Lipovich, L., Dachet, F., Cai, J., Bagla, S., Balan, K., Jia, H., & Loeb, J. A. (2012). Activity-

dependent human brain coding/noncoding gene regulatory networks. *Genetics*. https://doi.org/10.1534/genetics.112.145128

Lissin, D. V., Gomperts, S. N., Carroll, R. C., Christine, C. W., Kalman, D., Kitamura, M., … von Zastrow, M. (1998). Activity differentially regulates the surface expression of synaptic AMPA and NMDA glutamate receptors. *Proceedings of the National Academy of Sciences*. https://doi.org/10.1073/pnas.95.12.7097

Liston, C., Miller, M. M., Goldwater, D. S., Radley, J. J., Rocher, A. B., Hof, P. R., … McEwen, B. S. (2006). Stress-Induced Alterations in Prefrontal Cortical Dendritic Morphology Predict Selective Impairments in Perceptual Attentional Set-Shifting. *Journal of Neuroscience*. https://doi.org/10.1523/JNEUROSCI.1184-06.2006

Liu, C.-X., Li, X., Nan, F., Jiang, S., Gao, X., Guo, S.-K., … Chen, L.-L. (2019). Structure and Degradation of Circular RNAs Regulate PKR Activation in Innate Immunity. *Cell*, 1–16. https://doi.org/10.1016/j.cell.2019.03.046

Liu, J. S. (2011). Molecular genetics of neuronal migration disorders. *Current Neurology and Neuroscience Reports*. https://doi.org/10.1007/s11910-010-0176-5

Liu, S. J., Nowakowski, T. J., Pollen, A. A., Lui, J. H., Horlbeck, M. A., Attenello, F. J., … Lim, D. A. (2016). Single-cell analysis of long non-coding RNAs in the developing human neocortex. *Genome Biology*. https://doi.org/10.1186/s13059-016-0932-1

Livak, K. J., & Schmittgen, T. D. (2001). Analysis of relative gene expression data using real-time quantitative PCR and the 2-ΔΔCT method. *Methods*. https://doi.org/10.1006/meth.2001.1262

Lizarraga, S. B., Coser, K. R., Sabbagh, M., & Morrow, E. M. (2012). Methods for Study of Neuronal Morphogenesis: Ex vivo RNAi Electroporation in Embryonic Murine Cerebral Cortex. *Journal of Visualized Experiments*, (63), 3–6. https://doi.org/10.3791/3621

London, M., & Häusser, M. (2005). DENDRITIC COMPUTATION. *Annual Review of Neuroscience*. https://doi.org/10.1146/annurev.neuro.28.061604.135703

Lu, R., Liu, X., Long, H., & Ma, L. (2012). Effects of prenatal cocaine and heroin exposure on neuronal dendrite morphogenesis and spatial recognition memory in mice. *Neuroscience Letters*, *522*(2), 128–133. https://doi.org/10.1016/j.neulet.2012.06.023

Lu, Z., Filonov, G. S., Noto, J. J., Schmidt, C. A., Hatkevich, T. L., Wen, Y., … Gregory Matera, A. (2015). Metazoan tRNA introns generate stable circular RNAs in vivo. *RNA*. https://doi.org/10.1261/rna.052944.115

Lukiw, W. J. (2013). Circular RNA (circRNA) in Alzheimer ' s disease (AD), *4*(December), 1–2. https://doi.org/10.1007/BF00

Maaswinkel, H., Gispen, W. H., & Spruijt, B. M. (1997). Executive function of the hippocampus in social behavior in the rat. *Behavioral Neuroscience*. https://doi.org/10.1037/0735-7044.111.4.777

Magny, E. G., Pueyo, J. I., Pearl, F. M. G., Cespedes, M. A., Niven, J. E., Bishop, S. A., & Couso, J. P. (2013). Conserved regulation of cardiac calcium uptake by peptides encoded in small open reading frames. *Science*. https://doi.org/10.1126/science.1238802

Malenka, R. C., & Nicoll, R. A. (1997). Silent synapses speak up. *Neuron*.

https://doi.org/10.1016/S0896-6273(00)80362-1

Maletic-Savatic, M., Malinow, R., & Svoboda, K. (1999). Rapid dendritic morphogenesis in CA1 hippocampal dendrites induced by synaptic activity. *Science*, *283*(5409), 1923–1927. https://doi.org/10.1126/science.283.5409.1923

Marín-Padilla, M. (1992). Ontogenesis of the pyramidal cell of the mammalian neocortex and developmental cytoarchitectonics: A unifying theory. *Journal of Comparative Neurology*, *321*(2), 223–240. https://doi.org/10.1002/cne.903210205

Marraffini, L. A., & Sontheimer, E. J. (2008). CRISPR interference limits horizontal gene transfer in staphylococci by targeting DNA. *Science*, *322*(5909), 1843–1845. https://doi.org/10.1126/science.1165771

Marraffini, L. A., & Sontheimer, E. J. (2010). Self versus non-self discrimination during CRISPR RNA-directed immunity. *Nature*, *463*(7280), 568–571. https://doi.org/10.1038/nature08703

Martin, S. J., Grimwood, P. D., & Morris, R. G. M. (2000). S YNAPTIC P LASTICITY AND M EMORY : An Evaluation of the Hypothesis. *Annu Rev Neurosci*, *23*(Hebb 1949), 649–711. https://doi.org/10.1146/annurev.neuro.23.1.649

Matsuzaki, M, Ellis-Davies, G. C., Nemoto, T., Miyashita, Y., Iino, M., & Kasai, H. (2001). Dendritic spine geometry is critical for AMPA receptor expression in hippocampal CA1 pyramidal neurons. *Nature Neuroscience*, *4*(11), 1086–1092. https://doi.org/10.1038/nn736

Matsuzaki, Masanori, Honkura, N., Ellis-Davies, G. C. R., & Kasai, H. (2004). Structural basis of long-term potentiation in single dendritic spines. *Nature*, *429*(6993), 761–766. https://doi.org/10.1038/nature02617

Mattick, J. S. (2003). Challenging the dogma: The hidden layer of non-protein-coding RNAs in complex organisms. *BioEssays*. https://doi.org/10.1002/bies.10332

McConnell, S. K. (1995). Constructing the cerebral cortex: Neurogenesis and fate determination. *Neuron*. https://doi.org/10.1016/0896-6273(95)90168-X

McEwen, B. S., Coirini, H., Danielsson, A., Frankfurt, M., Gould, E., Mendelson, S., … Woolley, C. (1991). Steroid and thyroid hormones modulate a changing brain. *Journal of Steroid Biochemistry and Molecular Biology*, *40*(1–3), 1–14. https://doi.org/10.1016/0960-0760(91)90160-7

Mechan, A. O., Wyss, A., Rieger, H., & Mohajeri, M. H. (2009). A comparison of learning and memory characteristics of young and middle-aged wild-type mice in the IntelliCage. *Journal of Neuroscience Methods*, *180*(1), 43–51. https://doi.org/10.1016/j.jneumeth.2009.02.018

Memczak, S., Jens, M., Elefsinioti, A., Torti, F., Krueger, J., Rybak, A., … Rajewsky, N. (2013). Circular RNAs are a large class of animal RNAs with regulatory potency. *Nature*, *495*(7441), 333–338. https://doi.org/10.1038/nature11928

Memczak, S., Papavasileiou, P., Peters, O., & Rajewsky, N. (2015). Identification and characterization of circular RNAs as a new class of putative biomarkers in human blood. *PLoS ONE*. https://doi.org/10.1371/journal.pone.0141214

Ménoret, S., Fontaniére, S., Jantz, D., Tesson, L., Thinard, R., Rémy, S., … Anegon, I. (2013).

Generation of Rag1-knockout immunodeficient rats and mice using engineered meganucleases. *FASEB Journal*. https://doi.org/10.1096/fj.12-219907

Mercer, T. R., Qureshi, I. A., Gokhan, S., Dinger, M. E., Li, G., Mattick, J. S., & Mehler, M. F. (2010). Long noncoding RNAs in neuronal-glial fate specification and oligodendrocyte lineage maturation. *BMC Neuroscience*. https://doi.org/10.1186/1471-2202-11-14

Merkin, J., Russell, C., Chen, P., & Burge, C. B. (2012). Evolutionary dynamics of gene and isoform regulation in mammalian tissues. *Science*. https://doi.org/10.1126/science.1228186

Meyer, M., de Angelis, M. H., Wurst, W., & Kühn, R. (2010). Gene targeting by homologous recombination in mouse zygotes mediated by zinc-finger nucleases. *Proceedings of the National Academy of Sciences of the United States of America*, *107*(34), 15022–15026. https://doi.org/10.1073/pnas.1009424107

Mikuni, T., Nishiyama, J., Sun, Y., Kamasawa, N., & Yasuda, R. (2016). High-Throughput, High-Resolution Mapping of Protein Localization in Mammalian Brain by in Vivo Genome Editing. *Cell*, *165*(7), 1803–1817. https://doi.org/10.1016/j.cell.2016.04.044

Miyazaki, T., Fukaya, M., Shimizu, H., & Watanabe, M. (2003). Subtype switching of vesicular glutamate transporters at parallel fibre-Purkinje cell synapses in developing mouse cerebellum. *European Journal of Neuroscience*. https://doi.org/10.1046/j.1460-9568.2003.02698.x

Mizrahi, A., & Katz, L. C. (2003). Dendritic stability in the adult olfactory bulb. *Nature Neuroscience*, *6*(11), 1201–1207. https://doi.org/10.1038/nn1133

Mizutani, K. -i. (2005). Progenitors resume generating neurons after temporary inhibition of neurogenesis by Notch activation in the mammalian cerebral cortex. *Development*, *132*(6), 1295–1304. https://doi.org/10.1242/dev.01693

Mojica, F. J. M., Díez-Villaseñor, C., García-Martínez, J., & Almendros, C. (2009). Short motif sequences determine the targets of the prokaryotic CRISPR defence system. *Microbiology*, *155*(3), 733–740. https://doi.org/10.1099/mic.0.023960-0

Molina-Sánchez, M. D., Martinez-Abarca, F., & Toro, N. (2006). Excision of the Sinorhizobium meliloti group II intron RmInt1 as circles in vivo. *Journal of Biological Chemistry*. https://doi.org/10.1074/jbc.M602695200

Molyneaux, B. J., Goff, L. A., Brettler, A. C., Chen, H. H., Brown, J. R., Hrvatin, S., … Arlotta, P. (2015). DeCoN: Genome-wide analysis of invivo transcriptional dynamics during pyramidal neuron fate selection in neocortex. *Neuron*. https://doi.org/10.1016/j.neuron.2014.12.024

Moore, M. J., & Proudfoot, N. J. (2009). Pre-mRNA Processing Reaches Back toTranscription and Ahead to Translation. *Cell*. https://doi.org/10.1016/j.cell.2009.02.001

Murchison, E. P., & Hannon, G. J. (2004). miRNAs on the move: miRNA biogenesis and the RNAi machinery. *Current Opinion in Cell Biology*. https://doi.org/10.1016/j.ceb.2004.04.003

Murthy, V. N., Schikorski, T., Stevens, C. F., & Zhu, Y. (2001). Inactivity produces increases in neurotransmitter release and synapse size. *Neuron*. https://doi.org/10.1016/S0896-6273(01)00500-1

Nägerl, U. V, Eberhorn, N., Cambridge, S. B., & Bonhoeffer, T. (2004). Bidirectional activity-dependent morphological plasticity in hippocampal neurons. *Neuron*, *44*, 759–767. https://doi.org/10.1016/j.neuron.2004.11.016

Neff, A. T., Lee, J. Y., Wilusz, J., Tian, B., & Wilusz, C. J. (2012). Global analysis reveals multiple pathways for unique regulation of mRNA decay in induced pluripotent stem cells. *Genome Research*, *22*(8), 1457–1467. https://doi.org/10.1101/gr.134312.111

Nelson, B. R., Makarewich, C. A., Anderson, D. M., Winders, B. R., Troupes, C. D., Wu, F., … Olson, E. N. (2016). Muscle physiology: A peptide encoded by a transcript annotated as long noncoding RNA enhances SERCA activity in muscle. *Science*. https://doi.org/10.1126/science.aad4076

Nelson, S. B., & Valakh, V. (2015). Excitatory/Inhibitory Balance and Circuit Homeostasis in Autism Spectrum Disorders. *Neuron*, *87*(4), 684–698. https://doi.org/10.1016/j.neuron.2015.07.033

Neves, G., Cooke, S. F., & Bliss, T. V. (2008). Synaptic plasticity, memory and the hippocampus: a neural network approach to causality. *Nature Reviews Neuroscience*, *9*(1), 65–75. https://doi.org/nrn2303 [pii]\r10.1038/nrn2303 [doi]

Nigro, J. M., Cho, K. R., Fearon, E. R., Kern, S. E., Ruppert, J. M., Oliner, J. D., … Vogelstein, B. (1991). Scrambled exons. *Cell*, *64*(3), 607–613. https://doi.org/10.1016/0092-8674(91)90244-S

Nishina, P. M., North, M. A., Ikeda, A., Yan, Y., & Naggert, J. K. (1998). Molecular characterization of a novel tubby gene family member, TULP3, in mouse and humans. *Genomics*. https://doi.org/10.1006/geno.1998.5567

Noguchi, J., Matsuzaki, M., Ellis-Davies, G. C. R., & Kasai, H. (2005). Spine-neck geometry determines NMDA receptor-dependent Ca2+signaling in dendrites. *Neuron*, *46*(4), 609–622. https://doi.org/10.1016/j.neuron.2005.03.015

Norris, A. D., & Calarco, J. A. (2012). Emerging roles of alternative pre-mRNA splicing regulation in neuronal development and function. *Frontiers in Neuroscience*. https://doi.org/10.3389/fnins.2012.00122

North, M. A., Naggert, J. K., Yan, Y., Noben-Trauth, K., & Nishina, P. M. (1997). Molecular characterization of TUB, TULP1, and TULP2, members of the novel tubby gene family and their possible relation to ocular diseases. *Proceedings of the National Academy of Sciences of the United States of America*. https://doi.org/10.1073/pnas.94.7.3128

O'Brien, R. J., Kamboj, S., Ehlers, M. D., Rosen, K. R., Fischbach, G. D., & Huganir, R. L. (1998). Activity-dependent modulation of synaptic AMPA receptor accumulation. *Neuron*. https://doi.org/10.1016/S0896-6273(00)80624-8

O'Keefe, J., & Nadel, L. (1978). *The Hippocampus as a Cognitive Map.* https://doi.org/10.1097/00005053-198003000-00018

Pamudurti, N. R., Bartok, O., Jens, M., Ashwal-Fluss, R., Stottmeister, C., Ruhe, L., … Kadener, S. (2017). Translation of CircRNAs. *Molecular Cell*, 1–13. https://doi.org/10.1016/j.molcel.2017.02.021

Pan, Q., Shai, O., Lee, L. J., Frey, B. J., & Blencowe, B. J. (2008). Deep surveying of alternative splicing complexity in the human transcriptome by high-throughput sequencing. *Nature*

Genetics. https://doi.org/10.1038/ng.259

Peters, A., & Kaiserman-Abramof, I. R. (1970). The small pyramidal neuron of the rat cerebral cortex. The perikaryon, dendrites and spines. *American Journal of Anatomy*, *127*(4), 321–355. https://doi.org/10.1002/aja.1001270402

Peterson, A. C., Russell, J. D., Bailey, D. J., Westphall, M. S., & Coon, J. J. (2012). Parallel Reaction Monitoring for High Resolution and High Mass Accuracy Quantitative, Targeted Proteomics. *Molecular & Cellular Proteomics*, *11*(11), 1475–1488. https://doi.org/10.1074/mcp.O112.020131

Petralia, R. S., Esteban, J. A., Wang, Y. X., Partridge, J. G., Zhao, H. M., Wenthold, R. J., & Malinow, R. (1999). Selective acquisition of AMPA receptors over postnatal development suggests a molecular basis for silent synapses. *Nature Neuroscience*. https://doi.org/10.1038/4532

Phillips, G. R., Huang, J. K., Wang, Y., Tanaka, H., Shapiro, L., Zhang, W., … Colman, D. R. (2001). The presynaptic particle web: Ultrastructure, composition, dissolution, and reconstitution. *Neuron*, *32*(1), 63–77. https://doi.org/10.1016/S0896-6273(01)00450-0

Piwecka, M., Glažar, P., Hernandez-Miranda, L. R., Memczak, S., Wolf, S. A., Rybak-Wolf, A., … Rajewsky, N. (2017). Loss of a mammalian circular RNA locus causes miRNA deregulation and affects brain function. *Science*, *357*(6357). https://doi.org/10.1126/science.aam8526

Plotkin, J. L., & Surmeier, D. J. (2015). Corticostriatal synaptic adaptations in Huntington's disease. *Current Opinion in Neurobiology*. https://doi.org/10.1016/j.conb.2015.01.020

Qiu, M., Xia, W., Chen, R., Wang, S., Xu, Y., Ma, Z., … Xu, L. (2018). The circular RNA circPRKCI promotes tumor growth in lung adenocarcinoma. *Cancer Research*. https://doi.org/10.1158/0008-5472.CAN-17-2808

Quinn, J. J., & Chang, H. Y. (2016). Unique features of long non-coding RNA biogenesis and function. *Nature Reviews Genetics*, *17*(1), 47–62. https://doi.org/10.1038/nrg.2015.10

Radley, J. J., Rocher, A. B., Rodriguez, A., Ehlenberger, D. B., Dammann, M., McEwen, B. S., … Hof, P. R. (2008). Repeated stress alters dendritic spine morphology in the rat medial prefrontal cortex. *J Comp Neurol*, *507*(1), 1141–1150. https://doi.org/10.1002/cne.21588

Raj, B., & Blencowe, B. J. (2015). Alternative Splicing in the Mammalian Nervous System: Recent Insights into Mechanisms and Functional Roles. *Neuron*, *87*(1), 14–27. https://doi.org/10.1016/j.neuron.2015.05.004

Ramos, A. D., Diaz, A., Nellore, A., Delgado, R. N., Park, K. Y., Gonzales-Roybal, G., … Lim, D. A. (2013). Integration of genome-wide approaches identifies lncRNAs of adult neural stem cells and their progeny in vivo. *Cell Stem Cell*. https://doi.org/10.1016/j.stem.2013.03.003

Ran, F. A., Hsu, P. D. P. P. D., Wright, J., Agarwala, V., Scott, D. a, & Zhang, F. (2013). Genome engineering using the CRISPR-Cas9 system. *Nature Protocols*, *8*(11), 2281–2308. https://doi.org/10.1038/nprot.2013.143

Reisel, D., Bannerman, D. M., Schmitt, W. B., Deacon, R. M. J., Flint, J., Borchardt, T., … Rawlins, J. N. P. (2002). Spatial memory dissociations in mice lacking GluR1. *Nature*

Neuroscience, *5*(9), 868–873. https://doi.org/10.1038/nn910

Riccomagno, M. M., & Kolodkin, A. L. (2015). Sculpting Neural Circuits by Axon and Dendrite Pruning. *Annual Review of Cell and Developmental Biology*. https://doi.org/10.1146/annurev-cellbio-100913-013038

Richter, K., Wolf, G., & Engelmann, M. (2005). Social recognition memory requires two stages of protein synthesis in mice. *Learning and Memory*, *12*(4), 407–413. https://doi.org/10.1101/lm.97505

Rochefort, N. L., & Konnerth, A. (2012). Dendritic spines: From structure to in vivo function. *EMBO Reports*. https://doi.org/10.1038/embor.2012.102

Roelandse, M. (2004). Hypothermia-Associated Loss of Dendritic Spines. *Journal of Neuroscience*, *24*(36), 7843–7847. https://doi.org/10.1523/JNEUROSCI.2872-04.2004

Ronshaugen, M., McGinnis, N., Inglis, D., Chou, D., Zhao, J., & McGinnis, W. (2002). Structure and expression patterns of Drosophila TULP and TUSP, members of the tubby-like gene family. *Mechanisms of Development*, *117*(1–2), 209–215. https://doi.org/10.1016/S0925-4773(02)00211-3

Rosahl, T. W., Geppert, M., Spillane, D., Herz, J., Hammer, R. E., Malenka, R. C., & Südhof, T. C. (1993). Short-term synaptic plasticity is altered in mice lacking synapsin I. *Cell*, *75*(4), 661–670. https://doi.org/10.1016/0092-8674(93)90487-B

Rosahl, T. W., Spillane, D., Missler, M., Herz, J., Selig, D. K., Wolff, J. R., … Südhof, T. C. (1995). Essential functions of synapsins I and II in synaptic vesicle regulation. *Nature*. https://doi.org/10.1038/375488a0

Rupaimoole, R., Calin, G. A., Lopez-Berestein, G., & Sood, A. K. (2016). MiRNA deregulation in cancer cells and the tumor microenvironment. *Cancer Discovery*. https://doi.org/10.1158/2159-8290.CD-15-0893

Rybak-Wolf, A., Stottmeister, C., Glažar, P., Jens, M., Pino, N., Giusti, S., … Rajewsky, N. (2015). Circular RNAs in the Mammalian Brain Are Highly Abundant, Conserved, and Dynamically Expressed. *Molecular Cell*, 1–16. https://doi.org/10.1016/j.molcel.2015.03.027

Sadowski, I., Ma, J., Triezenberg, S., & Ptashne, M. (1988). GAL4-VP16 is an unusually potent transcriptional activator. *Nature*. https://doi.org/10.1038/335563a0

Saito, T. (2006). In vivo electroporation in the embryonic mouse central nervous system. *Nature Protocols*, *1*(3), 1552–1558. https://doi.org/10.1038/nprot.2006.276

Saito, T., & Nakatsuji, N. (2001). Efficient gene transfer into the embryonic mouse brain using in vivo electroporation. *Developmental Biology*, *240*(1), 237–246. https://doi.org/10.1006/dbio.2001.0439

Salzman, J. (2016). Circular RNA Expression: Its Potential Regulation and Function. *Trends in Genetics*, *32*(5), 309–316. https://doi.org/10.1016/j.tig.2016.03.002

Salzman, J., Chen, R. E., Olsen, M. N., Wang, P. L., & Brown, P. O. (2013). Cell-Type Specific Features of Circular RNA Expression. *PLoS Genetics*, *9*(9). https://doi.org/10.1371/journal.pgen.1003777

Salzman, J., Gawad, C., Wang, P. L., Lacayo, N., & Brown, P. O. (2012). Circular RNAs are the predominant transcript isoform from hundreds of human genes in diverse cell types.

PLoS ONE, *7*(2). https://doi.org/10.1371/journal.pone.0030733

Santagata, S., Boggon, T. J., Baird, C. L., Gomez, C. A., Zhao, J., Wei Song Shan, … Shapiro, L. (2001). G-protein signaling through tubby proteins. *Science*. https://doi.org/10.1126/science.1061233

Scoville, W. B., & Milner, B. (1957). Loss of recentmemory after bilateral hippocampal lesions. *Journal of Neurology, Neurosurgery & Psychiatry*, *20*(1), 11–21. https://doi.org/10.1136/jnnp.20.1.11

Segal, M. M. (1983). Rat hippocampal neurons in culture: responses to electrical and chemical stimuli. *Journal of Neurophysiology*. https://doi.org/10.1152/jn.1983.50.6.1249

Selkoe, D. J. (2002). Alzheimer's disease is a synaptic failure. *Science*. https://doi.org/10.1126/science.1074069

Sheng, M., & Hoogenraad, C. C. (2007). The Postsynaptic Architecture of Excitatory Synapses: A More Quantitative View. *Annual Review of Biochemistry*, *76*(1), 823–847. https://doi.org/10.1146/annurev.biochem.76.060805.160029

Shibata, M., Kurokawa, D., Nakao, H., Ohmura, T., & Aizawa, S. (2008). MicroRNA-9 Modulates Cajal-Retzius Cell Differentiation by Suppressing Foxg1 Expression in Mouse Medial Pallium. *Journal of Neuroscience*. https://doi.org/10.1523/JNEUROSCI.3219-08.2008

Siddiqui, T. J., & Craig, A. M. (2011). Synaptic organizing complexes. *Current Opinion in Neurobiology*. https://doi.org/10.1016/j.conb.2010.08.016

Skrede, K. K., & Westgaard, R. H. (1971). The transverse hippocampal slice: a well-defined cortical structure maintained in vitro. *Brain Research*, *35*(2), 589–593. https://doi.org/10.1016/0006-8993(71)90508-7

Smith, T. F., Gaitatzes, C., Saxena, K., & Neer, E. J. (1999). The WD repeat: A common architecture for diverse functions. *Trends in Biochemical Sciences*. https://doi.org/10.1016/S0968-0004(99)01384-5

Soma, A., Onodera, A., Sugahara, J., Kanai, A., Yachie, N., Tomita, M., … Sekine, Y. (2007). Permuted tRNA genes expressed via a circular RNA intermediate in Cyanidioschyzon merolae. *Science*. https://doi.org/10.1126/science.1145718

Song, H. J., Stevens, C. F., & Gage, F. H. (2002). Neural stem cells from adult hippocampus develop essential properties of functional CNS neurons. *Nature Neuroscience*. https://doi.org/10.1038/nn844

Soriano, E., Del Río, J. A., Martínez, A., & Supèr, H. (1994). Organization of the embryonic and early postnatal murine hippocampus. I. Immunocytochemical characterization of neuronal populations in the subplate and marginal zone. *Journal of Comparative Neurology*, *342*(4), 571–595. https://doi.org/10.1002/cne.903420406

Stagsted, L. V. W., Nielsen, K. M., Daugaard, I., & Hansen, T. B. (2018). Non-coding AUG circRNAs constitute an abundant and conserved subclass of circles. *BioRxiv*, *2*(3), 328104. https://doi.org/10.1101/328104

Starke, S., Jost, I., Rossbach, O., Schneider, T., Schreiner, S., Hung, L.-H., & Bindereif, A. (2015). Exon Circularization Requires Canonical Splice Signals. *Cell Reports*, *10*(1), 103–

111. https://doi.org/10.1016/j.celrep.2014.12.002

Stewart-Ornstein, J., & Lahav, G. (2016). Dynamics of CDKN1A in Single Cells Defined by an Endogenous Fluorescent Tagging Toolkit. *Cell Reports*, *14*(7), 1800–1811. https://doi.org/10.1016/j.celrep.2016.01.045

Stockmeier, C. A., Mahajan, G. J., Konick, L. C., Overholser, J. C., Jurjus, G. J., Meltzer, H. Y., … Rajkowska, G. (2004). Cellular changes in the postmortem hippocampus in major depression. *Biological Psychiatry*. https://doi.org/10.1016/j.biopsych.2004.08.022

Südhof, T. C. (2008). Neuroligins and neurexins link synaptic function to cognitive disease. *Nature*. https://doi.org/10.1038/nature07456

Sung, Y. H., Baek, I. J., Kim, D. H., Jeon, J., Lee, J., Lee, K., … Lee, H. W. (2013). Knockout mice created by TALEN-mediated gene targeting. *Nature Biotechnology*. https://doi.org/10.1038/nbt.2477

Supèr, H., & Uylings, H. B. (2001). The early differentiation of the neocortex: a hypothesis on neocortical evolution. *Cerebral Cortex (New York, N.Y. : 1991)*, *11*(12), 1101–1109. https://doi.org/doi: 10.1093/cercor/11.12.1101

Swerdlow, N. R., Geyer, M. A., & Braff, D. L. (2001). Neural circuit regulation of prepulse inhibition of startle in the rat: Current knowledge and future challenges. *Psychopharmacology*, *156*(2–3), 194–215. https://doi.org/10.1007/s002130100799

Talhouarne, G. J. S., & Gall, J. G. (2018). Lariat intronic RNAs in the cytoplasm of vertebrate cells. *Proceedings of the National Academy of Sciences*. https://doi.org/10.1073/pnas.1808816115

Tamás, G., Buhl, E. H., & Somogyi, P. (1997). Massive autaptic self-innervation of GABAergic neurons in cat visual cortex. *Journal of Neuroscience*. https://doi.org/10.1523/jneurosci.17-16-06352.1997

Tang, T. H. (2002). RNomics in Archaea reveals a further link between splicing of archaeal introns and rRNA processing. *Nucleic Acids Research*. https://doi.org/10.1093/nar/30.4.921

Tesson, L., Usal, C., Meǫnoret, S., Leung, E., Niles, B. J., Remy, S., … Cost, G. J. (2011). Knockout rats generated by embryo microinjection of TALENs. *Nature Biotechnology*. https://doi.org/10.1038/nbt.1940

Thiagarajan, T. C., Lindskog, M., & Tsien, R. W. (2005). Adaptation to synaptic inactivity in hippocampal neurons. *Neuron*. https://doi.org/10.1016/j.neuron.2005.06.037

Ting, J. T., Peça, J., & Feng, G. (2012). Functional Consequences of Mutations in Postsynaptic Scaffolding Proteins and Relevance to Psychiatric Disorders. *Annual Review of Neuroscience*. https://doi.org/10.1146/annurev-neuro-062111-150442

Trachtenberg, J. T., Chen, B. E., Knott, G. W., Feng, G., Sanes, J. R., Welker, E., & Svoboda, K. (2002). Long-term in vivo imaging of experience-dependent synaptic plasticity in adult cortex. *Nature*, *420*(6917), 788–794. https://doi.org/10.1038/nature01273

Truett, G. E., Heeger, P., Mynatt, R. L., Truett, A. A., Walker, J. A., & Warman, M. L. (2000). Preparation of PCR-quality mouse genomic dna with hot sodium hydroxide and tris (HotSHOT). *BioTechniques*, *29*(1), 52–54. https://doi.org/10.1016/j.jacc.2014.05.073

Turrigiano, G G, Leslie, K. R., Desai, N. S., Rutherford, L. C., & Nelson, S. B. (1998). Activity-

dependent scaling of quantal amplitude in neocortical neurons. *Nature*. https://doi.org/10.1038/36103

Turrigiano, Gina G., & Nelson, S. B. (2004). Homeostatic plasticity in the developing nervous system. *Nature Reviews Neuroscience*. https://doi.org/10.1038/nrn1327

Uekita, T., & Okanoya, K. (2011). Hippocampus lesions induced deficits in social and spatial recognition in Octodon degus. *Behavioural Brain Research*. https://doi.org/10.1016/j.bbr.2011.01.042

Urnov, F. D., Rebar, E. J., Holmes, M. C., Zhang, H. S., & Gregory, P. D. (2010). Genome editing with engineered zinc finger nucleases. *Nature Reviews Genetics*. https://doi.org/10.1038/nrg2842

Van Gaalen, M. M., & Steckler, T. (2000). Behavioural analysis of four mouse strains in an anxiety test battery. *Behavioural Brain Research*. https://doi.org/10.1016/S0166-4328(00)00240-0

Vannoni, E., Voikar, V., Colacicco, G., Sánchez, M. A., Lipp, H. P., & Wolfer, D. P. (2014). Spontaneous behavior in the social homecage discriminates strains, lesions and mutations in mice. *Journal of Neuroscience Methods*, *234*, 26–37. https://doi.org/10.1016/j.jneumeth.2014.04.026

Venø, M. T., Hansen, T. B., Venø, S. T., Clausen, B. H., Grebing, M., Finsen, B., … Kjems, J. (2015). Spatio-temporal regulation of circular RNA expression during porcine embryonic brain development. *Genome Biology*, *16*, 245. https://doi.org/10.1186/s13059-015-0801-3

Vetter, P., Roth, A., & Häusser, M. (2001). Propagation of action potentials in dendrites depends on dendritic morphology. *Journal of Neurophysiology*. https://doi.org/10.1152/jn.2001.85.2.926

Vicens, Q., & Westhof, E. (2014). Biogenesis of circular RNAs. *Cell*. https://doi.org/10.1016/j.cell.2014.09.005

Voikar, V., Colacicco, G., Gruber, O., Vannoni, E., Lipp, H. P., & Wolfer, D. P. (2010). Conditioned response suppression in the IntelliCage: Assessment of mouse strain differences and effects of hippocampal and striatal lesions on acquisition and retention of memory. *Behavioural Brain Research*. https://doi.org/10.1016/j.bbr.2010.05.019

Voikar, V., Krackow, S., Lipp, H. P., Rau, A., Colacicco, G., & Wolfer, D. P. (2018). Automated dissection of permanent effects of hippocampal or prefrontal lesions on performance at spatial, working memory and circadian timing tasks of C57BL/6 mice in IntelliCage. *Behavioural Brain Research*, *352*(September 2017), 8–22. https://doi.org/10.1016/j.bbr.2017.08.048

Wall, P. M., Blanchard, R. J., Yang, M., & Blanchard, D. C. (2003). Infralimbic D2 receptor influences on anxiety-like behavior and active memory/attention in CD-1 mice. *Progress in Neuro-Psychopharmacology and Biological Psychiatry*. https://doi.org/10.1016/S0278-5846(02)00356-1

Wan, L., Zhang, L., Fan, K., Cheng, Z. X., Sun, Q. C., & Wang, J. J. (2016). Circular RNA-ITCH Suppresses Lung Cancer Proliferation via Inhibiting the Wnt/β-Catenin Pathway. *BioMed Research International*. https://doi.org/10.1155/2016/1579490

Wang, E. T., Sandberg, R., Luo, S., Khrebtukova, I., Zhang, L., Mayr, C., … Burge, C. B. (2008). Alternative isoform regulation in human tissue transcriptomes. *Nature*. https://doi.org/10.1038/nature07509

Wang, H., Yang, H., Shivalila, C. S., Dawlaty, M. M., Cheng, A. W., Zhang, F., & Jaenisch, R. (2013). One-step generation of mice carrying mutations in multiple genes by CRISPR/cas-mediated genome engineering. *Cell*, *153*(4), 910–918. https://doi.org/10.1016/j.cell.2013.04.025

Wang, P. L., Bao, Y., Yee, M. C., Barrett, S. P., Hogan, G. J., Olsen, M. N., … Salzman, J. (2014). Circular RNA is expressed across the eukaryotic tree of life. *PLoS ONE*, *9*(3). https://doi.org/10.1371/journal.pone.0090859

Wang, Y., & Wang, Z. (2015). Efficient backsplicing produces translatable circular mRNAs. *Rna*, *21*(2), 172–179. https://doi.org/10.1261/rna.048272.114

Waterston, R. H., Lindblad-Toh, K., Birney, E., Rogers, J., Abril, J. F., Agarwal, P., … Lander, E. S. (2002). Initial sequencing and comparative analysis of the mouse genome. *Nature*, *420*(6915), 520–562. https://doi.org/10.1038/nature01262

Wefers, B., Meyer, M., Ortiz, O., Hrabe de Angelis, M., Hansen, J., Wurst, W., & Kuhn, R. (2013). Direct production of mouse disease models by embryo microinjection of TALENs and oligodeoxynucleotides. *Proceedings of the National Academy of Sciences*. https://doi.org/10.1073/pnas.1218721110

Wefers, Benedikt, Bashir, S., Rossius, J., Wurst, W., & Kühn, R. (2017). Gene editing in mouse zygotes using the CRISPR/Cas9 system. *Methods*, *121–122*, 55–67. https://doi.org/10.1016/j.ymeth.2017.02.008

Wefers, Benedikt, Ortiz, O., Wurst, W., & Kühn, R. (2014). Generation of targeted mouse mutants by embryo microinjection of TALENs. *Methods*, *69*(1), 94–101. https://doi.org/10.1038/nprot.2013.142

Westholm, J. O., Miura, P., Graveley, B. R., Lai, E. C., Olson, S., Shenker, S., … Celniker, S. E. (2014). Genome-wide Analysis of Drosophila Circular RNAs Reveals Their Structural and Sequence Properties and Age-Dependent Neural Accumulation. *Cell Reports*, *9*(5), 1966–1980. https://doi.org/10.1016/j.celrep.2014.10.062

Whitlock, J. R., Heynen, A. J., Shuler, M. G., & Bear, M. F. (2006). Learning induces long-term potentiation in the hippocampus. *Science*, *313*(5790), 1093–1097. https://doi.org/10.1126/science.1128134

Wiedholz, L. M., Owens, W. A., Horton, R. E., Feyder, M., Karlsson, R. M., Hefner, K., … Holmes, A. (2008). Mice lacking the AMPA GluR1 receptor exhibit striatal hyperdopaminergia and “schizophrenia-related” behaviors. *Molecular Psychiatry*, *13*(6), 631–640. https://doi.org/10.1038/sj.mp.4002056

Wilusz, J. E. (2018). A 360° view of circular RNAs: From biogenesis to functions. *Wiley Interdisciplinary Reviews: RNA*, *9*(4), 1–17. https://doi.org/10.1002/wrna.1478

Wojcik, S. M., Rhee, J. S., Herzog, E., Sigler, A., Jahn, R., Takamori, S., … Rosenmund, C. (2004). An essential role for vesicular glutamate transporter 1 (VGLUT1) in postnatal development and control of quantal size. *Proceedings of the National Academy of Sciences*, *101*(18), 7158–7163. https://doi.org/10.1073/pnas.0401764101

Wolfer, D. P., Litvin, O., Morf, S., Nitsch, R. M., Lipp, H.-P., & Würbel, H. (2004). Laboratory animal welfare: Cage enrichment and mouse behaviour. *Nature*. https://doi.org/10.1038/432821a

Woolley, C. S., Gould, E., Frankfurt, M., & McEwen, B. S. (1990). Naturally occurring fluctuation in dendritic spine density on adult hippocampal pyramidal neurons. *J Neurosci*, *10*(12), 4035–4039. https://doi.org/10.1523/JNEUROSCI.10-12-04035.1990

Wu, G. Y., Malinow, R., & Cline, H. T. (1996). Maturation of a central glutamatergic synapse. *Science*. https://doi.org/10.1126/science.274.5289.972

Xiong, H. Y., Alipanahi, B., Lee, L. J., Bretschneider, H., Merico, D., Yuen, R. K. C., … Frey, B. J. (2015). The human splicing code reveals new insights into the genetic determinants of disease. *Science*. https://doi.org/10.1126/science.1254806

Yang, H., Wang, H., Shivalila, C. S., Cheng, A. W., Shi, L., & Jaenisch, R. (2013). XOne-step generation of mice carrying reporter and conditional alleles by CRISPR/cas-mediated genome engineering. *Cell*, *154*(6). https://doi.org/10.1016/j.cell.2013.08.022

Yang, J., Thio, L. L., Clifford, D. B., & Zorumski, C. F. (1993). Electrophysiological properties of identified postnatal rat hippocampal pyramidal neurons in primary culture. *Developmental Brain Research*. https://doi.org/10.1016/0165-3806(93)90100-O

Yang, Yibing, Gao, X., Zhang, M., Yan, S., Sun, C., Xiao, F., … Zhang, N. (2018). Novel Role of FBXW7 Circular RNA in Repressing Glioma Tumorigenesis. *Journal of the National Cancer Institute*, *110*(3), 304–315. https://doi.org/10.1093/jnci/djx166

Yang, Yun, Fan, X., Mao, M., Song, X., Wu, P., Zhang, Y., … Wang, Z. (2017). Extensive translation of circular RNAs driven by N 6 -methyladenosine. *Cell Research*, *27*(5), 626–641. https://doi.org/10.1038/cr.2017.31

Yoon, E. J., Jeong, Y. T., Lee, J. E., Moon, S. J., & Kim, C. H. (2017). Tubby domain superfamily protein is required for the formation of the 7S SNARE complex in Drosophila. *Biochemical and Biophysical Research Communications*, *482*(4), 814–820. https://doi.org/10.1016/j.bbrc.2016.11.117

You, X., Vlatkovic, I., Babic, A., Will, T., Epstein, I., Tushev, G., … Chen, W. (2015). Neural circular RNAs are derived from synaptic genes and regulated by development and plasticity. *Nature Neuroscience*, *18*(4), 603–610. https://doi.org/10.1038/nn.3975

Yu, C.-Y., Li, T.-C., Wu, Y.-Y., Yeh, C.-H., Chiang, W., Chuang, C.-Y., & Kuo, H.-C. (n.d.). The circular RNA circBIRC6 participates in the molecular circuitry controlling human pluripotency. *Nature Communications*. https://doi.org/10.1038/s41467-017-01216-w

Yuste, R, & Bonhoeffer, T. (2001). Morphological changes in dendritic spines associated with long-term synaptic plasticity. *Annu Rev Neurosci*, *24*(1862), 1071–1089. https://doi.org/10.1146/annurev.neuro.24.1.1071

Yuste, Rafael, & Bonhoeffer, T. (2004). Genesis of dendritic spines: Insights from ultrastructural and imaging studies. *Nature Reviews Neuroscience*, *5*(1), 24–34. https://doi.org/10.1038/nrn1300

Zaghlool, A., Ameur, A., Wu, C., Westholm, J. O., Niazi, A., Manivannan, M., … Feuk, L. (2018). Expression profiling and in situ screening of circular RNAs in human tissues. *Scientific Reports*, *8*(1). https://doi.org/10.1038/s41598-018-35001-6

Zamanillo, D., Sprengel, R., Hvalby, Ø., Jensen, V., Burnashev, N., Rozov, A., … Sakmann, B. (1999). Importance of AMPA receptors for hippocampal synaptic plasticity but not for spatial learning. *Science*, *284*(5421), 1805–1811. https://doi.org/10.1126/science.284.5421.1805

Zaphiropoulos, P. G. (1996). Circular RNAs from transcripts of the rat cytochrome P450 2C24 gene: correlation with exon skipping. *Proceedings of the National Academy of Sciences of the United States of America*, *93*(13), 6536–6541. https://doi.org/10.1073/pnas.93.13.6536

Zeitelhofer, M., Vessey, J. P., Xie, Y., Tubing, F., Thomas, S., & Dahm, R. (2007). High-efficiency transfection of mammalian neurons via nucleofection. *Nature Protocols*, *2*(7), 1692–1704. https://doi.org/10.1038/nprot.2007.226

Zeringue, H. C., & Constantine-Paton, M. (2004). Post-transcriptional gene silencing in neurons. *Current Opinion in Neurobiology*. https://doi.org/10.1016/j.conb.2004.08.009

Zhang, M., Huang, N., Yang, X., Luo, J., Yan, S., Xiao, F., … Zhang, N. (2018a). A novel protein encoded by the circular form of the SHPRH gene suppresses glioma tumorigenesis. *Oncogene*, *37*(13), 1805–1814. https://doi.org/10.1038/s41388-017-0019-9

Zhang, M., Zhao, K., Xu, X., Yang, Y., Yan, S., Wei, P., … Zhang, N. (2018b). A peptide encoded by circular form of LINC-PINT suppresses oncogenic transcriptional elongation in glioblastoma. *Nature Communications*, *9*(1). https://doi.org/10.1038/s41467-018-06862-2

Zhang, X. O., Dong, R., Zhang, Y., Zhang, J. L., Luo, Z., Zhang, J., … Yang, L. (2016). Diverse alternative back-splicing and alternative splicing landscape of circular RNAs. *Genome Research*. https://doi.org/10.1101/gr.202895.115

Zhang, X. O., Wang, H. Bin, Zhang, Y., Lu, X., Chen, L. L., & Yang, L. (2014). Complementary sequence-mediated exon circularization. *Cell*, *159*(1), 134–147. https://doi.org/10.1016/j.cell.2014.09.001

Zhang, Y., Xue, W., Li, X., Zhang, J., Chen, S., Zhang, J. L., … Chen, L. L. (2016). The Biogenesis of Nascent Circular RNAs. *Cell Reports*, *15*(3), 611–624. https://doi.org/10.1016/j.celrep.2016.03.058

Zhang, Y., Zhang, X. O., Chen, T., Xiang, J. F., Yin, Q. F., Xing, Y. H., … Chen, L. L. (2013). Circular Intronic Long Noncoding RNAs. *Molecular Cell*. https://doi.org/10.1016/j.molcel.2013.08.017

Zhao, Y., Alexandrov, P., Jaber, V., & Lukiw, W. (2016). Deficiency in the Ubiquitin Conjugating Enzyme UBE2A in Alzheimer's Disease (AD) is Linked to Deficits in a Natural Circular miRNA-7 Sponge (circRNA; ciRS-7). *Genes*, *7*(12), 116. https://doi.org/10.3390/genes7120116

Zheng, Q., Bao, C., Guo, W., Li, S., Chen, J., Chen, B., … Huang, S. (2016). Circular RNA profiling reveals an abundant circHIPK3 that regulates cell growth by sponging multiple miRNAs. *Nature Communications*, *7*, 11215. https://doi.org/10.1038/ncomms11215

Zheng, S., & Black, D. L. (2013). Alternative pre-mRNA splicing in neurons: Growing up and extending its reach. *Trends in Genetics*. https://doi.org/10.1016/j.tig.2013.04.003

Zhou, Q., Homma, K. J., & Poo, M. M. (2004). Shrinkage of dendritic spines associated with

long-term depression of hippocampal synapses. *Neuron*, *44*(5), 749–757. https://doi.org/S0896627304007226 [pii]\n10.1016/j.neuron.2004.11.011

Zito, K., Scheuss, V., Knott, G., Hill, T., & Svoboda, K. (2009). Rapid Functional Maturation of Nascent Dendritic Spines. *Neuron*, *61*(2), 247–258. https://doi.org/10.1016/j.neuron.2008.10.054

Zucker, R. S., & Regehr, W. G. (2002). Short-term synaptic plasticity. *Scholarpedia*, *8*(10), 3153. https://doi.org/10.4249/scholarpedia.3153

12 List of abbreviations

4sU	4-thiouridine
aa	amino acids
ABR	auditory brainstem response
AD	Alzheimer's disease
AMPA	α-amino-3-hydroxy-5-methyl-4-isoxazolepropionic acid
AMPAR	α-amino-3-hydroxy-5-methyl-4-isoxazolepropionic acid receptor
ANOVA	analysis of variance
AS	alternative splicing
ASR	acoustic startle response
Beam	balance beam
bp	basepairs
Ca^{2+}	calcium
CA	cornu ammonis area
Cas	CRISPR-associated
cDNA	complementary DNA
CDS	coding sequence
CI	confidence interval
CMV	cytomegalovirus
CNS	central nervous system
CP	cross-point
Cre	cyclization recombinase
CRISPR	Clustered Regularly Interspaced Short Palindromic Repeats
crRNAs	CRISPR RNAs
C-terminus	carboxyl terminus
Ctrl	control
Da	Dalton
DAPI	4',6-diamidino-2-phenylindole
dB	decibel
DEPC	diethylpyrocarbonate
DH5α	*E. coli* strain DH5α
DIC	differential interference contrast
DIV	days *in vitro*
DMEM	Dulbecco's Modified Eagle's Medium
DMSO	dimethylsulfoxide
DNA	desoxyribonucleic acid
dNTP	desoxyribonucleotide triphosphate
DSBs	doubled-stranded breaks
E	embryonary day
EDTA	ethylenediaminetetraacetic acid
EIcircRNAs	Exon-intron circRNAs
EPM	elevated plus maze
EPSCs	excitatory post-synaptic currents
ES	embryonary stem cells
FCS	fetal calf serum
FISH	fluorescent *in situ* hybridization
FUS	fused in sarcoma
GABA	gamma aminobutyric acid
GFP	green fluorescent protein
GMC	german mouse clinic
gRNA	guide ribonucleic acid
h	hour
HBSS	Hanks´s balanced salt solution
HCl	hydrochloric acid
HEPES	4-(2-Hydroxyethyl)piperazine-1-ethanesulfonic acid

HR	homologous recombination
IPSCs	inhibitory post-synaptic currents
IRES	internal ribosome entry site
Kb	kilo basepairs
kDa	kilo Dalton
KO	knockout
lncRNAs	Long non-coding RNAs
loxP	locus of crossover in P1
LTD	long-term depression
LTP	long-term potentiation
mEPSCs	miniature excitatory post-synaptic currents
mESCs	mouse embryonary stem cells
mIPSCs	miniature inhibitory post-synaptic currents
miRNAs	micro RNAs
mRNA	messenger ribonucleic acid
min	minutes
ncRNAs	non-coding RNAs
NHEJ	non-homologous end joining
NLS	nuclear localization signal
NMDA	*N*-methyl-D-aspartic acid
NMDAR	*N*-methyl-D-aspartic acid receptor
N-terminus	amino terminus
o.n.	overnight
OE-circTulp4	circTulp4 overexpression construct
OF	open field
P	post-natal day
PAM	protospacer adjacent motif
PBS	phosphate buffered saline
PCR	polymerase chain reaction
PD	Parkinson's disease
PFA	paraformaldehyde
PIPs	phosphoinositides
piRNAs	piwi-interacting RNA
Pol II	RNA polymerase II
PPF	paired-pulse facilitation
PPI	pre-pulse inhibition
pre-mRNA	precursor mRNA
PRM	parallel reaction monitoring
PSD	post-synaptic density
pSico	plasmid for stable RNA interference, conditional
qRT-PCR	quantitative real time PCR
RACE	rapid amplification of cDNA ends
RBPs	RNA-binding proteins
RIPA	radioimmunoprecipitation assay
RFP	red fluorescent protein
RNA	ribonucleic acid
RNAi	RNA interference
RPL19	ribosomal protein L19
rRNA	Ribosomal RNA
RT	room temperature
s	seconds
SA	splice acceptor
SD	splice donor
SD	social discrimination
sgRNA	single-guide RNA
sh-circTulp4	short hairpin RNA against circTulp4
sh-RNA	short hairpin RNA

sh-scrambled	short hairpin RNA against a scrambled sequence
siRNAs	small interfering RNA
SLENDR	single-cell labelling of endogenous proteins by CRISPR/Cas9-mediated HDR
sncRNAs	small non-coding RNAs
SOCs	suppressor of cytokine signaling
SRM	selected reaction monitoring
SSC	saline-sodium citrate
ssDNA	single-stranded DNA
ssODN	single-stranded donor oligonucleotide
TAE	Tris acetate EDTA
TALENs	transcription activator-like effector nucleases
TBP	TATA-binding protein
TFBSs	transcription factor binding sites
tracrRNA	transactivating RNA
Tris	tris(hydroxylmethyl)-aminomethan
tRNA	transfer RNA
TULPs	Tubby-like protein family
TUSP	Tubby domain superfamily protein
UTR	untranslated region
VGlut	vesicular glutamate transporter
V/V	volume per volume
W/V	weight per volume
WB	western blot
WT	wild-type
ZFNs	zinc-finger nucleases

13 Acknowledgments

My deepest gratitude goes to my supervisor Dr. Daniela Vogt-Weisenhorn and the mentor of this project, Dr. Damián Refojo. Thank both of you for your continuous support, guidance, brain-storming sessions and feed-back during the past years.

I would also like to thank Prof. Dr. Wolfgang Wurst, for giving me the opportunity to work at the Institute of Developmental Genetics, for supervising and advising throughout this work. I would like to acknowledge Dr. Jan Deussing, member of my thesis committee together with the aforementioned, for his constructive comments and expertise in the mouse genetics field.

A heartfelt gratitude goes to Dr. Sebastián Giusti, who trained me, inspired me and encouraged me during the last years. Thank you for the fruitful discussions and for enabling me to develop and pursue my own ideas.

My gratitude also goes to our collaborators for their interest, support and input in their different areas of research. To the Neuronal Circuits group, led by Dr. Antonia Marin Burgin, for the electrophysiological measurements; to Dr. Dietrich Trümbach for all bioinformatic analyses; to the Genetics Tool Development group, led by Dr. Florian Giesert, for their assistance in mouse models generation; to the German Mouse Clinic for the behavioral analyses and, in particular, to the Behavioral Neuroscience group, led by PD Dr. Sabine Hölter-Koch, for the valuable discussions. Furthermore, several projects would not have been possible without the help and moral support of Annerose Kurz-Drexler, Susanne Badeke and Anja Folchert.

I would especially like to thank my colleagues María, Artem, Kristina and Chiara for their help, discussions and for creating a great working atmosphere. Not of less moral support has also been a group of not-work-related companions, the monkeys, without you my stay in Germany would have definitely been tougher and learning German would not have had continuity. Thank you for all the necessary leisure time.

To my parents and my brother goes the most profound gratitude. Thank you for supporting me in fulfilling my dreams, for having faith and for your love.

Michi, thank you for the unconditional support, for your advices and for believing in me. Finally, a very special thank you to the most influential persons in my life, my grandma and my daughter.

14 Affidavit

I hereby declare that the dissertation entitled “A circular RNA derived from the *Tulp4* gene regulates synaptic transmission and working memory” prepared under the guidance and supervision of Prof. Dr. Wolfgang Wurst, and submitted to the degree-awarding institution: Fakultät Wissenschaftszentrum Weihenstephan für Ernährung, Landnutzung und Umwelt of the Technical University of Munich is my own, original work undertaken in partial fulfillment of the requirements for the doctoral degree. I have made no use of sources, materials or assistance other than those specified in §6 (6) and (7), clause 2.

[ ] I have not employed the services of an organization that provides dissertation supervisors in return for payment or that fulfills, in whole or in part, the obligations incumbent on me in connection with my dissertation.

[ ] I have not submitted the dissertation, either in the present or in a similar form, as part of another examination process.

[ ] I have not yet been awarded the desired doctoral degree nor have I failed the last possible attempt to obtain the desired degree in a previous doctoral program.

I am familiar with the public available Regulations of the Award of Doctoral Degrees of the Technical University Munich, in particular §28 (invalidation of doctoral degree) and §29 (Revocation of doctoral degree). I am aware of the consequences of filling a false affidavit.

[ ] I agree, [ ] I do not agree

that my personal data is stored in the TUM alumni database.

Munich,